Table 13.5. The $E_{\mathrm{T}}^{\mathrm{miss}}$ + multi-jet SUSY search analysis path.

Requirement	Remark
Level 1	Level-1 trigger efficiency parametrisation
HLT, $E_{\mathrm{T}}^{\mathrm{miss}} > 200\,\mathrm{GeV}$	trigger/signal signature
primary vertex $\geqslant 1$	primary cleanup
$F_{em} \geqslant 0.175$, $F_{ch} \geqslant 0.1$	primary cleanup
$N_j \geqslant 3$, $\lvert\eta_d^{1j}\rvert < 1.7$	signal signature
$\delta\phi_{min}(E_{\mathrm{T}}^{\mathrm{miss}} - jet) \geqslant 0.3$ rad, $R1$, $R2 > 0.5$ rad,	
$\delta\phi(E_{\mathrm{T}}^{\mathrm{miss}} - j(2)) > 20^\circ$	QCD rejection
$Iso^{lead\,trk} = 0$	ILV (I) $W/Z/t\bar{t}$ rejection
$f_{em(j(1))}$, $f_{em(j(2))} < 0.9$	ILV (II), $W/Z/t\bar{t}$ rejection
$E_{\mathrm{T},j(1)} > 180\,\mathrm{GeV}$, $E_{\mathrm{T},j(2)} > 110\,\mathrm{GeV}$	signal/background optimisation
$H_{\mathrm{T}} \equiv E_{\mathrm{T}(2)} + E_{\mathrm{T}(3)} + E_{\mathrm{T}(4)} + E_{\mathrm{T}}^{\mathrm{miss}} > 500\,\mathrm{GeV}$	signal/background optimisation
SUSY LM1 signal efficiency 13%	

Table 13.6. Selected SUSY and Standard Model background events for 1 fb^{-1}.

Signal	$t\bar{t}$	single t	$Z(\rightarrow \nu\bar{\nu})$+ jets	$(W/Z, WW/ZZ/ZW)$ + jets	QCD
6319	53.9	2.6	48	33	107

Table 13.7. Standard Model background components and uncertainties for 1 fb^{-1}.

$t\bar{t}$, single top	$Z(\rightarrow \nu\bar{\nu})$+ jets	$(W/Z, WW/ZZ/ZW)$ + jets	QCD
56 ± 11(sys) $\pm$ 7.5(stat)	48 ± 3.5 (all)	33 ± 2.5 (all)	107 ± 25(sys) $\pm$10(stat)

significance computed with ScPf, defined in Appendix A.1. After $\sim 1.5\,\mathrm{fb}^{-1}$ the W/Z+jets backgrounds, including the invisible decays of the Z boson which constitutes a large irreducible background component, can be reliably normalised using the $Z \rightarrow \mu\mu$ and $Z \rightarrow ee$ + multi-jet data candle. The comparison of the signal, total background estimated and its components for the $M_{eff} \equiv E_{\mathrm{T}(1)} + E_{\mathrm{T}(2)} + E_{\mathrm{T}(3)} + E_{\mathrm{T}(4)} + E_{\mathrm{T}}^{\mathrm{miss}}$ can be found in section 4.2.

To perform the 5 σ reach scan (Fig. 13.5) in the mSUGRA parameter space, the HM1 test point is used as optimisation reference and the $E_{\mathrm{T}}^{\mathrm{miss}}$ and H_{T} requirements are raised to 600 GeV and 1500 GeV correspondingly. The analysis efficiency for HM1 is $\sim$12% while the total Standard Model background for 1 fb^{-1} is 4.36 events with a total uncertainty of 7% . The background composition is 67% Z invisible decays, 19% QCD jets and 14% W/Z+jets.

13.6. Inclusive muons with jets and missing transverse energy

We study the production and decay of new particles in mSUGRA via inclusive final states including muons, high p_{T} jets, and large missing transverse energy. Requiring at least one muon provides a relatively clean experimental signature (complementing searches involving only inclusive jets and missing energy), however requires a well-understood trigger shortly after the LHC start-up. In this work [675], the fully simulated and reconstructed LM1 mSUGRA point is taken as the benchmark for selection optimisation and study of systematic effects. Even though the study was performed within the context of mSUGRA, this method is not specific to the mSUGRA framework and should apply equally well in other contexts.

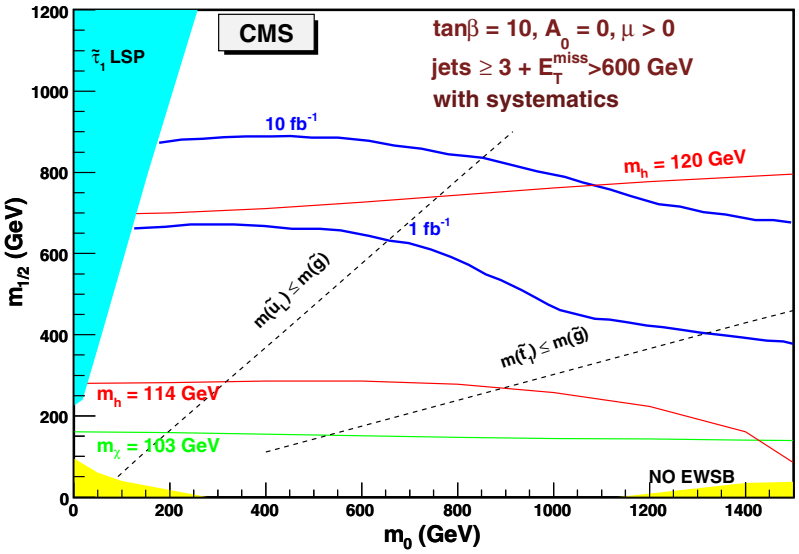

Figure 13.5. 5 σ reach for 1 and 10 fb^{-1} using multi-jets and missing transverse energy final state.

The strategy employed in this analysis is to optimise a set of selection cuts based on an objective function which provides a reasonable estimate of the significance to exclude the Standard Model null-hypothesis while explicitly including systematic uncertainties (thus avoiding regions of phase space which are prone to systematics). This work uses a Genetic Algorithm (GARCON [63]) for the optimisation of cuts.

13.6.1. Signal selection and backgrounds considered

Because this work is an inclusive study of mSUGRA signatures involving at least one muon accompanied by multiple jets and large $E_{\mathrm{T}}^{\mathrm{miss}}$, several Standard Model processes contribute as sources of background and must be taken into account. Accordingly, the main backgrounds studied in this analysis correspond to QCD dijet (2.8 million events with $0 < \hat{p}_{\mathrm{T}} < 4\,\mathrm{TeV/c}$), top ($t\bar{t}$) production (3.3 million events), electroweak single-boson production (4.4 million events with $0 < \hat{p}_{\mathrm{T}} < 4.4\,\mathrm{TeV/c}$) and electroweak dibosons production (1.2 million events). All backgrounds used in this work are fully simulated and reconstructed. This work uses only leading order cross-sections, consistently for both signal and all backgrounds. Considering NLO k-factors for the signal and background processes do not change the final results significantly.

The CMS trigger system is described in [76], and the current working trigger menu is described in Appendix E. This work uses an event sample which is triggered by either of two HLT triggers: the inclusive isolated single-muon trigger or the isolated dimuon trigger.

The following quality criteria are applied to muons and jets. The leading muon is required to have a transverse momentum above $p_{\mathrm{T}} = 30\,\mathrm{GeV/c}$ which ensures that the muon candidate is reconstructed with good efficiency, well above the trigger thresholds. Further, the leading muon is required to be isolated with less than 10 GeV of calorimeter energy within a cone of radius $R = 0.3$, reducing the effects due to fake muons, whilst preserving reasonable efficiency for signal acceptance. Finally, the three leading jets must each have an E_{T} of at least 50 GeV which guarantees that jets are reconstructed with good efficiency.

Table 13.8. Total number of selected events (for $10\,\text{fb}^{-1}$) and significance ("Signif.") with systematic uncertainties (but excluding uncertainties due to finite Monte Carlo simulation statistics and higher order QCD effects). "SM" represents the total of all Standard Model backgrounds considered.

Sample(s)	Events	Signif.	Sample	Events	Signif.	Sample	Events	Signif.
SM	2.54	–	LM4	246	29.2	LM6	277	31.6
LM1	311	34.0	LM5	165	22.9	HM1	13	5.0

The genetic algorithm GARCON [63] used for the optimisation of cuts results in: $E_{\text{T}}^{\text{miss}} > 130\,\text{GeV}$, $E_{\text{T}}^{\text{j1}} > 440\,\text{GeV}$, $E_{\text{T}}^{\text{j2}} > 440\,\text{GeV}$, $|\eta^{\text{j1}}| < 1.9$, $|\eta^{\text{j2}}| < 1.5$, $|\eta^{\text{j3}}| < 3$, $\cos\left[\Delta\phi(\text{j1},\text{j2})\right] < 0.2$, $-0.95 < \cos\left[\Delta\phi(E_{\text{T}}^{\text{miss}},\text{j1})\right] < 0.3$, $\cos\left[\Delta\phi(E_{\text{T}}^{\text{miss}},\text{j2})\right] < 0.85$. Assuming $10\,\text{fb}^{-1}$ of collected data, this set of cuts would expect to select a total of 2.54 background events from the Standard Model and 311 signal events from the mSUGRA LM1 benchmark signal point.

13.6.2. Results for 10 fb^{-1} using full detector simulation and reconstruction

After all selection cuts have been applied, several effects contribute as systematic uncertainties, including: jet energy scale (10%), jet energy resolution (5%), luminosity measurement (5%), and full GEANT simulation versus fast simulation differences (5%), used to determine the analysis reach in mSUGRA parameters in Section 13.6.3). Since this analysis is performed consistently at leading order, the inclusion of higher order effects involving ISR/FSR is not taken into account. A generator-level comparison of the parton shower method for inclusive $t\bar{t}$ used by PYTHIA [69] with the matrix element calculation for $t\bar{t}+1$jet from COMPHEP [355] suggests a $\approx 10\%$ enhancement in the acceptance of $t\bar{t}+1$jet events (generated via the matrix element method) compared with inclusive $t\bar{t}$. When combined with other expected effects – such as underlying event (5%), pile-up (5%), and parton distribution functions (5%) – a total theoretical systematic uncertainty of $\sim 13\%$ is estimated. The dominant uncertainty (32%) arises from an inability to precisely predict the number of background events, due to finite Monte Carlo simulation statistics. We note that by the time $10\,\text{fb}^{-1}$ of data is collected, many of the contributing background processes will be measured from real data, thereby reducing this uncertainty. If one includes the uncertainty due to finite Monte Carlo simulation statistics, the total systematic uncertainty for this work is 37%. Neglecting Monte Carlo simulation statistics, as well as higher order QCD effects, the total systematic uncertainty for this work is 19%.

Table 13.8 shows the main results of this study. For the fully simulated low mass mSUGRA point LM1, and assuming $10\,\text{fb}^{-1}$ of data, this work selects an expected 311 signal events (with an efficiency of 0.074%) compared with 2.54 expected background events, comprised of $t\bar{t}$ (0.73 events), $W+$ jets (1.56 events), and $Z+$ jets (0.24 events). The separation of signal from background for the different low mass mSUGRA points range in values from 23 to 34 in significance, including systematic uncertainties (but excluding uncertainties related to the limited number of simulated events). Such large values of significance merely indicate that the low mass mSUGRA region will either have been discovered or excluded, long before $10\,\text{fb}^{-1}$ of data is collected. We note that shortly after the LHC start-up, the systematic understanding of the CMS detector is expected to be quite different than what is presented in this work, which assumes $\mathcal{L} = 10\,\text{fb}^{-1}$. Nevertheless, if one assumes a similar systematic understanding and extrapolates the results of this work to early running, the expected

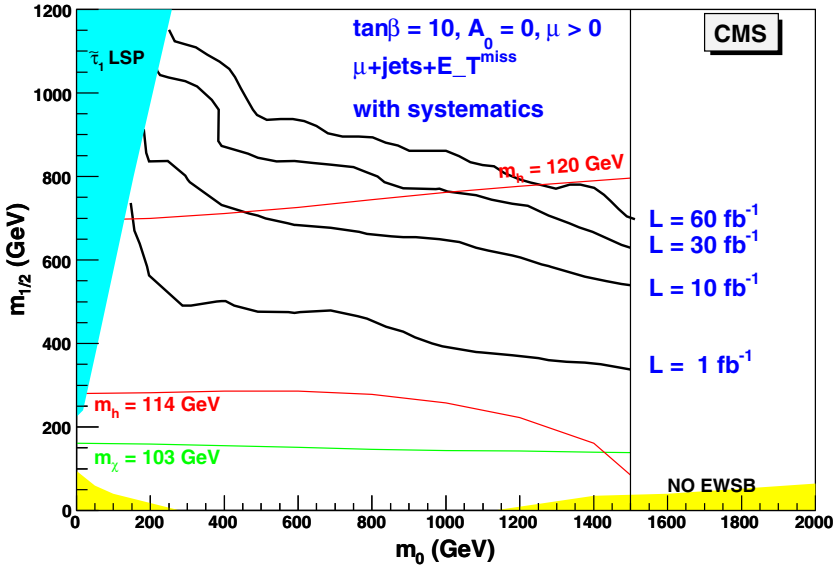

Figure 13.6. CMS discovery reach contours in the m_0–$m_{1/2}$ plane using inclusive muons with jets and missing energy for 10 fb^{-1} (lower contour), 30 fb^{-1} (middle contour), and 60 fb^{-1} (upper contour) including systematics.

luminosity required to discover the LM1 mSUGRA study point would be O(0.1) fb^{-1}. Hence, low mass SUSY is a prime candidate for possible discovery during the very early running of the LHC.

13.6.3. CMS Reach using inclusive muons with jets and missing energy

Since CMS will have either discovered or excluded the lower mass region well in advance of the time required to collect 10 fb^{-1} of data, the selection cuts for 30 fb^{-1} and 60 fb^{-1} are re-optimised using GARCON to select the HM1 mSUGRA point: $E_{\mathrm{T}}^{\mathrm{miss}} > 210\,\mathrm{GeV}$, $E_{\mathrm{T}}^{\mathrm{j1}} > 730\,\mathrm{GeV}$, $E_{\mathrm{T}}^{\mathrm{j2}} > 730\,\mathrm{GeV}$, $\cos\left[\Delta\phi(\mathrm{j1},\mathrm{j2})\right] < 0.95$, $\cos\left[\Delta\phi(\mathrm{E}_{\mathrm{T}}^{\mathrm{miss}},\mathrm{j1})\right] < -0.2$, $\cos\left[\Delta\phi(\mathrm{E}_{\mathrm{T}}^{\mathrm{miss}},\mathrm{j2})\right] < 0.95$. To estimate the reach for 30 fb^{-1} and 60 fb^{-1}, this same cut-set is applied in both cases and results in an estimated Standard Model background yield of $N_{\mathrm{B}} = 0.25$ for 30 fb^{-1}, and $N_{\mathrm{B}} = 0.49$ for 60 fb^{-1}. In both cases the uncertainty on the background levels is $\approx 71\%$, primarily due to a limited number of simulated events; if one neglects that uncertainty, the systematic uncertainty is $\approx 19\%$.

Fast simulation and reconstruction was also performed in order to scan the plane of universal scalar (m_0) and gaugino ($m_{1/2}$) masses for fixed mSUGRA parameters: $\tan\beta = 10$, $\mu > 0$ and $A_0 = 0$. Points were generated on a coarse grid with $\Delta m_0 = 100\,\mathrm{GeV/c^2}$ and $\Delta m_{1/2} = 100\,\mathrm{GeV/c^2}$, starting from the point $m_0 = 100\,\mathrm{GeV}$, $m_{1/2} = 100\,\mathrm{GeV}$. Figure 13.6 shows the discovery reach of this analysis (contours correspond to a significance value of 5), plotted in the mSUGRA m_0–$m_{1/2}$ plane. Assuming 10 fb^{-1} of data, CMS can observe SUSY mass scales of over $\approx 1.5\,\mathrm{TeV/c^2}$; assuming 30 fb^{-1} of integrated luminosity, several of the high mass CMS SUSY benchmark points become interesting for possible discovery; and, assuming 60 fb^{-1} of integrated luminosity, CMS is able to reach in this channel SUSY mass scales of up to $\approx 2\,\mathrm{TeV/c^2}$.

13.7. Inclusive analyses with same sign dimuons

The topology of two same sign isolated muons, high p_T jets, and large missing transverse energy is interesting as it allows for an efficient suppression of the Standard Model backgrounds, and at the same time allows much of the mSUGRA signal to be retained. Like-sign leptons can result from several signal processes because the gluino, being a Majorana particle, has equal probability of yielding either a positively or a negatively charged lepton in its decay chain. Squark production is another important source of like-sign dileptons, since the squark charge tends to be determined by the valence quarks in the proton-proton collision. The same-sign muon topology provides a clean experimental signature and has the extra advantage of an anticipated efficient and well-understood dimuon trigger soon after LHC start-up. Even though this study [676] is performed within the context of mSUGRA, this method is not specific to the mSUGRA framework.

The genetic algorithm GARCON [63] is used to determine the optimal set of cuts for each mSUGRA benchmark point. An interval for each physics cut-parameter is then defined corresponding to its minimal cut value and the maximum cut value, determined over all different optimal mSUGRA benchmark point cut-sets. The interval for each cut-parameter is then coarsely binned and the significance systematically calculated for each possible cut combination within this reduced sub-space.

13.7.1. Signal selection and backgrounds

Because this work is an inclusive study of mSUGRA signatures involving at least two like-sign muons accompanied by multiple jets and large missing transverse energy, several Standard Model processes contribute as sources of background and must be taken into account. Accordingly, the main backgrounds studied in this analysis correspond to QCD dijet (2.8 million fully simulated events with $0 < \hat{p}_T < 4\,\text{TeV/c}$), top ($t\bar{t}$) production (3.3 million fully simulated events), electro-weak single boson production (4.4 million fully simulated events with $0 < \hat{p}_T < 4.4\,\text{TeV/c}$) and electro-weak dibosons production (1.2 million fully simulated events). This work uses only leading order cross-sections, consistently for both signal and all backgrounds.

The dimuon HLT trigger (98% efficient) is required for this analysis. The following selection criteria are applied to muons and jets. The two leading muons are required to be of the same sign and to each have a transverse momentum above $10\,\text{GeV/c}$, ensuring that the muon candidate is reconstructed with good efficiency, above the symmetric thresholds of $7\,\text{GeV/c}$ in the dimuon trigger. Also this analysis requires at least three jets in the event, all of which are required to have $E_T > 50\,\text{GeV}$.

In order to select the particular SUSY diagrams responsible for prompt same-sign dimuons, we apply the following criteria. Each reconstructed muon is required to be separated by at least $\Delta R \geqslant 0.01$ from the other muons. The muon track fit is required to have $\chi^2_\mu \leqslant 3$ and the number of hits associated with the muon must be at least 13. Each muon is required to be isolated, both with respect to the tracker and calorimeter. A combined isolation parameter is used to account for correlations between the tracker (`IsoByTk`) and calorimeter (`IsoByCalo`) isolation variables, $\texttt{Iso} = \texttt{IsoByTk} + 0.75 \times \texttt{IsoByCalo}$, with $\texttt{Iso}_{\mu 1} \leqslant 10\,\text{GeV}$, $\texttt{Iso}_{\mu 2} \leqslant 6\,\text{GeV}$.

In addition to *a priori* requiring three jets in the event, the cut-set maximising the significance (with GARCON) to discover the lowest significant fully simulated mSUGRA test point is then chosen as the final optimal cut-set: $E_T^{j1} > 175\,\text{GeV}$, $E_T^{j2} > 130$ GeV, $E_T^{j3} > 55$ GeV, $E_T^{\text{miss}} > 200\,\text{GeV}$.

Table 13.9. Total number of selected events (for $\mathcal{L} = 10\,\text{fb}^{-1}$) and significance ("Signif.") with systematic uncertainties. "SM" represents the total of all Standard Model backgrounds considered.

Sample(s)	Events	Signif.	Sample	Events	Signif.	Sample	Events	Signif.
SM	1.5	–	LM5	61	14.0	LM10	4	2.2
LM1	341	>37.0	LM6	140	22.3	HM1	4	2.2
LM2	94	17.6	LM7	82	16.3	HM2	2	1.1
LM4	90	17.2	LM8	294	35.9			

13.7.2. Results for full detector simulated mSUGRA samples

After all selection cuts have been applied the main systematic uncertainty is due to the absolute jet energy scale, which is estimated to be 15% after $10\,\text{fb}^{-1}$. In addition, jet energy resolution (10%), muon identification efficiency and fake rate (negligible), luminosity (5%), theory (10%; cross sections, showering, ISR/FSR, etc.) and full simulation versus fast simulation (5%, used to determine the analysis reach in mSUGRA parameters in Section 13.7.3) have been evaluated. Since this analysis is performed consistently at leading order, the inclusion of higher order effects involving ISR/FSR is not taken into account. A generator-level comparison of the parton shower method for inclusive $t\bar{t}$ used by PYTHIA [69] with the matrix element calculation for $t\bar{t}$ + 1jet from COMPHEP [355] suggests a $\approx 10\%$ enhancement in the acceptance of $t\bar{t}$ + 1jet events (generated via the matrix element method) compared with inclusive $t\bar{t}$. The total systematic uncertainty on the number of background events is 24%.

Table 13.9 shows the main results of this study. For the fully simulated low mass mSUGRA point LM1, assuming $10\,\text{fb}^{-1}$ of data, this work selects an expected 341 signal events (with an efficiency of 0.081%) compared with 1.5 expected background events (comprised of $t\bar{t}$). For other fully simulated low mass mSUGRA points (excluding LM10) and an integrated luminosity $10\,\text{fb}^{-1}$ of data, the selection cuts (collectively optimised over all benchmark points) achieve a separation of signal from background with a statistical significance of between 16σ and greater than 37σ, including systematic uncertainties. Such a large significance merely indicates that the low mass mSUGRA region will either have been discovered or excluded, long before $10\,\text{fb}^{-1}$ of data is collected. Hence, low mass SUSY is a prime candidate for possible discovery during the very early running of the LHC. The discovery of high mass SUSY, represented by the fully simulated HM1 and HM2 points, is more difficult and requires more than $10\,\text{fb}^{-1}$ of data.

13.7.3. CMS inclusive reach

Fast simulation and reconstruction was also performed in order to scan the plane of universal scalar (m_0) and gaugino ($m_{1/2}$) masses for fixed mSUGRA parameters: $\tan\beta = 10$, $\mu > 0$ and $A_0 = 0$. Points were generated on a coarse grid with $\Delta m_0 = 100\,\text{GeV/c}^2$ and $\Delta m_{1/2} = 100\,\text{GeV/c}^2$, starting from the point $m_0 = 100\,\text{GeV/c}^2$, $m_{1/2} = 100\,\text{GeV/c}^2$.

The 5σ reach of this analysis, including systematic uncertainties, for different integrated luminosities and assuming no re-optimisation of the selection cuts is shown on Fig. 13.7. By the time CMS collects integrated luminosity $30\,\text{fb}^{-1}$, the high mass point HM1 becomes interesting for possible discovery. For comparison, $\mathcal{L} = 1\,\text{fb}^{-1}$ and $\mathcal{L} = 100\,\text{fb}^{-1}$ are also shown in the figure. Clearly, the systematics for $\mathcal{L} = 1\,\text{fb}^{-1}$ will be higher than that assumed in this work, nevertheless these results strongly suggest (provided systematics can be brought

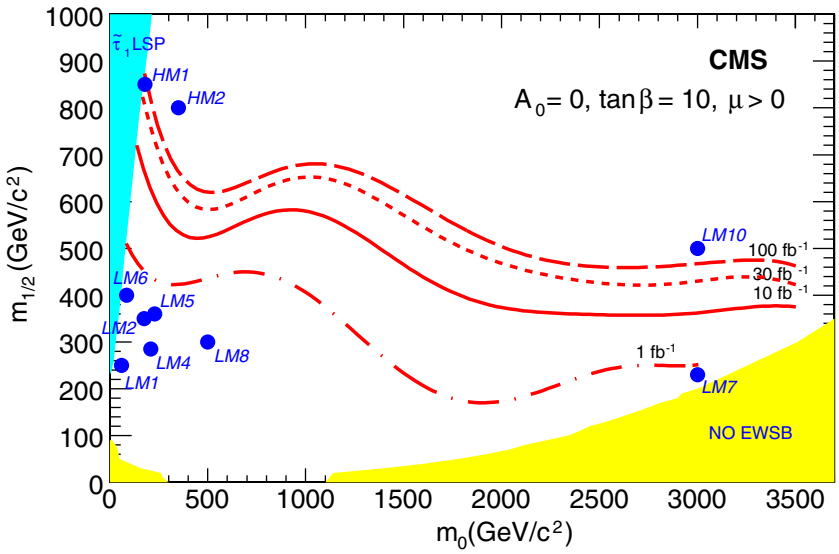

Figure 13.7. CMS reach contours (systematic uncertainties included) in the $(m_0, m_{1/2})$ plane for SUSY processes involving two prompt same-sign muons for $\mathcal{L} = 1\,\text{fb}^{-1}$ (dot-dashed line), $\mathcal{L} = 10\,\text{fb}^{-1}$ (solid line), $\mathcal{L} = 30\,\text{fb}^{-1}$ (short dashed line) $\mathcal{L} = 100\,\text{fb}^{-1}$ (dashed line). The other mSUGRA parameters are fixed to $\tan\beta = 10$, $\mu > 0$ and $A_0 = 0$. Points corresponding to the full detector simulation and reconstruction are also shown (solid circles).

under control) that most of the low mass mSUGRA points are well within reach of CMS during the early running of the LHC.

13.8. Inclusive analyses with opposite sign dileptons

Final states with opposite sign dileptons, originating from the decay $\tilde{\chi}_2^0 \to \tilde{l}_R l \to l^+ l^- \tilde{\chi}_1^0$ in the cascade decays of squarks and gluinos provide a clean signature of SUSY with isolated leptons, high p_T jets and missing transverse energy [677]. In addition, the dilepton invariant mass distribution for this decay is expected to have a triangular shape with a sharp upper edge, which renders this signature striking and useful for further characterisation of SUSY.

13.8.1. Signal selection and backgrounds

The analysis is performed at the LM1 mSUGRA test-point using GEANT-based detailed simulation of the CMS detector [8] and reconstruction [10]. The fast CMS simulation and reconstruction [11] is used to evaluate the discovery reach in the mSUGRA parameter space.

Signal events were generated by ISAJET 7.69 interfaced to PYTHIA 6.225 at the test point LM1, where the NLO cross section at NLO is about 52 pb, dominated by the production of $\tilde{q}\tilde{g}$, $\tilde{g}\tilde{g}$ and $\tilde{q}\bar{\tilde{q}}$. The gluino is the heaviest particle and decays to $\tilde{q}q$. While right squarks decay almost directly to the LSP, due to the bino-like nature of the $\tilde{\chi}_1^0$ at Point LM1, left-handed squarks decay to $\tilde{\chi}_2^0$ with a branching ratio $\sim 30\%$.

The SM backgrounds studied consist of $t\bar{t}$, $W+$ jets, $Z+$ jets, $WW+$ jets, $ZZ+$ jets, Zbb (with leptonic decays of the Z boson), Drell–Yan leptonic events and QCD dijet production processes.

Table 13.10. Cross section at NLO, selection efficiencies and number of events surviving cuts for signal and background processes.

Process	σ (pb)	Ev. analysed	ε	N_{ev} in 1 fb $^{-1}$
SUSY (LM1)	52	478 k	0.016	853
$t\bar{t}$	830	913 k	$1.9 \cdot 10^{-4}$	155
WW+ jets	188	197 k	$1.4 \cdot 10^{-4}$	26
Z+ jets	$5 \cdot 10^3$	606 k	$4.8 \cdot 10^{-6}$	24
DY $\rightarrow 2\mu$	$3.97 \cdot 10^3$	916 k	$< 1.1 \cdot 10^{-6}$	< 4
DY $\rightarrow 2\tau$	$3.97 \cdot 10^3$	514 k	$1.1 \cdot 10^{-6}$	4.5
$Zbb \rightarrow llbb(l = e, \mu, \tau)$ $P^T_{hat} > 60$ GeV/c	57.4	621 k	$8.4 \cdot 10^{-5}$	4.83
$t\bar{t}b\bar{b}$	3.3	50 k	$9.8 \cdot 10^{-4}$	3.2
ZZ+ jets	11	37k	$2.4 \cdot 10^{-4}$	2.7
W+ jets	$1.5 \cdot 10^5$	1765k	$6.7 \cdot 10^{-9}$	1

The SUSY final state studied contains at least two high-p_T isolated leptons, at least two high-p_T jets and large missing transverse energy. The event selection path includes the following requirements:

- the Level-1 and HLT path that requires a single isolated lepton (muon or electron);
- at least two same-flavour opposite-sign (SFOS) isolated leptons (e or μ) with $p_T \geqslant 10$ GeV/c and $\Delta R_{ll} \geqslant 0.2$ and 0.15 for ee and $\mu\mu$, respectively where ΔR_{ll} is the distance of the two leptons in the $\eta - \phi$ space;
- $E_T^{miss} > 200$ GeV;
- at least two jets with $p_T \geqslant 100$ and $\geqslant 60$ GeV/c within $|\eta| < 3$.

The isolation of the leptons is obtained requiring the sum of p_T of the tracks in a cone of $\Delta R = 0.25$ around the lepton track to be less than 5 GeV/c. The E_T^{miss} is computed from the vectorial sum of the jets and leptons.

These selection criteria result in 853 signal events (which correspond to 913 dilepton pairs) for a luminosity of 1 fb^{-1}. The Standard Model background consists of 155 $t\bar{t}$ events, 26 events from WW + jets and 24 events from Z + jets (Table 13.10). All other backgrounds have been found to be negligible and amount in total to at most 20 events.

13.8.2. Results for point LM1

The dilepton invariant mass distribution for 1 fb^{-1} is displayed in Fig. 13.8 showing a clear dilepton edge structure.

The presence of two SFOS leptons can also be due to other processes. Two leptons can result from independent leptonic decays, for example from two charginos or two W's. In that case the final state contains as many SFOS leptons as different-flavour opposite-sign (DFOS) ones and with identical distributions. The background to the SFOS contribution is removed by subtracting the DFOS events, which leads to the dilepton mass distribution of Figure 13.9. The $t\bar{t}$ and WW + jets backgrounds are also strongly reduced by the flavour subtraction. The resulting dilepton invariant mass distribution is fitted using a triangular function smeared (for resolution effects) with a Gaussian to extract the end-point related to the kinematics of the decay $\tilde{\chi}_2^0 \rightarrow \tilde{l}_R l \rightarrow l^+ l^- \tilde{\chi}_1^0$. The value obtained from 1 fb^{-1} of integrated luminosity is:

$$M_{ll}^{max} = 80.42 \pm 0.48 \text{ GeV/c}^2 \tag{13.19}$$

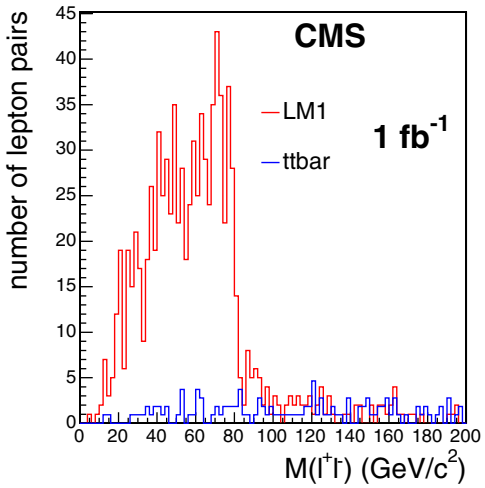

Figure 13.8. Invariant mass distribution of $\mu^+\mu^-$ + e^+e^- and $\mu^\pm e^\mp$ pairs at LM1 for 1 fb^{-1} luminosity. The contribution from the $t\bar{t}$ background is also shown.

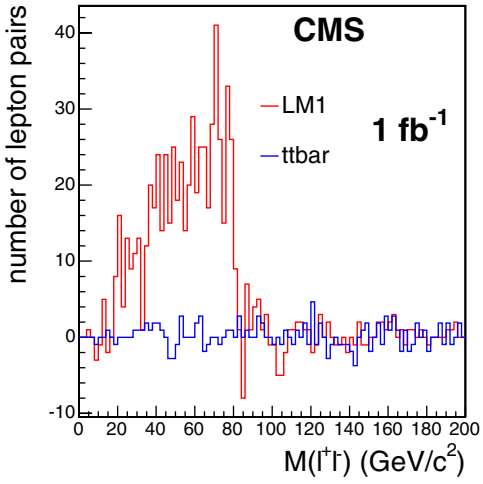

Figure 13.9. Invariant mass distribution of $\mu^+\mu^-$ + e^+e^- and $\mu^\pm e^\mp$ pairs at point LM1 for 1 fb^{-1} luminosity after subtracting $e^+\mu^-$ and μ^+e^- pairs. The contribution from the $t\bar{t}$ background is also shown.

to be compared to the expected value of 81.04 GeV/c^2 for the masses $m(\tilde{\chi}_1^0) = 95$, $m(\tilde{\chi}_2^0) = 180$ and $m(\tilde{l}_R) = 119$ GeV/c^2. The signal-to-background ratio at point LM1 is 4.1, the total signal efficiency is 1.6% and the background composition is 69% of total ttbar, 11.6% of total WW + jets, 10% Z + jets, 3% DY, 2% Zbb, 1% ttbb, 1% ZZ + jets, fractions the others. The total efficiency for the QCD background is too low to be directly calculated, and is then estimated through a factorisation, considering separately the effects due to the single selection cuts. Although the number of surviving QCD events is expected to be negligible, a residual QCD background is still possible, which will be measured using the real data. A statistical significance of 5 sigma, calculated using S_{cP} defined in Appendix A.1, is achieved with 14 pb^{-1} of integrated luminosity. At this luminosity 12.8 signal events are expected with 3.1 Standard Model background events. Therefore this signature is a strong probe for early discovery of low mass supersymmetry.

Systematic uncertainties have been evaluated under the assumption that control data are used for the Standard Model processes. Hence no uncertainties on the theory cross sections, showering, ISR/FSR, are taken into account. The main systematic uncertainty considered is due to the absolute jet energy scale. A $\simeq$ 7% uncertainty on the jet energy scale for 1 fb^{-1} of data is used while this is expected to be $\simeq$ 2% after 10 fb^{-1}. After applying the selection cuts this leads to a $\simeq$ 20% systematic uncertainty on the $t\bar{t}$ background and to a $\simeq$8% systematic uncertainty on the SUSY signal. The electron energy scale uncertainty, expected to be 0.25%, leads to a systematic uncertainty of less than 1% on the background, and less than 0.1% on the signal. The total considered systematic uncertainty on the Standard Model background is 20% at low luminosity, 5% at high luminosity. The effect on the signal of the Tracker and Muon System misalignment in the first months of LHC run has also been evaluated. The number of selected dimuon (dielectron) pairs is lowered by about 30% (10%) while the total signal selection efficiency is decreased by about 20%. The measurement of the distribution end-point is affected by about 1 GeV/c^2. The effect of the electron energy scale uncertainty on the dilepton measurement gives a systematic uncertainty of about 0.15 GeV/c^2.

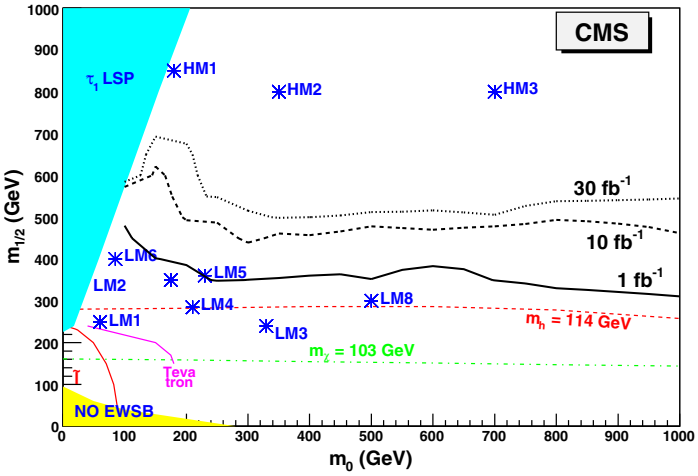

Figure 13.10. 5σ discovery reach for the dilepton final state, assuming $\tan\beta = 10$, $A = 0$, $\mu > 0$ and 1, 10, 30 fb^{-1} integrated luminosity (statistical uncertainties only).

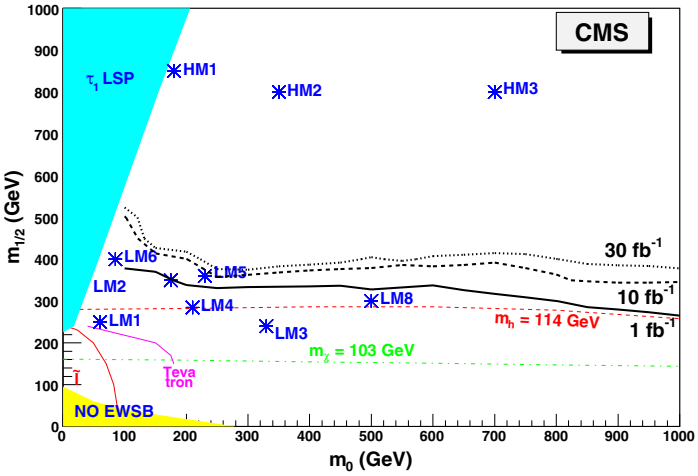

Figure 13.11. 5σ discovery reach for $\tan\beta = 10$ taking into account background systematic uncertainties.

Taking into account the systematic uncertainties on the Standard Model backgrounds expected after the first 1 fb^{-1} of data, the 5 sigma discovery can be achieved with 17 pb^{-1} of integrated luminosity.

13.8.3. CMS inclusive reach

Using the discussed selection path a scan was performed over the mSUGRA parameters in the $(m_0, m_{1/2})$ plane for $\tan\beta = 10$, $A = 0$, $\mu > 0$ to determine the $5\,\sigma$ discovery reach. The observability of the signal over the Standard Model background uses the dilepton estimates before flavour subtraction. The results of the survey are shown for integrated luminosities of 1, 10 and 30 fb^{-1} in Figs. 13.10 and 13.11. It is notable that most of the low mass test-points can be discovered with about 1 fb^{-1}.

13.9. Inclusive analyses with ditaus

In this section, $\tilde{\tau}$ production through the $\tilde{\chi}_2^0$ decays in $\tilde{q}$ or $\tilde{g}$ cascades is investigated. The $\tilde{\tau}$ is produced through $\tilde{\chi}_2^0 \to \tau^{\pm}\tilde{\tau}^{\mp}$, which further decays to $\tau\tilde{\chi}_1^0$ leaving a final state with two taus of opposite sign. The branching fraction of $\tilde{\tau}$ production through $\tilde{\chi}_2^0$ varying with mSUGRA parameters, the analysis is first carried out at large $\tan\beta$, at the LM2 test point, which parameters are given in Section 13.3.2, where the $\tilde{\chi}_2^0$ is predicted to decay 95% of the time into $\tau^{\pm}\tilde{\tau}^{\mp}$. Results are then generalised to any choice of mSUGRA parameters.

This section studies the opportunity of discovering such a model in the first years of data taking of LHC, with integrated luminosities as low as $0.1\,\text{fb}^{-1}$ and up to $10\,\text{fb}^{-1}$. The possibility of measuring the SUSY mass spectra associated to this cascade decay (in particular $\tilde{\chi}_2^0$, $\tilde{\chi}_1^0$ and $\tilde{\tau}$ masses) is investigated in Section 13.13.

13.9.1. Event selection and background studies

For this analysis, 93.5k events (corresponding to an integrated luminosity of $12.6\,\text{fb}^{-1}$) were generated at the LM2 test point using ISASUGRA. Those events were further passed through the full simulation of the CMS detector [8] then digitised and reconstructed [10]. The same procedure was applied to the Monte Carlo samples used as SM background in this analysis. However, in some cases, where large statistics were required, the fast simulation program [11] was used. All Monte Carlo samples used in this analysis are produced with leading order Parton Distribution Functions.

Physics processes responsible for W and Z production and $t\bar{t}$ which final states may contain several taus and jets are considered as potential background sources. In addition, because of its huge cross section ($1.3 \cdot 10^{-4}$ mb) QCD jet production is also considered. The latter can also represent an important source of fake taus as well as fake missing transverse energy ($E_{\text{T}}^{\text{miss}}$) due to imprecision in jet energy measurement.

13.9.1.1. Event selection using all reconstructed taus. In this analysis [678], only events passing the JETMET level1 and HLT triggers are accepted. The event selection is then carried out using only the $E_{\text{T}}^{\text{miss}}$, the reconstructed taus and jets. In order to increase the sensitivity of the selection both tau's decaying hadronically and leptonically are considered in this section.

The mSUGRA events are selected with the following requirement:

- $E_{\text{T}}^{\text{miss}}$ larger than 150 GeV.
  This cut removes a large fraction of Standard Model physics background.
- At least two tau candidates are required.
- At least two jets with $E_{\text{T}} > 150\,\text{GeV}$.
  This requirement is very aggressive on the LM2 events, however it allows to remove most of the Standard Model background.
- ΔR between any pair of tau's should be smaller than two.

This cut makes use of the fact that in $\tilde{\chi}_2^0$ decays, taus belonging to a same cascade decay will be produced relatively close to each other while in Standard Model physics processes taus as well as Supersymmetric physics processes such as chargino production (producing one tau in each cascade) tend to be produced in opposite direction. This cut also reduces the amount of wrong pairing.

Both theoretical and experimental systematic uncertainties are considered in this analysis. The theoretical systematic uncertainty is estimated for the signal according to standard CMS guidelines and involves changing the PDF [351] and varying generator parameters governing

both hard process and fragmentation. Each variation leads to the generation of a new LM2 sample which is then simulated and reconstructed using FAMOS and analysed in the same way as the main signal samples. Variations in the number of selected events are then taken as systematic uncertainty. The relative theoretical systematic uncertainty on the signal was found to be 12%. The experimental systematic uncertainties are coming from the Jet energy scale, the $E_{\mathrm{T}}^{\mathrm{miss}}$ and the tau-jet energy scale. These uncertainties are estimated following standard CMS procedure, see appendix B, by varying the jet and tau energies by an amount corresponding to their respective energy scales and redoing the analysis. The uncertainty on $E_{\mathrm{T}}^{\mathrm{miss}}$ is estimated in a similar way by varying the energy of the jets used to estimate $E_{\mathrm{T}}^{\mathrm{miss}}$ within their energy scale. The experimental systematic uncertainty affect the selection of signal events by 11% for low integrated luminosities (smaller than $1\,\mathrm{fb}^{-1}$) but for large integrated luminosities the systematic effect is less than 3.2%. The experimental systematic uncertainty on the background is 30% for integrated luminosities smaller than $1\,\mathrm{fb}^{-1}$ and 11% for larger integrated luminosities.

At $12.67\,\mathrm{fb}^{-1}$, $N_s = 2735 \pm 273(\mathrm{sys}) \pm 52(\mathrm{stat})$ events from the signal and $N_{bkg} = 938 \pm 103(\mathrm{sys}) \pm 114(\mathrm{stat})$ events from the background survive the selection. 50% of the remaining background is coming from QCD, 39% from $t\bar{t}$ and 11% from W+jets.

To this selection corresponds a ratio signal over background $S/B = 2.9$. The global efficiency of the selection of the signal is around 3% (of which 88% are SUSY events with at least two taus), while only 0.001% of the background remains after selection. Using S_{cL} significance, defined in Appendix A.1, it is possible to estimate that a 5σ discovery can be achieved with only $0.07\,\mathrm{fb}^{-1}$. Using S_{cP} significance [679], which takes into account systematic uncertainties on the background, a 5σ discovery can be expected with a luminosity of $0.125\,\mathrm{fb}^{-1}$.

13.9.1.2. Event selection using only reconstructed taus decaying hadronically. If only taus decaying hadronically are used in the selection described in 13.9.1.1, both signal and backgrounds are affected differently.

At $12.67\,\mathrm{fb}^{-1}$, $N_s = 1447 \pm 144(\mathrm{sys}) \pm 38(\mathrm{stat})$ events from the signal and $N_{bkg} = 543 \pm 60(\mathrm{sys}) \pm 112(\mathrm{stat})$ events from the background survive the selection. 70% of the remaining background is coming from QCD, 20% from $t\bar{t}$ and 10% from W + jets. To this selection corresponds a ratio signal over background $S/B = 2.6$. The global efficiency of the selection of the signal is around 1.5% (of which 88% are SUSY events with at least two taus), while only 0.0006% of the background remains after selection. This time, using S_{cL} a 5σ discovery is achieved with only $0.14\,\mathrm{fb}^{-1}$. Using S_{cP} significance [679], which takes into account systematic uncertainties on the background, a 5σ discovery can be expected with a luminosity of $0.26\,\mathrm{fb}^{-1}$.

13.9.2. Discovery potential of mSUGRA with ditaus final states

A scan of the mSUGRA $(m_0, m_{1/2})$ parameters plane is performed in order to delimit the mSUGRA parameter region where SUSY could be discovered with this analysis. Because the analysis focuses on ditau final states and since the respective branching ratio to ditaus and to other leptons from SUSY may vary by large amounts in the mSUGRA parameter space, allowing large contamination from leptons into ditaus final states the scan is performed using only hadronic tau decays as described in section 13.9.1.2.

This scan is achieved by generating many mSUGRA samples varying m_0 and $m_{1/2}$ values so that the entire region of the plane $(m_0, m_{1/2})$ below $m_0 < 1500\,\mathrm{GeV}$ and $m_{1/2} < 800\,\mathrm{GeV}$ is covered. The samples were generated with ISASUGRA 7.69 then simulated and reconstructed

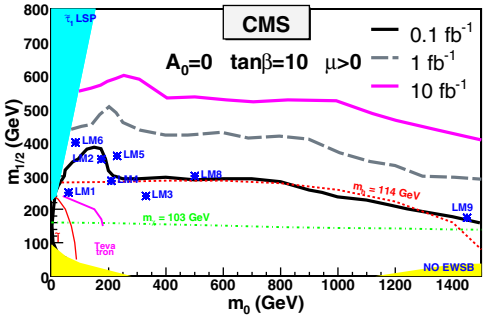

Figure 13.12. Inclusive ditau analysis discovery potential for mSUGRA between 0.1 and 30 fb^{-1} for $\tan\beta = 10$ including only statistical uncertainties.

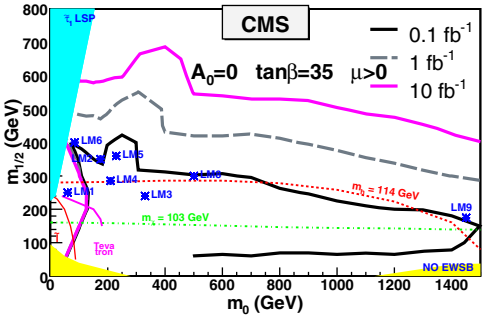

Figure 13.13. Inclusive ditau analysis discovery potential for mSUGRA between 0.1 and 30 fb^{-1} for $\tan\beta = 35$ including only statistical uncertainties.

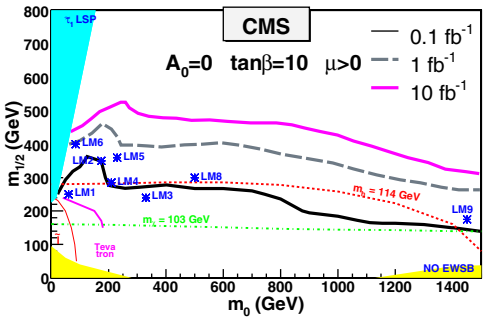

Figure 13.14. Inclusive ditau analysis discovery potential for mSUGRA between 0.1 and 30 fb^{-1} for $\tan\beta = 10$ where both statistical and systematic uncertainties are taken into account.

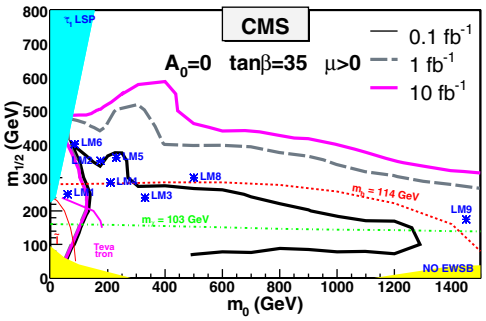

Figure 13.15. Inclusive ditau analysis discovery potential for mSUGRA between 0.1 and 30 fb^{-1} for $\tan\beta = 35$ where both statistical and systematic uncertainties are taken into account.

with FAMOS and analysed in the same way as the LM2 sample. The resulting number of events surviving the selection were used to estimate the significance at each point of the mSUGRA parameter plane. Two types of significance are estimated here, S_{cL} which accounts only for statistical uncertainties and S_{cp} which accounts for both statistical and systematics effects on the background. The resulting 5σ contours over the mSUGRA $(m_0, m_{1/2})$ parameter plane obtained with S_{cl} for several integrated luminosities between 0.1 and 30 fb^{-1} are shown in Figs. 13.12 and 13.13 for $\tan\beta = 10$ and $\tan\beta = 35$, respectively. Results obtained with S_{cp} are shown in Figs. 13.14 and 13.15. The region where a 5σ discovery is possible is somewhat shrunk, especially for the very early measurement at 0.1 fb^{-1} as a precise knowledge of the jet energy scale and of the measurement of the $E_{\mathrm{T}}^{\mathrm{miss}}$ will still be limited. However, a large region is accessible with larger integrated luminosities.

13.10. Inclusive analyses with Higgs

This section describes the potential of the CMS experiment to discover a light supersymmetric Higgs boson (h^0) produced at the end of a cascade of supersymmetric particles starting with the strong production of squarks ($\tilde{q}$) and gluinos ($\tilde{g}$). Because of the cascade production mechanism, the events can be efficiently triggered using inclusive SUSY triggers such as jet $+E_{\mathrm{T}}^{\mathrm{miss}}$, and the dominant $h^0 \to b\bar{b}$ decay mode of the Higgs boson can be exploited.

This analysis focuses on a full CMS detector simulation [8] and event reconstruction [10] at the mSUGRA point LM5, defined in Section 13.3.2. The total SUSY cross section at this parameter point is about 7.75 pb at NLO.

All SUSY channels leading to a light Higgs boson in the final state have been taken into account. The signal events are characterised by at least two b-tagged jets, an important missing transverse energy ($E_{\mathrm{T}}^{\mathrm{miss}}$) and multiple hard jets. This signature allows to suppress the majority of the $b\bar{b}$ background due to SM processes (mainly top pair production $t\bar{t}$, $W^{\pm}$+jets, Z^{0}+jets).

13.10.1. Signal selection and backgrounds

This analysis has been developed based on the CMS reconstruction. The two main algorithms used for the signal reconstruction are the jet reconstruction algorithm (the Iterative cone algorithm with a cone size of 0.5 radians and the GammaJet calibration) and the b-tagging algorithm (Combined b-tagging algorithm, see the PTDR Volume 1, Section 12.2).

A first rejection of the Standard Model backgrounds happens at the online trigger stage. The Level-1 and the High Level Trigger (HLT) efficiencies for the signal and background have been evaluated. The trigger path used for this analysis consists of the Level-1 and HLT Jet + $E_{\mathrm{T}}^{\mathrm{miss}}$ stream. This particular trigger is already an important tool in rejecting Standard Model backgrounds, for example it rejects 96% of the $t\bar{t}$ background while keeping 79% of the signal events.

In order to further remove the SM background events and reduce the SUSY background, a number of offline selection cuts are applied: a minimal number of four jets with a transverse energy above 30 GeV is required, of which at least two are b-tagged with high quality (i.e. a b-tag discriminator greater than 1.5).

The mean b-tagging efficiency is found to be 50% with a mistagging rate of about 1.6%, for u, d, s quarks and gluons, and 12% for c quarks. The mean b jet energy originating from the Higgs decay is approximately 70 GeV, corresponding to a b-tagging efficiency of about 50% at this energy. This means that approximately 25% of the signal events will pass the double b-tag criterion.

Other variables have been identified in order to improve the signal over background ratio, in particular for the most problematic $t\bar{t}$ background: the $E_{\mathrm{T}}^{\mathrm{miss}}$, the first, second and third highest jet P_t. The selection requires a $E_{\mathrm{T}}^{\mathrm{miss}} > 200$ GeV, the highest jet p_t in the event > 200 GeV/c, the second highest jet p_t in event > 150 GeV/c, the third highest jet p_t in event > 50 GeV/c.

Next, in order to select the b-jet pair coming from the Higgs decay, two methods are used. First, the Hemisphere separation technique (see section 13.4) is applied to identify two groups of jets in the detector, each group associated with an initial squark and/or gluino cascade. After that, the b-jet pairing is done only in each of these groups separately, reducing the number of possible combinations by a large factor. In addition, as the Higgs is relatively heavy, its decay products have an important boost leading to a small angle $\Delta R = \sqrt{\Delta\eta^2 + \Delta\phi^2}$ between the two b jets. Therefore, in case of multiple possible combinations inside one hemisphere, the pair with the smallest ΔR value within $\Delta R < 1.5$ is chosen. This procedure gives an efficiency of around 40% and strongly suppresses the combinatorial background.

The full selection chain leads to a signal efficiency of about 8% for all SUSY channels yielding a Higgs. The global rejection factor for $t\bar{t}$ events, including the rejection made by the Jet + $E_{\mathrm{T}}^{\mathrm{miss}}$ trigger, is close to $4.6 \cdot 10^4$. No Z + jets, W + jets nor QCD events from the full simulation samples pass the previously described series of cuts, hence the only remaining background is from $t\bar{t}$. The resulting SUSY signal over SM background ratio is >70. 61%

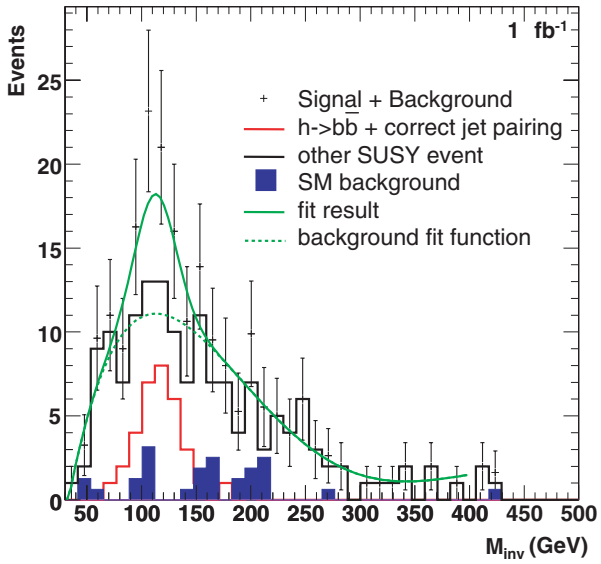

Figure 13.16. Invariant mass distribution of $b\bar{b}$ jets for the search of Higgs final states with 1 fb^{-1}.

of the SUSY signal comes from events with a true h^0, but only part of those have the correct b-jet pairing with both jets from the h^0.

13.10.2. Results at LM5 and systematics

The resulting invariant mass distribution, after the selection cuts described above, is shown in Fig. 13.16. The plot corresponds to the expected statistics equivalent to 1 fb^{-1} of integrated luminosity. A peak around 116 GeV/c^2 is visible. The main background is due to the remaining SUSY background events and some $t\bar{t}$ events.

A fit was performed representing the background by a fifth order polynomial and approximating the Higgs signal by a Gaussian. The r.m.s of the Gaussian has been fixed to 18 GeV, which is the Higgs mass resolution estimated using the Monte Carlo truth. In real data, this number will be determined from studying b-rich samples such as $t\bar{t}$. The results of the fit for the equivalent of 1 fb^{-1} of data are the following: the Higgs mass is found to be (112.9 ± 6.6) GeV/c^2 (for a generated mass of 116 GeV/c^2) and the fraction of signal in the distribution is evaluated to be 0.28 ± 0.08. The significance S_{CL}, directly extracted from the fraction of signal in the histogram, is found to be 4.5. A significance of 5 should be achieved with approximately 1.5 fb^{-1} luminosity.

For 1 fb^{-1}, the jet energy scale and $E_{\mathrm{T}}^{\mathrm{miss}}$ uncertainties have been estimated assuming a linear evolution from $\pm 15\%$ to $\pm 5\%$ for low energy jets (below 50 GeV) and then fixed at $\pm 5\%$ for higher energy jets. As the $E_{\mathrm{T}}^{\mathrm{miss}}$ is computed from the jets, a correction on the jet energy is automatically propagated to its estimation. The effects are about 15% on the SUSY event selection and 17% on the $t\bar{t}$ event rejection respectively. The impact on the Higgs mass measurement have been estimated to be ± 7.5 GeV/c^2; on the signal fraction, the effect is ± 0.04.

Another systematic uncertainty is introduced by the misalignment of the tracker. Both the short and long term misalignment scenarios have been investigated. The short term misalignment corresponds to a displacement of the tracker (strips/pixels) = (100 μm/10 μm), while the long term misalignment takes the following shift of the tracker (strips/pixels) = (20μ m/10 μm) into account. The misalignment of the tracker reduces the

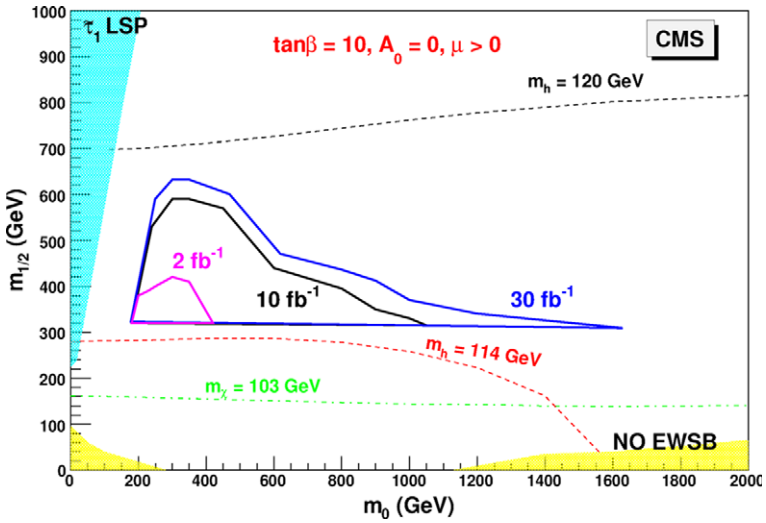

Figure 13.17. Higgs discovery reach in SUSY cascades for 2, 10 and 30 fb^{-1}.

track reconstruction resolution, which results in a reduced b-tagging efficiency and which in its turn causes a reduced signal event selection efficiency. The long term misalignment scenario results in a drop of the signal selection efficiency of (∼10%) compared to the case of an aligned detector; for the short term misalignment case, the reduction is (∼17%). No effect on the position/width of the Higgs mass peak was observed.

Finally, the systematics due to the choice of the background fit function has been estimated to be small (by changing the background function to a third, fourth, sixth or a seventh order polynomial): $\pm 0.3\,\mathrm{GeV/c^2}$ on the Higgs mass and ± 0.01 on the signal fraction.

The final result including all the previously discussed systematics for $1\,\mathrm{fb}^{-1}$ of integrated luminosity is then 112.9 ± 6.6 (stat) ± 7.5 (syst) $\mathrm{GeV/c^2}$ for the Higgs mass and 0.28 ± 0.08 (stat) $\pm$ 0.04 (syst) for the signal fraction.

13.10.3. CMS reach for inclusive Higgs production

After establishing the visibility of the signal for the LM5 point, a scan was performed in the (m_0, $m_{1/2}$) plane in order to determine the region where a 5σ discovery could be made with 2, 10 and 30 fb^{-1}.

First, an effective cross section ($\sigma \times BR(h0)$) was used (calculated with PROSPINO and ISASUGRA) to obtain an estimate of the reach. Using this first estimate, 40 points were chosen for which the full spectrum was calculated and a fast simulation was performed with FAMOS [11]. The same selection criteria as for LM5 point were applied, and the number of Higgs signal and background events was determined. Given that the background is dominated by SUSY events, the signal and background are similarly affected by the systematic uncertainties and the effect on the significance is small. The same significance definition (S_{CL}) was used in order to determine the 5-sigma contours. Comparing the ORCA/FAMOS results at LM5, the significances obtained with both programs were found to agree well.

The result of the scan is displayed in the reach plot in Fig. 13.17. Although for $1\,\mathrm{fb}^{-1}$ the sensitivity remains below 5σ, everywhere a sizeable region of the (m_0, $m_{1/2}$) plane, up to 1100 (1600) GeV in m_0 and 600 (650) GeV in $m_{1/2}$, can be covered with 10 (30) fb^{-1}. With $2\,\mathrm{fb}^{-1}$ of integrated luminosity, a small region of the plane can already be probed. The plot assumes $\tan\beta = 10$, $A_0 = 0$, and a positive sign of μ.

Table 13.11. Number of events for signal ($\tilde{\chi}_2^0 \to Z^0 + \tilde{\chi}_1^0,\ Z^0 \to e^+e^-, \mu^+\mu^-$) and background before and after selection criteria for 10 fb^{-1}. The numbers below Zj specify the range of partonic p_T in GeV/c.

	LM4 with $\tilde{\chi}_2^0$	LM4 no $\tilde{\chi}_2^0$	ZZj	ZWj	WWj	$t\bar{t}$	Zj 85–250
σ NLO (pb)	0.664	17.4	15.5	51.5	270	830	116.7
10 fb^{-1}							
total events	6640	173.8 K	155 K	515 K	2.7 M	8.3 M	1.17 M
L1+HLT	6032	81.7 K	12.6 K	24.4 K	174 K	973 K	462 K
OS leptons	4489	7147	9124	14.7 K	26.3 K	268 K	331 K
M_{ll}	3773	804	6999	11.5 K	2406	23.1 K	249 K
E_T^{miss}	1420	306	32	24	70	149	44
$\Delta\phi_{ll}$	1289	264	31	22	47	61	35

13.11. Inclusive SUSY search with Z^0

13.11.1. Topology of the signal

SUSY processes leading to final states with Z^0 can be detected in CMS using the Z^0 decays into same flavour opposite sign (SFOS) lepton pairs. The detection of SUSY in the mSUGRA framework through the decay $\tilde{\chi}_2^0 \to Z^0 + \tilde{\chi}_1^0$ is the scope of this study. The mSUGRA test-point LM4 with the parameters described in Section 13.3 is chosen. The $\tilde{\chi}_2^0$ is produced mainly through the cascade decays of gluinos ($M_{\tilde{g}} = 695$ GeV) and squarks (mainly the $\tilde{b}_1$ with $M_{\tilde{b}_1} = 601$ GeV). The decays of the second neutralino to Z^0 have a large branching ratio ($\sim$100%). The signal events are characterised by large missing E_T (due to the undetectable LSP) and the SFOS lepton pair from Z^0. The analysis details can be found in [680].

The main Standard Model backgrounds originate from the production of one or more Z^0 bosons in association with jets as well as $t\bar{t}$. In addition SUSY events contain dileptons that do not originate from the above neutralino decay chain and large missing transverse energy. These events are considered as signal for SUSY detection but as background for the $\tilde{\chi}_2^0$ detection. The following backgrounds were considered in this study: dibosons ($ZZ + j$, $ZW + j$, $WW + j$), inclusive top ($t\bar{t}$) and Z+ jets. The signal events were generated interfacing ISAJET 7.69 with PYTHIA. Unless otherwise stated all events are fully simulated and analysed using the CMS full detector simulation [8] and reconstruction [10] packages. The next to leading order (NLO) cross sections of the relevant processes are shown in Table 13.11.

13.11.2. Event selection

The following requirements are imposed in order to efficiently select the signal and reject the background events. All criteria were chosen so that the final SUSY search significance estimator S_{c1} [102, 681] for 10 fb^{-1} integrated luminosity is maximised. Very similar requirements maximise also significance estimator S_{L2} [102] used in the case of 1 fb^{-1} integrated luminosity. The effect of the selection requirements on the signal and on each background sample separately can be seen in Table 13.11 for 10 fb^{-1} integrated luminosity.

- Events are required to pass the HLT dielectron or dimuon triggers.
- An e^+e^- or $\mu^+\mu^-$ pair with lepton $p_T > 17$ GeV for electrons and $p_T > 7$ GeV for muons (as per L1 trigger requirements). Each lepton is required to be within $|\eta| < 2.4$.
- The SFOS lepton pair invariant mass is required to be consistent with the Z^0 mass, i.e. 81 GeV $< M_{ll} <$ 96.5 GeV. The reconstructed masses for the e^+e^- and the $\mu^+\mu^-$ pairs and

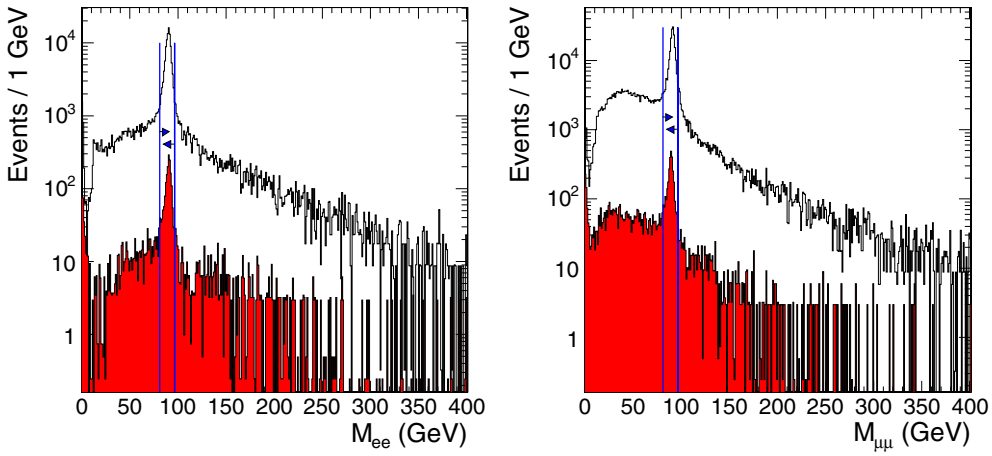

Figure 13.18. Reconstructed masses for (left) e^+e^- and (right) $\mu^+\mu^-$ pairs for the background and for the signal (shaded) events. SUSY events not involving $\tilde{\chi}_2^0$ are considered signal. The vertical lines denote the imposed mass requirement.

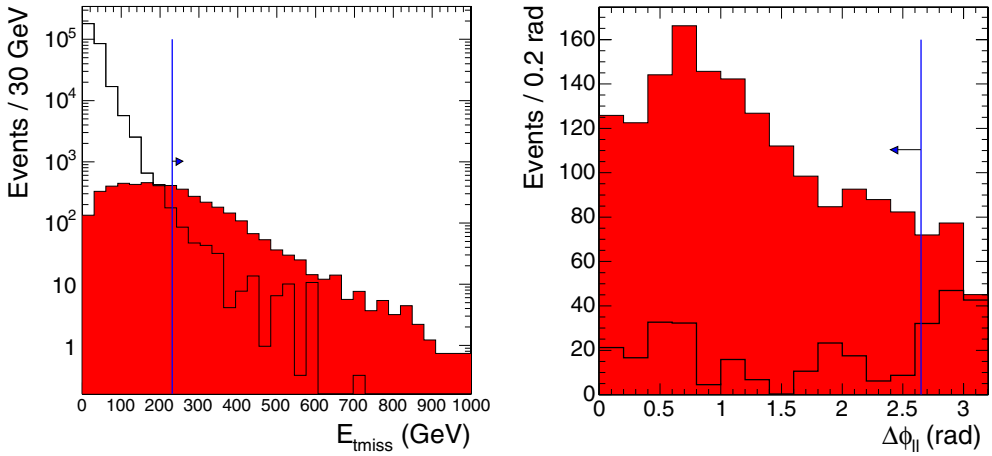

Figure 13.19. $E_{\mathrm{T}}^{\mathrm{miss}}$ (left) and $\Delta\phi$ between the two leptons (right) for background (black line) and signal (shaded) events. SUSY events not involving $\tilde{\chi}_2^0$ are considered signal. The vertical lines denote the $E_{\mathrm{T}}^{\mathrm{miss}}$ and $\Delta\phi$ requirements.

the mass requirements are shown in Figs. 13.18 (left) and (right) respectively. This cut reduces backgrounds not involving a Z^0 ($t\bar{t}$, WW+j) and the sample of SUSY events not involving $\tilde{\chi}_2^0$.

- The missing transverse energy $E_{\mathrm{T}}^{\mathrm{miss}}$ is required to be greater 230 GeV. This requirement reduces all backgrounds as seen in Fig. 13.19 (left). It allows, however, for enough signal and background events in order to maintain good statistics both for 1 fb^{-1} and for 10 fb^{-1} integrated luminosity.
- The angle $\Delta\phi$ between the two leptons of the lepton pair that reconstructs the mass of Z^0 is required to be less than 2.65 rad. The $\Delta\phi$ distribution is shown in Fig. 13.19 (right) for signal and background. This requirement targets the remainder of the $t\bar{t}$ and the WW + j backgrounds that survived the $E_{\mathrm{T}}^{\mathrm{miss}}$ requirement.

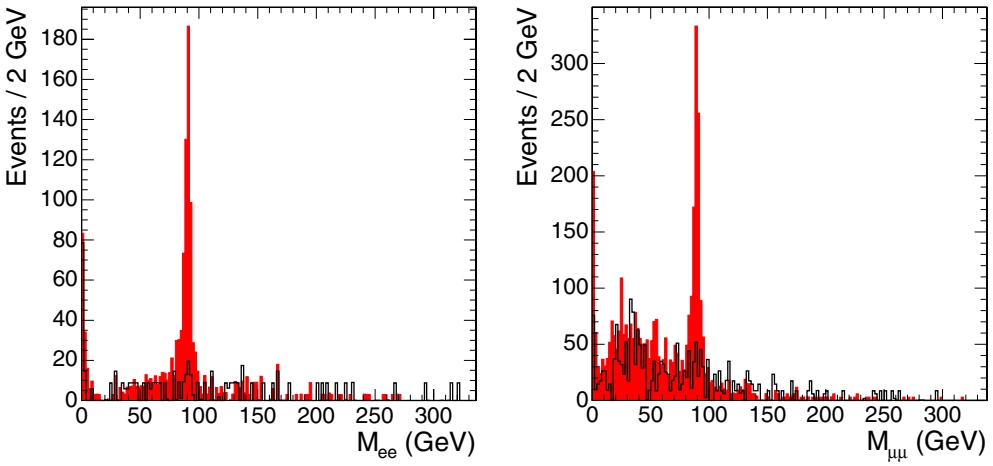

Figure 13.20. Reconstructed masses for (left) e^+e^- and (right) $\mu^+\mu^-$ pairs for the background and for the signal (shaded) events after the cut on $E_{\mathrm{T}}^{\mathrm{miss}}$. SUSY events not involving $\tilde{\chi}_2^0$ are considered signal.

13.11.3. Results and systematic uncertainties

The reconstructed masses for the e^+e^- and the $\mu^+\mu^-$ pairs without the Z^0 mass cut but after the cut on $E_{\mathrm{T}}^{\mathrm{miss}}$ are shown in Fig. 13.20 (left) and (right) respectively. A clear Z^0 peak from the signal is observed.

After the application of the above criteria and for 10 fb^{-1} integrated luminosity we have 1553 SUSY events and 196.5 Standard Model background events in the Z^0 window. This gives a signal over background ratio of 8 and inside the signal events 83% originate from a $\tilde{\chi}_2^0$ decay. The total efficiency for Z^0 events from a $\tilde{\chi}_2^0$ decay is 19.4%. The background is composed of 31% $t\bar{t}$, 24% WW, 18% Zj, 16% ZZ and 11% ZW.

The significance based on statistical uncertainties only has been evaluated by means of S_{cL}, defined in Appendix A.1. A significance of 5σ would be reached after 0.06 fb^{-1} if systematic effects were negligible.

When LHC will start running many uncertainties will be controlled from data. In this analysis relevant uncertainties are the lepton P_t resolution and the $E_{\mathrm{T}}^{\mathrm{miss}}$ uncertainty. The lepton P_t resolution ($\sim$3%) introduces an uncertainty of 2.7% in the number of background events. The dominant systematic, however, is the $E_{\mathrm{T}}^{\mathrm{miss}}$ energy scale uncertainty which is estimated to $\sim$5% and which introduces a 20% uncertainty in the number of background events, nearly independent of the background channel. The significance was recomputed after including the systematic uncertainties using S_{c12s} (see Appendix A.1), which increases the required integrated luminosity for a 5σ discovery to $\sim$0.1 fb^{-1}.

13.11.4. CMS reach for inclusive Z^0 search

A scan was performed over the mSUGRA $m_0, m_{1/2}$ parameter space in order to determine the range over which the above analysis can reveal new physics. The test points were taken at high density in the area where the Z^0 has high production cross section (especially due to the decay $\tilde{\chi}_2^0 \to Z^0 + \tilde{\chi}_1^0$). This is an almost horizontal band in the m_0–$m_{1/2}$ plane between $m_{1/2} \sim 240\,\mathrm{GeV/c^2}$ and $m_{1/2} \sim 340\,\mathrm{GeV/c^2}$. Points were also taken at higher and lower $m_{1/2}$ values, because there is an excess of lepton pairs created due to SUSY processes. These may have invariant mass close to the Z^0 mass and pass analysis cuts assisting in the detection

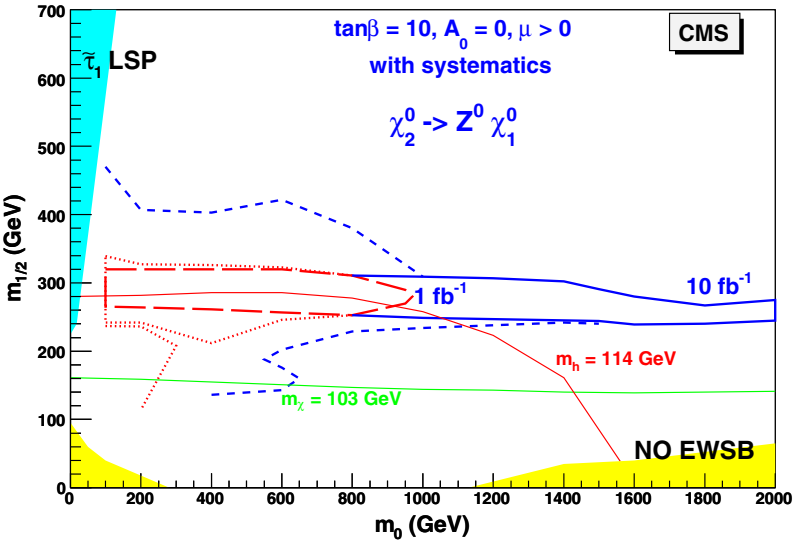

Figure 13.21. The 5σ significance contours of final states with Z^0 for $1\,\text{fb}^{-1}$ (dashed line) and $10\,\text{fb}^{-1}$ (full line) integrated luminosities, taking into account systematic uncertainties, in the region where the $\tilde{\chi}_2^0 \to Z^0\tilde{\chi}_1^0$ decay takes place. Also indicated as dotted and short dashed lines are the extensions at higher and lower $m_{1/2}$ where the Z^0 is off-shell.

of SUSY. For each point 2000 events were produced with an OS lepton pair close to the Z^0 mass. The events were generated interfacing ISAJET 7.69 with PYTHIA 6.227 and they were simulated, reconstructed and analysed using the FAMOS fast simulation package [11]. Systematic uncertainties were taken into account. The 5σ significance contour is shown for integrated luminosities of $1\,\text{fb}^{-1}$ and $10\,\text{fb}^{-1}$ in Fig. 13.21.

13.12. Inclusive analyses with top

The supersymmetric partner of the top quark in most of the supersymmetric scenarios is the lightest squark. Finding evidence of its existence can be a clear signature for supersymmetry. In the main part of the allowed m_0–$m_{1/2}$ plane, the stop can decay to a top plus a neutralino. This neutralino can be either the LSP ($\tilde{\chi}_1^0$) or a heavier neutralino which decays in turn to a LSP which appears as missing transverse energy ($E_{\text{T}}^{\text{miss}}$). Hence in the final state there is at least a top quark plus large $E_{\text{T}}^{\text{miss}}$.

The search for top was tuned on test point LM1, where the stop decays according to

$$\tilde{t}_1 \to t\tilde{\chi}_2^0 \to tl\tilde{l}_R \to tll\tilde{\chi}_1^0 \tag{13.20}$$

giving rise to a final state which also contains two leptons. Although this analysis consists primarily in a search for an excess of top quarks from any SUSY origin with respect to its SM production, it was also optimised for the selection of events where the top results from the production of $\tilde{t}$.

13.12.1. Top quark and lepton reconstruction and identification

Electrons and muons are requested to have $p_{\text{T}} \geqslant 5\,\text{GeV/c}$ and $\eta \leqslant 2.5$.

Electrons are separated from jets by requiring that the ratio of energy deposited in the HCAL to the ECAL $\leqslant 0.1$, the absolute difference in η between the electromagnetic cluster

in the ECAL and the associated track $\Delta\eta \leqslant 0.006$ and the energy weighted spread of the electron shower in η be $\sigma_{\eta\eta} \leqslant 0.015$.

Leptons were required to be isolated, namely that the ratio of p_T of the lepton to the p_T sum of other particles inside a cone of size $\Delta R = 0.1$ around the lepton track be greater than 2. Jets were reconstructed from ECAL and HCAL towers using an Iterative cone algorithm with cone size $\Delta R = 0.5$ and were selected if their uncalibrated transverse energy $E_T \geqslant 30$ GeV in the acceptance of $\eta \leqslant 2.5$. Their energy was calibrated using corrections from photon-jet balancing studies presented in Vol. 1 Section 11.6.3.

In this analysis only hadronic decays of the top quark were considered. A kinematic fit with constraints is utilised to find the best combination of jets to make the top quark. Since the purpose of this analysis is not to measure the top quark mass, its known value was used to constrain the invariant mass of the system of three jets. Among these three jets, one and only one must be tagged as a b-jet and the other two were constrained to be consistent with a hadronically decaying W. The fit then consisted in minimising the χ^2 as a function of the three jet energies and imposing the top and W mass constraints. The solution was obtained by an iterative method based on Lagrange multipliers. As several combinations may lead to a convergent fit for a given event, only the combination with the best χ^2 was kept, with the additional requirement that its χ^2 probability was greater than 0.1.

13.12.2. Signal selection and backgrounds

All events were fully simulated [8], digitised with low luminosity pileup and reconstructed [10].

The signal events consisted of an inclusive SUSY sample at the test point LM1 (see Section 13.3.2), where the total cross section at NLO is about 52 pb. Top quarks are found in the decay of $\tilde{t}$, but other important sources exist, e.g. $\tilde{b} \to t\tilde{\chi}_1^{\pm}$. At an integrated luminosity of 1 fb^{-1}, the total SUSY production amounts to 52000 events, out of which 8375 contain a top quark.

The main backgrounds, generated with PYTHIA 6.225 [69], consist of $t\bar{t}$, $WW + jets$, $WZ + jets$ and QCD. In addition, single top generated with TOPREX 4.11 [44] and $W + jets$ generated with ALPGEN V2.0 [161] were considered.

The selection of SUSY events containing a top quark was based on the following criteria:

- L1T: every event must pass the first level of the Trigger (L1T) cuts corresponding to "Jet/Met" (a jet with $E_T > 88$ and $E_T^{miss} > 46$ GeV/c).
- HLT: events were required to pass High level Trigger (HLT) cuts (a jet with $E_T > 180$ and $E_T^{miss} > 123$ GeV).
- $\geqslant$4 jets with $E_T^{raw} \geqslant 30$ GeV and $\eta \leqslant 2.5$.
- $\geqslant$1 b-jet with $E_T^{raw} \geqslant 30$ GeV and $\eta \leqslant 2.5$.
- $E_T^{miss} \geqslant 150$ GeV to suppress $t\bar{t}$ and other SM backgrounds.
- a convergent fit with $P(\chi^2) \geqslant 0.1$.
- $\Delta\Phi$ between the fitted top and $E_T^{miss} \leqslant 2.6$ rad to suppress semi-leptonic $t\bar{t}$ events.
- $\geqslant$1 isolated lepton (e or μ) with $p_T \geqslant 5$ GeV and $\eta \leqslant 2.5$ to suppress QCD background.

These criteria were simultaneously optimised to reject SM backgrounds and to maximise the ratio of events with a top quark at generator level, called SUSY(with top), to events without top at generator level, called SUSY(no top).

The effect of the cuts is shown in Table 13.12. As a result of the selection, the signal events remaining for a 1 fb^{-1} luminosity consist of 38 events SUSY(with top) and 17 events

Table 13.12. Effect of different cuts on different samples. In every row, the number of the remaining events after that cut is shown. "No.of.used.events" shows the number of events used in this analysis, "NEve(Nor.xsec)1 fb^{-1}" is the same number after normalising to the cross section times 1 fb^{-1} and "wT/noT" means $\frac{SUSY(withTop)}{SUSY(noTop)}$.

cut	SUSY (withTop)	SUSY (noTop)	ttInc	WW	ZW	Single t	wT/noT
x-sec(pb) NLO	52	830	269.91	51.5	250	-	
No.of.used.events	494261	1674500	305000	70000	100000	-	
NEve(Nor.xsec)1 fb^{-1}	8375	43625	830000	269910	51500	250000	0.19
L1T (Jet/Met)	6269	33582	75806	18498	598	10875	0.19
HLT (Jet/Met)	5070	29427	14430	4733	142	1750	0.17
MET $\geqslant$ 150 GeV	4183	25677	4930	2312	99	653	0.16
$n_{bj} \geqslant 1$	3457	14388	3718	792	32	355	0.24
$n_j^{b\ or\ light} \geqslant 4$	1789	4576	769	25	0	33	0.39
A convergent Fit	1335	3062	557	12	0	28	0.44
χ^2 probability >0.1	105	69	56	0	0	5	1.52
$\Delta\phi$ <2.6	79	52	12	0	0	5	1.51
$n_l > 0$	38	17	5	0	0	0	2.19

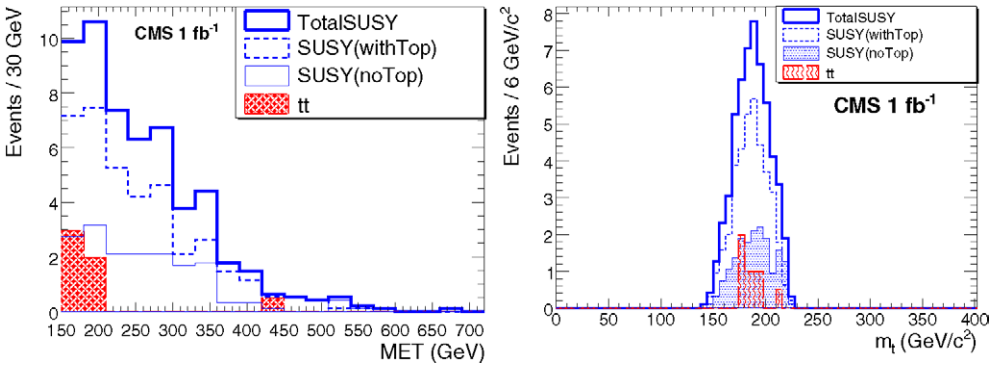

Figure 13.22. (left) Distributions of $E_{\mathrm{T}}^{\mathrm{miss}}$ and (right) fitted top mass after all selection criteria are applied.

SUSY(no top). The remaining backgrounds are 5 events from $t\bar{t}$. The resulting distributions of $E_{\mathrm{T}}^{\mathrm{miss}}$ and of the fitted top mass are displayed in Fig. 13.22.

13.12.3. Results at point LM1

The significance of a discovery was computed from statistical uncertainties only using the formula of S_{c12}, defined in Appendix A.1, where the number of signal events, S, is the sum of SUSY(with top) and SUSY(no top) and B represents the sum of all SM backgrounds. Using this formula, the integrated luminosity required to make a discovery at point LM1 with a significance of 5 amounts to $\sim$210 pb^{-1}.

Many systematic uncertainties (cross section, showering, ISR/FSR, ...) will be rendered very small by using real data. The main uncertainties remaining will be the absolute jet energy scale (estimated to 5% for jets and MET in 1 fb^{-1}), which leads to 5.1% from jets and 18.3% from MET in the $t\bar{t}$ sample and the b-tagging efficiency estimated to 8% for 1 fb^{-1}. Adding them in quadrature yields a total systematic uncertainty of 21%, considered common to all backgrounds. It is seen that this remains negligible compared to the statistical uncertainty.

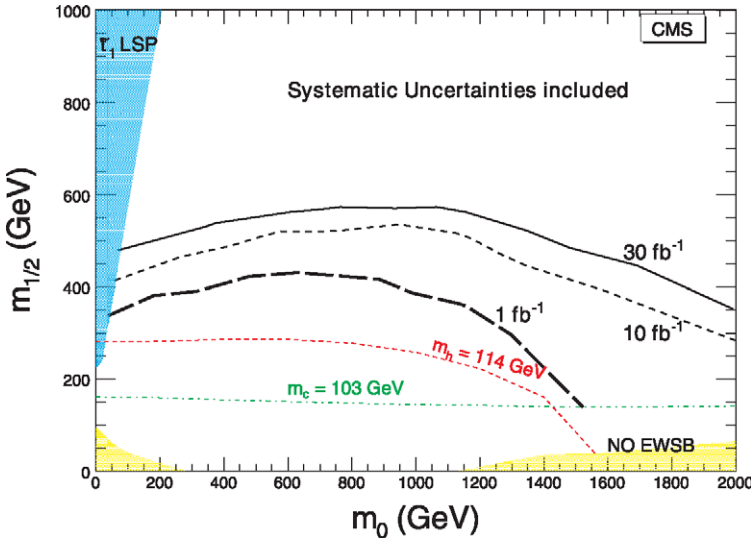

Figure 13.23. The 5σ reach in $m_0, m_{1/2}$ plane with 1, 10 and 30 fb^{-1} obtained for final states with a top quark.

13.12.4. CMS reach for inclusive top search

The CMS fast simulation, FAMOS, was used to find the reach of CMS in this channel in $m_0, m_{1/2}$ plane. In total 36 points have been tried. The ntuples were generated by using the CMS-official ISAPYTHIA. The NLO cross sections were derived by PROSPINO [682].

Figure 13.23 shows the 5σ reach in $m_0, m_{1/2}$ plane with 1, 10 and 30 fb^{-1}.

13.13. Mass determination in final states with ditaus

In this section the determination of the sparticle masses using invariant mass distributions in the ditau final state is investigated. The selection of the events is the same as presented in Section 13.9.

13.13.1. Extraction of mSUGRA mass spectra from the measurement of the end points of invariant mass distributions

Using the kinematics of the successive two body decays in $\tilde{q} \to q\tilde{\chi}_2^0 \to q\tau\tilde{\tau} \to q\tau\tau\tilde{\chi}_1^0$, it is possible to express the mass of the sparticles involved in that cascade as a fully resolved system of equations which depends only on the end-point of the invariant mass distributions obtained by combining the leptons and quark-jets observed in the final state.

However, the tau-lepton always decays, producing at least one undetected neutrino. Therefore, instead of observing a triangle-shaped distribution like for the dilepton invariant mass distribution of chapter 13.8, where the end-point coincides with the maximum of the distribution, the absence of the neutrino smears the resulting mass distribution to lower values. Even though the end-point of the distribution remains unchanged, it now lies at the tail of a gaussian-like distribution.

The $\tilde{\chi}_2^0$ cascade always produces a pair of opposite charge τ's, therefore signal samples are obtained by combining opposite charge tau pairs to the two most energetic jets of the event. In 75% of the cases the quark produced by the decay of the $\tilde{q}$ to $\tilde{\chi}_2^0$ is among these

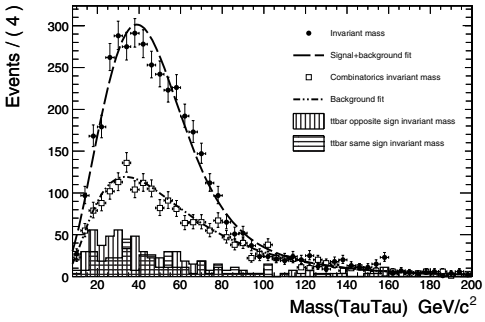

Figure 13.24. Ditau invariant mass distribution.

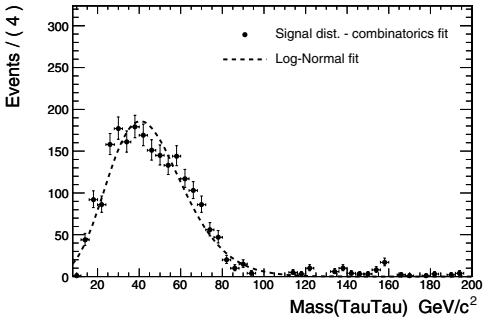

Figure 13.25. Difference between ditau invariant mass distribution and combinatorics fit together with log-normal fit.

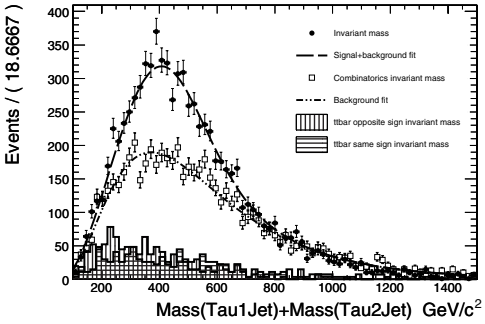

Figure 13.26. τ_1Jet + τ_2Jet invariant mass distribution.

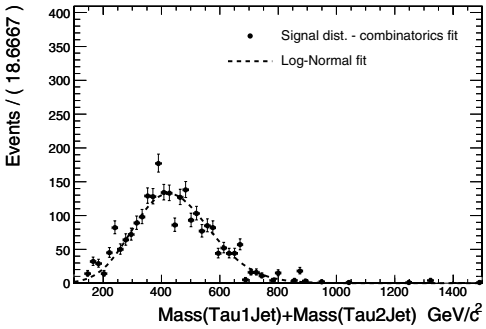

Figure 13.27. Difference between τ_1Jet + τ_2Jet invariant mass distribution and combinatorics fit together with log-normal fit.

two jets, due to the fact that the $\tilde{q}$ is much heavier than the $\tilde{\chi}_2^0$. This large number of tau's and jets is responsible for a high combinatorial background. A good description of this combinatorial background, in particular of its tail, is essential for extracting the true end-points. The combinatorial background in the opposite sign invariant ditau mass is estimated by taking same sign tau pairs. The combinatorial background from the jets is estimated by combining all tau pairs to a jet taken among the 2 most energetic jets of a previous event selected randomly to insure that the jet and tau's are uncorrelated.

Five invariant mass and their associated combinatorial background distributions are then obtained: $M(\tau\tau)$, $M(\tau\tau\text{Jet})$, $M(\tau_1 Jet)$, $M(\tau_2 Jet)$ and $M(\tau_1\text{Jet}) + M(\tau_2\text{Jet})$. ($\tau_1$ is defined as the one which maximises the invariant mass formed by its association with a jet, $M(\tau_1 Jet) > M(\tau_2 Jet)$).

The distributions of combinatorial background are first fitted. Then, the resulting fit parameters are used together with a Log-normal distribution, which gives a good description of the tail of the true distributions, to fit the distributions of the signal. Since it is possible to express the log-normal distribution as a function of the end-point, the end-point can be extracted directly from the fit.

The ditau invariant mass and $M(\tau_1\text{Jet}) + M(\tau_2\text{Jet})$ are fitted first (Figs 13.24–13.27). The three other invariant mass distributions are built using only candidates found to have values for the two previous distributions below the measured end-points. Then, they are fitted using the same procedure. The sparticle masses are evaluated by solving the system of four equations giving the end-points as a function of the sparticle mass [683].

Table 13.13. End-point obtained with the lognormal fit together with sparticle masses measured with the end-point technique for LM2 for integrated luminosities around 40 fb^{-1}.

End-points (GeV)	case 1 (GeV)	case 2 (GeV)
$m(\tau_1\tau_2)^{\max} = 95 \pm 3$	$M(\tilde{\chi}_1^0) = 213 \pm 14$	$M(\tilde{\chi}_1^0) = 147 \pm 23$
$m(\tau_1 Q)^{\max} = 559 \pm 11$	$M(\tilde{\chi}_2^0) = 337 \pm 17$	$M(\tilde{\chi}_2^0) = 265 \pm 10$
$m(\tau_2 Q)^{\max} = 298 \pm 7$	$M(\tilde{\tau}) = 310 \pm 17$	$M(\tilde{\tau}) = 165 \pm 10$
$m(\tau_1\tau_2 Q)^{\max} = 596 \pm 12$	$M(\tilde{q}) = 839 \pm 19$	$M(\tilde{q}) = 763 \pm 33$
$E_5^{meas} = 780 \pm 20$	$E_5^{calc} = 815 \pm 26$	$E_5^{calc} = 765 \pm 30$

Table 13.14. sparticle masses measured with end-point method for LM2 together with theoretical value.

	LM2 benchmark point	
	measured	theory
$M(\tilde{\chi}_1^0)$ (GeV)	$147 \pm 23(\text{stat}) \pm 19(\text{sys})$	138.2
$M(\tilde{\chi}_2^0)$ (GeV)	$265 \pm 10(\text{stat}) \pm 25(\text{sys})$	265.5
$M(\tilde{\tau})$ (GeV)	$165 \pm 10(\text{stat}) \pm 20(\text{sys})$	153.9
$M(\tilde{q})$ (GeV)	$763 \pm 33(\text{stat}) \pm 58(\text{sys})$	753–783 (light $\tilde{q}$)

When several solutions are possible for the SUSY mass spectrum (as it is the case here, where two valid solutions exist), the choice is made by comparing the measured $M(\tau_1\text{Jet}) + M(\tau_2\text{Jet})$ end-point value, E_5, to the one computed from the sparticle masses found by solving the systems of equations.

The most probable mass hypothesis is then chosen as the one for which E_5 computed for each mass spectrum is the closest to the measured one. The measured end-point was found to be 780±20 GeV while the calculations for the mass hierarchy in case 1 and case 2 yield to 815±26 GeV and 765±30 GeV respectively (Table 13.14). The second hypothesis, which corresponds to the correct LM2 mass hierarchy, gives a result compatible with the measured end-point value.

Three main systematic uncertainties are considered, the jet energy scale and tau-jet energy scale as well as systematics uncertainties arising from the extraction procedure.

Results obtained are shown in Table 13.14 for 40 fb^{-1}, together with LM2 generated sparticle masses. They are found to be in good agreement with the theoretical values. Using a 40 fb^{-1} LM2 sample, it is possible to measure the SUSY mass spectra and in particular $\tilde{\tau}$ mass with a precision of 30 GeV.

13.14. Direct $\chi_2^0\chi_1^\pm$ production in tri-leptons

The exclusive tri-lepton final state appears in $pp \to \tilde{\chi}_2^0\tilde{\chi}_1^\pm$ channel with subsequent three body decays of the second neutralino, $\tilde{\chi}_2^0 \to \tilde{\chi}_1^0 ll$, and chargino, $\tilde{\chi}_1^\pm \to \tilde{\chi}_1^0 W^* \to \tilde{\chi}_1^0 l\nu$; or via sleptons in two body decay, $\tilde{\chi}_2^0 \to l\tilde{l} \to l\tilde{\chi}_1^0 l$, and $\tilde{\chi}_1^\pm \to l\tilde{\nu} \to l\tilde{\chi}_1^0\nu$, $\tilde{\chi}_1^\pm \to \nu\tilde{l} \to \nu\tilde{\chi}_1^0 l$. The final signatures are two Opposite-Sign Same-Flavour (SFOS) leptons (e, μ) from the neutralino $\tilde{\chi}_2^0$ decay plus any lepton from the chargino $\tilde{\chi}_1^\pm$. Jets are expected to be only due to gluon state radiation or pile up events. In spite of the escaping $\tilde{\chi}_1^0$, the $E_{\text{T}}^{\text{miss}}$ is relatively small at low $m_{1/2}$ and is comparable with the one of SM backgrounds, especially for three body decays at large m_0. The invariant mass of the SFOS dileptons exhibits a particular shape with a kinematic end point M_{ll}^{max} that depends upon the event topology, see section 13.3.

13.14.1. Datasets

The tri-lepton cross section σ_{3l} was calculated with ISAJET (7.69) and PYTHIA (6.225 CTEQ5L) at LO, the K_{NLO} factor calculated with PROSPINO is in the range of 1.30–1.25 (for $m_{\tilde{\chi}_2^0} = 150-300\,\mathrm{GeV/c^2}$) [684]. The σ_{3l} drops rapidly with the neutralino mass $m_{\tilde{\chi}_2^0} \sim 0.8 m_{1/2}$, $\sigma_{3l} \sim m_{1/2}^{-4}$. This study is restricted to the low $m_{1/2}$ region, where σ_{3l} contributes, for instance, $\sim 0.5\%$ to the total SUSY cross section at $m_0 > 1000\,\mathrm{GeV/c^2}$. The three body decays are dominant in this m_0, $m_{1/2}$ region, except for $m_0 < 150\,\mathrm{GeV/c^2}$ and $\tan\beta \leqslant 20$. The kinematic end point in the invariant mass is approximately $M_{ll}^{max} \sim 0.42^* m_{1/2} - 18.4$ $\mathrm{GeV/c^2}$ (at $m_0 \sim 1000\,\mathrm{GeV/c^2}$), thus moving into the Z-peak region at $m_{1/2} > 250\,\mathrm{GeV/c^2}$ where the SM background is high. Among the CMS benchmark points in this region, LM9 ($m_{1/2} = 175$, $m_0 = 1450$, $\tan\beta = 50$, $A_0 = 0$) has the largest cross section, ~ 3700 events are produced for $30\,\mathrm{fb}^{-1}$, and it was used as a reference.

13.14.2. Backgrounds and trigger path

The main background results from the Drell–Yan, Z + jets, $\mathrm{t\bar{t}} \to WbWb$, ZW, ZZ, Wt+jets, WW+jets, W+jets and inclusive SUSY channels. For all backgrounds, except ZW and ZZ, some leptons originate from jets, mostly $b \to l + j$. The background events were produced with PYTHIA (ALPGEN and TOPREX are also used) and their cross section corrected to NLO. The Z and W bosons are forced to decay leptonically to e, μ, $\tau \to e$, μ. The DY and Z+jets cross section is large ($\sigma_{DY,Zj} \sim 10\,\mathrm{nb}$) and events were preselected by requiring three leptons with $p_\mathrm{T} > 5\,\mathrm{GeV/c}$ and $|\eta| < 2.4$ at the generator level. The full data samples of $30\,\mathrm{fb}^{-1}$ for the LM9 test point and backgrounds are simulated with the CMS fast simulations (FAMOS) validated with smaller statistics samples produced with the full GEANT based simulation (OSCAR, ORCA). Low luminosity pile-up was included.

All events were required to pass Level-1 and HLT triggers. The main trigger paths for LM9 are the dimuons (74%) and dielectrons (25%). The trigger efficiency is 86% at Level-1 and 91% at HLT for LM9 and is increasing for larger $m_{1/2}$ where the leptons become harder. In the off-line selection, at least three isolated leptons in $|\eta| < 2.4$ and $P_\mathrm{T}^{\mu,e} > 10\,\mathrm{GeV/c}$ are required for each event. The leptons are reconstructed using standard reconstruction algorithms. Electrons and muons are required to be isolated, *i.e.* other tracks may only contribute up to $\sum P_\mathrm{T}$ of $1.5\,\mathrm{GeV/c}$ inside a cone of $\Delta R < 0.3$. Moreover, for muons the energy deposit in calorimeters should be $E_\mathrm{T} < 5\,\mathrm{GeV}$ in a cone of $\Delta R < 0.3$. In addition, electron candidates are required to satisfy quality criteria based on a likelihood function, > 0.65. The muons and electrons reconstruction efficiencies in ORCA are found to be 78% ($\mathrm{P}_\mathrm{T}^{\mu} > 5\,\mathrm{GeV/c}$) and 66% ($\mathrm{P}_\mathrm{T}^{e} > 10\,\mathrm{GeV/c}$) respectively. The jets are reconstructed using an iterative cone algorithm with the seed energies $E_\mathrm{T}^{seed} > 0.5\,\mathrm{GeV}$ in a cone $\Delta R < 0.5$.The $E_\mathrm{T}^{\mathrm{miss}}$ was reconstructed from the calorimeter towers. Since the $E_\mathrm{T}^{\mathrm{miss}}$ for the signal events is relatively small and its reconstruction at low energy scale is limited by the $\mathrm{E_T}$ resolution, a $E_\mathrm{T}^{\mathrm{miss}}$ requirement is not as efficient as in other SUSY channels.

13.14.3. Analysis path

The reconstructed events are selected in two steps. First, sequential cuts are applied: 1) No central jets with corrected energy $E_\mathrm{T} > 30\,\mathrm{GeV}$ in $|\eta| < 2.4$, 2) Two SFOS isolated leptons (e, μ) in $|\eta| < 2.4$ with $P_\mathrm{T}^{\mu} > 10\,\mathrm{GeV/c}$, $P_\mathrm{T}^{e} > 17\,\mathrm{GeV/c}$ and the dilepton invariant mass below the Z peak $M_{ll} < 75\,\mathrm{GeV/c^2}$. 3) The third lepton is with $P_\mathrm{T}^{\mu,e} > 10\,\mathrm{GeV/c}$ in $|\eta| < 2.4$. The evolution of statistics and the efficiencies of the selection cuts are presented in Table 13.15.

Table 13.15. Evolution of signal and background statistics with the cuts as expected for 30 fb^{-1}. The last column gives the results of a neural network selection applied after the sequential cuts.

channel	N_{ev} 30 fb^{-1} ($\sigma \times BR$ [pb])	L1+HLT	No Jets	2 SFOS+l SFOS $M_{ll} < 75$ GeV/c^2	NN_{LM9}
LM1	2640 (0.088)	1544 (58%)	864 (56%)	70 (8%)	17 (24%)
LM7	1540 (0.051)	1250 (82%)	738 (59%)	91 (12%)	57 (62%)
LM9	3700 (0.125)	2896 (78%)	1740 (60%)	239 (14%)	158 (68%)
SUSY	$4{\cdot}10^5$ ($13.1^{\,NLO}$)	$2.5{\cdot}10^5$ (63%)	$1.8{\cdot}10^4$ (7%)	34 (0.2%)	22 (65%)
ZW	$5{\cdot}10^4$ ($1.68^{\,NLO}$)	$3.6{\cdot}10^4$ (73%)	$1.9{\cdot}10^4$ (53%)	173 (1%)	44 (25%)
ZZ	$4.8{\cdot}10^3$ ($0.16^{\,NLO}$)	$3.5{\cdot}10^3$ (73%)	$1.7{\cdot}10^3$ (48%)	38 (2.3%)	15 (39%)
$t\bar{t}$	$2.6{\cdot}10^6$ ($88^{\,NLO}$)	$1.8{\cdot}10^6$ (70%)	$1.3{\cdot}10^5$ (7%)	239 (0.2%)	89 (37%)
Z+jets(3l)	$4.6{\cdot}10^5$ ($15.4^{\,LO}$)	$3.7{\cdot}10^5$ (80.5%)	$9.8{\cdot}10^4$ (26.5%)	504 (0.5%)	129 (26%)
DY(3l)	$4.5 \cdot 10^5$ ($15.1^{\,LO}$)	$3.2{\cdot}10^5$ (71%)	$1.4{\cdot}10^5$ (44%)	670 (0.5%)	131 (20%)
$Zb\bar{b}$(3l)	$8.4{\cdot}10^4$ ($2.8^{\,LO}$)	$7.3{\cdot}10^4$ (87%)	$1.5{\cdot}10^4$ (20%)	69 (0.6%)	18 (26%)
Wt+jets	$3{\cdot}10^5$ ($10^{\,NLO}$)	$2.1{\cdot}10^5$ (70%)	$3.9{\cdot}10^4$ (18.5%)	52 (0.1%)	20 (38%)
WW+jets	$6{\cdot}10^5$ ($19.8^{\,LO}$)	$3.8{\cdot}10^5$ (63%)	$1.9{\cdot}10^4$ (50%)	7 (0.04%)	2 (29%)
Tot. bkg	$\sim 4.9 \cdot 10^6$			1786	470 (26%)

In a second step the background suppression is improved with a Neural Network (NN). Five networks for DY, Z+jets, $t\bar{t}$, ZW and ZZ backgrounds are trained on the LM9 signal sample using the following variables: $P_T^{1,2,3}$, $\sum P_T$, M_{ll}, P_T^{2l} (transverse momentum of two SFOS leptons), $A = \frac{P_T^1 - P_T^2}{P_T^1 + P_T^2}$, Θ_{ll} (angle between two SFOS leptons), Φ_{ll} (angle in transverse plane), E_T^{miss}, N_{jets} (number of jets passing the jets veto), E_t^{hj} (of the highest E_T jet), η_{hj} (rapidity of the highest jet). The selection cuts on the NN outputs were optimised for the maximum significance at LM9 with the genetic algorithm GARCON [63]. The efficiency of the NN selection is also shown in Table 13.15.

13.14.4. Results at LM9 and systematics

After the selection based on cuts the S_{cp} significance calculated for all SFOS pair combination is 6.1 at point LM9 for an integrated luminosity of 30 fb^{-1}. The NN improves the S_{cp} for all SFOS combinations to 7.8.

In addition to the real tri-lepton final state, leptons can be produced in the detector volume from $\pi^{\pm}$, $K^{\pm}$ decays, bremsstrahlung, punch-through or faked by jets. The rate per event of such fake leptons was estimated individually for each background by matching the reconstructed lepton with the generated one and is $\sim 10^{-4}$ for electrons and $\sim 10^{-5}$ for muons. The expected fake leptons substantially increase the background, especially for the preselected channels like DY or Z + jets, by $\sim 221 \pm 48$ events and $\sim 31 \pm 16$ events respectively for the tri-muon final state where the fake rate is smaller. The S_{cP} significance defined in Appendix A.1 including fakes but without other systematic uncertainties for all SFOS combinations and for the tri-muon state at LM9 is 6.5 and 5.1 respectively.

The reconstruction uncertainties related to the jet energy scale (5%) and the lepton momentum resolution (2%) contribute 1% to the uncertainties on the background. The average theoretical uncertainty from the PDFs, calculated with the LHPDF subsets using the re-weighting technique for each background channel, amounts to 1.7%. These uncertainties reduce the significances to 5.8 and 4.8 for the all SFOS pairs and for the tri-muon final state, respectively. However the largest uncertainties are coming from the Monte Carlo statistical

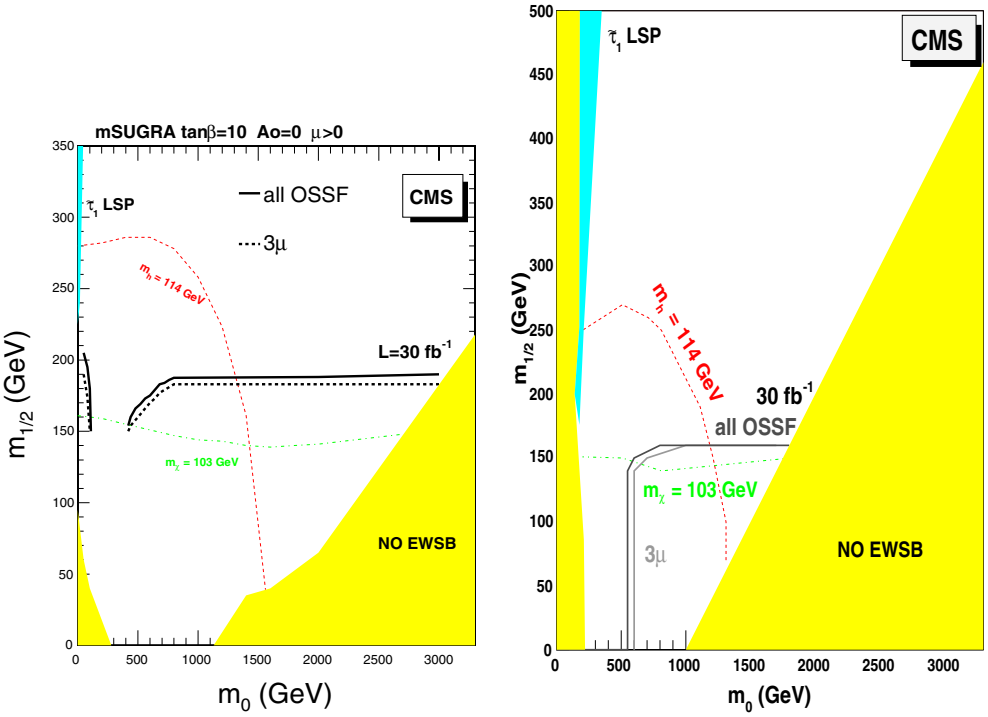

Figure 13.28. Discovery reach of tri-lepton from the $pp \to \tilde{\chi}_2^0 \tilde{\chi}_1^{\pm}$ production at $\mathcal{L}_{int}$=30 fb^{-1} for all SFOS lepton combinations (dashed) and for the tri-muon final state (solid) including systematic uncertainties from reconstruction, for (left) $\tan\beta = 10$ and (right) $\tan\beta = 50$.

errors in the fake rate estimation which contribute ∼7% to the background uncertainties rendering the signal hardly observable, $S_c p \sim 3.3$. These fake rate uncertainties can be reduced with larger simulation samples.

In summary, for the tri-lepton mSUGRA study presented here, the final signal to background ratio is 0.23, the total signal efficiency is 4.4% and the background composition is 28% Drell–Yan, 27% Z + jets, 19% $t\bar{t}$, 9% WZ, and 17% ZZ, WW, SUSY, W+ jets and QCD. The total considered theoretical and reconstruction systematic uncertainties on the Standard Model background is 2.2%. The Monte Carlo statistics systematic errors in the fake rates increases this to 7.5%.

13.14.5. CMS reach for the tri-lepton final state

Figure 13.28 shows the 5σ discovery reach in m_0 and $m_{1/2}$ plane at $L_{int} = 30\,\text{fb}^{-1}$ for all SFOS combinations and for the tri-muon final state including the systematic uncertainties due to the reconstruction. The signal can be observed at large $m_0 > 1000\,\text{GeV/c}^2$ in a narrow band below $m_{1/2} < 180\,\text{GeV/c}^2$. At low $m_0 < 100\,\text{GeV/c}^2$ the two body decays are visible although a better optimisation is possible in this region, see Sections 13.8 and 13.15. The tri-lepton final state from direct neutralino-chargino production is complementary to the inclusive SFOS dilepton search and provides an additional verification for the leptonic decays of the neutralino at low $m_{1/2}$.

13.15. Production of $\tilde{l}\tilde{l}$

The aim of this section is the study of the possibility of detecting sleptons. Note the previous related papers where the sleptons detection was studied at the level of a toy detector [685–689].

13.15.1. Simulation details

ISASUSY 7.69 [672] was used for the calculation of coupling constants and cross sections in the leading order approximation for SUSY processes. For the calculation of the next-to-leading order corrections to the SUSY cross sections the PROSPINO code [682] was used. Cross sections of the background events were calculated with PYTHIA 6.227 [69] and COMPHEP 4.2pl [355]. For considered backgrounds the NLO corrections are known and they were used. Official datasets (DST) production was used for the study of CMS test point LM1 and backgrounds ($t\bar{t}$, ZZ, WW, Wt, Z $b\bar{b}$, DY2e, DY2τ). For WZ, DY2μ and W + jet backgrounds the events were generated with PYTHIA 6.227. The detector simulation and hits production were made with full CMS simulation [8], digitised and reconstructed [10]. The DY2μ and W + jet backgrounds were simulated with fast simulation [11].

Jets were reconstruction using an iterative cone algorithm with cone size 0.5 and their energy corrected with the GammaJet calibration.

The events are required to pass the Global Level 1 Trigger (L1) and the High Level Trigger (HLT). The events have to pass at least one of the following triggers: single electron, double electron, single muon, double muon.

The CMS fast simulation code was used for the determination of the sleptons discovery plot.

13.15.2. Sleptons production and decays

When sleptons are heavy relative to $\tilde{\chi}_1^{\pm}$, $\tilde{\chi}_2^0$, they are produced significantly at the LHC through the Drell–Yan mechanism (direct sleptons production), via $q\bar{q}$ annihilation with neutral or charged boson exchange in the s-channel, namely, $pp \to \tilde{l}_L\tilde{l}_L, \tilde{l}_R\tilde{l}_R, \tilde{\nu}\tilde{\nu}, \tilde{\nu}\tilde{l}, \tilde{l}_L\tilde{l}_R$. The left sleptons decay to charginos and neutralinos via the following (kinematically accessible) decays:

$$\tilde{l}_L^{\pm} \to l^{\pm} + \tilde{\chi}_{1,2}^0 , \tag{13.21}$$

$$\tilde{l}_L^{\pm} \to \nu_l + \tilde{\chi}_1^{\pm} , \tag{13.22}$$

$$\tilde{\nu} \to \nu_l + \tilde{\chi}_{1,2}^0 , \tag{13.23}$$

$$\tilde{\nu} \to l^{\pm} + \tilde{\chi}_1^{\pm} . \tag{13.24}$$

For right sleptons only decays to neutralino are possible and they decay mainly to LSP:

$$\tilde{l}_R^{\pm} \to l^{\pm} + \tilde{\chi}_1^0 . \tag{13.25}$$

If sleptons are light relative to $\tilde{\chi}_1^{\pm}$, $\tilde{\chi}_2^0$, they can be abundantly produced, besides the Drell–Yan mechanism, also from chargino and neutralino decays $\tilde{\chi}_1^{\pm}$, $\tilde{\chi}_2^0$ (indirect production), equations (13.8), (13.9), (13.13) and (13.14).

13.15.3. Signature and backgrounds

The slepton production and decays described previously lead to the signature with the simplest event topology: *two leptons* $+E_{\mathrm{T}}^{\mathrm{miss}} + jet\ veto$. This signature arises for both direct and indirect slepton pair production. In the case of indirectly produced sleptons not only the event topology with two leptons but with single, three and four leptons is possible. Besides, indirect slepton production from decays of squarks and gluino through charginos, neutralinos can lead to an event topology *two leptons* $+E_{\mathrm{T}}^{\mathrm{miss}} + (n \geqslant 1)\ jets$.

The cut set close to the optimal one is the following:

(a) for leptons:
- p_{T} - cut on leptons ($p_{\mathrm{T}}^{lept} > 20\,\mathrm{GeV/c}$, $|\eta| < 2.4$) and lepton isolation within $\Delta R < 0.3$ cone containing calorimeter cells and tracker;
- effective mass of two opposite-sign and the same-flavour leptons is outside ($M_Z - 15\,\mathrm{GeV}$, $M_Z + 10\,\mathrm{GeV}$) interval;
- $\Phi(l^+l^-) < 140^\circ$ cut on angle between two leptons;

(b) for $E_{\mathrm{T}}^{\mathrm{miss}}$:
- $E_{\mathrm{T}}^{\mathrm{miss}} > 135\,\mathrm{GeV}$ cut on missing E_{T};
- $\Phi(E_{\mathrm{T}}^{\mathrm{miss}}, ll) > 170^\circ$ cut on relative azimuthal angle between dilepton and $E_{\mathrm{T}}^{\mathrm{miss}}$;

(c) for jets:
- jet veto cut: $N_{jet} = 0$ for a $E_{\mathrm{T}}^{jet} > 30\,\mathrm{GeV}$ (corrected jets) threshold in the pseudorapidity interval $|\eta| < 4.5$.

The Standard Model (SM) backgrounds are: $\mathrm{t\bar{t}}$, WW, WZ, ZZ, Wt, $\mathrm{Zb\bar{b}}$, DY, W + jet. The main contributions come from WW and $\mathrm{t\bar{t}}$ backgrounds. There are also internal SUSY backgrounds which arise from $\tilde{q}\tilde{q}$, $\tilde{g}\tilde{g}$ and $\tilde{q}\tilde{g}$ productions and subsequent cascade decays with jets outside the acceptance or below the threshold. Note that when we are interested in new physics discovery we have to compare the calculated number of SM background events N_{SMbg} with new physics signal events $N_{new\ physics} = N_{slept} + N_{SUSYbg}$, so SUSY background events increase the discovery potential of new physics.

13.15.4. Results

For the point LM1 with the used set of cuts for the integral luminosity $\mathcal{L} = 10\,\mathrm{fb}^{-1}$ the number of signal events (direct sleptons plus sleptons from chargino/neutralino decays) is $N_S = 60$, whereas the number of SUSY background events is $N_{SUSYbg} = 4$ and the number of SM background events is $N_{SMbg} = 41$. The total signal efficiency is 1.16×10^{-4} and the background composition is 1.32×10^{-6} of the total ttbar, 1.37×10^{-5} of the total WW, 4×10^{-6} of the total WZ, 4.4×10^{-5} of the total ZZ, 8.1×10^{-6} of the total Wt, 0 of the total Zbb, DY, W + jet.

The SUSY background is rather small compared to the signal, so we can assume $N_S = N_{direct\ sleptons} + N_{chargino/neutralino} + N_{SUSYbg} = 64$. It corresponds to the significances $S_{c12} = 7.7$ and $S_{cL} = 8.3$, defined in Appendix A.1.

Taking into account the systematic uncertainty of 23% related with in exact knowledge of backgrounds leads to the decrease of significance S_{c12} from 7.7 to 4.3.

The ratio of the numbers of background events from two different channels $N(e^+e^- + \mu^+\mu^-)/N(e^\pm\mu^\mp)$=1.37 will be used to keep the backgrounds under control.

The CMS discovery plot for $two\ leptons + E_{\mathrm{T}}^{\mathrm{miss}} + jet\ veto$ signature is presented in Fig. 13.29.

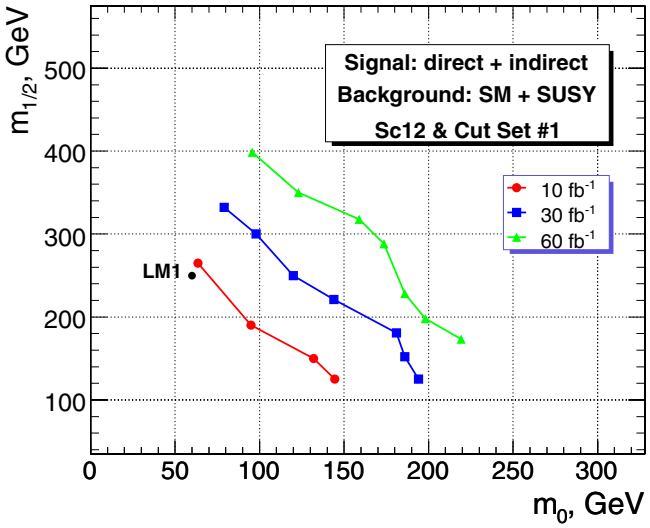

Figure 13.29. Discovery plot ($\tan\beta = 10$, sign(μ) = +, $A = 0$) for final states with l^+l^-, missing transverse energy and a jet veto.

13.16. Lepton flavour violation in neutralino decay

The aim of this section is the study of the possibility to detect SUSY and Lepton Flavour Violation (LFV) using the $e^{\pm}\mu^{\mp} + E_{\mathrm{T}}^{\mathrm{miss}}$ signature.

13.16.1. Signal selection and backgrounds

The simulation details of this study could be found in the Section 13.15.

The SUSY production $pp \to \tilde{q}\tilde{q}^{'}, \tilde{g}\tilde{g}, \tilde{q}\tilde{g}$ with subsequent decays leads to the event topology $e^{\pm}\mu^{\mp} + E_{\mathrm{T}}^{\mathrm{miss}}$. In the MSSM with lepton flavour conserving neutralino decays into leptons $\tilde{\chi}^0_{2,3,4} \to l^+l^-\tilde{\chi}^0_1$ do not contribute to this signature and contribute only to $l^+l^- + E_{\mathrm{T}}^{\mathrm{miss}}$ signature (here $l = e$ or μ). The main backgrounds which contribute to the $e^{\pm}\mu^{\mp}$ events are: $t\bar{t}$, ZZ, WW, WZ, Wt, $Zb\bar{b}$, DY2τ, Z+jet. It has been found that $t\bar{t}$ background is the biggest one and it gives more than 50% contribution to the total background.

Our set of cuts is the following:

- p_{T} - cut on leptons ($p_{\mathrm{T}}^{lept} > 20\,\mathrm{GeV/c}$, $|\eta| < 2.4$) and lepton isolation within $\Delta R < 0.3$ cone.
- $E_{\mathrm{T}}^{\mathrm{miss}} > 300\,\mathrm{GeV}$ cut on missing E_{T}.

13.16.2. Results at CMS test points and reach

For integrated luminosity $\mathcal{L} = 10\,\mathrm{fb}^{-1}$ the number of background events is $N_B = 93$. The results for this luminosity are presented in Table 13.16. At point LM1 the signal over background ratio is 3 and the signal efficiency is 6×10^{-4}. The background composition is 9.5×10^{-6} of the total ttbar, 3.4×10^{-6} of the total WW, 4×10^{-6} of the total WZ, 3.2×10^{-6} of the total Wt, 2.2×10^{-6} of the total Z + jet, 0 of the total ZZ, $Zb\bar{b}$, DY2τ.

The CMS discovery plot for the $e^{\pm}\mu^{\mp} + E_{\mathrm{T}}^{\mathrm{miss}}$ signature is presented in Fig. 13.30.

In the MSSM the off-diagonal components of the slepton mass terms violate lepton flavour conservation. As it was shown in Refs. [690–692] it is possible to look for lepton

Table 13.16. Number of signal events and significances S_{c12} [50] and S_{cL} [100, 102], defined in Appendix A.1, for $\mathcal{L} = 10\,\text{fb}^{-1}$.

Point	N events	S_{c12}	S_{cL}
LM1	329	21.8	24.9
LM2	94	8.1	8.6
LM3	402	25.2	29.2
LM4	301	20.4	23.1
LM5	91	7.8	8.3
LM6	222	16.2	18.0
LM7	14	1.4	1.4
LM8	234	16.9	18.8
LM9	137	11.0	11.9

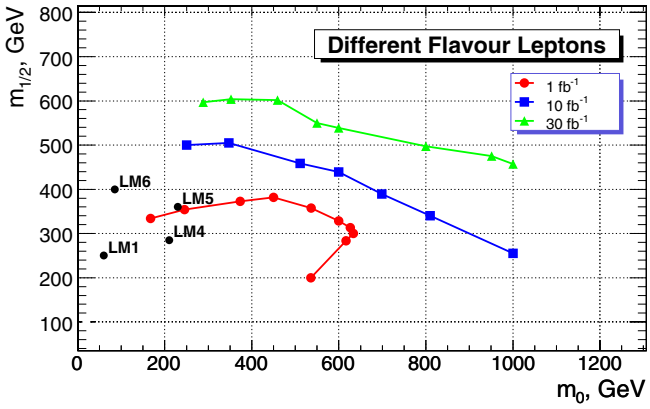

Figure 13.30. Discovery plot ($\tan\beta = 10$, $\text{sign}(\mu) = +$, $A = 0$) for the luminosities $\mathcal{L} = 1$, 10, $30\,\text{fb}^{-1}$ for the $e^{\pm}\mu^{\mp} + E_{\text{T}}^{\text{miss}}$ signature.

flavour violation at supercolliders through the production and decays of the sleptons. For the LFV at the LHC one of the most promising processes is the LFV decay of the second neutralino [693, 694] $\tilde{\chi}_2^0 \to \tilde{l}l \to \tilde{\chi}_1^0\, ll'$, where the non zero off-diagonal component of the slepton mass matrix leads to the different flavours for the leptons in the final state. By using the above mode, LFV in $\tilde{e} - \tilde{\mu}$ mixing has been investigated in Refs. [693, 694] at a parton model level for a toy detector. In this section we study the perspectives of the LFV detection in CMS on the base of full simulation of both signal and background is studied. To be specific, we study the point LM1. We assume that the LFV is due to nonzero mixing of right-handed smuon and selectron. The signal of the LFV $\tilde{\chi}_2^0$ decay is two opposite-sign leptons ($e^+\mu^-$ or $e^-\mu^+$) in the final state with the characteristic edge structure. In the limit of lepton flavour conservation, the process $\tilde{\chi}_2^0 \to \tilde{l}l \to ll\tilde{\chi}_1^0$ has the edge structure for the distribution of the lepton-pair invariant mass m_{ll} and the edge mass m_{ll}^{max} is expressed by the slepton mass $m_{\tilde{l}}$ and the neutralino masses $m_{\tilde{\chi}_{1,2}^0}$ as follows:

$$(m_{ll}^{max})^2 = m_{\tilde{\chi}_2^0}^2 \left(1 - \frac{m_{\tilde{l}}^2}{m_{\tilde{\chi}_2^0}^2}\right)\left(1 - \frac{m_{\tilde{\chi}_1^0}^2}{m_{\tilde{l}}^2}\right). \tag{13.26}$$

The SUSY background for the LFV comes from uncorrelated leptons from different squark or gluino decay chains. The SM background comes mainly from

$$t\bar{t} \to bWbW \to blbl'\nu\nu'. \tag{13.27}$$

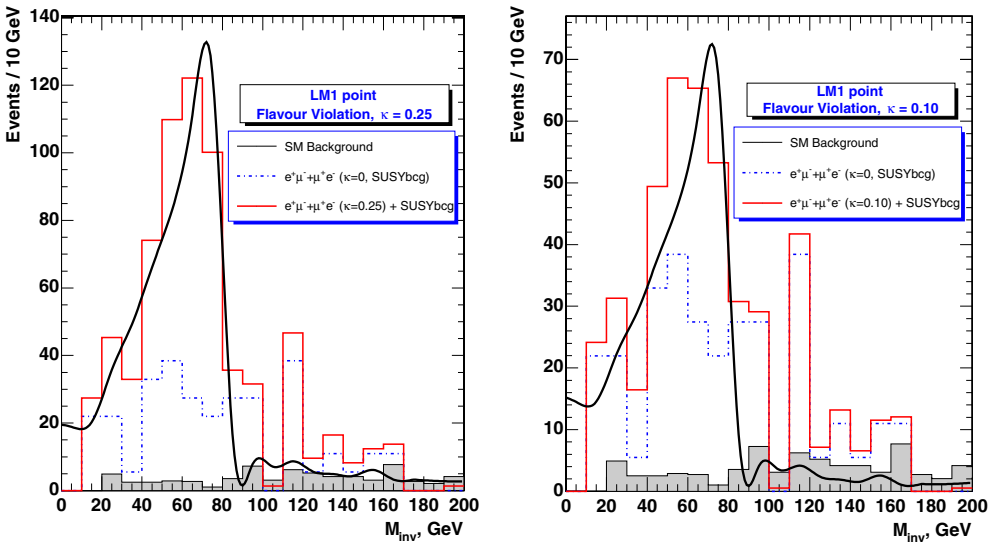

Figure 13.31. The distribution of dilepton invariant mass after selection of two isolated $e^{\pm}\mu^{\mp}$ leptons with $p_{\mathrm{T}}^{lept} > 20\,\mathrm{GeV/c}$ and $E_{\mathrm{T}}^{\mathrm{miss}} > 300\,\mathrm{GeV}$ for flavour violation parameter $k = 0.25$ (left) and $k = 0.1$ (right). The superimposed curves are fits to the invariant mass distribution for the case of 100% LFV.

The Drell–Yan background from $pp \to \tau\tau \to e\mu \ldots$ is negligible. It should be stressed that for the signature with $e^{\pm}\mu^{\mp}$ in the absence of the LFV we do not have the edge structure for the distribution on the invariant mass $m_{inv}(e^{\pm}\mu^{\mp})$. As the result of the LFV the edge structure for $e^{\pm}\mu^{\mp}$ events arises too. Therefore the signature of the LFV is the existence of an edge structure in the $e^{\pm}\mu^{\mp}$ distribution. The rate for a flavour violating decay is

$$Br(\tilde{\chi}_2^0 \to e^{\pm}\mu^{\mp}\tilde{\chi}_1^0) = \kappa\, Br(\tilde{\chi}_2^0 \to e^+e^-\tilde{\chi}_1^0, \mu^+\mu^-\tilde{\chi}_1^0), \tag{13.28}$$

where

$$Br(\tilde{\chi}_2^0 \to e^+e^-\tilde{\chi}_1^0, \mu^+\mu^-\tilde{\chi}_1^0) = Br(\tilde{\chi}_2^0 \to e^+e^-\tilde{\chi}_1^0) + Br(\tilde{\chi}_2^0 \to \mu^+\mu^-\tilde{\chi}_1^0), \tag{13.29}$$

$$\kappa = 2x \sin^2\theta \cos^2\theta, \tag{13.30}$$

$$x = \frac{\Delta m^2_{\tilde{e}\tilde{\mu}}}{\Delta m^2_{\tilde{e}\tilde{\mu}} + \Gamma^2}, \tag{13.31}$$

$$Br(\tilde{\chi}_2^0 \to e^{\pm}\mu^{\mp}) = Br(\tilde{\chi}_2^0 \to e^+\mu^-) + Br(\tilde{\chi}_2^0 \to e^-\mu^+). \tag{13.32}$$

Here θ is the mixing angle between $\tilde{e}_R$ and $\tilde{\mu}_R$ and Γ is the sleptons decay width. The parameter x is the measure of the quantum interference effect. There are some limits on $\tilde{e} - \tilde{\mu}$ mass splitting from lepton flavour violating processes but they are not very strong.

For $\kappa = 0.25$, $\kappa = 0.1$ the distributions of the number of $e^{\pm}\mu^{\mp}$ events on the invariant mass $m_{inv}(e^{\pm}\mu^{\mp})$ (see Figure 13.31) clearly demonstrates the existence of the edge structure [695], i.e. the existence of the lepton flavour violation in neutralino decays. It appears that for the point LM1 the use of an additional cut

$$m_{inv}(e^{\pm}\mu^{\mp}) < 85\,\mathrm{GeV} \tag{13.33}$$

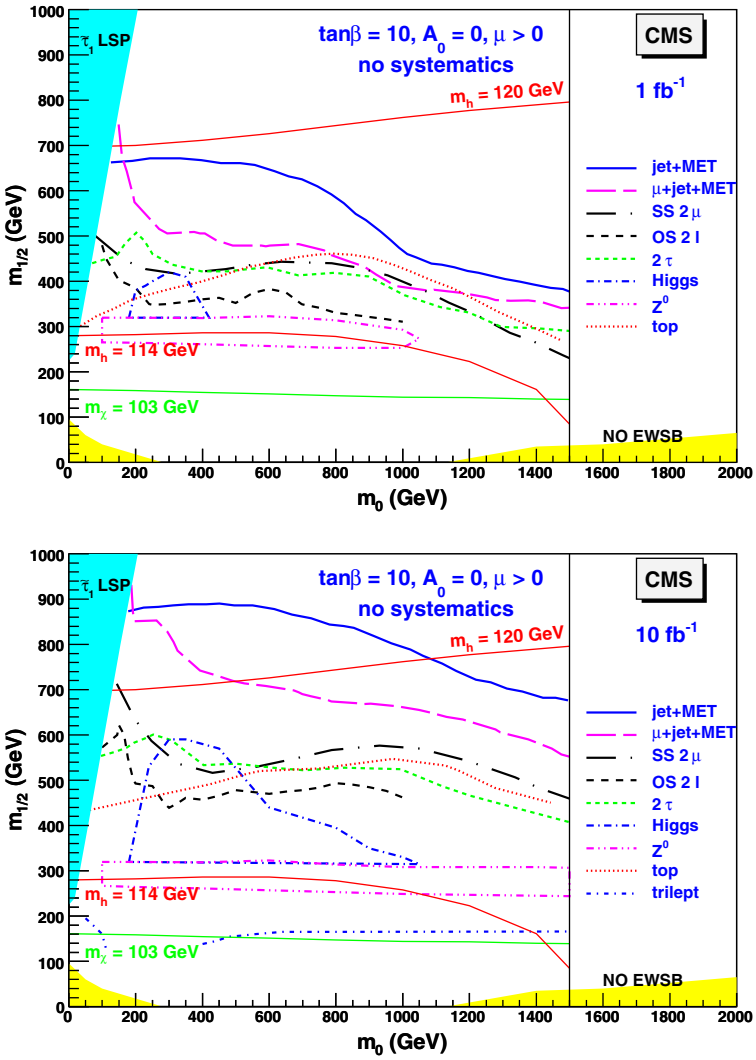

Figure 13.32. Regions of the m_0 versus $m_{1/2}$ plane showing CMS the reach when only statistical uncertainties are taken into account. (Top) for 1 fb^{-1} integrated luminosity, except the Higgs case which assumes 2 fb^{-1}. (Bottom) for 10 fb^{-1}.

reduces both the SM and SUSY backgrounds and increases the discovery potential in the LFV search. For the point LM1 we found that in the assumption of exact knowledge of the background (both the SM and SUSY backgrounds) for the integrated luminosity $\mathcal{L} = 10\,\text{fb}^{-1}$ it would be possible to detect LFV at 5σ level in $\tilde{\chi}_2^0$ decays for $\kappa \geqslant 0.04$.

13.17. Summary of the reach with inclusive analyses

13.17.1. Summary of the mSUGRA studies

In previous sections, several characteristic topologies (or signatures) for MSSM were studied and it was shown that many are already detectable with rather low integrated luminosity

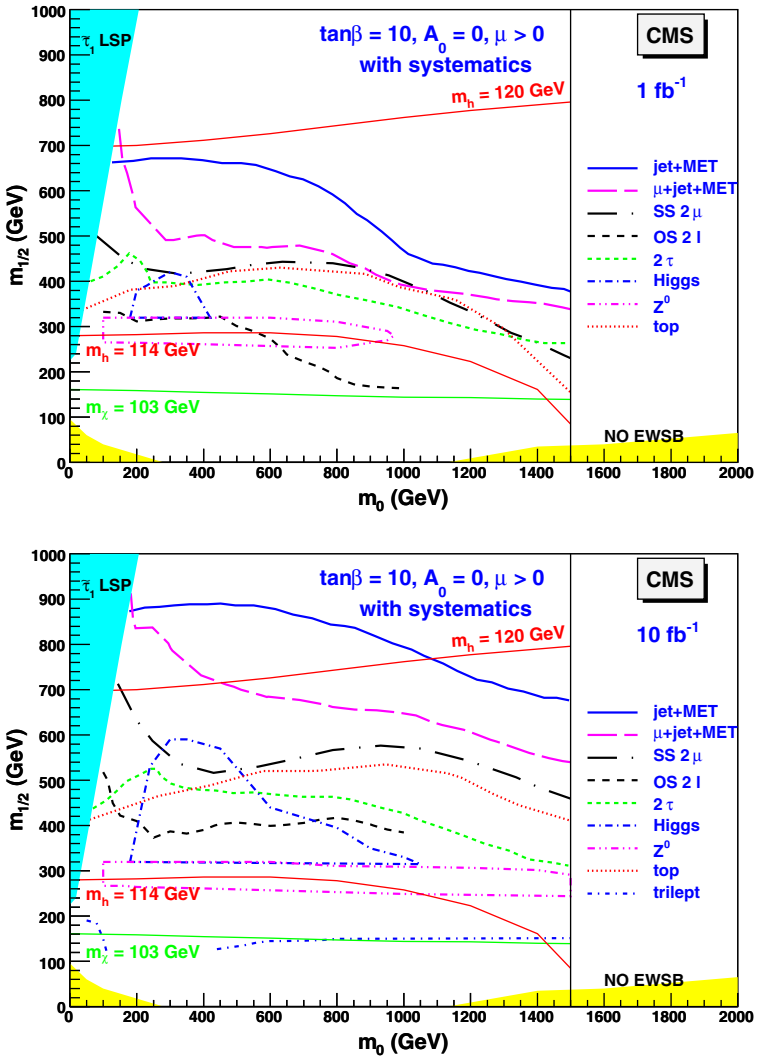

Figure 13.33. Regions of the m_0 versus $m_{1/2}$ plane showing CMS the reach when systematic uncertainties are included. (Top) for 1 fb^{-1} integrated luminosity, except the Higgs case which assumes 2 fb^{-1}. (Bottom) for 10 fb^{-1}.

(few years of LHC running) over a sizeable part of the parameter space, extending well beyond the Tevatron reach.

The curves in Fig. 13.32 summarise the reach estimated for the various topologies of the preceding sections for integrated luminosities of 1 and 10 fb^{-1} when only statistical uncertainties are taken into account. The same results are shown in Fig. 13.33 when systematic uncertainties are included. It is seen that the systematic uncertainties do not degrade the reach very much for integrated luminosities up to 10 fb^{-1}. It should be noted that the analyses have not been reoptimised for the inclusion of systematics nor for higher masses which could be reached with higher luminosity. Moreover, the reach will be further improved by the addition of topologies with electrons, which are presently missing for the muon + jet + MET and same sign dimuon searches.

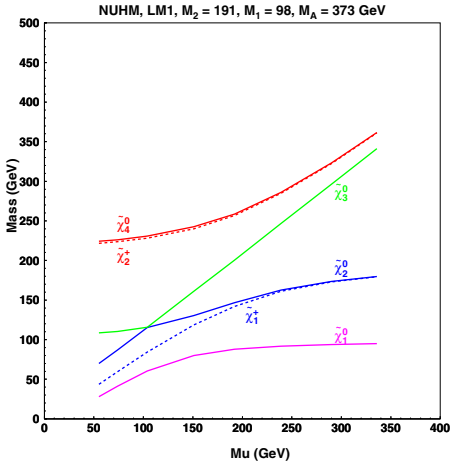

Figure 13.34. Variation of the chargino and neutralino masses as a function of μ for the CMS test point LM1.

The best reach is obtained with the most inclusive channels, the jets + MET and muons + jet + MET. The range of gluino and squark masses up to about 1.5 TeV can be probed with an integrated luminosity of only 1 fb^{-1} and is extended to about 2 TeV with 10 fb^{-1}. Moreover, a large part of the area is covered by several search topologies. The simultaneous observation of a signal in various topologies will help unravel the underlying physics. Examples are the triangular dilepton mass distribution, the observation of the Z^0 or the h^0 in less inclusive channels, which provide a hint that their origin may be the decay of a $\tilde{\chi}_2^0$. If discovered, yet more exclusive analyses should then allow a more quantitative study, e.g. the reconstruction of the sparticle masses and cross section measurements of relevant sub-processes and their ratios.

13.18. Look beyond mSUGRA

13.18.1. Non-universal Higgs masses

It was emphasised in Section 13.3 that the signatures of SUSY with a stable LSP result from the fundamental Supersymmetry gauge couplings, together with the composition of the lightest charginos and neutralinos. As all previous analyses were based on mSUGRA, it is interesting to verify their robustness when relaxing some of the assumptions which might affect the signal observability. As full generality, including giving up all universality assumptions, would lead to an intractable model, a choice needs to be made. Here, a mild extension is considered whereby the two Higgsino mass parameters at the GUT scale are no longer supposed to be degenerate with the other scalar masses, which is sometimes called the Non Universal Higgs Masses (NUHM [696]) scenario. This scenario is conveniently parameterised in terms of two low scale parameters, the mass of the CP-odd Higgs (m_A) and the parameter μ. More specifically, we will analyse the effect of lowering the value of μ compared to its mSUGRA value on the observability of the signatures, as this modifies the composition of the charginos and neutralinos as a function of the gaugino and Higgsino fields. For simplicity, m_A is kept at a fixed value. As exemplified in Fig. 13.34 for the test point LM1, lowering μ also lowers the gaugino masses and in particular their splittings, which affect the

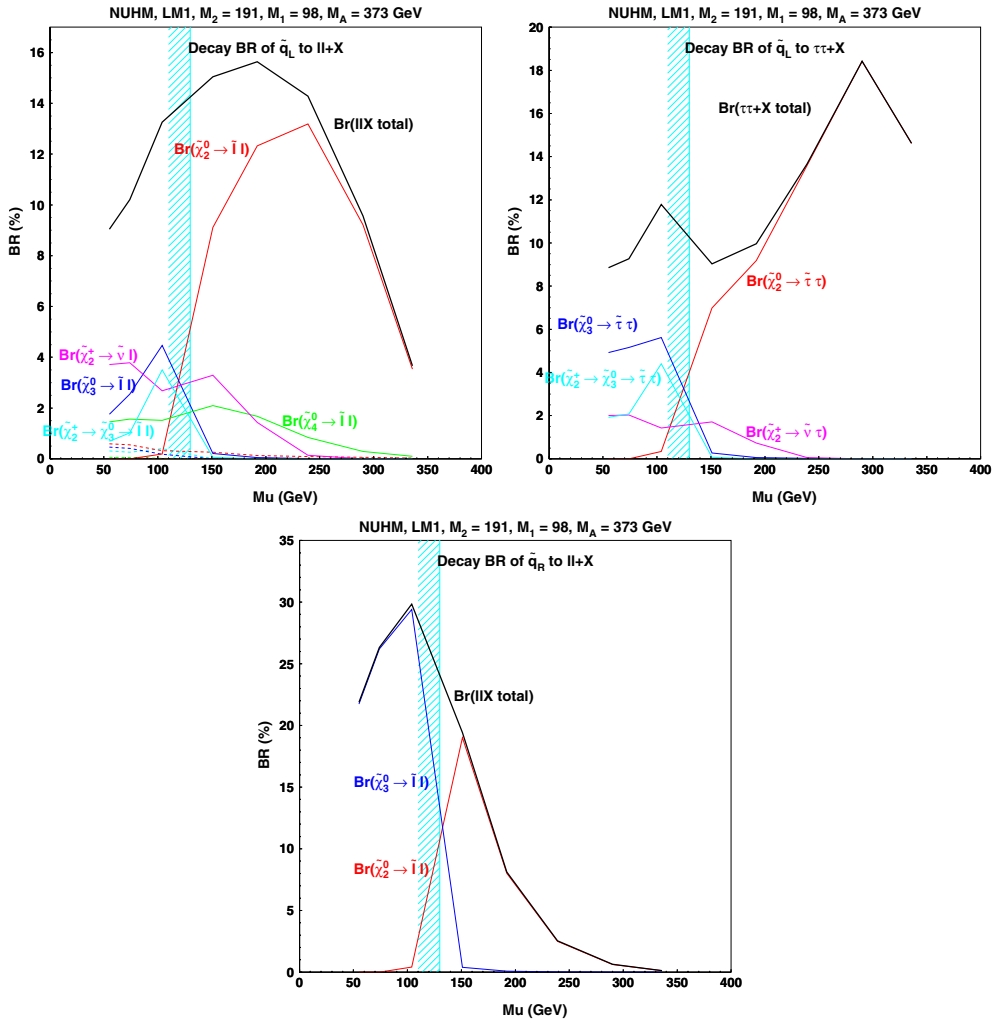

Figure 13.35. Decay branching ratios as a function of μ for $\tilde{q}_L$ into ll and $\tau\tau$ and for $\tilde{q}_R$ into ll at the test point LM1.

branching ratios through phase space effects (a similar behaviour is observed for the other test points). The $\tilde{q}$ and $\tilde{l}$ spectra are almost unaffected. As for low values of μ the lightest chargino becomes lighter than the exclusion from LEP, $m_(\tilde{\chi}_1^{\pm}) \geqslant 103\,\text{GeV}$, this region is excluded and is indicated on Fig. 13.35 by a grey (blue) shaded strip.

13.18.1.1. Signatures at point LM1. The test point LM1 was studied above for its detectability in cascade decays via a $\tilde{\chi}_2^0$ into $\tilde{l}_R l$. Figure 13.35 shows the variation of some branching ratios from the value of μ near the region where radiative electroweak symmetry breaking is not possible up to its value in mSUGRA.

It is seen that by lowering μ, $B(\tilde{q}_L \to q\tilde{\chi}_2^0 \to q\tilde{l}_R l)$ first increases (due to closing the competing decay to $\tilde{\nu}\nu$), then decreases when the $\tilde{\chi}_2^0$ becomes Higgsino-like, but it remains considerably larger than its mSUGRA value for all values of μ down to the LEP limit. In

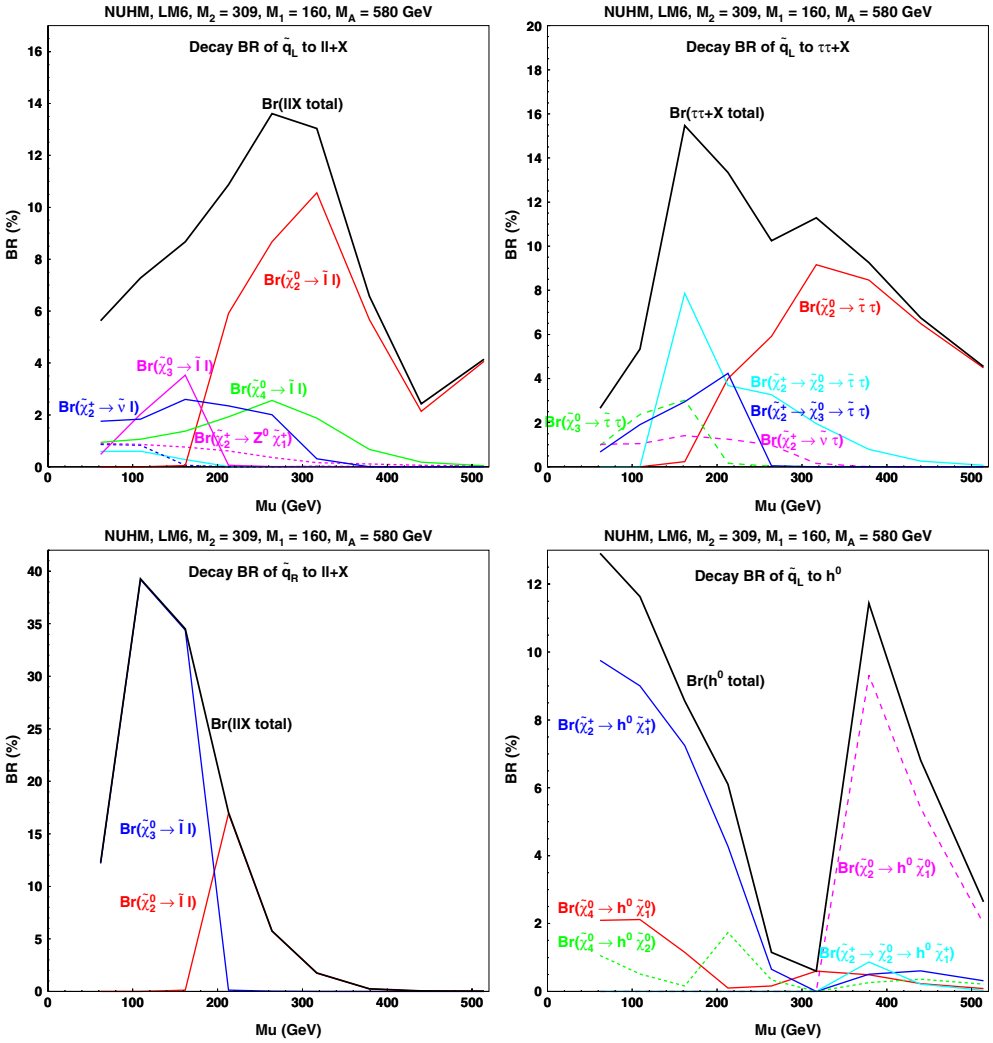

Figure 13.36. Decay branching ratios as a function of μ for $\tilde{q}_L$ into ll, $\tau\tau$ and h^0 and for $\tilde{q}_R$ into ll at the test point LM6.

addition, some new channels open up, like the decay via $\tilde{\chi}_4^0$ into left and right sleptons and the decay via a $\tilde{\chi}_2^\pm \to \tilde{\nu}_l \bar{l}$ followed by $\tilde{\nu}_l \to \tilde{\chi}_1^\pm l$ (the $\tilde{\chi}_4^0$ and $\tilde{\chi}_2^\pm$ become more Wino-like). Other decays via $\tilde{\chi}_3^0$ might also contribute, but only in the region excluded by LEP.

The branching for the decay to $\tilde{\tau}\tau$ shows qualitatively the same behaviour, but is larger than its mSUGRA value in only a small region of μ. Also here a small contribution from the decay $\tilde{\chi}_2^\pm \to \tilde{\nu}\tau$ is present at small μ.

It is interesting to note that, although for mSUGRA the $\tilde{q}_R$ decays exclusively directly to the LSP, it may have for lower μ a non negligible branching ratio to $\tilde{\chi}_2^0$ and also contributes to the dilepton signature.

Finally, there is a non-zero branching ratio for the $\tilde{q}_L$ to the light Higgs via the $\tilde{\chi}_2^\pm$ or $\tilde{\chi}_4^0$ (not shown), but it remains below 1% over the whole range of μ above the LEP limit and will be difficult to detect.

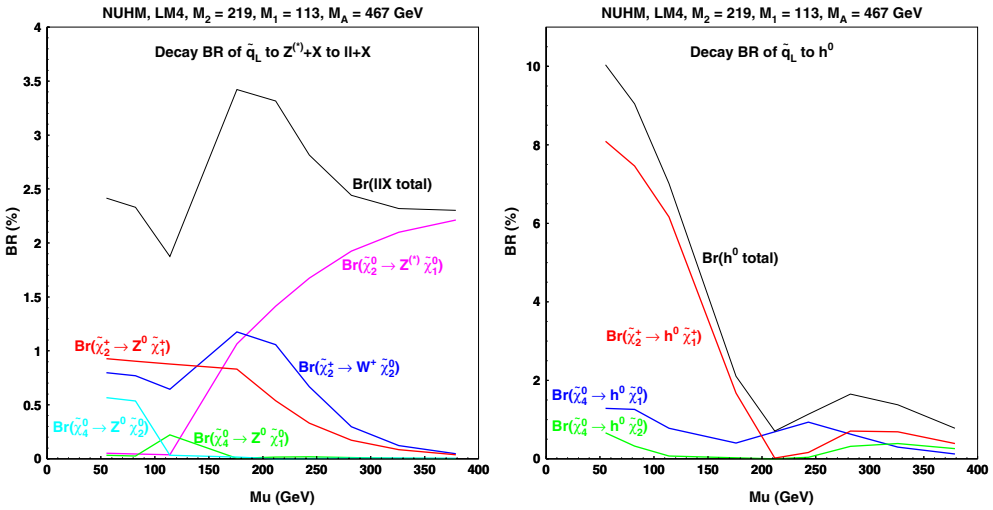

Figure 13.37. Decay branching ratios as a function of μ for $\tilde{q}_L$ into ll and h^0 at the test point LM4.

13.18.1.2. Signatures at point LM6. The test point LM6 has many features in common with LM1, but the $\tilde{\chi}_2^0$ decays mainly to $\tilde{l}_L l$ with a small admixture of $\tilde{l}_R l$. Moreover the decay $\tilde{\chi}_2^0 \to h^0 \tilde{\chi}_1^0$ is kinematically allowed, although suppressed due to the strong gaugino dominance in the $\tilde{\chi}_1^0$ and $\tilde{\chi}_2^0$. The variation of the branching ratios as a function of μ is displayed in Fig. 13.36.

The cascade decays of $\tilde{q}_L$ to $\tilde{l}l$ and $\tilde{\tau}\tau$ via $\tilde{\chi}_2^0$ show grossly the same behaviour as for LM1, with an increase at intermediate values of μ followed by a decrease at low μ. Again, the contributions from other charginos and neutralinos are non negligible near the LEP exclusion limit. Also $\tilde{q}_R$ decays contribute to the dilepton signal via $\tilde{\chi}_2^0$ and $\tilde{\chi}_3^0$ intermediate states.

A distinctive feature of LM6 is its production of final states with h^0. The $\tilde{q}_L$ branching ratio via $\tilde{\chi}_2^0 \to h^0 \tilde{\chi}_1^0$, which is only 2% for mSUGRA increases drastically for lower μ due to the increased Higgsino components in $\tilde{\chi}_1^0$ and $\tilde{\chi}_2^0$, then it drops as the decay becomes kinematically forbidden. After a gap where the branching ratio is below 1%, a strong increase is again visible for lower μ from the cascade dominated by $\tilde{\chi}_1^\pm \to h_0 \tilde{\chi}_1^\pm$ down to the LEP limit. Such an effect is not observed at LM1 due to the smaller spacing of the masses.

13.18.1.3. Signatures at point LM4. Point LM4 was chosen for its characteristic decay of $\tilde{\chi}_2^0$ into $Z^0 \tilde{\chi}_1^0$. Figure 13.37 shows the variation of the branching ratios as a function of μ.

As the decay $\tilde{\chi}_2^0 \to Z^0 \tilde{\chi}_1^0$ requires Higgsino components in both the $\tilde{\chi}_1^0$ and $\tilde{\chi}_2^0$, its branching ratio remains above 90% for all values of μ allowed by the LEP limit. The branching ratio of the $\tilde{q}_L$ into $Z^{(+)}$ via a $\tilde{\chi}_2^0$ decreases mainly due to the decrease of $B(\tilde{q}_L \to q \tilde{\chi}_2^0)$ (the $\tilde{\chi}_2^0$ becomes less gaugino-like). This loss is, however, compensated by the contributions from cascades via $\tilde{\chi}_2^\pm \to W \tilde{\chi}_2^0$ and $\tilde{\chi}_2^\pm \to Z^0 \tilde{\chi}_1^\pm$ and the overall effect is a net increase of the branching ratio of the $\tilde{q}_L$ to final states with a Z^0.

For low values of μ there is also a contribution to h^0 final states via the decay $\tilde{\chi}_2^\pm \to h^0 \tilde{\chi}_1^\pm$, but it remains small above the limit imposed by LEP.

13.18.1.4. Signatures at point LM5. At point LM5, the main signature for mSUGRA is provided by the cascade via $\tilde{\chi}_2^0 \to h^0 \tilde{\chi}_1^0$. The variation of the branching ratios with μ are shown in Fig. 13.38.

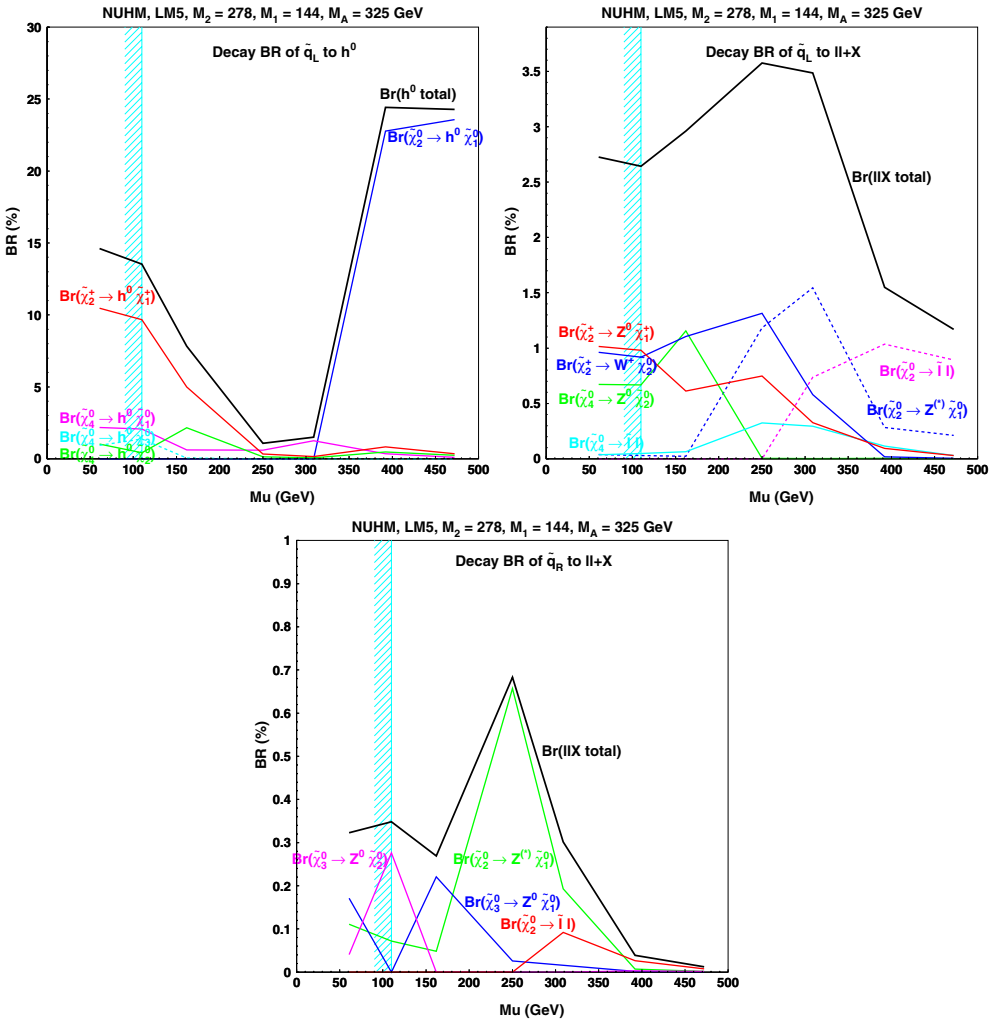

Figure 13.38. Decay branching ratios as a function of μ for $\tilde{q}_L$ into h^0 and ll and for $\tilde{q}_R$ into ll at the test point LM5.

The sharp drop in the branching ratio of $\tilde{\chi}_2^0$ to h^0 below the mSUGRA value of μ results from the decrease in the mass splitting between $\tilde{\chi}_2^0$ and $\tilde{\chi}_1^0$ which suppresses the decay to h^0. For lower values of μ, final states with h^0 are again produced mainly via the $\tilde{\chi}_2^{\pm} \to h^0 \tilde{\chi}_1^{\pm}$. In between these two decay chains, a narrow gap is left where the Higgs branching ratio is less than 2% and hence very difficult to detect.

It is seen that this loss of sensitivity to Higgs final states is to some extent compensated by an increase of the dilepton final states in the region of the gap. The cascade decays of both $\tilde{q}_L$ and $\tilde{q}_R$ contribute in this region, the main contributions being through $\tilde{\chi}_2^0 \to Z^* \tilde{\chi}_1^0$, $\tilde{\chi}_2^{\pm} \to Z^0 \tilde{\chi}_1^{\pm}$ and $\tilde{\chi}_2^{\pm} \to W \tilde{\chi}_2^0$. It gives a branching ratio of up to 3.5% for the dilepton decay of $\tilde{q}_L$ and less than 1% for $\tilde{q}_R$ and hence should be detectable. However, the mixture of intermediate states leading to the dileptons will make the sparticle mass reconstruction very challenging.

13.18.1.5. Conclusion. It can be concluded that the same flavour dilepton signatures originating from the decay of $\tilde{l}l$ or Z^* are quite robust with respect to the chargino and neutralino composition. Lowering μ with respect to its mSUGRA value, a sizeable increase of the branching ratio is even observed for the test points LM1, LM4 and LM6. The h^0 signature at point LM5 is less robust and a region with low branching ratio exists at intermediate values of μ. It is compensated by an increase of dilepton final states. It may be noted that the loss of $\tilde{\chi}_2^0$ decay to h^0 is due to the reduction of the $\tilde{\chi}_2^0$ and $\tilde{\chi}_1^0$ mass splitting. It is therefore a consequence of the low mass spectrum chosen and should disappear at larger values of $m_{1/2}$. Another feature of the NUHM scenario is that for small μ the cascades from $\tilde{q}_R$ also contribute to the signatures, unlike the mSUGRA case. Moreover the signatures at low to intermediate μ tend to be produced by several intermediate neutralino and chargino states. This points to the difficulty of identifying which sparticles are at the origin of the observed end points in the effective mass distributions.

Chapter 14. Extra Dimensions and New Vector Boson High Mass States

14.1. Introduction

The theoretical and phenomenological landscape of beyond the standard model searches extends to a multitude of exotic tendencies today in collider physics. Most are conceived within one kind or another of extra dimensions and supersymmetric scenarios. The strict or loose dualities between different frameworks for physics "beyond the Standard Model" have a direct experimental consequence: the final states and signatures of the models are very similar. This renders the characterisation of an excess or a deviation a fine and probably long challenge. To mention a couple of examples: the question "is it extra dimensions (e.g. UED/ TeV) or is it SUSY?" or "is it a Randall–Sundrum graviton mode or a Z′" is not going to be answered immediately when the excess is observed. The results from all the collider data to date, together with the as yet unobserved Higgs and including the data on the neutrino masses and the composition of the universe, impose a wide program of searches that the LHC experiments are preparing for.

In the present chapter and as well as the "alternatives" chapter that follows, a series of searches is presented with signatures (corresponding to models) as indicated below:

- Dilepton, dijet, diphoton resonances
  - ∗ using ee, $\mu\mu$, $\gamma\gamma$, dijets
  - ∗ searching for Z' (leptons, jets), RS Extra Dimensions (leptons, photons, jets), Z_{KK} in TeV^{-1} (electrons) (can also be interpreted in the context of Little Higgs models)
- Dilepton, dijet continuum modification
  - ∗ using $\mu\mu$, dijets
  - ∗ searching for ADD graviton exchange (dimuons), contact interactions (dimuons, dijets)
- Dilepton + dijets
  - ∗ using ee, $\mu\mu$ + dijets
  - ∗ searching for heavy neutrino from right-handed W (can also be interpreted in the context of leptoquark searches)
- Single photon + missing E_{T}
  - ∗ using γ + missing $\mathrm{E_T}$
  - ∗ searching for ADD direct graviton emission (can also be interpreted in the context of GMSB gravitino-type searches)
- Single lepton + missing E_{T}
  - ∗ using μ + missing $\mathrm{E_T}$
  - ∗ searching for W' (can also be interpreted in the context of little Higgs or W_{KK} excitation in TeV^{-1} models)
- Multilepton + multijet
  - ∗ using top, W and Z reconstruction and constraints
  - ∗ searching for technicolour, littlest Higgs (can also be interpreted in the context of leptoquark searches)
- Same-sign dileptons
  - ∗ using ee, $\mu\mu$, $e\mu$
  - ∗ searching for same-sign top (can be interpreted in the context of technicolour, charged Higgs or SUSY searches)

- High multiplicity/sphericity
  - searching for microscopic black holes in large extra dimensions scenarios

Although not included here, a number of searches are being developed for signatures that involve heavy highly-ionising charged particles and split-SUSY type R-hadrons as well as low P_{T} multi-lepton signatures in UED scenarios. Strategies are being developed to extract the Standard Model backgrounds from data and control its systematic uncertainties. Fake rates are being estimated as possible while machine and cosmic ray induced backgrounds are not included although methods to suppress them are being developed.

14.1.1. Models with heavy vector bosons

Additional heavy neutral gauge bosons (Z') are predicted in many superstring-inspired [87, 88] and grand unified theories (GUTs) [89], as well as in dynamical symmetry breaking [90] and "little Higgs" [91] models. There are no reliable theoretical predictions, however, of the Z' mass scale. Current lower limits on the Z' mass are (depending on the model) of the order of 600–900 $\mathrm{GeV}/\mathrm{c}^2$ [54]. The mass region up to about 1 $\mathrm{TeV}/\mathrm{c}^2$ is expected to be explored at Run II at the Tevatron [92, 93]. The LHC offers the opportunity to search for Z' bosons in a mass range significantly larger than 1 $\mathrm{TeV}/\mathrm{c}^2$. In the Z' studies presented here (Sections 14.3 and 14.2) six models which are frequently discussed and whose properties are representative of a broad class of extra gauge bosons are used:

- $\mathrm{Z}_{\mathrm{SSM}}$ within the Sequential Standard Model (SSM), which has the same couplings as the Standard Model Z^0.
- Z_ψ, $\mathrm{Z}\eta$ and Z_χ, arising in E_6 and SO(10) GUT groups with couplings to quarks and leptons as derived in Refs. [96, 97].
- $\mathrm{Z}_{\mathrm{LRM}}$ and $\mathrm{Z}_{\mathrm{ALRM}}$, arising in the framework of the so-called "left–right" [98] and "alternative left–right" [92, 93] models with couplings as derived in Ref. [92, 93], with the choice of $g_R = g_L$.

The W' search presented in Section 14.4 uses a reference model by Altarelli [697], in which the W' is a heavy copy of the W, with the very same left-handed fermionic couplings (including CKM matrix elements), while there is no interaction with the Standard Model gauge bosons or with other heavy gauge bosons such as a Z'.

14.1.2. Arkani-Hamed–Dimopoulos–Dvali (ADD) models

ADD refers to the class of models which incorporate the large extra dimensions scenario of Arkani-Hamed, Dvali, and Dimopoulos [698]. These were the first extra dimensions models in which the compactified dimensions can be of macroscopic size, consistent with all current measurements, and they are referred to as "large extra dimensions" models. In the most basic version, n extra spatial dimensions are compactified on a torus with common circumference R, and a brane is introduced which extends only in the three infinite spatial directions. Strictly speaking, the brane should have a very small tension (energy per unit volume) in order that it does not significantly warp the extra dimensional space. It is assumed that all standard model fields extend only in the brane. This can be considered as a toy version of what happens in string theory, where chiral gauge theories similar to the standard model are confined to reasonably simple brane configurations in reasonably simple string compactifications [699].

A consequence of these assumptions is that the effective 4d Planck scale is related to the underlying fundamental Planck scale of the $4+n$-dimensional theory and to the volume of

the compactified space. This relation follows from Gauss' law, or by dimensional analysis

$$M_{\text{Planck}}^2 = M_*^{2+n}\, R^n, \tag{14.1}$$

where M_{Planck}^2 is defined by Newton's constant: $M_{\text{Planck}} = 1/\sqrt{G_N} = 1.2 \times 10^{19}\,\text{GeV/c}^2$. M_*^{2+n} is defined as the gravitational coupling which appears in the $4+n$-dimensional version of the Einstein–Hilbert action. It is the quantum gravity scale of the higher dimensional theory.

If M_{Planck}, M^* and $1/R$ are all of the same order, as is usually assumed in string theory, this relation is not very interesting. But it is plausible and experimentally allowed that M^* is equal to some completely different scale. Taking $M^* \sim 1\,\text{TeV/c}^2$ [700] the hierarchy problem of the standard model is translated from an ultraviolet problem to an infrared one. Note that if there is any interface with string theory, ADD-like models must arise from string ground states in which the string scale (and thus the ultraviolet cutoff for gravity) is also in the TeV range. This is difficult to achieve but has been studied in [701].

The ADD scenario renders observations of quantum gravity at the LHC possible. In such models only the graviton, and possibly some non-SM exotics like the right-handed neutrino, probe the full bulk space. There is a Kaluza–Klein (KK) tower of graviton modes, where the massless mode is the standard 4d graviton, and the other KK modes are massive spin 2 particles which also couple to SM matter with gravitational strength.

Whereas bremsstrahlung of ordinary gravitons is a completely negligible effect at colliders, the total cross section to produce *some* massive KK graviton is volume enhanced, and effectively suppressed only by powers of M^* and not M_{Planck}. From Eq. (14.1) it follows:

$$\sigma \sim \frac{1}{M_{\text{Planck}}^2}(E\,R)^n \sim \frac{1}{M_*^2}(E\,M_*)^n, \tag{14.2}$$

where E is the characteristic energy of the subprocess.

For graviton phenomenology it is useful to replace the ADD parameter M^* by other rescaled parameters. The two most useful choices are taken from the work of Giudice, Rattazzi and Wells (GRZ) [702], and Han, Lykken and Zhang (HLZ) [703]:

$$M_*^{n+2} = \frac{S_{n-1}}{(2\pi)^n} M_s^{n+2}\,, \tag{14.3}$$

$$M_*^{n+2} = \frac{8\pi}{(2\pi)^n} M_D^{n+2}\,, \tag{14.4}$$

where M_s is the HLZ scale, M_D is the GRW scale, and S_{n-1} is the surface area of a unit n-sphere:

$$S_{n-1} = \frac{2\pi^{n/2}}{\Gamma(n/2)}\,. \tag{14.5}$$

Both notations are equivalent. To obtain a complete dictionary between ADD, GRZ and HLZ, one also needs to relate the ADD parameter R to those used by the other authors: $R = R_{\text{HLZ}} = 2\pi\, R_{GRW}$, and take note of the different notations for Newton's constant:

$$\kappa^2 = 16\pi\, G_N \text{ (HLZ)}; \quad \overline{\text{M}}_{\text{P}}^2 = \frac{1}{8\pi \text{G}_{\text{N}}} \text{ (GRW)}\,. \tag{14.6}$$

A Kaluza–Klein graviton mode has a mass specified by an n-vector of integers $\vec{k}$:

$$m^2(\vec{k}) = \frac{\vec{k}^2}{R_{\text{GRW}}^2}\,. \tag{14.7}$$

Let $r = |\vec{k}|$. Then for large r (as is often the relevant case for ADD phenomenology) the number of KK graviton states of a given polarisation with $r \leqslant r_{\max}$ is given by the integral

$$S_{n-1}\int_0^{r_{\max}} dr\, r^{n-1} = \frac{1}{n} S_{n-1}\, r_{\max}^n = \int_0^{m_{\max}} \rho(m)\, dm, \tag{14.8}$$

where the KK density of states is

$$\rho(m) = \frac{m^{n-1}}{G_N M_s^{n+2}}. \tag{14.9}$$

M_s is the natural scaling parameter for KK graviton production. The density of states formulation can be applied to a much more general class of models than ADD, and can also include graviton wavefunction factors when the extra dimensions are not flat.

Consider an on-shell production of a KK graviton from a pp or collision. To leading order this is a $2 \to 2$ process with two massless partons in the initial state, plus a massive KK graviton and a massless parton in the final state. Let p_1, p_2 denote the 4-momenta of the initial state partons, p_3 the 4-momentum of the graviton, and p_4 the 4-momentum of the outgoing parton. The total cross section for any particular variety of partonic subprocess has the form

$$\sigma(1+2 \to \mathrm{KK}+4) = \int dx_1 dx_2\; f_1(x_1,\hat{s})\, f_2(x_2,\hat{s}) \int d\hat{t} \int_0^{\sqrt{\hat{s}}} dm\, \rho(m)\, \frac{d\sigma_m}{d\hat{t}}(\hat{s},\hat{t}), \tag{14.10}$$

where $f_1(x_1,\hat{s})$, $f_2(x_2,\hat{s})$ are the parton distribution functions (PDFs) for the initial state partons, $\hat{s} = x_1 x_2 s = (p_1+p_2)^2$ is the square of the total centre of mass (cm) energy of the subprocess, and $\hat{t} = (p_1 - p_3)^2$ is the usual Mandelstam invariant. The formulae for $d\sigma_m/d\hat{t}$, the differential subprocess cross sections for KK gravitons of mass m, are given in [702].

14.1.2.1. Graviton production above the cutoff. At the LHC, proton–proton collisions will probe a distribution of partonic subprocess energies $\sqrt{\hat{s}}$. This creates a problem for the consistent analysis of missing energy signatures in the framework of ADD models. These models are simple low energy effective theories which are only valid for $\sqrt{\hat{s}}$ below some cutoff. This cutoff is at most $2M^*$, and could be a factor of a few smaller if the ultraviolet completion of the model is weakly coupled string theory [704]. The same is true for the Lykken–Randall model [705], which is a low energy description of gravity in a single infinite warped extra dimension, valid up to a cutoff $\sim M^*$. It is inconsistent to use either type of model to describe LHC collisions with subprocess energies greater than the cutoff.

This problem was first noted by the authors of [702], who suggested replacing the ADD graviton density of states $\rho(m)$ by $\rho(m)\theta(\sqrt{\hat{s}} - M_D)$, where θ is a step function. This introduces a systematic theory error into the analysis. The size of this error is very sensitive to the values of M_D and n. For initial LHC data sets, we will be probing the lower range of M_D values, beginning at the current $\simeq 1\,\mathrm{TeV/c^2}$ bounds from Tevatron and LEP. This increases the theory systematic from the cutoff for any fixed n. For fixed M_D, the theory systematic increases rapidly for increasing n. For $n = 2$, the theory uncertainty in the total cross section remains below about 20% even for M_D approaching $1\,\mathrm{TeV/c^2}$.[49] For $n = 6$ and above, the effect of the cutoff is enormous for modest values of M_D, because the rapid rise in the graviton density of states is not compensated by the rapid falloff of the pdfs. The theory error for the total cross section in this case can be as large as an order of magnitude.

[49] To avoid strong astrophysical constraints, $n = 2$ ADD models also require an *ad hoc* infrared cutoff, truncating the massive graviton spectrum for masses below about 20 MeV. This has a negligible effect on LHC analysis.

The resolution of this problem depends upon whether or not there is a signal in the missing energy channels (we will not discuss the related problems which arise in channels affected by virtual graviton exchanges). If there is a signal, the optimal procedure is to measure the observables $d^2\sigma/dp_T d\eta$ as accurately as possible, perhaps at more than one collider energy as suggested in [706, 707]. No theory systematic should be included in these analyses. Instead, one should use the data to find the best fit form for $\rho(m, \sqrt{\hat{s}})$. Simple trial forms can be obtained, for example, from multiplying the ADD density of states by the form factors obtained in models with strings [704, 708, 709] or branes [710]. For the lower range of M_D values, the sensitivity to n suggested in [706, 707] will tend to be washed out. This is not a bad outcome, since it is a result of convolving the n dependence with the effects of strings, branes or other new physics. Thus the theory systematic is replaced by likelihood fits to theories of Planck scale physics.

More problematic is the case where there is no graviton signal in a given data set. Since in this case we are trying to set a limit, we need an estimate of the theory systematic. The simplest possibility is to implement the GRW cutoff defined above, and estimate the theory error by varying the cutoff. For ADD with $n \geqslant 6$, one expects to obtain no lower bound at all on M_D, as noted in [702].

14.1.3. Virtual graviton exchange

The second class of collider signals for large extra dimensions is that of virtual graviton exchange[702, 711] in $2 \to 2$ scattering. This leads to deviations in cross sections and asymmetries in Standard Model processes with difermion final states. It may also give rise to new production processes which are not present at tree-level in the Standard Model, such as $gg \to \ell^+\ell^-$. The signature is similar to that expected in composite theories and provides a good experimental tool for searching for large extra dimensions for the case $\sqrt{s} < M_D$.

Graviton exchange is governed by the effective Lagrangian

$$\mathcal{L} = i\frac{4\lambda}{M_H^4} T_{\mu\nu} T^{\mu\nu} + \text{h.c.} \tag{14.11}$$

The amplitude is proportional to the sum over the propagators for the graviton KK tower which may be converted to an integral over the density of KK states. However, in this case, there is no specific cut-off associated with the process kinematics and the integral is divergent for $n > 1$. This introduces a sensitivity to the unknown ultraviolet physics which appears at the fundamental scale. This integral needs to be regulated and several approaches have been proposed: (i) a naive cut-off scheme [702, 711], (ii) brane fluctuations [710], or (iii) the inclusion of full weakly coupled TeV-scale string theory in the scattering process [704, 708]. The most model independent approach which does not make any assumptions as to the nature of the new physics appearing at the fundamental scale is that of the naive cut-off. Here, the cut-off is set to $M_H \neq M_D$; the exact relationship between M_H and M_D is not calculable without knowledge of the full theory. The parameter $\lambda = \pm 1$ is also usually incorporated in direct analogy with the standard parametrisation for contact interactions [123] and accounts for uncertainties associated with the ultraviolet physics. The substitution

$$\mathcal{M} \sim \frac{i^2\pi}{M_{\text{Pl}}^2} \sum_{\vec{n}=1}^{\infty} \frac{1}{s - m_{\vec{n}}^2} \to \frac{\lambda}{M_H^4} \tag{14.12}$$

is then performed in the matrix element for s-channel KK graviton exchange with corresponding replacements for t- and u-channel scattering. As above, the Planck scale suppression is removed and superseded by powers of $M_H \sim \text{TeV/c}^2$.

The resulting angular distributions for fermion pair production are quartic in $\cos\theta$ and thus provide a unique signal for spin-2 exchange.

The experimental analyses also make use of the cut-off approach. Using virtual Kaluza–Klein graviton exchange in reactions with diphoton, dibosons and dilepton final states, ($G_n \to \gamma\gamma$, VV, $\ell\ell$), the LEP and Tevatron experiments exclude exchange scales up to $\sim 1.1\,\mathrm{TeV/c^2}$.

In the dimuon studies presented here (14.3.2) with $1\,\mathrm{fb}^{-1}$ a 5-sigma effect from the virtual contributions of ADD gravitons to Drell–Yan process is observable for effective fundamental Planck scale of 4.0 TeV and for $n = 6$ extra dimensions.

14.1.4. Inverse TeV sized extra dimensions

The possibility of TeV $^{-1}$-sized extra dimensions naturally arises in braneworld theories [700]. By themselves, they do not allow for a reformulation of the hierarchy problem, but they may be incorporated into a larger structure in which this problem is solved. In these scenarios, the Standard Model fields are phenomenologically allowed to propagate in the bulk. This presents a wide variety of choices for model building: (i) all, or only some, of the Standard Model gauge fields exist in the bulk; (ii) the Higgs field may lie on the brane or in the bulk; (iii) the Standard Model fermions may be confined to the brane or to specific locales in the extra dimension. The phenomenological consequences of this scenario strongly depend on the location of the fermion fields. Unless otherwise noted, our discussion assumes that all of the Standard Model gauge fields propagate in the bulk.

The masses of the excitation states in the gauge boson KK towers depend on where the Higgs boson is located. If the Higgs field propagates in the bulk, the zero-mode state of the Higgs KK tower receives a vacuum expectation value (vev) which is responsible for the spontaneous breaking of the electroweak gauge symmetry. In this case, the resulting mass matrix for the states in the gauge boson KK towers is diagonal and the excitation masses are shifted by the mass of the gauge zero-mode, which corresponds to the Standard Model gauge field, giving

$$m_{\vec{n}} = (m_0^2 + \vec{n}\cdot\vec{n}/R_c^2)^{1/2} \tag{14.13}$$

where $\vec{n} = (n_1, n_2, \ldots)$ labels the KK excitation levels. However, if the Higgs is confined to the brane, its vev induces mixing, amongst the gauge KK states of order $(m_0 R_c)^2$. The KK mass matrix must then be diagonalised in order to determine the excitation masses. For the case of 1 extra TeV $^{-1}$-sized dimension, the coupling strength of the gauge KK states to the Standard Model fermions on the brane is $\sqrt{2}g$, where g is the corresponding Standard Model gauge coupling.

In the case where the Standard Model fermions are rigidly fixed to the brane, they do not feel the effects of the additional dimensions. For models in this class, precision electroweak data place strong constraints on the mass of the first gauge KK excitation. Contributions to electroweak observables arise from the virtual exchange of gauge KK states and a summation over the contributions from the entire KK tower must be performed. For $D > 5$, this sum is divergent. In the full higher dimensional theory, some new, as of yet unknown, physics would regularise this sum and render it finite. An example of this is given by the possibility that the brane is flexible or non-rigid, which has the effect of exponentially damping the sum over KK states. Due to our present lack of knowledge of the full underlying theory, the KK sum is usually terminated by an explicit cut-off, which provides a naive estimate of the magnitude of the effects.

Since the $D = 5$ theory is finite, it is the scenario that is most often discussed and is sometimes referred to as the 5-dimensional Standard Model (5DSM). In this case, a global

fit to the precision electroweak data including the contributions from KK gauge interactions yields $m_1 \sim R_c^{-1} \gtrsim 4\,\mathrm{TeV/c^2}$. In addition, the KK contributions to the precision observables allow for the mass of the Higgs boson to be somewhat heavier than the value obtained in the Standard Model global fit. Given the constraint on R_c from the precision data set, the gauge KK contributions to the anomalous magnetic moment of the muon are small. The first gauge KK state can be produced as a resonance at the LHC in the Drell–Yan channel provided $m_1 \lesssim 6\,\mathrm{TeV/c^2}$. In the studies presented here using the Z_{KK} in the dielectron channel a 5-sigma reach for $m_1 \sim R_c^{-1} \sim 4.97\,\mathrm{TeV/c^2}$ is obtained with $10\,\mathrm{fb}^{-1}$.

In the scenario where the Standard Model fermions are localised at specific points in the extra TeV^{-1}-sized dimensions, the fermions have narrow gaussian-like wave functions in the extra dimensions with width much smaller than R_c^{-1}. The placement of the different fermions at distinct locations in the additional dimensions, along with the narrowness of their wavefunctions, can then naturally suppress operators mediating dangerous processes such as proton decay. The exchange of gauge KK states in $2 \to 2$ scattering processes involving initial and final state fermions is sensitive to the placement of the fermions and can be used to perform a cartography of the localised fermions, i.e., measure the wavefunctions and locations of the fermions. At very large energies, it is possible that the cross section for such scattering will tend rapidly to zero since the fermions' wavefunctions will not overlap and hence they may completely miss each other in the extra dimensions.

14.1.5. Randall–Sundrum (RS) models

Randall–Sundrum refers to a class of scenarios, also known as warped extra dimensions models, originated by Lisa Randall and Raman Sundrum [94, 646]. In these scenarios there is one extra spatial dimension, and the five-dimensional geometry is "warped" by the presence of one or more branes. The branes extend infinitely in the usual three spatial dimensions, but are sufficiently thin in the warped direction that their profiles are well-approximated by delta functions in the energy regime of interest. If we ignore fluctuations of the branes, we can always choose a "Gaussian Normal" coordinate system, such that the fifth dimension is labelled y and the usual 4d spacetime by x^μ. The action for such a theory contains, at a minimum, a 5d bulk gravity piece and 4d brane pieces. The bulk piece has the 5d Einstein–Hilbert action with gravitational coupling M^3, and a 5d cosmological constant Λ. The brane pieces are proportional to the brane tensions V_i, which may be positive or negative. These act as sources for 5d gravity, contributing to the 5d stress-energy terms proportional to

$$\sum_i V_i \delta(y - y_i) \tag{14.14}$$

where the y_i are the positions of the branes. Combined with a negative Λ, this results in a curved geometry, with a 5d metric of the form:

$$\begin{aligned} &g_{\mu\nu}(x^\rho, y) = a^2(y)\, \tilde{g}_{\mu\nu}(x^\rho)\,, \\ &g_{\mu y} = 0\,, \quad g_{yy} = 1\,, \end{aligned} \tag{14.15}$$

where $a(y)$ is called the warp factor, $\tilde{g}$ is a 4d metric, and we have made a useful choice of coordinates. Warping refers to the fact that a 4d distance d_0 measured at $y = y_0$ is related to an analogous 4d distance d_1 measured at $y = y_1$ by $a(y_0)d_0 = a(y_1)d_1$. Thus in Randall–Sundrum scenarios 4d length, time, energy and mass scales vary with y.

Most collider physics phenomenology done with warped extra dimensions so far is based upon one very specific model, the original simple scenario called RSI. In this model the extra dimension is compactified to a circle of circumference $2L$, and then further orbifolded by identifying points related by $y \to -y$. The fifth dimension then consists of two periodically

identified mirror copies of a curved 5d space extending from $y = 0$ to $y = L$. It is assumed that there is a brane at $y = 0$, with positive tension V_0; it is known as the Planck brane – strong gravity resides on that brane. There is another brane at $y = L$, with negative tension V_L, known as the TeV brane–the entire 4d universe is confined to the TeV brane.

Randall and Sundrum showed that, for a tuned choice of input parameters $V_0 = -V_L = -M^2\Lambda$, the 5d Einstein equations have a simple warped solution on $0 < y < L$ with metric:

$$g_{\mu\nu}(x^\rho, y) = \mathrm{e}^{-2ky}\,\eta_{\mu\nu}\,,$$
$$g_{\mu y} = 0\,, \quad g_{yy} = 1\,, \tag{14.16}$$

where $\eta_{\mu\nu}$ is the 4d flat Minkowski metric, and $k = \sqrt{-\Lambda}$. Away from the branes, the 5d curvature is constant and negative; it is thus equivalent locally to AdS_5, with the anti-de Sitter radius of curvature given by $1/k$. At the locations of the branes the curvature is discontinuous, due to the fact that the branes are delta function sources for curvature.

The RSI model is completely described by three parameters: k, M, and L. Restricting the scenario to a low energy effective description implies considering k, $1/L \ll M$. In fact in RSI it is assumed that k is merely parametrically small compared to the 5d Planck scale M, i.e. $k \sim M/10$. The effective 4d Planck scale, which is the same as the coupling of the graviton zero mode, is given by dimensional truncation:

$$M^2_{\mathrm{Planck}} = \frac{M^3}{2k}\left(1 - \mathrm{e}^{-2kL}\right). \tag{14.17}$$

Then, within an order of magnitude, $M \sim k \sim M_{\mathrm{Planck}}$. In RSI the distance L is fixed by requiring that $a(L)M_{\mathrm{Planck}} \simeq 1\,\mathrm{TeV}$, thus $kL \sim 30$. This is *not* a large extra dimension: its inverse size is comparable to the grand unification scale.

Since the standard model fields live on the TeV brane as in ADD models, the phenomenology of RSI is concerned with the effects of the massive KK modes of the graviton. These modes as measured on the TeV brane have their mass splittings of the order of a TeV, and have TeV suppressed couplings to the standard model fields. In RSI, the Standard Model is replaced at the TeV scale by a new effective theory in which gravity is still very weak, but there are exotic heavy spin-two particles.

At the LHC the KK gravitons of RSI would be seen as difermion or dibosons resonances, since (unlike the KK gravitons of ADD) the coupling of each KK mode is only TeV suppressed [712]. The width of these resonances is controlled by the ratio $c = k/M$; the resonances become more narrow as the coupling parameter $c = k/M$ is reduced, as shown in Fig. 14.1.

The studies presented here focus on dilepton and diphoton final states while results using dijets can be found in Section 14.4.1. Note that due to the spin-2 nature of the graviton its branching ratio to diphotons is roughly twice that of a single dilepton channel.

14.2. High mass dielectron final states

This section presents the CMS experiment discovery potential for new heavy resonances, decaying into an electron pair. The $\mathrm{e^+e^-}$ decay channel provides a clean signature in the CMS detector. The presence of a heavy particle would be detected in CMS by the observation of a resonance peak in the dielectron mass spectrum over the Drell–Yan process ($\mathrm{pp} \to \gamma/\mathrm{Z} \to \mathrm{e^+e^-}$) which constitutes the main Standard Model background.

Heavy resonances with mass above $1\,\mathrm{TeV/c^2}$ are predicted by several models beyond the Standard Model. Three models are considered here: Kaluza–Klein (KK) excitations of a Z boson (TeV^{-1} model, see Section 14.1.4) and KK excitation of a graviton (Randall–Sundrum

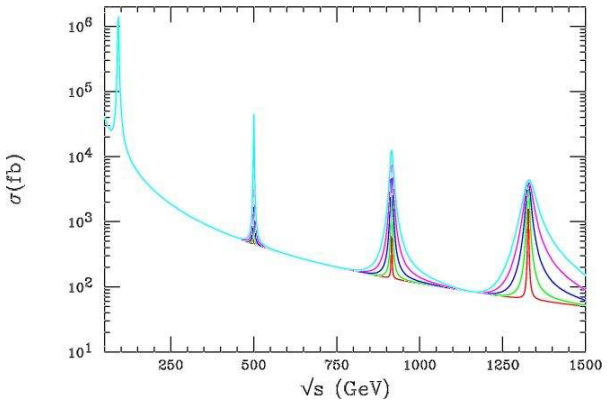

Figure 14.1. The cross section for $e^+e^- \to \mu^+\mu^-$ including the exchange of KK gravitons in the RSI model. The narrowest resonances correspond to $k/M = 0.05$, the widest to $k/M = 0.14$. (Taken from Ref. [713].)

(RS) model, see Section 14.1.5), both predicted in extra dimensions models, and neutral heavy Z' boson predicted by Grand Unified Theories (GUT) (see Section 14.1.1). For the Z' bosons, 6 models are studied, as for the $Z' \to \mu^+\mu^-$ channel [100] that is discussed in Section 14.3.

Details of the analyses presented in this section can be found in [714] and [715].

14.2.1. Event selection and correction

Two electrons are required for this analysis. They are reconstructed as super-clusters (SC) in the ECAL calorimeter in the barrel and the endcap regions [716]. For endcap SC, the energy loss in the preshower detector is taken into account. The two SC with highest energies are selected as the electron candidates.

Reducible backgrounds (like QCD jets and γ-jets) are suppressed by applying the following requirements:

- The ratio of the HCAL to ECAL energy deposits is required to be $H/E < 10$ %.
- The two SC must be isolated: the total additional transverse energy in a cone of radius $0.1 < \Delta R < 0.5$ is required to be below 2% of the SC transverse energy (where $\Delta R = \sqrt{\Delta\eta^2 + \Delta\phi^2}$).
- To identify electrons and reject neutral particles, a track is requested to be associated for each electron candidate. If a track is associated with only one of these SC, the event is however kept if it contains a third SC with $E > 300$ GeV with an associated track and satisfying the H/E and isolation cuts described above.

The selected events are then corrected for the following effects:

- Saturation correction. For very energetic electrons and photons, saturation occurs in the ECAL electronics because of the limited dynamical range of the Multi-Gain-Pre-Amplifier. The saturation threshold has been established to be at 1.7 TeV in crystals of the barrel and 3.0 TeV in the endcaps. A correction method (for barrel only) has been developed using the energy deposit in crystals surrounding the saturated crystal. The correction allows the energy deposits of clusters suffering from saturation to be estimated with a resolution of about 7% [717].

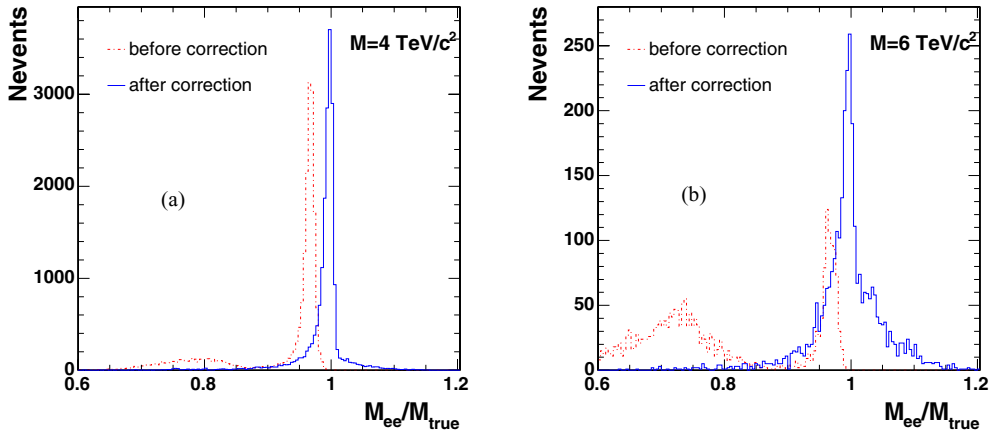

Figure 14.2. Ratio M_{ee}/M_{true} before and after corrections for KK Z boson production, for $M = 4\,\mathrm{TeV/c^2}$ (a) and $M = 6\,\mathrm{TeV/c^2}$ (b).

- Energy correction. The ECAL measured electron energy after preshower, HCAL and saturation corrections, is smaller than the generated energy. Dedicated energy correction factors for very energetic electrons have been determined using calibration files. These factors depend on both energy, η and whether saturation occurs or not. The resolution on the corrected SC energy is 0.6% at $E = 1000\,\mathrm{GeV}$.
- z-vertex distribution. The measurement in η takes into account the knowledge of the z-vertex position.
- FSR recovery. Hard photon emission from Final State Radiation can induce the detection in the event of a third energetic SC If a SC with $E > 300\,\mathrm{GeV}$ satisfying the H/E and isolation cuts is observed very close to the SC of the electron candidates ($\Delta R < 0.1$), this additional SC is associated to the corresponding electron.

14.2.2. Mass peak distributions

The resonance mass is reconstructed from the energies and angles of the 2 electron candidates, after the selection cuts and energy corrections mentioned above. Figures 14.2a and 14.2b show the ratio of the reconstructed and the true masses, M_{ee}/M_{true}, before and after energy corrections for KK Z production with $M = 4$ and $6\,\mathrm{TeV/c^2}$, respectively. The peaks at low values of M_{ee}/M_{true} correspond to events with saturated ECAL electronics. The final resolution on the resonance mass is around 0.6% for events with no saturation, and 7% in case of saturation.

Figure 14.3a presents the signal and the Drell–Yan background for KK Z boson production with $M = 4\,\mathrm{TeV/c^2}$; Fig. 14.3b for Z' boson production with $M = 1.5\,\mathrm{TeV/c^2}$; Fig. 14.3c for graviton production with $M = 1.5\,\mathrm{TeV/c^2}$ and coupling parameter, defined in Section 14.1.5, $c = 0.01$.

14.2.3. Discovery potential of CMS

The discovery potential of a new physics resonance is determined using the likelihood estimator S_{cL} (defined in Appendix A.1) based on event counting, suited for small event samples. The discovery limit is defined by $S_{cL} > 5$.

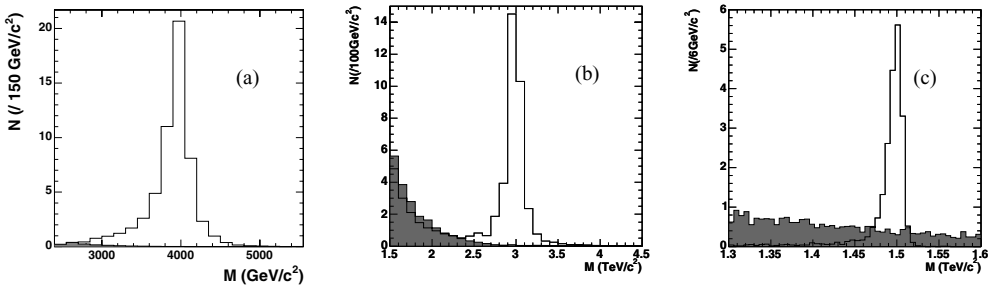

Figure 14.3. Resonance signal (white histograms) and Drell–Yan background (shaded histograms) for KK Z boson production with $M = 4.0\,\mathrm{TeV/c^2}$ (a), SSM Z' boson production with $M = 3.0\,\mathrm{TeV/c^2}$ (b), and graviton production with $M = 1.5\,\mathrm{TeV/c^2}$, coupling parameter $c = 0.01$ (c), for an integrated luminosity of $30\,\mathrm{fb^{-1}}$.

Table 14.1. Number of events for resonant signal, N_s, and for Drell–Yan background, N_b, and corresponding significances S_{cL} for an integrated luminosity of $30\,\mathrm{fb^{-1}}$. The masses M and the mass windows M_w are in $\mathrm{TeV/c^2}$.

	KK Z		G, $c = 0.01$	G, $c = 0.1$	SSM Z'	
M	4.0	6.0	1.5	3.5	1.0	5.0
M_w	3.5–4.5	5.0–6.7	1.47–1.52	3.30–3.65	0.92–1.07	4.18–5.81
N_s	50.6	1.05	18.8	7.30	72020	0.58
N_b	0.13	0.005	4.16	0.121	85.5	0.025
S	22.5	3.0	6.39	6.83	225	1.63

The number of signal and background events, N_s and N_b, computed for a given mass window around the peak, are presented in Table 14.1 for the three models, together with the corresponding significance, for an integrated luminosity of $30\,\mathrm{fb^{-1}}$.

The 5σ discovery limits as a function of mass are given in Fig. 14.4a and Fig. 14.4b, for KK Z boson production and Z' production (for the 6 considered models), respectively. In the graviton case, the 5σ discovery plane as a function of the coupling parameter c and the resonance mass is given in Fig. 14.4c.

For KK Z bosons, a 5σ discovery can be achieved for a resonance mass up to $M = 4.97\,\mathrm{TeV/c^2}$ for an integrated luminosity of $10\,\mathrm{fb^{-1}}$, $M = 5.53\,\mathrm{TeV/c^2}$ for $30\,\mathrm{fb^{-1}}$ and $M = 5.88\,\mathrm{TeV/c^2}$ for $60\,\mathrm{fb^{-1}}$. For gravitons, with an integrated luminosity of $30\,\mathrm{fb^{-1}}$, a 5σ discovery can be extracted for masses up to $1.64\,\mathrm{TeV/c^2}$ for $c = 0.01$ and up to $3.81\,\mathrm{TeV/c^2}$ for $c = 0.1$. For Z' boson production, with an integrated luminosity of $30\,\mathrm{fb^{-1}}$, a 5σ discovery can be extracted for masses up to $3.31\,\mathrm{TeV/c^2}$ for model ψ and up to $4.27\,\mathrm{TeV/c^2}$ for model ARLM. The 5σ discovery limits on the resonance masses for 10, 30 and $60\,\mathrm{fb^{-1}}$ are summarised in Table 14.2.

For KK Z boson production, the luminosities needed for a five σ discovery are 1.5, 4.0, 10.8, 29.4, and $81.4\,\mathrm{fb^{-1}}$ for $M = 4.0$, 4.5, 5.0, 5.5 and $6.0\,\mathrm{TeV/c^2}$, respectively; for SSM Z' boson production, they are 0.015, 3.0 and $260\,\mathrm{fb^{-1}}$ for $M = 1$, 3 and $5\,\mathrm{TeV/c^2}$; for graviton production, most of the interesting region of the (mass, coupling) plane is already covered with $10\,\mathrm{fb^{-1}}$.

For KK Z and Z' production, a K factor of 1 was conservatively taken for both the signal and the Drell–Yan background, since heavy Z production interferes with Z/γ Drell–Yan production. For the graviton analysis, as little interference is present with the Standard Model

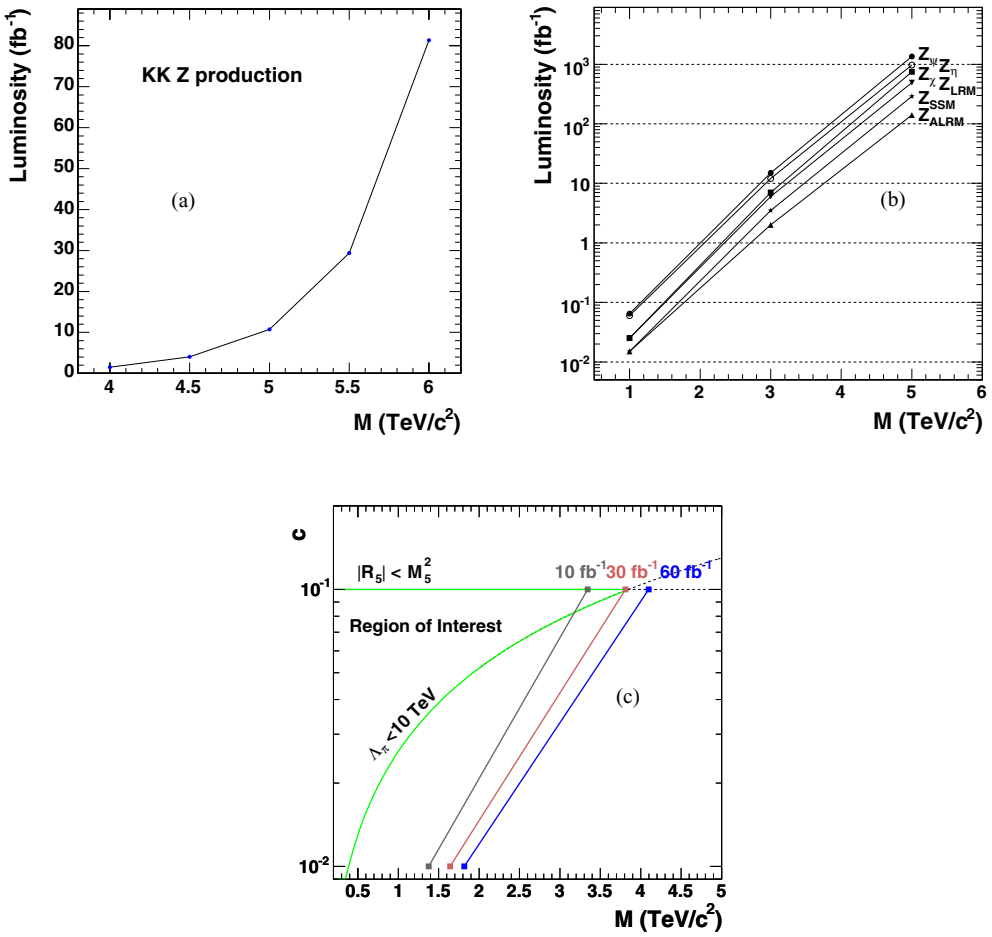

Figure 14.4. Five σ discovery limit as a function of the resonance mass for KK Z boson production (a), for the 6 Z' models (b); five σ discovery plane for graviton production as a function of the coupling parameter c and the graviton mass (c).

Table 14.2. The 5σ discovery limit on the resonance mass (given in TeV/c^2) for the three models, for an integrated luminosity of 10, 30 and 60 fb^{-1}.

Model	Luminosity (fb^{-1})		
	10	30	60
KK Z	4.97	5.53	5.88
G ($c = 0.01$)	1.38	1.64	1.82
G ($c = 0.1$)	3.34	3.81	4.10
Z' (ψ)	2.85	3.31	3.62
Z' (ALRM)	3.76	4.27	4.60

processes, a K factor of 1.0 is used for the signal and of 1.3 for the Drell–Yan background, in order to take into account the higher order terms in the cross section. The latter number comes from the CDF analysis [718] and is compatible with the K factor obtained from theoretical computations [348].

14.2.4. Systematic uncertainties

The uncertainty coming from the choice of the parton distribution function (PDF) was investigated using the set of 20 positive and 20 negative errors, of the CETQ6.1M "best fit" parametrisation [12, 719, 720]. For each event, a weight factor is computed according to the x_1, x_2, and Q^2 variables, for each of the 40 PDF errors, in the case of graviton production with $M = 1.5\,\mathrm{TeV/c^2}$ ($c = 0.01$) and $M = 3.5\,\mathrm{TeV/c^2}$ ($c = 0.1$). The uncertainties on the PDF modify the number of signal events by a factor 1.20 (positive deviations) and 0.86 (negative deviations) for $M = 1.5\,\mathrm{TeV/c^2}$ ($c = 0.01$). The corresponding numbers for $M = 3.5\,\mathrm{TeV/c^2}$ ($c = 0.1$) are 1.47 and 0.78. For the Drell–Yan background, the re-weighting effects on the numbers of events are 1.07 and 0.94 for masses around $1.5\,\mathrm{TeV/c^2}$, and 1.19 and 0.88 for masses around $3.5\,\mathrm{TeV/c^2}$. For an integrated luminosity of $30\,\mathrm{fb^{-1}}$, the significances with the "best fit" and with the positive/negative deviations are equal respectively to 6.40 and 7.25/5.78 for $M = 1.5\,\mathrm{TeV/c^2}$, and to 6.83 and 8.54/5.93 for $M = 3.5\,\mathrm{TeV/c^2}$. The main effect of the variation comes from the gluon-fusion contribution to the graviton production cross section. A lower dependence is observed for the KK Z and Z' channels, which are produced by quark-anti-quark annihilation. For KK Z boson production at $M = 4\,\mathrm{TeV/c^2}$ with an integrated luminosity of $30\,\mathrm{fb^{-1}}$, the significances with the "best fit" and with the positive/negative errors are equal respectively to 22.5 and 23.3/21.9.

Changing to 1 the value of the K factor of the Drell–Yan background for RS graviton production increases the significance from 6.39 to 6.87 ($M = 1.5\,\mathrm{TeV/c^2}$, $c = 0.01$) and from 6.83 to 7.09 ($M = 3.5\,\mathrm{TeV/c^2}$, $c = 0.1$). The discovery limits increase respectively from 1.64 to $1.68\,\mathrm{TeV/c^2}$ and from 3.81 to $3.84\,\mathrm{TeV/c^2}$.

The data themselves will be used to estimate and cross-check the Drell–Yan background at very high energy. For resonance discovery, the number of events in the side-bands of the resonance and their mass dependence will be used to estimate the number of background events under the resonance peak, provided there is enough data in the side-bands. In this approach, the uncertainties on the background cross-sections, the PDF and the luminosity measurement are highly reduced.

14.2.5. Identification of new particles

Once a resonance is found, information will be gained on its characterisation from the study of other decay channels, like $\gamma\gamma$ (see Section 14.6), of angular distributions and of asymmetries, in view of the spin determination (see also Section 14.3).

As an example, RS gravitons with spin 2 can be distinguished from the Standard Model background and Z' bosons with spin 1 using the distribution of the $\cos\theta^*$ variable, computed as the cosine of the polar angle between the electron and the boost direction of the heavy particle in the latter rest frame. In addition to the cuts defined above, the electron and positron candidates are requested to have opposite charges, in order to identify the electron, from which the $\cos\theta^*$ variable is computed.

The $\cos\theta^*$ distributions for graviton production with $M = 1.25\,\mathrm{TeV/c^2}$, $c = 0.01$ and $M = 2.5\,\mathrm{TeV/c^2}$, $c = 0.1$, are presented in Fig. 14.5, for an integrated luminosity of $100\,\mathrm{fb^{-1}}$. The error bars represent the corresponding statistical uncertainties, applied to the signal distribution obtained from a large statistics simulation. The spin-2 hypothesis is compared to the spin-1 hypothesis (dashed red curve in the figures), formed by the Drell–Yan production (Figs. 14.5a and 14.5b) or the ALRM Z' production (Figs. 14.5c and 14.5d). For graviton production, the expected background is included in the $\cos\theta^*$ distributions.

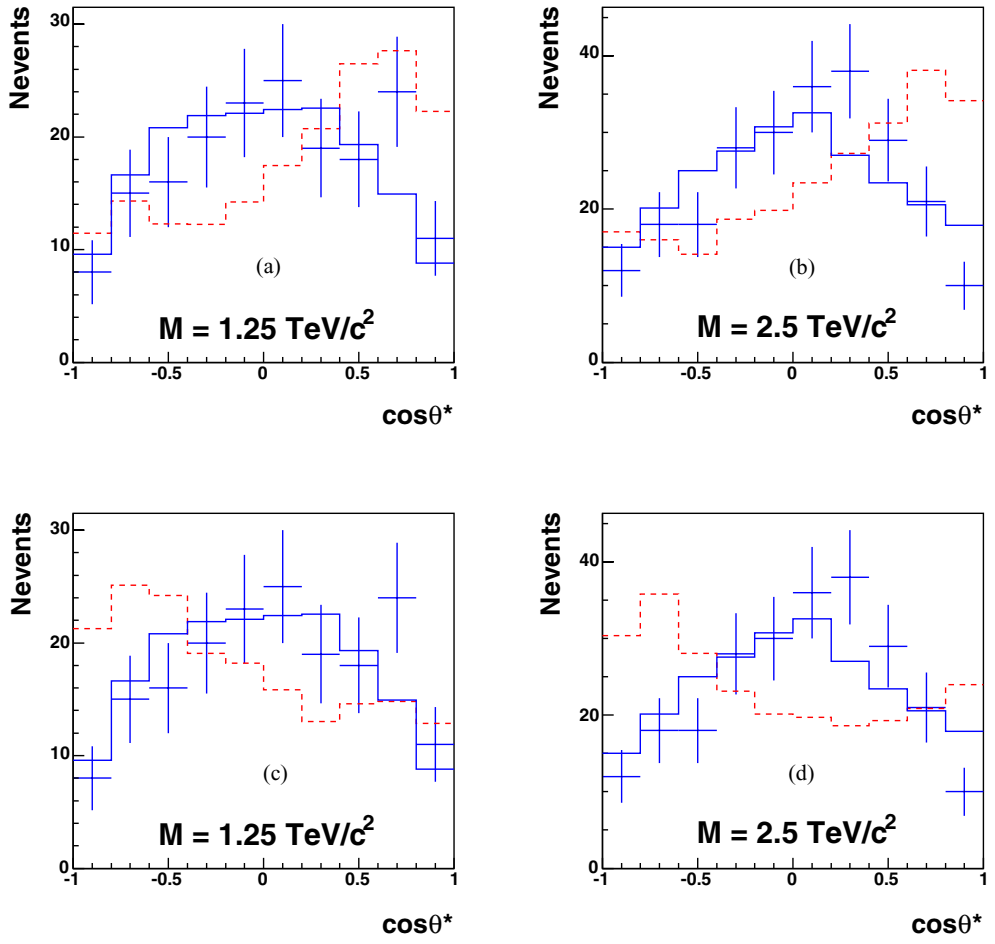

Figure 14.5. Distributions of $\cos\theta^*$ for graviton production (full blue curves) and for Drell–Yan production (dashed red curves) normalised to the signal, for $M = 1.25\,\mathrm{TeV/c^2}$ (a) and $2.5\,\mathrm{TeV/c^2}$ (b), and for Z' boson (ALRM model) (dashed red curves), normalised to the signal, for $M = 1.25\,\mathrm{TeV/c^2}$ (c) and $2.5\,\mathrm{TeV/c^2}$ (d), with an integrated luminosity of $100\,\mathrm{fb}^{-1}$. The error bars represent the "1-experiment" distribution for the graviton production. The expected background is included in the $\cos\theta^*$ distributions.

The spin 2 nature of RS gravitons can be determined in contrast to the Drell–Yan production or the Z' boson production for an integrated luminosity of $100\,\mathrm{fb}^{-1}$ up to $1.25\,\mathrm{TeV/c^2}$ for $c = 0.01$ and $2.5\,\mathrm{TeV/c^2}$ for $c = 0.1$.

14.3. High mass dimuon final states

Many scenarios beyond the Standard Model are expected to manifest themselves through modifications in the mass spectrum of high-mass dimuon pairs. The potential of the CMS experiment to discover dimuon decays of a new heavy neutral gauge boson, Z′, is discussed in Section 3.3.4; the discovery reach for a representative set of Z′ models was found to be in the range between 2.9 and $3.8\,\mathrm{TeV/c^2}$ for an integrated luminosity of $10\,\mathrm{fb}^{-1}$. In this section, we discuss the observability of $\mu^+\mu^-$ final states predicted in two classes of

large extra dimensions models, RS and ADD. While the RS scenario gives rise to relatively narrow resonances, the ADD model is expected to be observed via non-resonant modifications of the dimuon spectrum; therefore, these two searches require somewhat different experimental approaches. The search for compositeness in the dimuon channel is described in Section 15.2.

Once a new physics is discovered, observables other than dimuon invariant mass can be used to determine the theoretical framework to which it belongs. The measurement of the forward-backward asymmetries of leptonic decay products has long been known as a powerful tool to identify Z′; some aspects of such a measurement at the LHC are discussed in Section 3.3.5. Spin discrimination of new heavy resonances based on an unbinned likelihood ratio statistic incorporating the angles of the decay products is described in Section 3.3.6.

14.3.1. The Randall–Sundrum model in the dimuon channel

We consider the range of RS1 graviton masses in the range $1 < m < 4\,\mathrm{TeV/c^2}$ and the dimensionless coupling constant in the expected theoretical range $0.01 \leqslant c \leqslant 0.1$ [721]. A full simulation with PYTHIA [69] version 6.227 and with the GEANT4-based CMS program [8] and reconstruction with the CMS full-reconstruction package [10], including pile-up of minimum-bias collisions is carried out. We derive both the CMS discovery potential for Randall–Sundrum gravitons and the performance of spin determination in this channel (see details in Ref. [117]). The non-reducible backgrounds are the Drell–Yan process, vector boson pair production ZZ, WZ, WW, $t\bar{t}$ production, etc. In the SM the expected leading-order cross section of the Drell–Yan process dominates the other contributions (see the Section 9.2 for details). The trigger simulation is based on the reconstruction package, using the on-line reconstruction algorithm. We require the single or double muon trigger, no requirement for calorimeter isolation of high-p_{T} muons is made. The total trigger + reconstruction efficiency varies between 95% and 90% for dimuons in the mass range $1 < m < 4\,\mathrm{TeV/c^2}$. Only the events which passed both the Level-1 and HLT cuts are selected. Note that the trigger efficiency is significantly decreased after applying of the calorimeter isolation cuts (down to 15%). This drop is caused by electromagnetic showers accompanying high-energy muons. In the following, no cuts on calorimeter isolation of muon tracks are applied at the HLT level.

14.3.1.1. The Randall–Sundrum model discovery potential. The significance estimators used for studying the discovery potential of the RS1 model were S_{cP}, S_{cL} and S_L, defined in Appendix A.1 (see discussion of S_L in Section 3.3.4.1).

Figure 14.6a shows the integrated luminosity required for a 5σ discovery as a function of the dimuon mass. The results for different values of integrated luminosity are summarised in Table 14.3 and Fig. 14.6b. The CMS experiment can observe a RS1 graviton with mass up to $2.3\,\mathrm{TeV/c^2}$ with an integrated luminosity of $\int L\,dt = 1\,\mathrm{fb}^{-1}$ if the coupling c is equal to 0.1. For $c = 0.01$ the mass reach does not exceed $1.9\,\mathrm{TeV/c^2}$, even for the asymptotic regime of LHC operation with $\int \mathcal{L}\,dt = 300\,\mathrm{fb}^{-1}$. The asymptotic reach limit for $c = 0.1$ is $4.5\,\mathrm{TeV/c^2}$.

A combined analysis [721] in the RS1 scenario shows that the value of the coupling constant c is strongly restricted (Fig. 14.6b) due to the theoretical constraints to assure that the model does not introduce a new hierarchy (the scale parameter $\Lambda_\pi = M_{Pl}e^{kL} < 10\,\mathrm{TeV/c^2}$ with the symbols defined in Section 14.1.5). The direct comparison of results on a mass reach region for c with the data of the Fig. 14.6 shows that a luminosity of $100\,\mathrm{fb}^{-1}$ is needed to test the RS1 model everywhere in ($c - M_{\mathrm{grav}}$) space of model parameters. However, these conclusions are not definitive since the initial theoretical constraints are quite arbitrary.

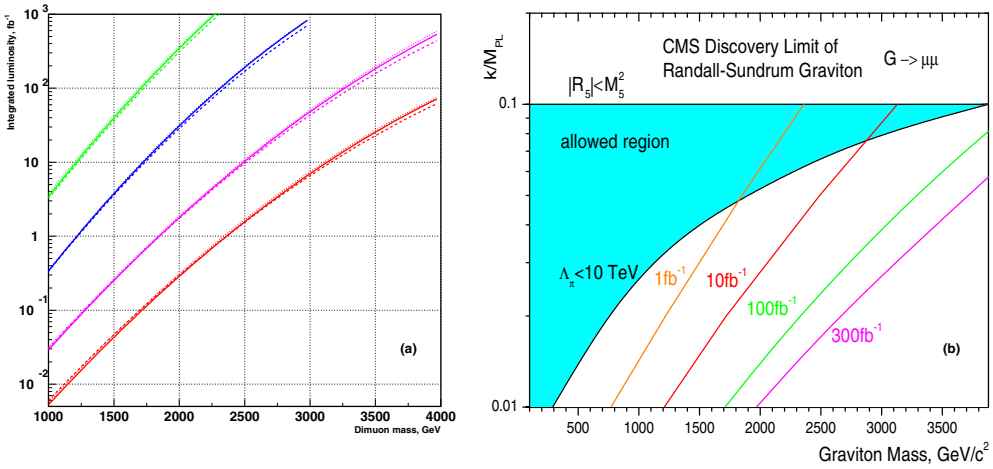

Figure 14.6. (a) Discovery limit for RS1 graviton with $\mu^+\mu^-$ decay mode for different values of RS1 coupling constant $c = 0.01$, 0.02, 0.05 and 0.1 (from top to bottom). Used discovery limit $S > 5$ for the S_{cP} estimator (solid lines), S_L (dashed lines), S_{cL} (dotted lines). (b) Reach of the CMS experiment as a function of the coupling parameter c and the graviton mass for various values of integrated luminosity. The left part of each curve is the region where significance exceeds 5σ.

Table 14.3. CMS discovery potential invariant mass reach (in TeV) to observe the RS1 graviton in $\mu^+\mu^-$ channel.

Coupling constant c	Estimator	1 fb^{-1}	10 fb^{-1}	100 fb^{-1}	300 fb^{-1}
	S_{cP}	0.75	1.20	1.69	1.95
0.01	S_{cL}	0.77	1.21	1.71	1.97
	S_L	0.78	1.23	1.73	1.99
	S_{cP}	1.21	1.72	2.30	2.63
0.02	S_{cL}	1.22	1.72	2.31	2.64
	S_L	1.22	1.74	2.34	2.68
	S_{cP}	1.83	2.48	3.24	3.67
0.05	S_{cL}	1.85	2.49	3.26	3.71
	S_L	1.85	2.51	3.31	3.79
	S_{cP}	2.34	3.11	4.12	4.52
0.1	S_{cL}	2.36	3.13	4.14	4.54
	S_L	2.36	3.16	4.23	4.73

14.3.1.2. Systematic uncertainties. The results taking into account the systematic uncertainties are shown in Fig. 14.7. The expected effects of misalignment are considered in two misalignment scenarios: the First Data and the Long Term scenarios [99], which correspond to different stages of the alignment corrections for the positions of the tracker and muon chambers. The current estimate is that the transition to the Long Term scenario can be achieved at an integrated luminosity of about 1 fb^{-1} [86]. In contrast to Fig. 14.6 which assumed a K-factor equal to unity, a K-factor of $K = 1.30 \pm 0.05$ is used both for the RS1 signal and Drell–Yan background. Additional variations due to EW corrections, hard-scale and PDF uncertainties have been considered, the details being found in Ref. [117].

14.3.1.3. Spin discrimination in angular analysis. A study of muon angular distributions allows a discrimination between the hypotheses of Graviton (spin-2 particle) and Z' (spin-1 particle) – see the discussion and the results in Section 3.3.6.

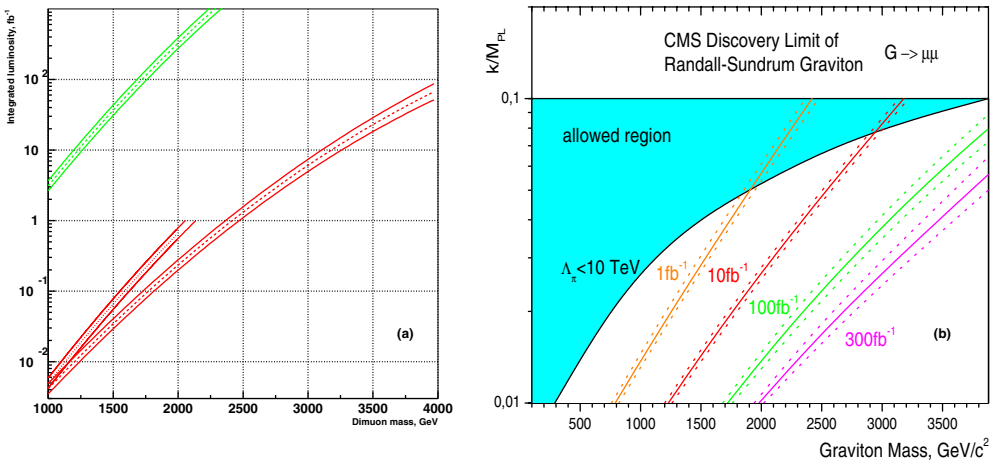

Figure 14.7. (a) Discovery limit for coupling constants $c = 0.01$, 0.1 (upper and lower curves, respectively) after taking into account the systematic uncertainties including misalignment in two scenarios: the curves ending at integrated luminosity of $1\,\text{fb}^{-1}$ correspond the First Data misalignment scenario, the other ones correspond to the Long Term scenario. The ranges show the expected variations due to the systematic uncertainties. (b) The ranges of the expected variations due to the systematic uncertainties for the mass reach of the CMS experiment.

14.3.2. The ADD model in the dimuon channel

We consider the fundamental Planck scale of the ADD model in the range of $3.0 < M_S < 10.0\,\text{TeV/c}^2$ and numbers of extra dimensions in the range of $3 \leqslant n \leqslant 6$ [698]. The contribution of KK-modes of ADD gravitons to the Drell–Yan processes is computed using the leading-order matrix element [722] which was implemented in STAGEN generator collection as external matrix element in PYTHIA [69] version 6.227. A full simulation [8] of the CMS detector and reconstruction [10], without a pile-up of minimum-bias collision is performed to derive the CMS discovery potential for ADD virtual gravitons (see details in Ref. [723]). The non-reducible backgrounds are the Drell–Yan process, vector boson pair production ZZ, WZ, WW, $t\bar{t}$ production, etc. In the SM the expected leading-order cross section of the Drell–Yan process dominates the other contributions (see Section 9.2 for details). The trigger simulation is realised in the reconstruction package, using the on-line reconstruction algorithm. A single or double muon trigger is required, but no requirement for calorimeter isolation of high-p_T muons is made. The total trigger + reconstruction efficiency varies between 70% and 90% for dimuons dependent on the model parameters. Only the events which passed both the Level-1 and HLT cuts are selected.

14.3.2.1. The ADD discovery limit. The CMS discovery potential was estimated using as significance S_{cP} and S_{cL}, defined in Appendix A.1. The computed significance values for the ideal detector as a function of a fundamental theory scale, M_S, are presented in Fig. 41.8 for integrated luminosities of 0.1, 1.0, 10, 100, 300, $1000\,\text{fb}^{-1}$. The main observations are:

- $\int \mathcal{L}\text{d}t = 1\,\text{fb}^{-1}$, even a low luminosity regime allows us to measure the effect from the virtual contributions of ADD gravitons to Drell–Yan process for an effective fundamental Planck scale up to 4.0 TeV for the most unfavourable case with $n = 6$. For a scenario where the number of extra dimensions is $n = 3$ the reach limit is extended to 5.8 TeV.
- $\int \mathcal{L}\text{d}t = 10\,\text{fb}^{-1}$, M_S values of 4.8 and 7.2 TeV can be reached for $n = 3$ and $n = 6$ respectively.

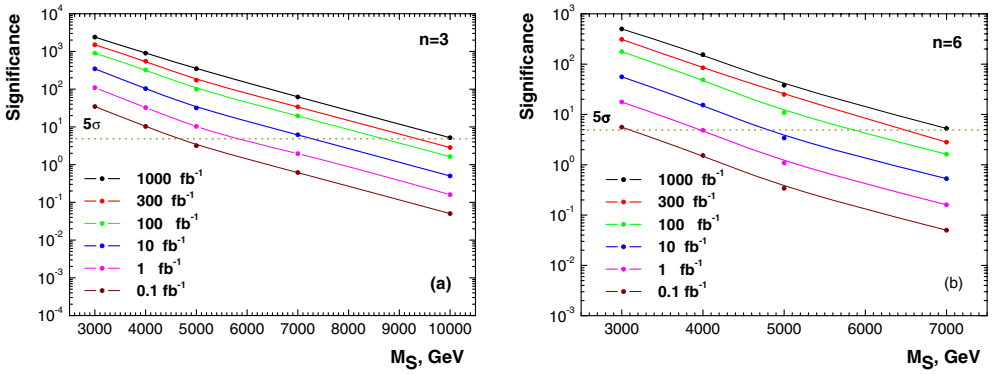

Figure 14.8. Significance as a function of M_S for (a) $n = 3$ and (b) $n = 6$.

- $\int \mathcal{L}dt = 100\,\text{fb}^{-1}$, for LHC operation in a high luminosity regime allow the observation of the ADD signal at $5.8 \div 8.7$ TeV of model scale dependent on a number of extra dimensions.
- $\int \mathcal{L}dt = 300\,\text{fb}^{-1}$, in the asymptotic regime the CMS sensitivity to fundamental Planck scale is increased to values of $6.5 \div 9.3$ TeV.

14.3.2.2. Systematics. The results taking into account the systematical uncertainties with the S_{cP} estimator are shown in Fig. 14.8. To take into account the misalignment effect two scenario of misalignment were considered during reconstruction procedure: *First Data* scenario [99] for 0.1 and $1.0\,\text{fb}^{-1}$ and *Long Term* scenario [99] for 10, 100, 300, $1000\,\text{fb}^{-1}$. The K-factor of $K = 1.30 \pm 0.05$ is used both for ADD signal and Drell–Yan background. Additional variations due to hard-scale and PDF uncertainties as well as trigger and selection uncertainties have been considered, the details being given in Ref. [723].

14.4. High energy single lepton final states

14.4.1. Introduction

Several theoretical models predict, in addition to the well known electroweak vector bosons γ, W, Z, further heavy gauge bosons. These additional particles are postulated for example in Left–Right Symmetric Models [724–727], based on the gauge group $\text{SU(3)}_\text{C} \times \text{SU(2)}_\text{L} \times \text{SU(2)}_\text{R} \times \text{U(1)}_{\text{B}-\text{L}}$ (B, L: baryon-, lepton-number) in theories predicting a substructure of the known "elementary particles", and in Little Higgs Models [91].

Here we investigate the detection capabilities for a hypothetical heavy partner of the W, a charged spin-1 boson W'. We do not assume one of the specific models mentioned above, but derive the W' properties from the Reference Model by Altarelli [697], which has been used in several earlier experiments, so that the resulting limits can be compared easily. In this Reference Model the W' is a carbon copy of the W, with the very same left-handed fermionic couplings (including CKM matrix elements), while there is no interaction with the Standard Model gauge bosons or with other heavy gauge bosons as a Z'. Thus the W' decay modes and corresponding branching fractions are similar to those for the W, with the notable exception of the $\text{t}\bar{\text{b}}$ channel, which opens for W' masses beyond 180 GeV.

In hadron collisions W' bosons can be created through $q\bar{q}$ annihilation, in analogy to W production. Previous searches for the Reference W' at LEP and at the Tevatron give rise to lower bounds approaching 1 TeV [728].

This analysis is based on the decay $W' \to \mu\nu$, with a branching ratio of roughly 10%. The resulting signature of a high energy muon accompanied by missing energy allows an easy separation of signal and background reactions. More details are found in [729].

14.4.2. Data samples

For this study we assume an integrated luminosity of $10\,\text{fb}^{-1}$ and an average instantaneous luminosity of $\mathcal{L} = 2 \times 10^{33}\,\text{cm}^{-2}\,\text{s}^{-1}$ corresponding to an average pile-up of 3.5 pp-collisions per bunch crossing.

Reference Model W' events decaying into muon and neutrino have been generated with PYTHIA v6.227 [69], based on the leading order cross section and the parton density functions CTEQ 5L (leading order) [719]. In total about 300 000 events have been produced for W' masses between 1 TeV and 8 TeV. The product of LO cross section and branching fraction varies between 3.0×10^3 fb (1 TeV) and 3.3×10^{-4} fb (8 TeV), to be compared with 1.7×10^7 fb for Standard Model W production and muonic decay. The detector response was simulated with the full CMS simulation [8] and reconstruction [10] software. Both the signal events and the following background samples were analysed: $\text{W} \to \mu\nu$, $Z \to \mu\mu$, WW inclusive, ZZ inclusive, ZW inclusive, $t\bar{t}$ inclusive. These data sets have been produced in the CMS Data Challenge 2004. On average 3.5 minimum bias reactions have been overlaid to each event.

14.4.3. Event selection and analysis

Events have been preselected requiring at least one globally reconstructed muon which pass the trigger criteria.

The final cuts to select $W' \to \mu\nu$ candidate events are:

- muon quality: at least 13 hits along the global track, $\chi^2/N_{dof} < 50$ for the fit;
- single muon requirement;
- muon isolation: no additional track ($p_\text{T} > 0.8\,\text{GeV}$) within a cone of size $\Delta R = 0.17$.

These cuts have been chosen to maximise the signal/background ratio.

For the selected events the transverse mass

$$M_\text{T} = \sqrt{2 p_{\text{T}_\mu} E_\text{T}^\text{miss} (1 - \cos \Delta\phi_{\mu, E_\text{T}^\text{miss}})}$$

is calculated from the muon transverse momentum p_{T_μ}, the missing energy component in the transverse plane E_T^miss and the angular $\Delta\phi_{\mu, E_\text{T}^\text{miss}}$ between both in this plane. Figure 14.9 shows the resulting distribution for signal (1 and 5 TeV) and background events. The W' boson distributions show a Jacobian peak which is spread out for large M_T due to the detector resolution. It can be seen immediately, that a 1 TeV boson can be discovered or excluded easily, while for higher masses a statistical analysis is needed to quantify the sensitivity.

14.4.4. Discovery and exclusion potential

To interpret the results, the CL_s method [508] is applied, which is based on the likelihood ratios, calculated for all bins of the M_T distribution. CL_s is defined as ratio of the confidence levels for the signal and background hypotheses, $\text{CL}_\text{s} = \text{CL}_{\text{s+b}}/\text{CL}_\text{b}$.

Figure 14.10 shows, that for an integrated luminosity of $10\,\text{fb}^{-1}$, a limit of 4.7 TeV at the 95% CL is reachable, if no signal is present in the CMS data. Both the expected discovery and exclusion limits are displayed in Fig. 14.11 as a function of integrated luminosity and W' mass. To investigate the sensitivity to the signal and background cross sections, they have been varied in a wide range; relative changes by factors of 2 and 10, respectively, lead to a lowering of the accessible mass range by about 0.5 TeV in the worst case.

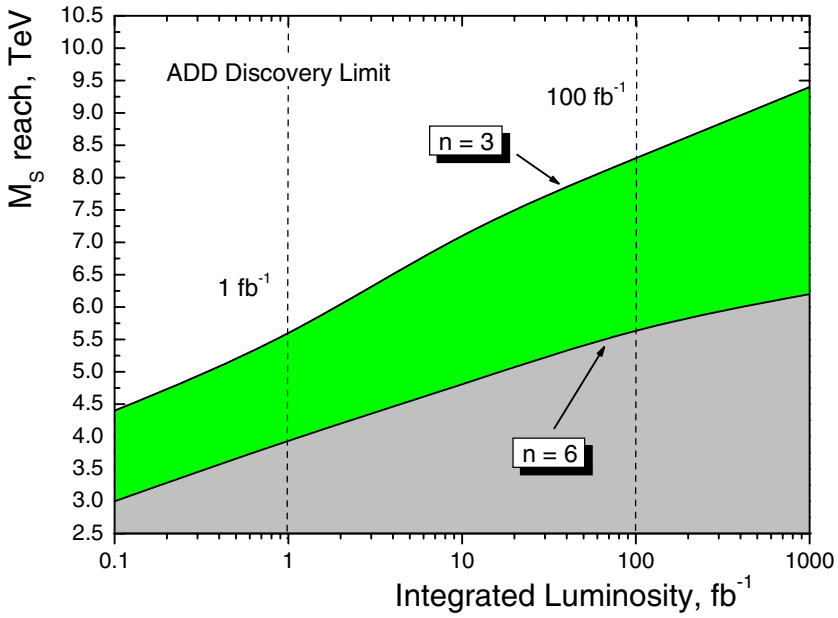

Figure 14.9. 5σ limit on M_S for the number of extra dimensions $n = 3$ and 6.

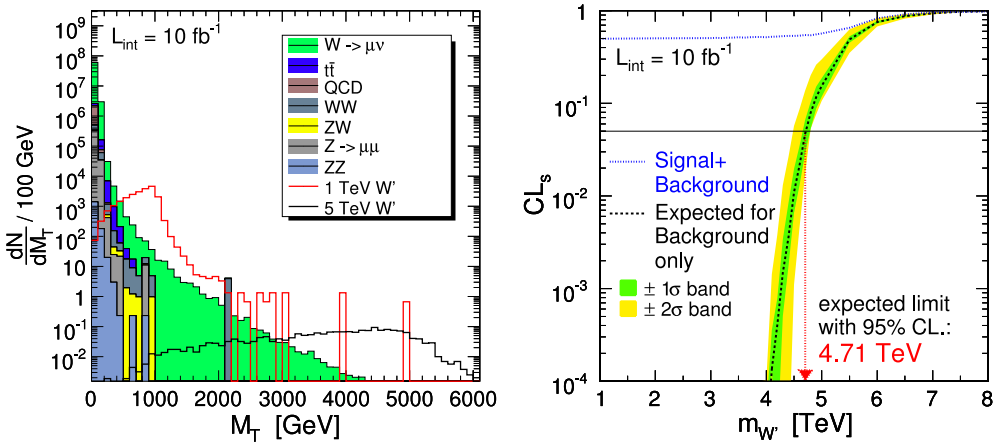

Figure 14.10. (Left) transverse invariant mass spectrum of signal (1 and 5 TeV, non-stacked) and background (stacked) after applying the selection cuts. (Right) result of the CL_s-method: with an integrated luminosity of 10 fb^{-1}. Reference W' bosons can be excluded up to a mass of 4.7 TeV.

14.4.5. Systematic uncertainties

The uncertainties arising from an imperfect knowledge of the PDFs at LHC energies and the error from the hard scale parameters have been investigated by using the Les Houches Accord PDFs [95] and varying the hard scale, respectively. The relative errors on the cross-section of the signal are listed in Table 14.4. The error on the background is comparable to that of the W' at the corresponding invariant mass.

The steep falling invariant mass distribution especially of the W background holds a potential danger for the detection of W' bosons: if only a small fraction of these events is

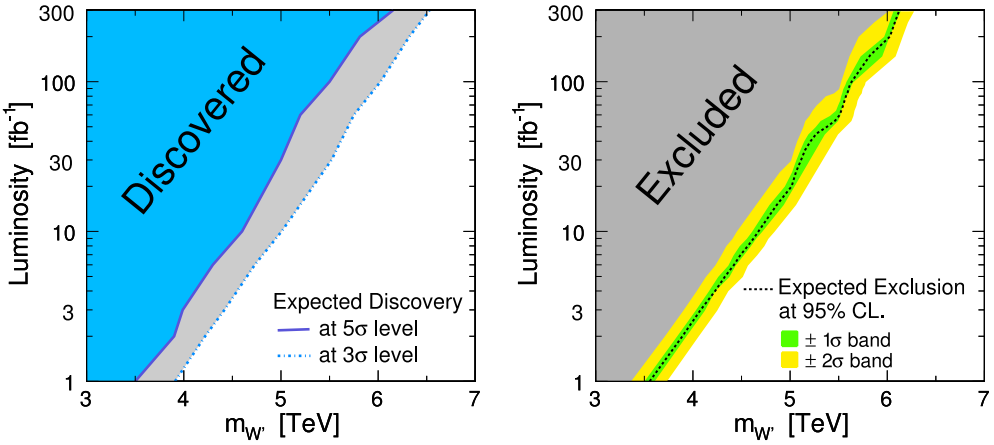

Figure 14.11. The plots show which integrated luminosity is needed to discover (left) or exclude (right) W' bosons of a certain mass.

Table 14.4. Relative systematic uncertainties in percent, arising from an imperfect theoretical knowledge (parton density functions, hard scale) and the expected luminosity error for an integrated luminosity of 10 fb^{-1}.

	Systematic Uncertainties				
Type	1 TeV W'	2 TeV W'	3 TeV W'	4 TeV W'	5 TeV W'
PDF $\Delta\sigma/\sigma$	$^{+3.6}_{-4.3}$	$^{+6.8}_{-5.9}$	$^{+6.2}_{-8.3}$	$^{+17.1}_{-10.6}$	$^{+33.7}_{-18.9}$
Hard Scale $\Delta\sigma/\sigma$	$^{+4.1}_{-4.1}$	$^{+7.5}_{-6.9}$	$^{+10.4}_{-9.2}$	$^{+13.1}_{-10.3}$	$^{+14.8}_{-12.7}$
Luminosity $\Delta\mathcal{L}/\mathcal{L}$	$\pm5\%$	$\pm5\%$	$\pm5\%$	$\pm5\%$	$\pm5\%$

reconstructed with a by far too large mass, which might result from a mis-measured muon momentum, the detection of a W' becomes extremely difficult. Such a behaviour would be visible in non-gaussian tails for example in the p_T resolution distribution. Using a large sample of a W events it could be demonstrated, that the alignment precision expected after an integrated luminosity of 10 fb^{-1} has only a small influence on the non-gaussian tails of the muon p_T resolution distribution.

The luminosity uncertainty at the considered integrated luminosity of 10 fb^{-1} is expected to be 5%, while other experimental errors (neutron background, dead detector components, etc.) are expected to be negligible.

14.4.6. Summary

For an integrated luminosity of 10 fb^{-1}, W' bosons of the Reference Model can be discovered or excluded up to a mass of 4.5–5 TeV, from an analysis of the muonic decay mode.

14.5. High mass dijet final states

14.5.1. Dijet resonances and contact interactions

Dijet resonances and contact interactions are the two major signals of new physics with dijets. Dijet resonances are direct and compelling observations of a new physical object at a mass M, requiring an incoming parton-parton collision energy equal to the mass. Contact interactions

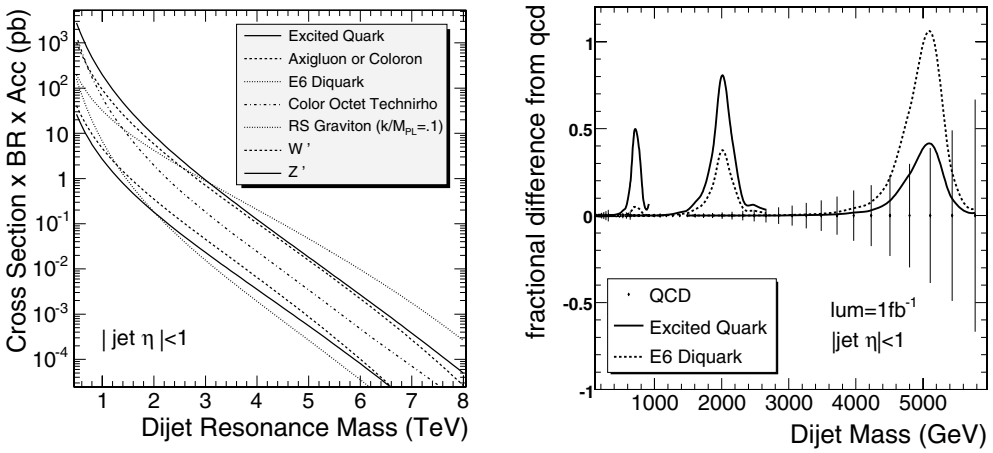

Figure 14.12. (Left) The total cross section times branching ratio times acceptance for dijet resonances from eight different models (see text). (Right) For resonance masses of 0.7, 2.0, and 5.0 TeV/c^2, the fractional difference between an excited quark (solid curve) or an E6 diquark (dashed curve) and the QCD dijet background is compared to the QCD statistical errors (vertical lines).

(discussed in Section 15.3) are indirect observations of an energy scale of new physics, Λ, which can be significantly larger than the available collision energy. Resonances are clear signals but contact interactions are often observed first.

14.5.2. Dijet resonance search

We search for processes producing narrow resonances, X, decaying to dijets: $pp \to X \to$ jet + jet (inclusive) [730]. Our experimental motivation is that LHC is a parton-parton collider, and resonances made from partons must decay to the same partons giving two jets in the final state. The theoretical motivation is broad, since there are many models that predict narrow dijet resonances.

14.5.2.1. Dijet resonance models. In Fig. 14.12 we show the cross section times branching ratio times acceptance calculated to lowest order for eight benchmark models. Here we introduce them in order of descending cross section at low mass. Excited states of composite quarks [731] are strongly produced giving large cross sections ($qg \to q^*$). Axigluons (A) [732] or colorons (C) [733] from an additional colour interaction are also strongly produced, but require an anti-quark in the initial state ($q\bar{q} \to A$ or C) slightly reducing the cross section compared to excited quarks. Diquarks [734] from superstring inspired E_6 grand unified models are produced with electromagnetic coupling from the valence quarks of the proton ($ud \to D$). The cross section for E_6 diquarks at high mass is the largest of all the models considered, because at high parton momentum the probability of finding a quark in the proton is significantly larger than the probability of finding a gluon or anti-quark. Colour octet technirhos [735] from topcolour-assisted technicolour are produced for either gluons or quark-anti-quark pairs in the initial state through a vector-dominance model of mixing between the gluon and the technirho ($q\bar{q}, gg \to g \to \rho_{T8}$). Randall–Sundrum gravitons [94] from a model of large extra dimensions are produced with a significant cross section at masses below 1 TeV/c^2 primarily from gluons in the initial state ($q\bar{q}, gg \to G$). Heavy W bosons [736] inspired by left-right symmetric grand unified models have electroweak couplings and

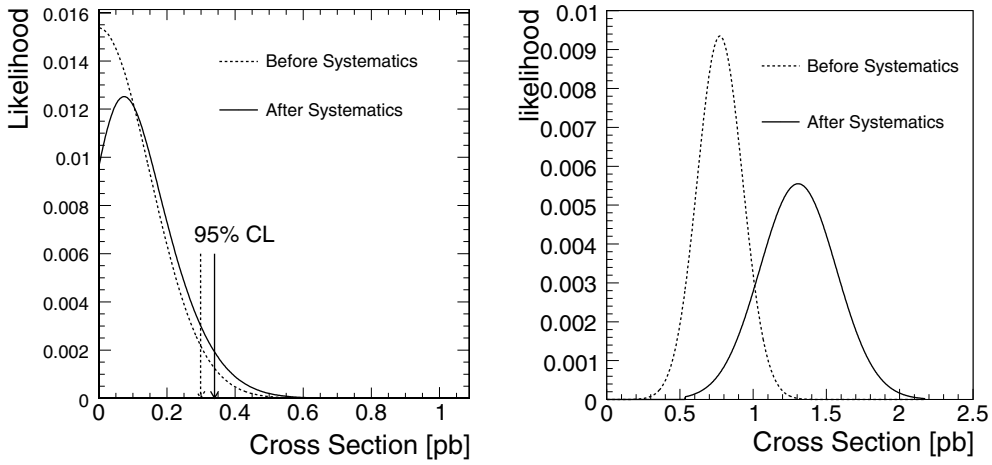

Figure 14.13. Likelihoods for observing a narrow dijet resonance of mass 2 TeV/c^2 in a 1 fb^{-1} data sample that contains only QCD background (left) and a data sample that also contains a resonance with a significance of 5σ (right) are shown with statistical uncertainties only (dashed) and including systematics (solid).

require anti-quarks for their production ($q_1\bar{q}_2 \to W'$) giving small cross sections. Heavy Z bosons [736] inspired by grand-unified models are widely anticipated by theorists, but they are weakly produced, and require an anti-quark in the initial state ($q\bar{q} \to Z'$), so their production cross section is around the lowest of the models considered. Lower limits from CDF [120] and D0 [121] on the mass of these models range from 0.4 to 1.0 TeV/c^2.

14.5.2.2. Dijet resonance sensitivity estimates. The signal and background dijet mass distributions for narrow resonances were presented in Section 4.1.4. In Fig. 14.12 we demonstrate the size of the signal for excited quarks and E_6 diquarks compared to the QCD background and it's statistical uncertainty. It is clear that we will be sensitive to such large signals for strongly produced dijet resonances. Here we quantify our sensitivity to any model of narrow dijet resonances. In Fig. 14.13 we show examples of likelihoods for excluding or observing a narrow resonance signal on a QCD background as a function of the signal cross section. In the case where the observed sample is QCD only, the signal likelihood peaks around zero cross section, and the 95% CL excluded signal cross section is shown. In the case where the observed sample is QCD plus a resonance signal, we have varied the signal size until the Gaussian distributed likelihood is 5σ above zero. In Fig. 14.13 we have included estimates of our systematic uncertainties. For a resonance mass of 0.7 (5.0) TeV/c^2 the systematic uncertainty on the observable signal cross section due to the jet energy uncertainty in the background rate is 15% (25%), the uncertainty due to jet resolution in the resonance shape is 10% (10%), the uncertainty due to radiation's affect on the resonance shape is 10% (25%), and the uncertainty due to luminosity is 10% (10%). For resonance masses just above the dijet mass thresholds where the trigger prescale decreases, there is an additional systematic uncertainty from the jet energy uncertainty. Systematic uncertainties have a greater effect on discovery than exclusion, because exclusions occur at a smaller signal cross section and are dominated by statistical uncertainties.

Figure 14.14 demonstrates that the 95% CL exclusion and 5σ discovery signal cross sections, including statistical uncertainties only, have reasonable values when compared to the size of the QCD statistical errors. Also in Fig. 14.13 we present the resonance cross

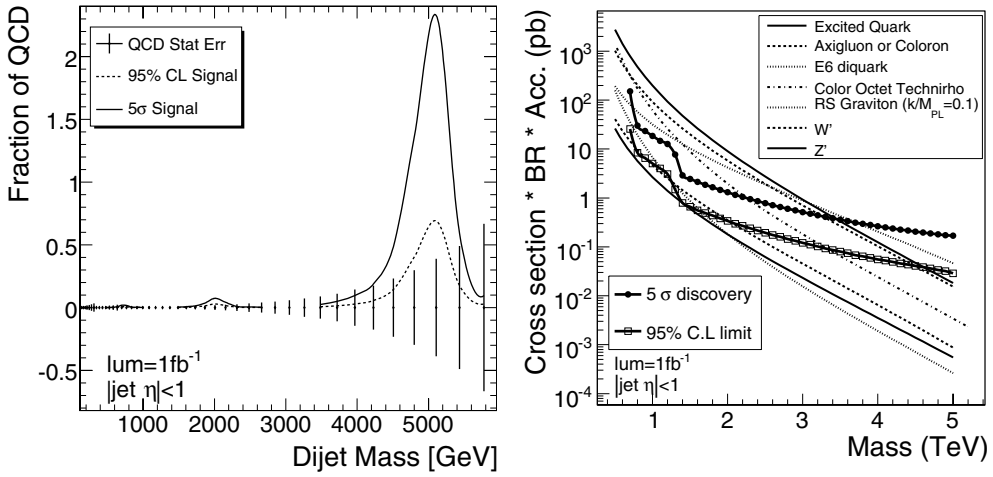

Figure 14.14. (Left) For resonances of mass 0.7, 2.0 and 5.0 TeV/c^2, the rate as a fraction of QCD that CMS expects to exclude (dashed) or discover (solid) including statistical uncertainties only. (Right) The resonance cross section that CMS expects to exclude (boxes) or discover (circles), including systematic uncertainties, is compared to the cross section for eight resonance models.

Table 14.5. Sensitivity to dijet resonances with 100 pb^{-1}, 1 fb^{-1} and 10 fb^{-1}. For each resonance model, we show the range of masses we expect to be able to exclude at a confidence level of 95% or greater, and the range of masses we expect to be able to discover with a significance of 5σ or greater. All estimates are with both statistical and systematic uncertainties.

Resonance Model	95% CL Excluded Mass (TeV/c^2)			5σ Discovered Mass (TeV/c^2)		
	100 pb^{-1}	1 fb^{-1}	10 fb^{-1}	100 pb^{-1}	1 fb^{-1}	10 fb^{-1}
Excited Quark	0.7–3.6	0.7–4.6	0.7–5.4	0.7–2.5	0.7–3.4	0.7–4.4
Axigluon or Colouron	0.7–3.5	0.7–4.5	0.7–5.3	0.7–2.2	0.7–3.3	0.7–4.3
E_6 diquarks	0.7–4.0	0.7–5.4	0.7–6.1	0.8–2.0	0.8–3.7	0.8–5.1
Colour Octet Technirho	0.7–2.4	0.7–3.3	0.7–4.3	0.7–1.5	0.7–2.2	0.7–3.1
Randall–Sundrum	0.7–1.1	0.7–1.1	0.7–1.1			
Graviton		1.3–1.6	1.3–1.6	N/A	N/A	N/A
			2.1–2.3			
W′	0.8–0.9	0.8–0.9	0.8–1.0	N/A	N/A	N/A
		1.3–2.0	1.3–3.2			
Z′	N/A	N/A	2.1–2.5	N/A	N/A	N/A

section values for jet $|\eta| < 1$ that CMS can expect to exclude at 95% CL or discover at 5σ significance for an integrated luminosity of 1 fb^{-1}. These can be compared with the cross section of any model of narrow dijet resonances, and here we compare with our benchmark models. From Fig. 14.14 we can read off the mass limits or discoveries that are possible with 1 fb^{-1} of data, which are listed in Table 14.5 along with the results of repeating the same analysis for 100 pb^{-1} and 10 fb^{-1}. The resonances that are produced via the colour interaction (excited quarks, axigluons, colorons and colour octet technirhos) or from the valence quarks of each proton (E_6 diquarks) have large cross sections and can be discovered up to a mass of a few TeV. A single search for resonances in the dijet mass distribution provides CMS with a sensitive test of many different models of the widely anticipated New Physics at the TeV scale.

14.6. High mass diphoton final states

14.6.1. Introduction

The study of the Randall–Sundrum (RS) graviton decaying into the two photons is particularly interesting as the detection of such few $\mathrm{TeV/c^2}$ mass resonance in such channel together with its observation in the dilepton channel will sign a RS graviton, distinguishing it from a Z′ production. The model is governed by two parameters: the graviton mass M and its coupling to Standard Model particles c, the latter being related to the natural width of the resonance.

14.6.2. Event generation and kinematics pre-selection

The search for the $\mathrm{G} \to \gamma\gamma$ signal at LHC is affected by four types of backgrounds:

- The prompt diphoton production from the quark annihilation and gluon fusion diagrams, which provides an intrinsic or 'irreducible' background.
- The γ + jets production consisting of two parts: i) prompt photon from hard interaction + the second photon coming from the outgoing quark due to final state radiation and ii) prompt photon from hard interaction + the decay of a neutral hadron (mostly isolated π^0) in a jet, which could fake a real photon.
- The background from QCD hadronic jets, where electromagnetic energy deposits result from the decay of neutral hadrons (especially isolated π^0s) in both jets.
- Drell–Yan process with e^+e^- in a final state which could mimic photons when correspondent electron tracks will not be assigned to the superclusters during the reconstruction.

Generator-level pre-selection and parameters used for QCD and bremsstrahlung backgrounds is described in [737].

14.6.3. Offline selection and analysis

The requirements for the analysis were as follows:

1 Two super-clusters (SCs) with $E_\mathrm{T} > 150\,\mathrm{GeV}$ and two HLT trigger bits triggered at the same time: 2p (two photons) and r2p (two photons relaxed).
2 Calorimeter isolation criteria: for each SC the energy in a cone of $\Delta R = 0.5$ (excluding SC itself) should be $< 0.02 E_\mathrm{T}(SC)$
3 $E(HCAL)/E(ECAL) < 0.05$
4 Tracker isolation: the sum of the energy of all tracks in a cone $\Delta R = 0.5$ around the SC should be $< 0.01 E_\mathrm{T}(SC)$
5 Photon energy corrections are done in a simple way so far:
   - For E1 energy $< 1.7\,\mathrm{TeV}$, only a simple energy dependent part of correction is applied (just a shift of the peak).
   - For E1 energy $> 1.7\,\mathrm{TeV}$, the MGPA saturation correction (1d) was applied (see and [738]).

14.6.4. K-factors

To produce the final results and to calculate the expected statistical significance for RS-1 graviton search recently calculated next-to-leading order corrections (K factors) to the cross sections of different types of background are used: $\mathrm{K} = 1.5$ for quark annihilation [26], $\mathrm{K} = 1.2$ for gluon fusion [29], $\mathrm{K} = 1$ for the γ + hadronic jets [29] and $\mathrm{K} = 1$ for QCD jets. For signal, a conservative $\mathrm{K} = 1$ value is taken.

Table 14.6. Number of events passed through the analysis cuts defined above for $M_G = 1.5\,\mathrm{TeV/c^2}$, $c = 0.01$ and $\mathcal{L} = 30\,\mathrm{fb}^{-1}$. Leading column is non-saturated events, all saturated events, passed through the analysis, were added in brackets, where applied.

	signal	Born (K = 1.5)	Box (K = 1.2)	Brem (K = 1)	QCD (K = 1)	DY (K = 1)
trigger + 2SC	28.9	8.6	0.10	29.2	798.7	4.3
+ EM isolation	24.5	5.5	0.08	20.3	361.8	3.5
+ HCAL/ECAL	24.3	5.4	0.08	4.4	12.8	3.5
+ tracker isolation	17.6	4.2(+0.2)	0.05	0.17	0.0	0.0

Table 14.7. Number of events passed through the analysis cuts defined above for $M_G = 3.5\,\mathrm{TeV/c^2}$, $c = 0.1$ and $\mathcal{L} = 30\,\mathrm{fb}^{-1}$. Leading column is non-saturated events, all saturated events, passed through the analysis, were added in brackets, where applied.

	signal	Born (K = 1.5)	Box (K = 1.2)	Brem (K = 1)	QCD (K = 1)	DY (K = 1)
trigger + 2SC	11.6	0.20	$4.4 * 10^{-4}$	0.78	821.9	0.10
+ EM isolation	10.8	0.14	$3.6 * 10^{-4}$	0.32	164.4	0.095
+ HCAL/ECAL	10.6	0.13	$3.4 * 10^{-4}$	0.016	0.0	0.095
+ tracker isolation	8.9(+1.0)	0.10(+0.02)	$2.7(+0.24) * 10^{-4}$	$1.7 * 10^{-3}$	0.0	$7.2 * 10^{-4}$

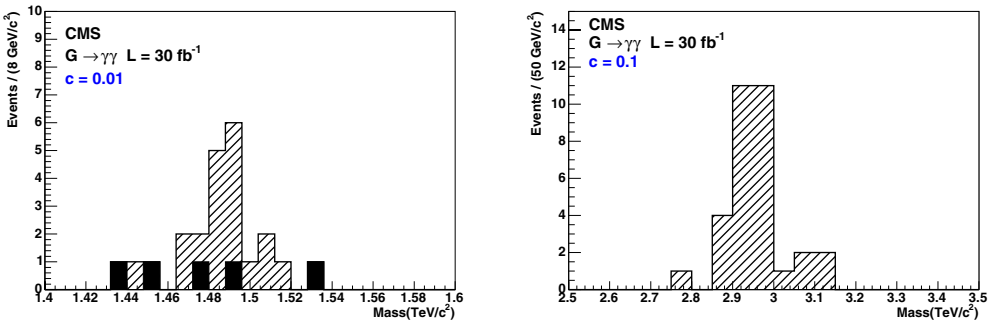

Figure 14.15. Number of events passing all cuts for (1.5 TeV/c^2, 0.01) (left) and (3.0 TeV/c^2,0.1) (right) RSI gravitons for 30 fb^{-1} integrated luminosity.

14.6.5. Results

The numbers of events passing the analysis cuts described above, for the signal and for the backgrounds, are presented in Table 14.6 (1.5 TeV/c^2, 0.01) and in Table 14.7 (3.5 TeV/c^2, 0.1).

Figure 14.15 shows the number of events satisfying all cuts for both signal and backgrounds for the cases (1.5 TeV/c^2, 0.01) and (3.0 TeV/c^2, 0.1) after 30 fb^{-1} luminosity. The results for one year low luminosity of 10 fb^{-1} are presented in Fig. 14.16.

Taking into account the K-factors described above, the number of events for signal and background and the significance S_{cL} (defined in Appendix A.1) for $c = 0.01$ and $c = 0.1$ are shown respectively in Tables 14.8 and 14.9 for an integrated luminosity of 30 fb^{-1}.

The significance as a function of the graviton mass (M_G) for integrated luminosities of 10 fb^{-1}, 30 fb^{-1} and 60 fb^{-1} are displayed in Fig. 14.17.

The discovery region in the plane of the coupling parameter c and the graviton mass is shown in Fig. 14.18.

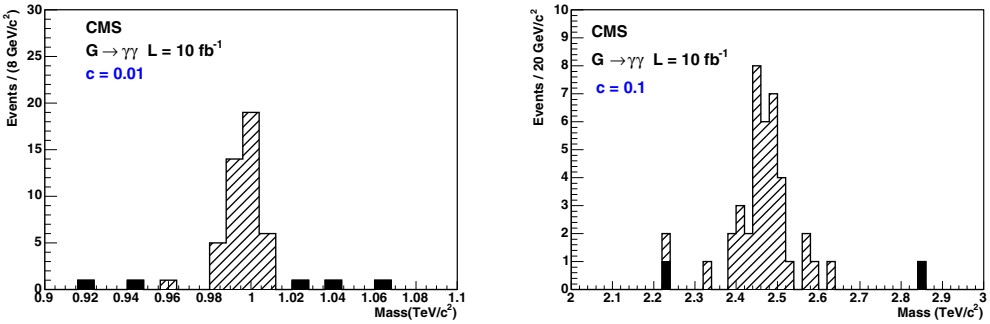

Figure 14.16. Number of events passing all cuts for (1.0 TeV/c^2, 0.01) (left) and (2.5 TeV/c^2,0.1) (right) RS-1 gravitons for 10 fb^{-1} integrated luminosity.

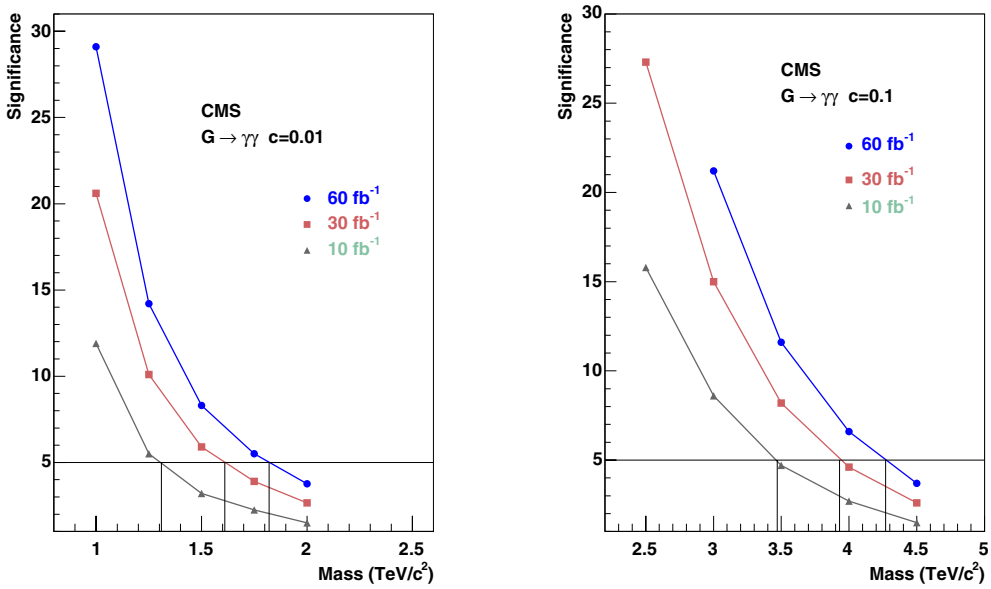

Figure 14.17. Significance as a function of the graviton mass for 10 fb^{-1}, 30 fb^{-1} and 60 fb^{-1} integrated luminosities, with c = 0.01 (left) and c = 0.1 (right).

Table 14.8. Significance for $c = 0.01$ and $\mathcal{L} = 30\,\text{fb}^{-1}$.

	$M_G = 1.0$ TeV/c^2	$M_G = 1.25$ TeV/c^2	$M_G = 1.5$ TeV/c^2	$M_G = 1.75$ TeV/c^2	$M_G = 2.0$ TeV/c^2
N_s	135.8	44.0	17.6	7.3	3.9
N_{bkg}	15.0	8.8	4.6	1.8	1.2
Significance	20.6	10.1	5.9	3.9	2.6

Table 14.9. Significance for $c = 0.1$ and $\mathcal{L} = 30\,\text{fb}^{-1}$.

	$M_G = 2.5$ TeV/c^2	$M_G = 3.0$ TeV/c^2	$M_G = 3.5$ TeV/c^2	$M_G = 4.0$ TeV/c^2	$M_G = 4.5$ TeV/c^2
N_s	103.8	31.6	9.9	3.44	1.11
N_{bkg}	1.11	0.35	0.13	0.06	0.02
Significance	27.3	15.0	8.2	4.6	2.6

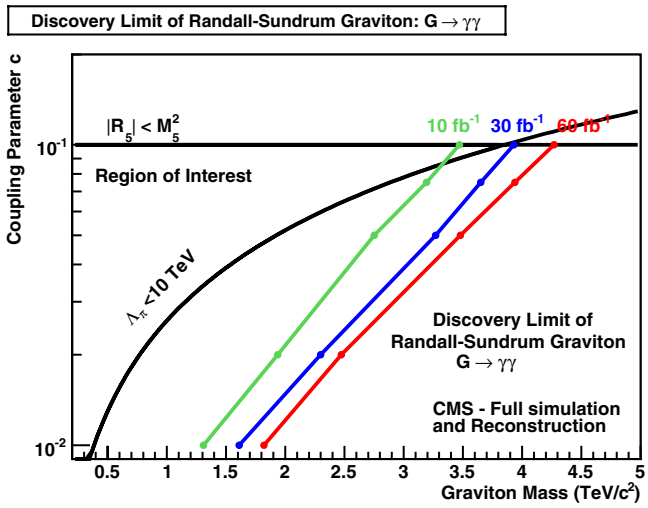

Figure 14.18. Reach of the CMS experiment in the search for the Randall–Sundrum graviton decaying into diphoton channel as a function of the coupling parameter c and the graviton mass for 10 fb^{-1}, 30 fb^{-1} and 60 fb^{-1}. The left part of each curve is the region where the significance exceeds 5σ.

Table 14.10. Hard scale confidence limits uncertainties for 30 fb^{-1}.

	$4\hat{s}$	$0.25\hat{s}$
$c = 0.01$	$-62\,\mathrm{GeV/c^2}$	$+56\,\mathrm{GeV/c^2}$
$c = 0.1$	$-47\,\mathrm{GeV/c^2}$	$+42\,\mathrm{GeV/c^2}$

The discovery region for 60 fb^{-1} extends to $M_G = 1.82\,\mathrm{TeV/c^2}$ if $c = 0.01$ and to $M_G = 4.27\,\mathrm{TeV/c^2}$ if $c = 0.1$. For 30 fb^{-1} it is $M_G = 1.61\,\mathrm{TeV/c^2}$ if $c = 0.01$ and $M_G = 3.95\,\mathrm{TeV/c^2}$ if $c = 0.1$. For 10 fb^{-1} it reaches to $M_G = 1.31\,\mathrm{TeV/c^2}$ if $c = 0.01$ and $M_G = 3.47\,\mathrm{TeV/c^2}$ if $c = 0.1$.

14.6.6. Systematic uncertainties for 30 fb^{-1}

Several systematic uncertainties and their effect on the mass reach have been evaluated for an integrated luminosity of 30 fb^{-1}. The effect of hard scale uncertainties is given in Table 14.10, computed by multiplying and dividing the scale $\hat{s}$ by a factor 2. The uncertainties from the pdfs, computed with LHAPDF, amount for $c = 0.01$ to $-55\,\mathrm{GeV/c^2}$ and for $c = 0.1$ to $-152\,\mathrm{GeV/c^2}$. There is another source of uncertainties due to the fact, that we have used K-factor = 1.5 for the Born process, while the most recent measurements at the Tevatron pointed to a K-factor closer to 2 [739]. The effect of such a change on the mass reach is $-50\,\mathrm{GeV/c^2}$ for $c = 0.01$ and $-30\,\mathrm{GeV/c^2}$ for $c = 0.1$.

14.7. Single γ final state with E_T^{miss} from extra dimensions

14.7.1. Topology of single-photon final states

An introduction to the signals involving direct graviton emission in ADD type of extra dimensions frameworks is given is Section 14.3.2. The topology of single photon events can

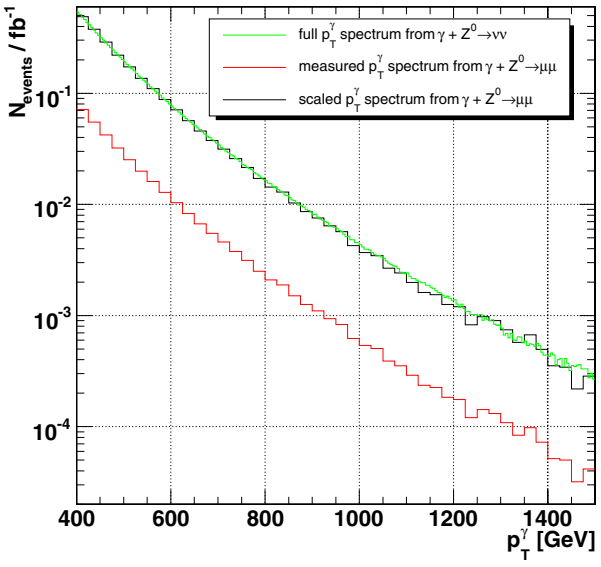

Figure 14.19. Number of expected p_T^γ events per 25 GeV bin at 1 fb^{-1} from measured $\gamma+Z^0 \to \mu^+\mu^-$ events before and after transformation compared with the generator distribution for $\gamma+Z^0 \to \nu_i\bar{\nu}_i$ – the transformed muon distribution models the $\nu_i\bar{\nu}_i$ spectrum well.

be identified by:

- a single high p_T photon in the central η region;
- high missing p_T back-to-back to the photon in the azimuthal plane with a similar p_T distribution.

These characteristics are not strongly dependent on the ADD model parameters. The details of this analysis can be found in [740].

14.7.2. Backgrounds from the Standard Model

All signal and background samples used in the following were simulated using the CMS fast detector simulation [11]. Fully simulated reference samples were generated for the signal and the largest irreducible background, $Z^0\gamma \to \nu\bar{\nu}+\gamma$. A detailed comparison of the resolution, efficiency and purity of all reconstructed objects used in this analysis to the GEANT-based CMS simulation confirmed that the fast simulation provides a very good approximation of the expected detector response. All samples were consistently generated using a generator level cut in PYTHIA $\hat{p_T} > 400$ GeV. The backgrounds considered in the study are, $Z^0\gamma \to \nu\bar{\nu}+\gamma$, $W^\pm \to \ell\nu$ where ℓ is electron, muon or tau, $W^\pm\gamma \to e\nu+\gamma$ γ+Jets, QCD, di γ and Z^0 + jets. For the main background, a normalisation method from measured data is developed employing the reconstructed leptonic decays of the Z^0 into muon and electron pairs.

The detector acceptance for selecting the leptons is parameterised using a two-dimensional function $\alpha(p_T^\gamma, \eta_\gamma)$. Figure 14.19 shows the measured and the p_T^γ spectrum from $\gamma+Z^0 \to \mu^+\mu^-$ after the (acceptance $\times$ efficiency) parameterisation is applied, in comparison with the generator spectrum for $\gamma+Z^0 \to \nu_i\bar{\nu}_i$ events. For $p_T^\gamma > 100$ GeV/c there is 1170 $Z^0 \to \mu^+\mu^-/e^+e^-$ events expected after all selection cuts for 30 fb^{-1}. These can be used as the candle sample that provides a direct normalisation of the $\gamma+Z^0 \to \nu_i\bar{\nu}_i$ with a statistical precision of 3%.

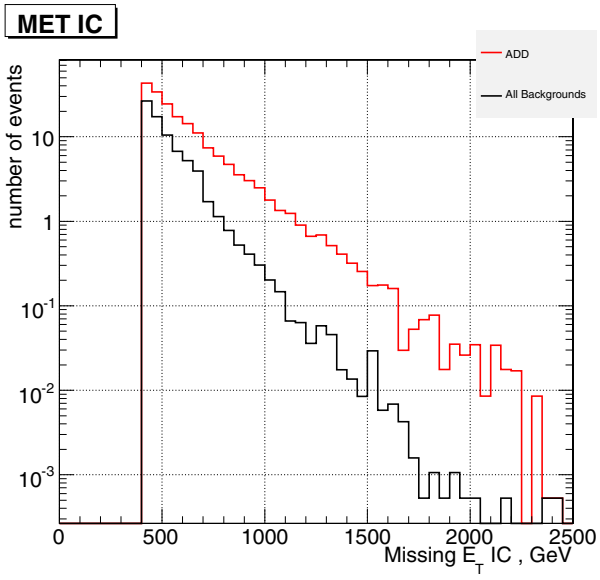

Figure 14.20. Spectrum of the missing E_{T} for all backgrounds (black histogram) and for an example signal sample ($M_{\mathrm{D}} = 2.5$ TeV, $n = 2$). The number of events corresponds to an integrated luminosity of 30 fb^{-1}.

14.7.3. Event selection

The main trigger path for the selection of signal and background events will be the single photon trigger, both at the Level-1 and the HLT. Presently the single photon trigger has a HLT level threshold of 80 GeV, which is far below the selection cut for events with isolated photons above 400 GeV used here. Hence the expected trigger efficiency is close to 100% and its efficiency can be monitored from data with a $E_{\mathrm{T}}^{\mathrm{miss}}$ trigger which will have a threshold in the range of 200–300 GeV, well below the acceptance of the bulk of the signal. Both the topological characteristic and the necessity to reduce the Standard Model background lead to the following selection criteria:

- At least a $E_{\mathrm{T}}^{\mathrm{miss}} > 400$ GeV is required and the photon p_{T} has to be above 400 GeV.
- $|\eta|$ of the photon < 2.4.
- $\Delta\phi(E_{\mathrm{T}}^{\mathrm{miss}}, \gamma) > 2.5$.
- A track veto for high p_{T} tracks > 40 GeV is applied. This is a powerful criterion to reduce all backgrounds containing high-energetic charged particles (such as $e^{\pm}$, $\mu^{\pm}$, jets).
- An Isolated Photon Likelihood criterion is applied to remove residual background from hard photon emission from jets as well as fake photons from jets.

Figure 14.20 shows the missing transverse energy spectra for events surviving the selection path for both the signal and the backgrounds. As expected the $Z^0\gamma$ is by far the most dominant component of the background, followed by $W^{\pm}\gamma$ while the contributions of the other Standard Model backgrounds are small. For all ADD cross section the hard truncation approach is used (see Section 14.1), i.e. events with $M_G < M_D$ are rejected.

14.7.4. Systematic uncertainties and discovery potential

We consider an uncertainty of 2% for the measurement of the photon p_{T}^{γ} in the electromagnetic calorimeter and an uncertainty of 5% for the $E_{\mathrm{T}}^{\mathrm{miss}}$ measurement. The

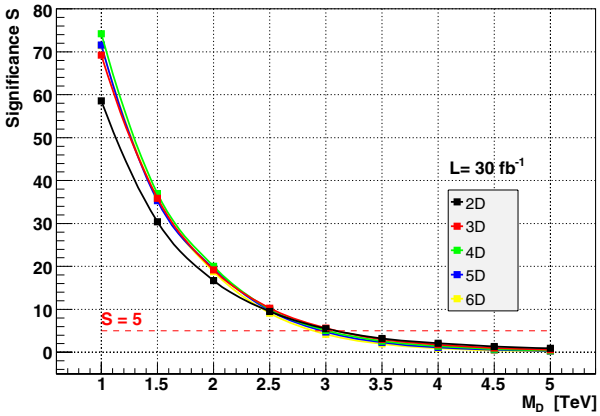

Figure 14.21. Expected significances as function of M_{D} for different number n of extra dimensions.

resulting decrease of the significance is 1.0% and 1.6% respectively. For the main background the systematics can be reduced to the luminosity measurement using the Z^0 candle calibration method. It can thus be measured with a precision of 3% after 30 fb^{-1}. The 5σ discovery reach is achievable for M_D <2.5 TeV/c^2 and all values of extra dimensions while for M_D < 3 TeV/c^{2}5σ reach is achievable for n between 2 and 4. Figure 14.21 shows the expected significances as function of M_{D}.

14.8. Black holes

14.8.1. Introduction to higher-dimensional black holes

One of the consequences of large extra dimensions is the possibility to produce microscopic black hole (BH) at LHC energies. Such a BH formed in a (4+n)-dimensional space-time has a Schwarzschild radius

$$r_{s(4+n)} = \frac{1}{\sqrt{\pi}\,M_{(4+n)}}\left(\frac{M_{BH}}{M_{(4+n)}}\left(\frac{8\Gamma((n+3)/2)}{n+2}\right)\right)^{1/(n+1)} \tag{14.18}$$

where $M_{(4+n)}$ is the reduced Planck scale and n is the number of large extra dimensions [741]. A high energy collision of two partons can result in the formation of a BH when the impact parameter is smaller than $r_{s(4+n)}$. In the semi-classical approach the BH cross section is given by $\sigma(M_{\mathrm{BH}}) = \pi r^2_{s(4+n)}$ at the parton level. If for low masses $M_{(4+n)}$, i.e. around 2 TeV, the BH production cross sections at the LHC is in the pb range.

Once produced, these BHs are expected to decay thermally via Hawking radiation [742]. The Hawking temperature for a BH in 4 + n dimensions is [743]

$$T_{(4+n)} \sim M_{(4+n)}(M_{(4+n)}/M_{\mathrm{BH}})^{1/(n+1)}. \tag{14.19}$$

These BHs have a very short lifetime typically of $\sim 10^{-27}$ seconds.

BH events are expected to evaporate democratically by emission of all particle types that exist in nature, independent of their spin, charge, quantum numbers or interaction properties. Therefore they can be a source of new particles. BH physics at the LHC can provide the possibility of probing quantum gravity in the lab.

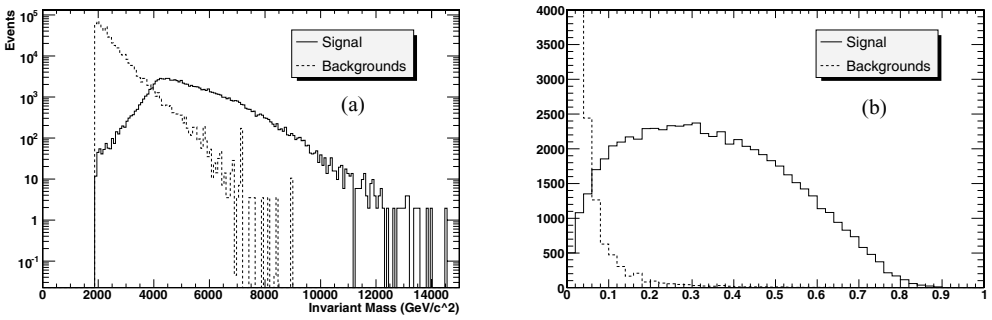

Figure 14.22. (a) Reconstructed invariant mass distribution and (b) event sphericity for black hole and standard model background events.

14.8.2. Analysis selection path and results

Black hole event samples were produced using the CHARYBDIS event generator [744]. As a benchmark the case which is analysed has the following parameters: a) 2 TeV/c^2 effective Planck scale, b) 4 TeV/c^2 minimum and 14 TeV/c^2 maximum black hole mass c) 3 extra dimensions. Time evolution during Hawking radiation and gray body effects are included. The detector response was simulated by us using the CMS fast simulation (FAMOS, version 1.4.0) after validation against the detailed CMS GEANT-based simulation. The Standard Model backgrounds taken into account include QCD jets, top production and boson plus jet production. The invariant mass of all final state objects (electrons, photons, jets and muons) in the event is found to be correlated with the input black hole mass. In addition since the black hole formation can only occur if $M_{\mathrm{BH}} > M_{(4+n)}$, the event invariant mass can indicate the effective Planck scale $M_{(4+n)}$. In the benchmark scenario the invariant mass is required to be greater than 2 TeV/c^2. BH events are characterised by a high multiplicity of the final state particles, which increase as a function of the BH mass (and decreases as a function of Hawking temperature). In particular the ratio of jets to leptons is found to be 5 to 1. In this study with a simple jet and lepton multiplicity counting the jet/lepton ratio is formed. The average value of this ratio is found to be 4.5. The thermal nature of Hawking radiation requires the distribution of BH remnants to be spherical as shown and a sphericity of 0.28 is required which eliminates drastically the Standard Model backgrounds. The invariant mass distribution and sphericity for the signal and background events is shown in Fig. 14.22.

Events are counted when the total sum of the P_{T} of all reconstructed objects plus the missing transverse energy is larger than 2500 GeV. A study of the Level-1 and HLT trigger path shows that the 4 jet trigger has a 93% efficiency for the signal events and is used in the analysis.

The event selection criteria applied to the reconstructed events and the efficiencies of the requirements are listed in Table 14.11.

The minimum integrated luminosity needed for 5σ significance and for the benchmark point is $\sim$2 pb^{-1}. A survey of the parameter space using 25 points shows that for effective Planck scale of 2–3 TeV, minimum black hole mass up to 4 TeV and 2–6 extra dimensions the 5 sigma significance can be obtained with luminosity between fraction of pb^{-1} and 100's of pb^{-1}. For effective Planck scale of 4 TeV a few fb^{-1} is needed for discovery. To account for the systematic uncertainties in the number of signal events, the effect of PDF distribution on cross section is calculated using the CTEQ6 NLO PDF set with the help of LHAPDF interface. PDF uncertainties for the chosen benchmark point is found to be $^{+24.2\%}_{-9.07\%}$. Using these uncertainties, the error in significance calculation was computed to be 12%.

Table 14.11. Event selection and background rejection for signal events and major background processes.

Cut	Signal	tt+nJ	W+nj	Z+nJ	QCD Dijet	WW+nJ
Cross Section (pb)	18.85	371	896	781.84	33076.8	269.91
Events ($10\,\mathrm{fb}^{-1}$)	188500	3.71×10^{6}	8.96×10^{6}	7.82×10^{6}	3.31×10^{8}	2.70×10^{6}
$M\mathrm{Inv} > 2\,\mathrm{TeV/c^2}$	18.71	13.29	6.53	3.85	2634.94	20.53
Tot. Multiplicity > 4	17.72	13.25	6.43	3.84	2613.18	20.42
Sphericity > 0.28	9.27	1.60	0.23	0.10	53.74	0.07
Final No. Events ($10\,\mathrm{fb}^{-1}$)	92740	15990	2328	982	537391	740

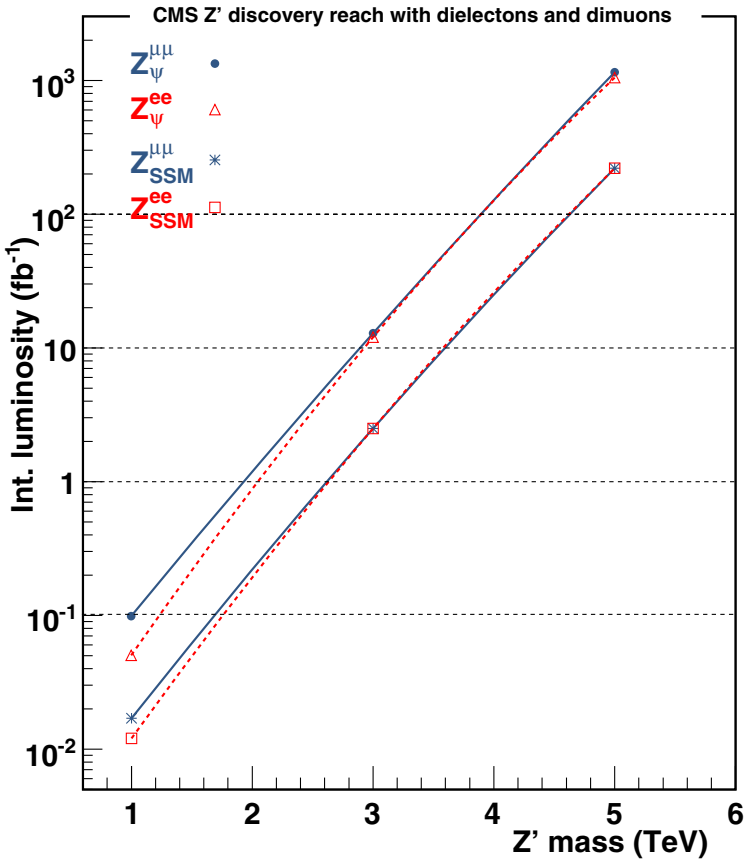

Figure 14.23. Z′ discovery reach for two of the models studied in the dielectron and dimuon channels. The reach for the rest of the models studied is within the band between the two shown here.

14.9. Discussion

The results on Z′s and RS gravitons in the channels studied in this chapter are summarised here.

In Fig. 14.23 the summary of the discovery reach in the dielectron and dimuon channels is shown for two representative Z' models. The reach for the rest of the models studied lies within the band of the two shown in the figure. The results for the dielectron channel are using

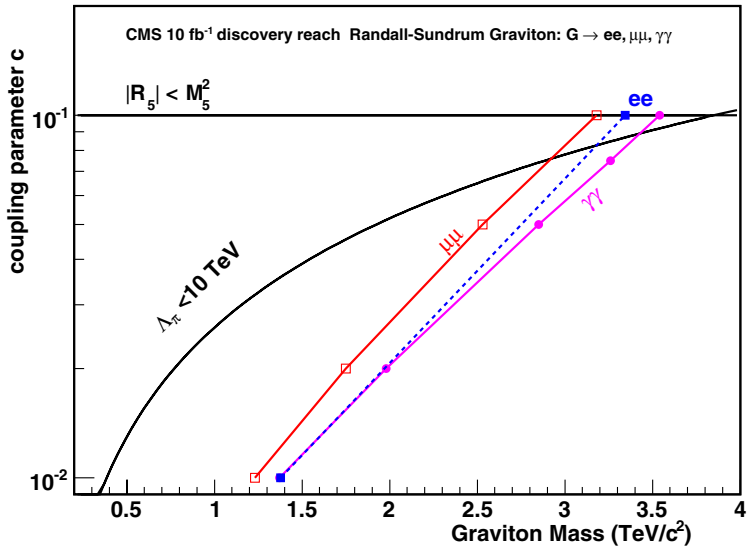

Figure 14.24. RS graviton discovery mass reach as a function of the model coupling parameter in the dielectron, dimuon and diphoton channels for 10 fb^{-1}. The dielectron reach is shown as dashed because only the boundary points (c = 0.01 and c = 0.1) where studied.

here K-factor of 1.3 for the signal and background in order to be directly compared with the dimuon results[50]. Although the analysis strategies and significance computation is different between the two analyses the results are compatible. For low luminosity and mass reach up to 3 TeV/c^2 the muons suffer from misalignment effects which are recovered after 10 fb^{-1}. For high mass reach (above 3 TeV/c^2) the saturation in the ECAL is causing a degradation of the resolution in the dielectron channel. The reach using the dielectron channel is up to 3 TeV better than the dimuons due to less than 1% resolution. Optimising the analysis in the dielectron channel to extract the background from the data and detailed studies of the saturation is expected to further improve the reach in the dielectron channel for high masses. The combined reach of the two channels requires a detailed analysis and is not presented here. Note that a 1 TeV/c^2 Z' is observable with less than 0.1 fb^{-1} for all models and with a single channel while every TeV/c^2 in mass reach corresponds to approximately an order of magnitude increase in integrated luminosity.

In Fig. 14.24 the summary of the RS graviton discovery reach in the dielectron, dimuon and diphoton channels is shown. Here the results for the diphoton channel are using CTEQ6M PDFs to be directly compared with the dielectron and dimuon channels.[51] Although the branching ratio to photons is roughly twice that of electrons or muons the reach for low coupling and graviton mass is comparable between dielectrons and diphotons due to the QCD and prompt photon backgrounds in the photon channel which are harder to efficiently suppress. For higher masses and coupling the diphoton is leading the reach due to the higher branching ratio. The dimuon channel is trailing the reach compared to the dielectrons merely due to resolution.

[50] Recent calculation of K-factors for several of the processes discussed here can be found in reference [745].

[51] In the main analysis the diphoton channel uses CTEQ5L while the dielectron and dimuon analyses use CTEQ6M where the gluon-gluon contribution is enhanced compared to the CTEQ5L; while the Drell–Yan background is largely insensitive to this choice, at low masses the gluon-gluon is the dominant graviton production process while at high masses the qq dominates where CTEQ5L and CTEQ6M are comparable.

Chapter 15. Alternative BSM Signatures

15.1. Technicolour

15.1.1. The $\rho_{TC} \to W + Z$ channel

Technicolour (TC) provides an alternative to the elementary Higgs mechanism of the Standard Model. It introduces a new strong interaction [746] providing a dynamical nature to Electroweak Symmetry Breaking. Technicolour is a QCD-like force, acting on technifermions at an energy scale $\Lambda_{TC} \sim v_{weak} = 246\,\text{GeV}$. A number N_D of technifermion doublet condensates yield the pseudo-Goldstone bosons π_{TC}, together with a wide spectroscopy of excited technimesons. The present simulation is performed using the phenomenology of the lowest-lying technihadrons, commonly referenced as the "Technicolour Straw Man" model (TCSM) [735]. The colour-singlet sector includes the spin-zero π_{TC} and the spin-one technimesons ρ_{TC} and ω_{TC}. The decay cross-section of the ρ_{TC} is expressed as an admixture of π_{TC} and the Standard Model Z and W bosons:

$$\rho_{TC} \to \cos^2\chi\,\langle\pi_{TC}\pi_{TC}\rangle + \cos\chi\,\sin\chi\,\langle\pi_{TC}V_L\rangle + \sin^2\chi\,\langle V_L V_L\rangle \qquad (15.1)$$

where V_L is the longitudinal mode of the $V = Z, W$ and $\sin\chi \simeq 1/\sqrt{N_D} \sim 1/3$. The branching fraction $\text{BR}(\rho_{TC} \to W + Z)$ is competing with the two first terms in Eq. 15.1, hence changing with $\text{M}(\pi_{TC})$.

The decay channel $\rho_{TC} \to W + Z$ is the subject of this analysis [747] as it has the advantage of a very clean final state, namely $3\ell + \nu$. The background contributions arise mainly from Standard Model processes involving weak boson production and decays. Other technicolour decay modes that include jets such as $\rho_{TC} \to \pi_{TC} + W$, have higher branching fractions but are much harder to disentangle from the Standard Model background processes.

15.1.1.1. Event selection. All signal and backgrounds samples used in this analysis are generated with PYTHIA 6.2 [24] with the requirement of at least 3 prompt leptons in the CMS fiducial region. The $Zb\bar{b}$ background is generated using COMPHEP [355] interfaced to PYTHIA. Contributions from processes of type $Z \to 2\ell$ plus an additional fake lepton from a jet have been taken into account in the systematic uncertainties, see Sect. 15.1.1.2. A set of 14 different ρ_{TC} samples are generated within the $[\text{M}(\rho_{TC}), \text{M}(\pi_{TC})]$ phase space.

Nominal CMS Level-1 and High-Level Trigger requirements are applied [76]. The CMS fast simulation [11] is used for detector simulation and event reconstruction. The main reconstructed objects and their efficiencies have been validated against the detailed GEANT-based CMS detector simulation [8, 10].

The analysis is designed to reduce the main Standard Model background contributions WZ, ZZ, $Zb\bar{b}$ and $t\bar{t}$, while retaining high signal efficiency. It is summarised as follows:

(i) Lepton selection: 3 high-p_T and isolated electrons or muons.
(ii) Lepton trigger: single- or two-electron or muon mode (Level-1 and HLT).
(iii) Z : same-flavour and opposite-charge ℓ-pair closest to $\text{M}(Z)$, with $p_T(\ell_{1,2}) > (30, 10)\,\text{GeV/c}$.
(iv) W : solution to 3rd lepton with $p_T > 10\,\text{GeV/c}$ + Missing E_T + $\text{M}(W)$ constraint.
(v) $|\text{M}(\ell^+\ell^-) - \text{M}(Z)| \leqslant 3\sigma_{\text{M}_Z} \cong 7.8\,\text{GeV/c}^2$.
(vi) $p_T(Z)$ and $p_T(W) > 30\,\text{GeV/c}$. For benchmark points with $\text{M}(\rho_{TC}) = 200\,\text{GeV/c}^2$, the minimum $p_T(Z)$ and $p_T(W)$ threshold is $10\,\text{GeV/c}$.
(vii) $|\Delta[\eta(Z) - \eta(W)]| \leqslant 1.2$.

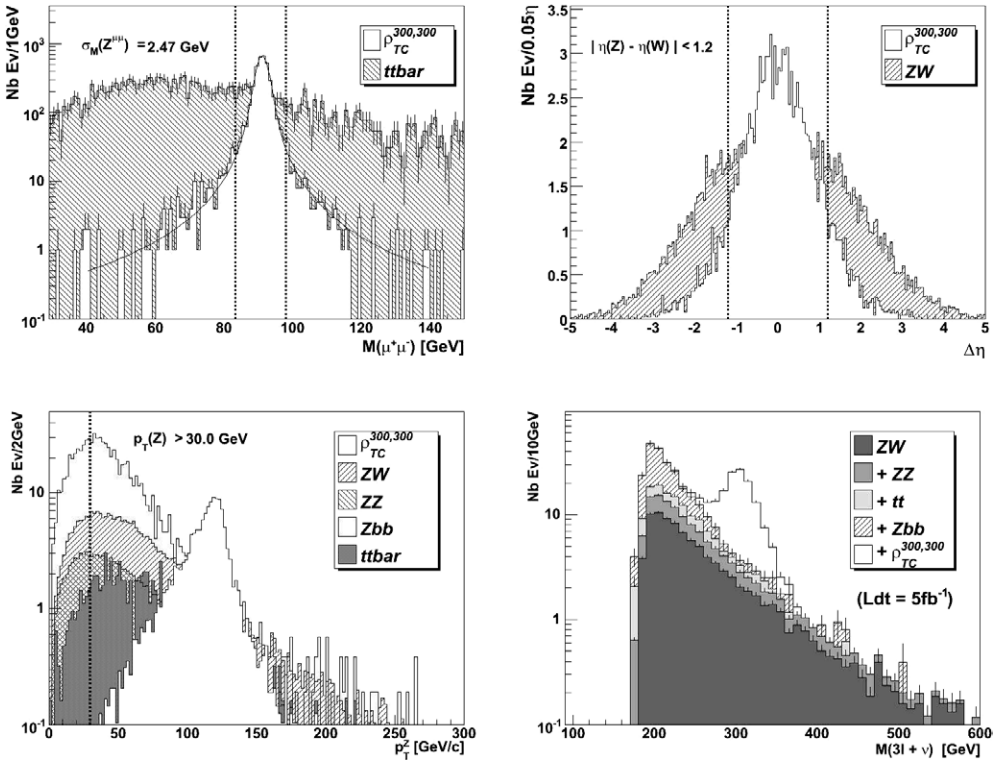

Figure 15.1. (a) M($\mu^+\mu^-$) for $\rho_{TC}(300, 300)$ and $t\bar{t}$; (b) $\Delta[\eta(\mathrm{Z}) - \eta(\mathrm{W})]$ for $\rho_{TC}(300, 300)$ and WZ; (c) $p_T(Z)$ for $\rho_{TC}(300, 300)$ and all backgrounds ($p_T(W)$ is similar); (d) Reconstructed M($3\ell + \nu$) for $\rho_{TC}(300, 300)$ and all backgrounds. The vertical lines indicate the applied requirements.

The Z and W are reconstructed with a purity of $\sim$99%, using the 3 highest-p_T leptons in the event, and the Missing Transverse Energy (MET), obtained as the vector sum of the jets and leptons in the event. The M(W) constraint yields a 2 fold ambiguity in the p_Z component of the reconstructed neutrino: it is found that the most efficient choice for the ρ_{TC} signal is the minimum p_Z solution. The kinematic cuts are illustrated in Fig. 15.1. The main $t\bar{t}$ reduction is obtained via the Z-mass window requirement (v). The irreducible background $WZ \to 3\ell + \nu$ is most efficiently separated from the signal via the $\eta(Z) - \eta(W)$ correlation requirement (vii).

The p_T cut on Z and W further improves the signal to background ratio, however it is kept modest in order to preserve the exponential background hypothesis of the $3\ell + \nu$ invariant mass spectrum, used to compute the signal sensitivity. The $\rho_{TC}(300, 300)$ signal and background yields are shown in Fig. 15.1d and the corresponding reconstruction efficiencies are listed in Table 15.1.

15.1.1.2. Signal sensitivity and systematic uncertainties. The sensitivity of each ρ_{TC} benchmark point is computed by taking into account realistic statistical fluctuations for a given integrated luminosity. The sensitivity estimator is defined as the likelihood-ratio S_L, defined in Appendix A.1. The signal probability density function (p.d.f.) is assumed Gaussian (dominated by detector resolution) and the background p.d.f. is exponential in all ρ_{TC} fit regions. The output of the fitting procedure is shown in the contour plot over the

Table 15.1. $\sigma \times \mathrm{BR}(\ell = e \text{ or } \mu)$, 3-lepton pre-selection efficiency, total efficiency and final yield within 3σ of the signal region (Nev), for $\mathcal{L} = 5\,\mathrm{fb}^{-1}$. $\rho_{TC}(300, 300)$ and the main background contributions are shown. The simulation is repeated for all ρ_{TC} benchmark points.

Sample	$\sigma \times$ BR(pb)	ε(3-lept)	ε(Reco) (%)	Nev($5\,\mathrm{fb}^{-1}$)
$\rho_{TC} \to W + Z \to 3\ell + \nu$	0.13	0.635	25.88 ± 0.40	103
$WZ \to 3\ell + \nu$	0.39	0.471	9.91 ± 0.11	27
$ZZ \to 4\ell$	0.07	0.719	15.80 ± 0.14	10
$Zb\bar{b} \to 2\ell + X$	332	0.046	0.23 ± 0.01	12
$t\bar{t}$	489.72	0.065	0.019 ± 0.001	8

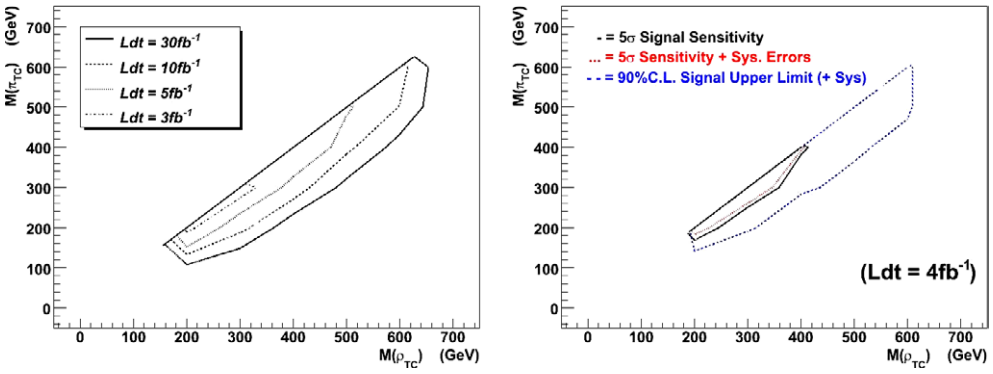

Figure 15.2. Left: Signal 5σ Sensitivity curves for various integrated luminosities. Right: sensitivity for $\mathcal{L} = 4\,\mathrm{fb}^{-1}$: the dotted (resp. dashed) curve shows the sensitivity (resp. the 90% C.L. signal upper limit) after including systematic uncertainties.

$[\mathrm{M}(\rho_{TC}), \mathrm{M}(\pi_{TC})]$ phase space in Fig. 15.2 (left), for various integrated luminosities. A signal sensitivity above 5 is expected for $\mathcal{L} = 3\,\mathrm{fb}^{-1}$ (before including systematic uncertainties).

The ρ_{TC} sensitivity has been simulated for the early CMS data taking phase. Expected detector related systematic uncertainties for $\mathcal{L} = 1\,\mathrm{fb}^{-1}$ are taken into account. While no substantial contribution is found from the tracker and muon system misalignment or the calorimeter miscalibration, the accuracy at which the lepton efficiency will be determined from data affects the result: a 2% uncertainty is considered. Moreover, the lepton fake rate has been simulated on $Zb\bar{b}$ and extrapolated to any $Z + jet(s)$ type background, in order to take into account additional contaminations from pion/kaon decays or from wrongly identified lepton candidates. A production cross-section of 1047 pb per lepton flavour is assumed for $Z + n\text{-}jets$, $n \geqslant 0$. A single lepton fake rate of $\mathrm{O}(10^{-3})$ is obtained using the fast simulation [11], affecting the ρ_{TC} sensitivity as shown below. Finally, a 7.5% uncertainty on the missing transverse energy measurement is considered. The above uncertainties result in the following relative ρ_{TC} sensitivity drop:

$$\Delta^{\mathrm{tot}}_{\mathrm{SYS}} = \sqrt{\left(\Delta^{\mathrm{Eff}}_{\mathrm{SYS}}\right)^2 + \left(\Delta^{\mathrm{Fake}}_{\mathrm{SYS}}\right)^2 + \left(\Delta^{\mathrm{MET}}_{\mathrm{SYS}}\right)^2} = \sqrt{(2.7\%)^2 + (8.5\%)^2 + (6.6\%)^2} = 11\%. \qquad (15.2)$$

Introducing K-factors from next-to-leading-order (NLO) expectations for the signal (a K-factor 1.35 is assumed in similarity with the Drell–Yan process) and background leads to a relative signal sensitivity increase of 6%; however the latter estimate has not been included in the final result.

Table 15.2. Contact interaction models.

Model	LL	RR	LR	RL	VV	AA	LL + RR	LR + RL
	Non-parity conserving				Parity conserving			
η_{LL}	±1	0	0	0	±1	±1	±1	0
η_{RR}	0	±1	0	0	±1	±1	±1	0
η_{LR}	0	0	±1	0	±1	∓1	0	±1
η_{RL}	0	0	0	±1	±1	∓1	0	±1

In summary, the technicolour signature $\rho_{TC} \to W + Z$ in the context of the Straw Man model is studied. The 5 sigma discovery reach is obtained for an integrated luminosity $\mathcal{L} \simeq 4\,\text{fb}^{-1}$.

15.2. Search for contact interactions with dimuons

Contact interactions offer a general framework for describing a new interaction with typical energy scale $\Lambda \gg \sqrt{s}$. The presence of operators with canonical dimension $N > 4$ in the Lagrangian gives rise to effects $\sim 1/\Lambda^{N-4}$. Such interactions can occur for instance, if the SM particles are composite, or when new heavy particles are exchanged.

In the following we will consider lepton-pair production. The lowest order flavour-diagonal and helicity-conserving operators have dimension six [123].

The differential cross section takes the form

$$\frac{d\sigma}{d\Omega} = SM(s,t) + \varepsilon \cdot C_{Int}(s,t) + \varepsilon^2 \cdot C_{NewPh}(s,t) \tag{15.3}$$

where the first term is the Standard Model contribution, the second comes from interference between the SM and the contact interaction, and the third is the pure contact interaction effect. The Mandelstam variables are denoted as s, t and u.

Usually the coupling is fixed, and the structure of the interaction is parameterised by coefficients for the helicity amplitudes:

$$\begin{aligned} &g && \text{coupling (by convention } g^2/4\pi = 1), \\ &|\eta_{ij}| \leqslant 1 && \text{helicity amplitudes } (i,\ j = \text{L, R}), \\ &\varepsilon && \frac{g^2}{4\pi}\frac{\text{sign}(\eta)}{\Lambda^2} \text{ for } f\bar{f}. \end{aligned}$$

Some often investigated models are summarised in Table 15.2. The models in the second half of the table are parity conserving, and hence not constrained by the very precise measurements of atomic parity violation at low energies. The results presented in this contribution cover the LL model, which has the highest sensitivity at LHC energies from the models in the first half of the table. More details can be found in [349].

15.2.1. Analysis

The topology under study is high-mass muon pairs with opposite sign. More details on the analysis are found in [349]. The Global Muon Reconstructor (GMR, described in PTDR, Volume 1, Section 9.1.2) output is used. The dimuon events are triggered by the single and dimuon triggers. We have processed events, generated to cover the whole region of interest

up to dimuon masses of 6 TeV/c^2, through full simulation with OSCAR and reconstruction with ORCA. The dimuon mass resolution is parameterised in two ways:

- as mass dependent one standard deviation (RMS);
- by fitting the mass resolution with a sum of two Gaussians to account for the long tail of less well reconstructed masses.

The results are remarkably stable as a function of the dimuon mass: the second Gaussian contributes around 14% and has a standard deviation 3.3 times bigger than the first Gaussian.

Our strategy is to generate events with PYTHIA and apply parametrisations of the dimuon mass efficiency and resolution obtained from full simulation. We have verified our approach by comparing the resulting mass spectra with the ones obtained with OSCAR/ORCA or FAMOS for Drell–Yan and selected contact interactions samples, observing good agreement in all cases.

Two mass regions: 500–1000 GeV and 1000–6000 GeV are considered. The total cross section and the forward–backward asymmetry as function of the dimuon mass are studied. Our analysis shows that the sensitivity to contact interactions comes almost exclusively from the cross section measurements for the LL model.

In order to reduce the systematic uncertainties both on the experimental and theory sides a "double ratio" method is developed. The number of observed events for a given bin in invariant mass is

$$N_{obs} = L \cdot \sigma \cdot \varepsilon \tag{15.4}$$

where L is the luminosity, σ the differential cross section for the given mass bin, and ε the experimental efficiency. We select a zeroth "normalisation" bin for invariant masses between 250–500 GeV/c^2, both well above the Z pole and in an area well covered by the Tevatron, and define the experimental ratios

$$R_i^{DATA} = \frac{N_i^D}{N_0^D} = \frac{\sigma_i^D \cdot \varepsilon_i^D}{\sigma_0^D \cdot \varepsilon_0^D}. \tag{15.5}$$

Here the cross sections and efficiencies are the ones for the real LHC data. The index i runs for all measured bins with masses above 500 GeV/c^2. The luminosity cancels in the ratio. The choice of this mass bin is not random. If we compare the flavour composition of partons initiating the hard interaction (Table 15.3), at the Z peak 32.1% are heavier flavours (not u or d quarks), with their own parton density functions (PDF) uncertainties. At 250–500 GeV/c^2 the u and d quarks are "initiators" already in 85.6% of the cases, increasing to 96.3% above 1 TeV/c^2, etc. Moreover, at the Z peak d quarks are most abundant, while at higher masses u quarks dominate, asymptotically approaching a ratio 4:1. It is clear that our choice of normalisation bin gives flavour composition much closer to the most interesting high mass events, compared to a normalisation using Z pole events. The PDF uncertainty on cross sections is estimated using LHAPDF [95, 351]. It is interesting to note that this uncertainty reaches a minimum for masses 250–600 GeV/c^2, corresponding to medium values of the parton momentum fractions X, reinforcing our choice of normalisation bin.

We define similar ratios for the Monte Carlo (theory) predictions. The *absolute* values of the cross sections and efficiencies are not important for the ratios, what matters is *the shape* of these quantities as function of invariant mass. For example, the absolute value of K-factors, a way to compensate for missing higher order N(N)LO terms and enable the comparison of leading order Monte Carlo predictions to data (similarly for the electroweak radiative corrections) disappears from the ratios and only the *shape* of the K-function as depending on invariant mass remains – a much smaller effect. And part of the uncertainties introduced due to our limited knowledge of PDFs cancels in the ratio, leaving smaller residual uncertainties due to the change of phase space for changing masses.

Table 15.3. Flavour composition of partons initiating the hard Drell–Yan interaction.The PDF uncertainty on the cross sections (positive and negative asymmetric errors) is estimated using LHAPDF.

Mass [GeV/c^2]	d [%]	u [%]	s [%]	c [%]	b [%]	PDF+ [%]	PDF− [%]
Z peak	35.9	32.1	17.2	9.77	5.10	+4.7	−5.7
250–500	24.3	61.3	6.22	6.64	1.54	+3.4	−4.2
500–600	22.8	68.4	4.03	3.95	0.89	+3.5	−4.1
1000+	21.7	74.6	1.86	1.48	0.33	+5.0	−5.8
2000+	19.9	78.4	0.91	0.63	0.14	+9.0	−7.7

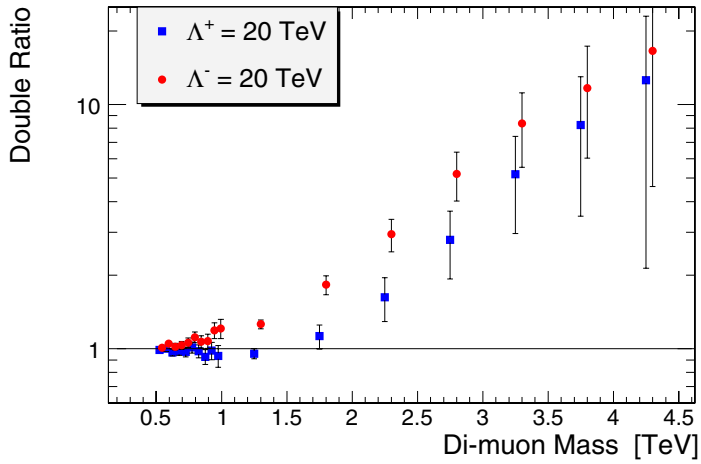

Figure 15.3. Double ratios for contact interactions in the dimuon channel, LL model, scale $\Lambda = 20\,\mathrm{TeV/c^2}$, positive and negative interference, and luminosity $100\,\mathrm{fb^{-1}}$. The errors shown are statistical.

Now let us define the double ratios

$$DR_i = \frac{R_i^{DATA}}{R_i^{MC}}. \tag{15.6}$$

This method is inspired by a study of Drell–Yan events and extraction of proton and pion PDFs at lower masses [748], as well as by the SuperKamiokande double ratio method for measuring atmospheric neutrino oscillations [749]. If our theory understanding and detector modelling are both perfect, we expect $DR_i \equiv 1$. The experimental or Monte Carlo errors introduced in the ratios from the uncertainties in the zeroth bin are negligible, as due to the steeply falling Drell–Yan spectrum this bin has much more data compared to the high mass bins.

An example of double ratios for positive and negative interference is shown in Fig. 15.3. As can be seen, for scale $\Lambda = 20\,\mathrm{TeV/c^2}$ the expected effects are quite sizable (note the log scale), with the sensitivity for negative interference starting around dimuon masses of $750\,\mathrm{GeV/c^2}$, while for positive interference masses above $2\,\mathrm{TeV/c^2}$ are required.

The experimental systematic effects in the cross section measurement are estimated to be 2% from the total muon efficiency and no more than 1.4% from momentum resolution. The former can be controlled quite well with the huge sample of Z events decaying to dimuons, and the effects for TeV muons are taken into account on top of this. The latter is important at high mass as smearing from lower masses from the steeply falling Drell–Yan spectrum can contaminate the high mass measurements, especially if the tails of the momentum resolution

Table 15.4. The PDF uncertainty on the cross section ratios (positive and negative asymmetric errors) as estimated using LHAPDF. Clearly normalising to the 250–500 GeV/c^2 mass bin is superior compared to a normalisation relative to the Z peak (70–120 GeV/c^2).

	$R\left(\frac{M}{250-500}\right)$		$R\left(\frac{M}{Zpeak}\right)$	
Mass [GeV/c^2]	PDF+ [%]	PDF− [%]	PDF+ [%]	PDF− [%]
500–600	+1.5	−1.5	+4.6	−4.2
1000+	+5.2	−4.8	+7.8	−7.1
2000+	+10.7	−7.8	+12.9	−9.4

are not under control. It is estimated by varying the two parametrisations of the mass resolution by ±40%, giving consistent results. The main source of systematic uncertainties on the momentum resolution comes from the alignment of the muon chambers and the central tracker, both at start-up and at high luminosity.

The systematic uncertainties from our limited knowledge of PDFs is estimated using the CTEQ6M PDF set from LHAPDF. From Table 15.4 our estimate of the PDF uncertainty on the cross section ratio is $^{+5.2}_{-4.8}$% above 1 TeV or $^{+10.7}_{-7.8}$% above 2 TeV.

The genuine electro-weak radiative corrections change by ∼10% in the relevant mass range [158, 350]. The K-function changes faster below 250–300 GeV. From our normalisation bin to the highest masses first estimates show a change below 8% on the cross section[52]. Taking conservatively half of these changes with mass as an upper limit on the systematic uncertainty we arrive at 5% and 4% respectively.

Combining all effects in quadrature, we arrive conservatively at systematic uncertainties below 2.5% experimental, 11.5% from theory, 12% total at nominal conditions, 15% shortly after start-up. With the accumulation of data and improved calculations there is hope to improve this number by making progress in our understanding of PDF, electro-weak radiative corrections and K-functions.

The discovery reach for a given model is determined by constructing a negative log-likelihood function combining the deviations between measurements and predictions, including the contact interaction contributions, for all simulated data points. The error on a deviation consists of three parts, which are combined in quadrature: a statistical error, an experimental systematic error and a theoretical uncertainty. The log-likelihood function is integrated in the physically allowed region (all positive Λ for positive interference and all negative Λ for negative interference) to derive the five standard deviations σ discovery reach and one-sided lower limits at 95% confidence level on the scale.

The discovery reach is summarised in Fig. 15.4. The sensitivity is dominated by the cross section measurement, the contribution of the forward-backward asymmetry is minor. The sensitivity for negative interference is substantially better. Even at the highest luminosities the statistical errors at LHC play a major role, as evident from the comparison of the cases with total systematic uncertainties of 3, 15 and 30%. This is not surprising as the Drell–Yan process is probing directly masses up to ∼4–5 TeV/c^2, where due to the steeply falling cross sections the statistical errors remain important for all considered luminosities.

[52] Calculations by M. Schmitt with the program PHOZPRMS [348].

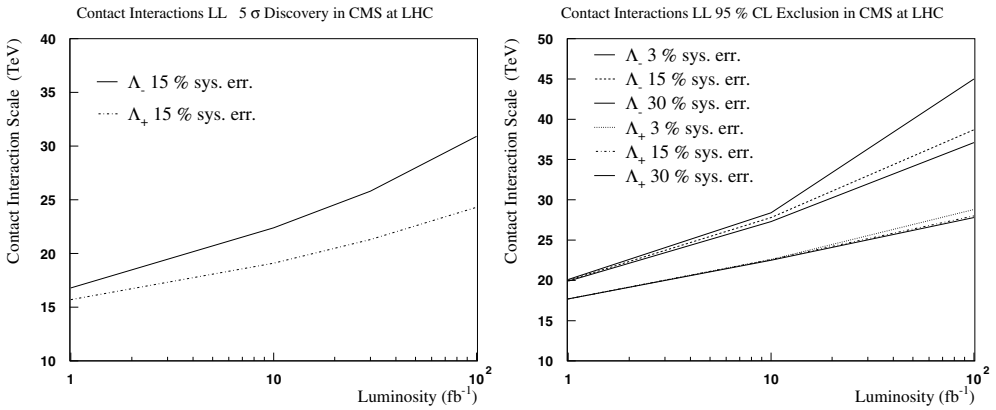

Figure 15.4. Five sigma discovery reach (left) and sensitivity at 95% CL (right) for contact interactions in the dimuon channel for different luminosities and signs of the interference.

15.3. Search for contact interactions with dijets

New physics at a scale Λ above the mass of the final state is effectively modelled as a contact interaction. Here the propagator for a particle of mass $M \sim \Lambda$ exchanged between quarks, or exchanged between constituent particles inside two interacting composite quarks, shrinks to a single point and gives a contact interaction. Quark contact interactions, for example those that arise from a left-handed interaction among composite quarks [123, 124], will always produce a rise in rate relative to QCD at high dijet mass or high inclusive jet E_{T}. However, observation in the mass distribution alone requires precise understanding of the QCD rate as a function of dijet mass, which is complicated by the large systematic uncertainties discussed in Section 4.1.6. Angular distributions benefit from much smaller systematic uncertainties. The contact interaction is often more isotropic than the QCD background, since QCD is dominated by t-channel scattering and produces jets predominantly in the forward direction. Our analysis uses the dijet ratio, discussed in section 4.1.5, to measure the angular distribution as a function of dijet mass, and see any contact interactions which affect the dijet angular distribution [750].

15.3.0.1. Contact interaction sensitivity estimates. The QCD background distribution for the dijet ratio was discussed in section 14.5. In Fig. 15.5 we show a smooth dijet ratio for QCD, estimated at 0.6 from the fit to the full simulation. The error bars shown in Fig. 15.5 are the statistical uncertainties expected with 1 fb^{-1} and the jet trigger prescales discussed in section E.4.3.2. The uncertainties are calculated using Poisson statistics at high dijet mass, where few events are expected and Gaussian statistics is less accurate. In Fig. 4.7 we presented a lowest order calculation of both QCD and a contact interaction among left-handed quarks. The signal in Fig. 15.5 is estimated by scaling the lowest order contact interaction calculation of Fig. 4.7 by the ratio of our full simulation prediction for QCD to the lowest order QCD calculation: signal = contact $\times$ 0.6/QCD. Systematic uncertainties on the dijet ratio are small, as discussed in section 4.1.6 and demonstrated in Fig. 4.8. The calculated chisquared between QCD and the contact interaction signal, including all uncertainties on the dijet ratio, is listed in Table 15.5. In Fig. 15.5 we show the significance in σ, estimated as $\sqrt{\chi^2}$, compared to a smooth fit as a function of $1/\Lambda^+$. The anticipated capability of CMS with 1 fb^{-1} to exclude contact interactions at 95% CL or discover them at 5σ can be read off Fig. 15.5, and they are listed in Table 15.6. This includes the uncertainty on Λ due to the anticipated 5% uncertainty on the observed jet energy. The same analysis is repeated for 100 pb^{-1} and 10 fb^{-1} and the

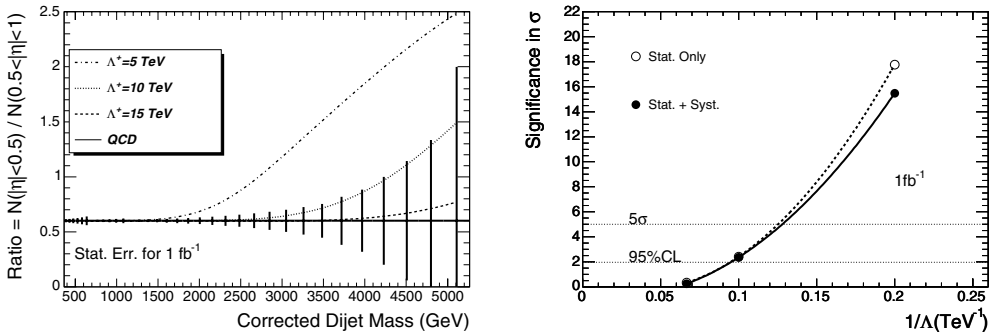

Figure 15.5. Left: The expected value and statistical error of the dijet ratio of QCD in the CMS detector for 1 fb^{-1} (solid) is compared with QCD plus a quark contact interaction at a scale Λ^+ of 15 TeV (dashed), 10 TeV (dotted) and 5 TeV (dot-dashed). Right: The significance with statistical uncertainties only (open circles) and with all uncertainties (solid circles) of the difference between QCD alone and QCD plus a quark contact interaction is plotted vs $1/\Lambda^+$ and fit with a quadratic function. Horizontal lines show the 5σ and 95% CL levels.

Table 15.5. Chisquared between signal and background. For each luminosity and contact interaction scale considered we list the chisquared between QCD alone and QCD plus a contact interaction, for the case where only statistical uncertainties are included (Stat), and for the case where both statistical and systematic uncertainties are included (All).

Luminosity	$100\,\text{pb}^{-1}$			$1\,\text{fb}^{-1}$			$10\,\text{fb}^{-1}$		
Λ^+(TeV)	5	10	15	5	10	15	5	10	15
χ^2 (Stat)	18.3	0.090	0.0037	316	5.82	0.107	3652	133	4.15
χ^2 (All)	16.7	0.082	0.0011	240	5.55	0.061	1340	124	3.56

Table 15.6. Sensitivity to contact interactions with $100\,\text{pb}^{-1}$, $1\,\text{fb}^{-1}$, and $10\,\text{fb}^{-1}$. We list the largest value of the contact interaction scale we expect to be able to exclude at a confidence level of 95% or greater, and the largest value we expect to be able to discover with a significance of 5σ or greater. Estimates include both statistical and systematic uncertainties.

	95% CL Excluded Scale			5σ Discovered Scale		
Luminosity	$100\,\text{pb}^{-1}$	$1\,\text{fb}^{-1}$	$10\,\text{fb}^{-1}$	$100\,\text{pb}^{-1}$	$1\,\text{fb}^{-1}$	$10\,\text{fb}^{-1}$
Λ^+ (TeV)	<6.2	<10.4	<14.8	<4.7	<7.8	<12.0

results are also listed in Table 15.6. The systematic uncertainties on the dijet ratio reduced the CMS sensitivity to a contact interaction between 0.1 and 0.3 TeV/c^2 depending on luminosity and level of significance. To see how quickly CMS jet data will extend the search for new physics, we note that with $100\,\text{pb}^{-1}$ our anticipated 95% CL sensitivity, $\Lambda^+ < 6.3\,\text{TeV}$, is more than twice the sensitivity of the DØ search($\Lambda^+ < 2.7\,\text{TeV}$ at 95% CL) [122]. We note that our contact interaction sensitivity to composite quarks in Table 15.6 is roughly twice our mass resonance sensitivity to excited states of composite quarks in Table 14.5, and is equivalent to observing or excluding a quark radius of order 10^{-18} cm.

15.4. Heavy Majorana neutrinos and right-handed bosons

15.4.1. Introduction

This study is exploring the left–right (LR) symmetric model $SU_C(3) \otimes SU_L(2) \otimes SU_R(2) \otimes U(1)$ [724, 725, 751] at LHC. The model embeds the SM at the scale of the order of 1 TeV

and naturally explains the parity violation in weak interactions as a result of the spontaneously broken parity. It necessarily incorporates three additional gauge bosons W_R and Z' and the heavy right-handed Majorana neutrino states N. The Ns can be the partners (N_l) of the light neutrino states ν_l ($l = e, \mu, \tau$) and can provide their non-zero masses through the see-saw mechanism [726]. Given the results from the atmospheric, solar and reactor neutrino experiments the LR model is very attractive. In the framework of the LR symmetric model, we have studied the production and the experimental signature of heavy Majorana neutrinos and the associated heavy gauge bosons. The detailed analysis is presented in [752].

Existing experimental data constrain the Z' mass to the values $O(1)\,\mathrm{TeV/c^2}$ [753]. The lower bound on the W' mass derived from the $K_L - K_S$ mass difference is quite stringent, $M_{W'} \gtrsim 1.6\,\mathrm{TeV}$ [754], however with some uncertainties from the low energy QCD corrections to the kaon system. The direct searches for W' at the Tevatron yield bounds $M_{W'} \gtrsim 720\,\mathrm{GeV/c^2}$ assuming a light (keV-range) N, and $M_{W'} \gtrsim 650\,\mathrm{GeV/c^2}$ assuming $M_N < M_{W'}/2$ [755]. These bounds are less stringent in more general LR models.

15.4.2. Heavy Majorana neutrino production and decay

The cross sections of $pp \to W_R \to l + N_l + X$ (the process studied here), and $pp \to Z' \to N_l + N_l + X$ (where $N_l \to l + j_1 + j_2$) depend on the value of the coupling constant g_R, the parameters of the CKM mixing matrix for the right-handed sector, the $W_R - W_L$ and $Z' - Z$ mixing strengths, and the masses of the partners N_l of the light neutrino state. In the study presented here the mixing angles are assumed small, the right-handed CKM matrix is identical to the left-handed one and $g_R = g_L$. With these assumptions the Z' is about 1.7 times heavier than W_R and the production cross-section for $pp \to W_R \to eN_e$ is found to be at least one order of magnitude higher than for the $pp \to Z' \to N_eN_e$ process. Finally it is assumed that only the lightest M_{N_e} is reachable at the LHC. In the case of degenerated masses of N_l, the channels with μ's and τ's are open resulting in the increase of the cross section of the process studied here by a factor of $\sim$1.2. The analysis is performed in the M_{W_R}, M_{N_e} parameter space. For the benchmark point considered (referred to as (LRRP)) $M_{N_e} = 500\,\mathrm{GeV/c^2}$ and $M_{W_R} = 2000\,\mathrm{GeV/c^2}$.

For the signal event generation and calculation of cross sections, the PYTHIA Monte Carlo program is used that includes the LR symmetric model with the standard assumptions mentioned above and CTEQ5L parton distribution functions. The fraction of $pp \to W_R^+$ ($pp \to W_R^-$) reactions as a function of M_{W_R} changes from $\simeq$70%($\simeq$ 30%) at $M_{W_R} \simeq 1\,\mathrm{TeV/c^2}$ to $\simeq$ 95%($\simeq$ 5%) at $M_{W_R} \simeq 10\,\mathrm{TeV/c^2}$. For W_R boson masses higher than $M_{W_R} \simeq 2\,\mathrm{TeV/c^2}$ the production of W_R^+ boson dominates. The W_R mass region above $1\,\mathrm{TeV/c^2}$ is studied since smaller masses are excluded by indirect analyses [756].

The signal and background data sample are simulated using the GEANT based CMS full detector simulation [8] and reconstruction package [10].

15.4.3. Analysis

The two major backgrounds considered in this study are the Z+jets and $t\bar{t}$ production. In the event selection two isolated electrons and at least two jets are required. The dielectron invariant mass M_{ee} is required to be above $200\,\mathrm{GeV/c^2}$ to suppress the Z+jets Standard Model background. The invariant mass of each electron with the two leading jets M_{ejj} ($M_{N_e}^{\mathrm{cand}}$ is formed. The M_{eejj} (W_R boson candidate) invariant mass is required to be above $1\,\mathrm{TeV/c^2}$. After this requirement the Standard Model background is suppressed as shown in Fig. 15.6.

The total W_R mass the reconstruction efficiency for $M_{W_R} = 2\,\mathrm{TeV/c^2}$ and for neutrino masses above $500\,\mathrm{GeV/c^2}$ is between 20% and 25% while for neutrino masses much smaller

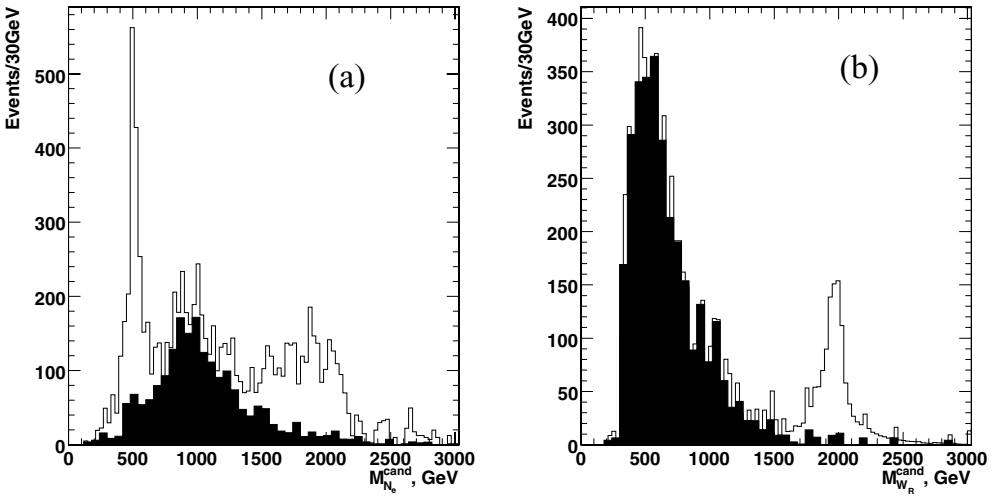

Figure 15.6. M_{ejj} for the signal overlaid with the SM background (shaded histogram) for 30 fb^{-1}: (a) M_{eejj} >1 TeV/c^2, (b) M_{eejj} <1 TeV/c^2.

than the W_R mass the reconstruction efficiency drops due to the significant overlap of the heavy neutrino decay products in $\eta - \phi$.

15.4.4. Results

The 5 sigma discovery contour in the (M_{W_R}; M_{N_e}) plane is shown in Fig. 15.7 for 1 and 30 fb^{-1}. With 30 fb^{-1} a 5 sigma observation of W_R and N_e with masses up to 4 TeV/c^2 and 2.4 TeV/c^2 respectively can be achieved. The signal at the LRRP test point (W_R of 2 TeV/c^2 and N_e 500 GeV/c^2) is observable already after one month of running at low luminosity.

15.5. Little Higgs models

15.5.1. Introduction

The Little Higgs model [656] provides an alternative mechanism of electroweak symmetry breaking keeping a light Higgs boson free from one-loop divergences of SM. It breaks a global symmetry spontaneously and invokes a number of new particles of masses in TeV scale. A heavy singlet quark of charge 2/3, marked as T, is the lightest among them and hence we study the viability of its observation with limited integrated luminosity.

The heavy quark T acquires its mass via Yukawa interactions of two gauge groups with couplings λ_1 and λ_2 which are of similar order. T has three dominant decay modes, the corresponding branching ratios following the relation: $BR(T \to th) = BR(T \to tZ) = \frac{1}{2} BR(T \to bW)$.

15.5.2. Analysis

The decay channel T $\to$ tZ, with leptonic decays of Z and W bosons, provides a clean signature at the LHC environment. This channel has not been previously studied in CMS and the work presented here is a feasibility study. Further details can be found in [757].

The signal samples were generated with PYTHIA 6.227 [24] and the T production was mimicked by activating the fourth quark generation through the W-b fusion. The T quark mass

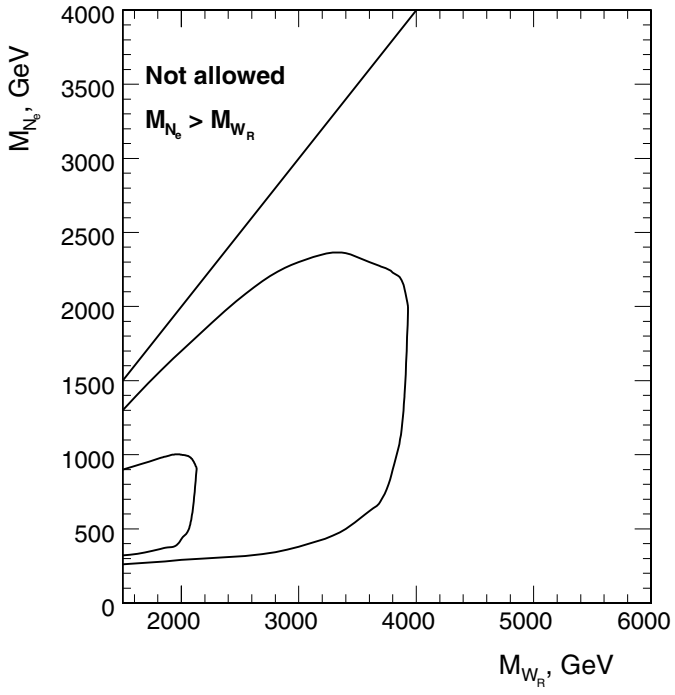

Figure 15.7. CMS discovery potential of the W_R boson and right-handed Majorana neutrinos of the Left–Right Symmetric model for the integrated luminosity $L_t = 30\,\text{fb}^{-1}$ (outer contour) and for $L_t = 1\,\text{fb}^{-1}$ (inner contour).

was set to $1\,\text{TeV/c}^2$ and was treated as a narrow resonance. The CMS full detector simulation was performed with OSCAR [8] and ORCA [10] while pile-up events corresponding to the low luminosity running period of the LHC were taken into account. The major backgrounds considered in this analysis were: $t\bar{t}$, ZW + jets, ZZ + jets, WW + jets, $Zb\bar{b}$, and Z+ jets.

The main selection requirements are summarised below:

- Events are required to pass the "double electron" or "double muon" L1 and HLT trigger criteria.
- Electrons are required to have $p_T > 20\,\text{GeV/c}$ and muons $p_T > 10\,\text{GeV/c}$.
- The combined transverse momentum of the same flavour opposite sign lepton pair is required to be $p_T^{\ell\ell} > 100\,\text{GeV/c}$. The invariant mass of the pair is required to be consistent with the nominal Z mass within $10\,\text{GeV/c}^2$.
- A further third lepton is required in the event ($e^{\pm}$ with $p_T > 20\,\text{GeV/c}$ or $\mu^{\pm}$ with $p_T > 15\,\text{GeV/c}$). The combined transverse momentum of the third lepton with the missing transverse energy is required to be greater than 60 GeV/c. In addition the transverse mass of the third lepton with the missing transverse energy is required to be less than $120\,\text{GeV/c}^2$, to be consistent with the W boson transverse mass.
- Exactly one jet compatible with a b-jet and with calibrated transverse momentum more than $30\,\text{GeV/c}$ is required.
- The combined transverse momentum of the W boson and the b-jet should be more than 150 GeV/c, while their invariant mass is required to be in the range (110–220) GeV/c^2.
- The combined ZWb system invariant mass is required to be in the mass range of the search for heavy quark, namely (850–1150) GeV/c^2.

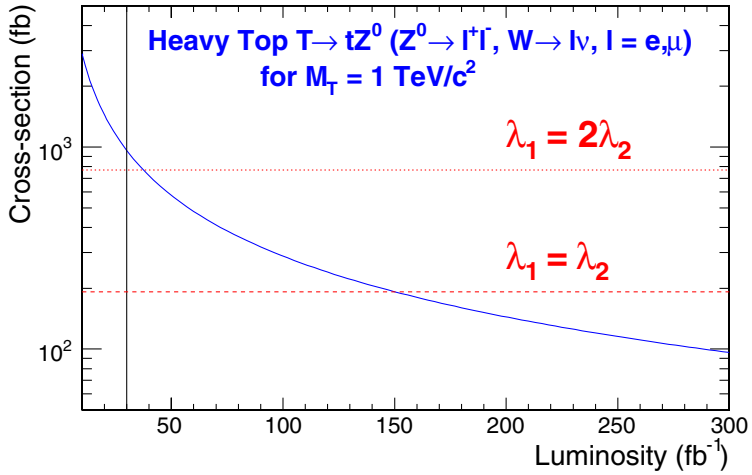

Figure 15.8. Minimum cross section required for a 5σ discovery for a heavy quark of mass $M_{\mathrm{T}} = 1\,\mathrm{TeV/c^2}$ as a function of the luminosity. The horizontal lines correspond to the cross section values for the two cases of λ_1/λ_2. The vertical line indicates the luminosity of $30\,\mathrm{fb}^{-1}$ used for this analysis.

The SM background ZZ $\rightarrow$ leptonic, is the only background that gives non-zero contribution (still less than 1 event at luminosity $30\,\mathrm{fb}^{-1}$). The total efficiency for the signal selection is $(9.7 \pm 0.4)\%$. Assuming the production cross section of T $\rightarrow$ tZ to be 192 fb for $M_{\mathrm{T}} = 1\,\mathrm{TeV/c^2}$ (for the case of $\lambda_1 = \lambda_2$) and folding in the branching ratios involved, a total of $N_S = 2.1 \pm 0.1$ signal events are expected for $30\,\mathrm{fb}^{-1}$. This implies that the discovery potential of the channel is rather limited.

The statistical significance of the channel (S_{c12}, defined in Appendix A.1) is 2.5 with a signal-to-background ratio of 41 for $30\,\mathrm{fb}^{-1}$. Taking into account systematic uncertainties from the electron energy scale, jet and missing energy scale and b-tagging efficiency uncertainty, the significance drops down to 2.0. Figure 15.8 shows the signal cross section as a function of the integrated luminosity at the LHC, for establishing at 5σ level, single production of a heavy quark of mass $= 1\,\mathrm{TeV/c^2}$. The luminosity needed for 5σ evidence is estimated to be around $150\,\mathrm{fb}^{-1}(40\,\mathrm{fb}^{-1})$ for choices of parameters $\lambda_1 = \lambda_2$ ($\lambda_1 = 2\lambda_2$). The vertical line corresponds to the luminosity used for this analysis and demonstrates the inadequacy of statistics for a luminosity of $30\,\mathrm{fb}^{-1}$.

15.6. Same sign top

At the LHC dileptonic $t\bar{t}(+jets)$ events can be selected with a relatively high signal-to-noise ratio and efficiency. Within the clean sample of such events, both leptons (electrons and muons) have an opposite electric charge. In several models beyond the Standard Model however, $tt/\bar{t}\bar{t}(+jets)$ topologies are predicted where both leptons have an equal electric charge. The signal excess is highly enhanced by the application of a combined likelihood variable described in [284]. The likelihood variable is designed to differentiate the lepton from the W boson decay from leptons arising for example in QCD jets or from fake reconstructions. The signal of new physics can be diluted by the mis-identification of the electric charge of the leptons in Standard Model $t\bar{t}(+jets)$ events and the mis-identification of the leptons from the W decay themselves. The observability of an excess of same-sign signals above

Table 15.7. Overview of the selection criteria applied on the events using simulated events with pile-up collisions included. The expected number of events are rescaled to a dataset of 1 fb^{-1} taking into account the respective Leading-Order cross-sections of the processes.

	$\mu\mu$	μe and ee	$t\bar{t} \to \tau + X$	Other $t\bar{t}$	$W^{\pm}W^{\mp}$	$Z + jets$	S/N
Before selection	6915.0	20745.0	34606.2	485973.2	189951.7	578033.3	0.0078
Trigger	6114.7	16314.8	17415.6	100137.2	41288.4	266366.7	0.017
Two jets $E_T > 25$ GeV	4398.2	11982.7	13560.9	93858.2	20593.8	66146.7	0.032
b-tag criteria	989.8	2485.4	2289.6	8784.7	133.5	240.0	0.13
Two leptons identified	888.2	30.1	375.8	801.6	1.7	73.3	1.30
Two leptons selected	481.5	0.07	48.4	3.01	0.4	53.3	4.7
Efficiency (in %)	6.96	0.0003	0.14	0.0006	0.00022	0.0092	
Opposite-sign	481.3	0	48.3	2.19	0	53.3	
Same-sign	0.2	0.07	0.1	0.82	0.4	0	
	ee	μe and $\mu\mu$	$t\bar{t} \to \tau + X$	Other $t\bar{t}$	$W^{\pm}W^{\mp}$	$Z + jets$	S/N
Before selection	6915.0	20745.0	34606.2	485973.2	189951.7	578033.3	0.0078
Trigger	5354.8	17074.7	17415.6	100137.2	41288.4	266366.7	0.015
Two jets $E_T > 25$ GeV	3960.9	12420.0	13560.9	93858.2	20593.8	66146.7	0.029
b-tag criteria	802.7	2672.4	2289.6	8784.7	133.5	240.0	0.11
Two leptons identified	724.5	34.6	453.8	2283.6	73.1	126.7	0.57
Two leptons selected	285.0	0.3	37.5	5.2	0.8	53.3	3.1
Efficiency (in %)	4.12	0.0013	0.11	0.0011	0.00044	0.0092	
Opposite-sign	279.6	0.3	36.8	4.1	0.4	46.7	
Same-sign	5.4	0	0.7	1.1	0.4	6.7	
	$e\mu$	$\mu\mu$ and ee	$t\bar{t} \to \tau + X$	Other $t\bar{t}$	$W^{\pm}W^{\mp}$	$Z + jets$	S/N
Before selection	13830.0	13830.0	34606.2	485973.2	189951.73	578033.3	0.016
Trigger	10960.0	11469.5	17415.6	100137.2	41288.4	266366.7	0.030
Two jets $E_T > 25$ GeV	8021.8	8359.1	13560.9	93858.2	20593.8	66146.7	0.061
b-tag criteria	1682.7	1792.5	2289.6	8784.7	133.5	240.0	0.25
Two leptons identified	1500.6	66.4	822.1	3001.6	30.2	20.0	0.88
Two leptons selected	722.7	0.9	85.2	6.3	0.4	0	8.3
Efficiency (in %)	5.23	0.0065	0.25	0.0013	0.00022	0	
Opposite-sign	715.5	0.9	83.8	4.9	0	0	
Same-sign	7.2	0	1.3	1.4	0.4	0	

the mis-reconstruction of the Standard Model background is determined. The details of the analysis are mentioned in [758].

The jets in the final state are reconstructed with an Iterative Cone jet clustering algorithm using a cone size of $\Delta R = 0.5$. Input objects for the cones are selected from all calorimeter towers above a pseudo-rapidity dependent energy threshold determined from the average underlying event energy deposits [165]. The energy scale of the reconstructed jets is calibrated with corrections from Monte Carlo studies. The primary vertices in the proton bunch crossing are determined, and the vertex with the highest transverse momentum is taken as the one of the hard scattering. Via a track-based algorithm, jets are rejected if they do not match with this hard primary vertex.

The leptons are reconstructed and identified using the methods described in [284]. A likelihood variable is used to suppress leptons from the heavy flavour quark background exploiting several reconstruction aspects of leptons in the CMS detector. This likelihood is determined for each muon or electron in the final state in order to enhance the purity of choosing the correct lepton from the leptonic W decay. The combined likelihood

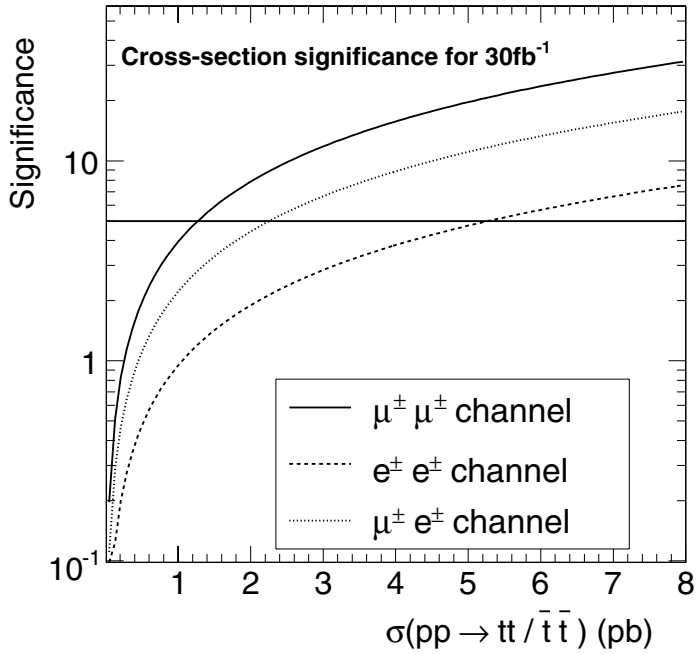

Figure 15.9. For an integrated luminosity of $30\,\mathrm{fb}^{-1}$ the significance of the same-sign tt or $\overline{tt}$ excess above the Standard Model events is indicated as a function of the cross-section of the inclusive process $pp \to tt/\overline{tt}$.

includes observables as tracker isolation, calorimeter isolation, vertex matching significance, transverse momentum of the lepton and angular distance to the closest jet. For the electron likelihood a variable reflecting the reconstruction quality is added. The two muons or electrons having the largest combined likelihood ratio value are taken as the hard leptons of interest.

The inclusive single-muon, single-electron, double muon and double electron triggers are applied as described in [506]. The event should be triggered in at least one of these streams. In total 88.4%, 77.4% and 79.2% of respectively the $\mu\mu$, the ee and the μe signal events remain after applying the trigger criteria. The event is required to have at least 2 jets with a calibrated E_{T} above 25 GeV. These jets need to have a pseudo-rapidity in the range $|\eta| < 2.4$ and a b-tag discriminant larger than 0.5 [157]. The reconstructed hard leptons are required to have transverse momentum p_{T} exceeding $25\,\mathrm{GeV/c}$ in the pseudo-rapidity range of $|\eta| < 2.4$ and a combined likelihood variable larger than 0.05.

In Table 15.7 the efficiencies and signal-to-noise ratios are shown after each selection step. Applying all cuts a signal-to-noise ratio of 4.7, 3.1 and 8.3 is obtained for respectively the $\mu\mu$, the ee and the $e\mu$ final state. Cross-talk between these three considered final states is by construction not possible. As the amount of selected WW and $Z + jets$ events in Table 15.7 is small, their contribution is alternatively estimated by multiplying the efficiencies of the event selection without the b-tagging and the individual b-tagging selection cut efficiency under the assumption that both selection cuts are uncorrelated.

It is illustrated [758] that from the selected topology of dilepton $t\bar{t}$ events, a ratio $R = \frac{N_{++,--}}{N_{+-}}$ can be determined which is sensitive to physics beyond the Standard Model. In the ratio the total amount of events with equally charged leptons is divided by the total amount of events with opposite charged leptons. As the efficiency of reconstructing the leptons electric charge is very high, we can neglect the amount of selected $pp \to tt$ or $pp \to \overline{tt}$

events observed with two opposite-charged leptons. Using the uncertainty on the ratio R, the significance of the observation of new physics channels $pp \to tt$ or $pp \to \overline{tt}$ is determined as a function of the cross section (see Fig. 15.9). The dimuon channel has a larger sensitivity compared to the decay channels with electrons. This is caused by the electron reconstruction where a large fraction of electron energy clusters are matched with a wrong track resulting in a charge ambiguity.

It is assumed that the new physics processes beyond the Standard Model have a similar kinematic topology compared to the $t\bar{t}$ process, therefore the selection efficiency of the new physics channels is taken equal to that of the Standard Model $t\bar{t}$ process. Several models predict an excess of events with same-sign leptons in this topology, via the process $pp \to tt/\overline{tt}$ or $pp \to tt/\overline{tt} + b/c$. These models are motivated by Flavour Changing Neutral Currents (FCNC) [759, 760], topcolour-assisted Technicolour (TC2) [761] or supersymmetry [762]. With a measurement of R these kinematically similar processes $pp \to tt/\overline{tt}$ can be observed with 30 fb^{-1} of integrated luminosity if they have a cross section above 1 pb. Because a ratio of kinematically similar event topologies is measured, most of the experimental and theoretical systematic uncertainties cancel. The uncertainty of the background cross sections on the significances shown in Fig. 15.9 is found to be negligible. A feasibility study is performed to estimate the potential uncertainty on the mis-identification efficiency of the electric charge of electrons and muons from Z boson decays [758]. The effect on the significance of the excess of $tt/\overline{tt}$ events is found to be negligible.

Appendix A. 95% CL limits and 5σ discoveries

A.1. Estimators of significance

Several methods exist to quantify the statistical "significance" of an expected signal at future experiments. Following the conventions in high energy physics, the term significance usually means the "number of standard deviations" an observed signal is above expected background fluctuations. It is understood implicitly that S should follow a Gaussian distribution with a standard deviation of one. In statistics, the determination of the sensitivity is a typical problem of hypothesis testing, aiming at the discrimination between a null-hypothesis H_0 stating that only background and no signal is present, and a alternative hypothesis H_1, which states the presence of a signal on top of the background. The "significance level" is the probability to find a value of a suitably constructed test statistic beyond a certain pre-specified critical value, beyond which the validity of H_1 is assumed. The significance level has to be converted into an equivalent number of Gaussian sigmas to arrive at the common terminology of a high-energy physicist.

Since a signal is usually searched for in many bins of a distribution, and in many channels, a very high value of the significance of a local excess of events must be demanded before an observed "peak" found somewhere in some distribution can be claimed to be an observation of a signal. If the position of the signal peak is not known a-priori and treated as a free parameter in searches for new physics, the probability of background fluctuations is much higher. This is quantified in a case study in Section A.2 below, and this aspect will need careful consideration in the near future before first data taking at the LHC. The general, somewhat arbitrary convention is that the value of S of a local signal excess should exceed five, meaning that the significance level, or the corresponding one-sided Gaussian probability that a local fluctuation of the background mimics a signal, is 2.9×10^{-7}.

Here, the recommendations for the procedures to be used for the studies presented in this document are summarised. The aim of many of these studies is the prediction of the average expected sensitivity to the observation of a new signal in a future experiment. The real experiment might be lucky, i.e. observe a higher significance than the average expectation, or a downward fluctuation of the expected signal could lead to a lower observed significance. The proposed methods have been checked in a large number of pseudo-experiments using Monte Carlo simulation in order to investigate whether the probability of a background fluctuation having produced the claimed significance of the discovery is properly described.

Counting methods use the number of signal events, s, and the number of background events, b, observed in some signal region to define the significance S. These event numbers can be turned into a significance, S_{cP}, by using either the Poisson distribution for small numbers of events, or, in the high-statistics limit, the Gaussian distribution, leading to

$$S_{c1} = \frac{s}{\sqrt{b}}. \tag{A.1}$$

The significance may also be obtained from the ratio of the likelihoods, $\mathcal{L}_1$ and $\mathcal{L}_0$, belonging to the hypothesis H_0 and H_1,

$$S_L = \sqrt{2 \ln Q}, \text{ with } Q = \frac{\mathcal{L}_0}{\mathcal{L}_1}. \tag{A.2}$$

This approach is theoretically well founded and is applicable also to the simple approach of the counting method, leading to

$$S_{cL} = \sqrt{2\left((s+b)\,\ln\left(1+\frac{s}{b}\right)-s\right)}, \tag{A.3}$$

which follows directly from the Poisson distribution. In the Gaussian limit of large numbers s and b, S_{cL} becomes equivalent to S_{c1}. The likelihood approach can be extended to include the full shapes of the signal and background distributions for the hypothesis H_0 and H_1, and the likelihood may be obtained from binned or unbinned likelihood fits of the background-only and the background-plus-signal hypotheses to the observed distributions of events.

Another estimator,

$$S_{c12} = 2\left(\sqrt{s+b}-\sqrt{b}\right), \tag{A.4}$$

has been suggested in the literature [79, 763]. The formula for S_{c12} is strictly only valid in the Gaussian limit, but tabulated values exist for small statistics.

The presence of systematic errors deserves some special care. Two cases must be separated clearly:

(a) If the background and signal contributions can be determined from the data, e.g. by extrapolating the background level into the signal region from sidebands, systematic errors may be irrelevant, and the systematic errors only influence our ability to predict the average expected sensitivity. In this case, simple propagation of the theoretical errors on s and b applied to the above formulae for the various significances is all that is needed.

(b) If systematic errors on the background will affect the determination of the signal in the real experiment, e.g. because an absolute prediction of the background level or a prediction of the background shape are needed, the theoretical uncertainty must be taken into account when estimating the sensitivity. This can be done by numerical convolution of the Poisson distribution, or the Gaussian distribution in the high-statistics limit, with the probability density function of the theoretical uncertainty. Numerical convolutions of the Poisson distribution with a theoretical error of a Gaussian shape, leading to a variant of S_{cP} including systematic errors, were used for this document [679]. Numerical convolutions of the Poisson distribution with a systematic error of a Gaussian shape, leading to a variant of S_{cP} including systematic errors, were used for this document. The program ScPf [679] computes the significance by Monte Carlo integration with the assumption of an additional Gaussian uncertainty Δb on b. The significance can be approximated by an extension of S_{c12}:

$$S_{c12s} = 2\left(\sqrt{s+b}-\sqrt{b}\right)\,\frac{b}{b+\Delta b^2}. \tag{A.5}$$

In the Gaussian limit it leads to

$$S_{c1} = s/\sqrt{b+\Delta b^2}. \tag{A.6}$$

The most crucial point in this context is a realistic description of the probability density function of the systematic theoretical uncertainty, which can be anything ranging from a flat distribution between $b \pm \Delta b$ to a pathological distribution with a significant non-Gaussian tail, but, in practice, is hardly ever known precisely.

The distribution of a significance estimator S in a series of experiments, its probability density function (p.d.f.), is of prime importance for the calculation of discovery probabilities in the presence of a real signal, or of fake probabilities due to fluctuations of the background. In the large-statistics limit, the likelihood-based significance estimators are expected to follow a χ^2-distribution with a number of degrees of freedom given by the difference in the number of free parameters between the alternative hypothesis and the null hypothesis [103]. When

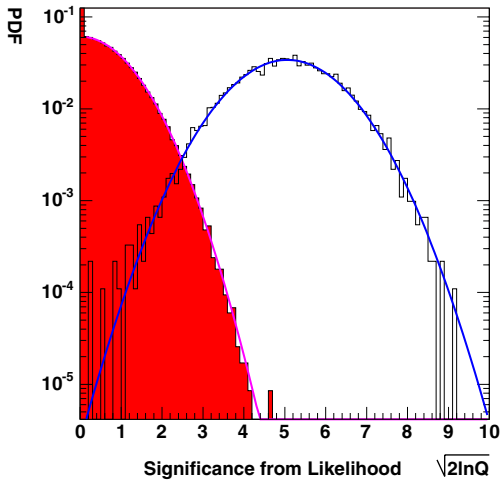

Figure A.1. Probability density functions of the estimator of significance S_L for small statistics (11 signal events over a background of 1.5 events). Filled histogram: pure background sample from 200 000 toy experiments, open histogram: background plus signal from 10 000 toy experiments. Gaussian fits are overlayed; the distribution of S_L for the background-only sample has a mean of -0.004 and a width of $\sigma = 1.0$, the background-plus-signal sample has a width of 1.1.

testing for the presence of a signal on top of background at a fixed peak position, $2 \ln Q = S_L^2$ is expected to follow a χ^2 distribution with one degree of freedom, i.e. a standard Gaussian distribution. All of the above estimators have been tested in a large number of toy experiments, see e.g. [60, 100, 102]. In particular the likelihood based estimators were found to be well-behaved, i.e. the distribution of the values of significance followed the expected behaviour already at moderate statistics, as is shown for one example in Fig. A.1. Good scaling with the square root of the integrated luminosity was also observed in these studies. On the other hand, the estimator S_{c1} cannot be considered a useful measure of significance at low statistics.

A quantitative comparison as a function of the number of background events for fixed values of $s/\sqrt{b}$ of the various estimators discussed above is shown in Fig. A.2. S_{cL} and S_{cP} are found to agree very well, while S_{c12} tends to slightly underestimate the significance, a result which was also verified in the above Monte Carlo studies with large samples of toy experiments. While S_{cL} and S_{cP} remain valid independent of the value of b, the simpler estimator S_{c1} can only be used for background levels larger than 50 events.

A.2. On the true significance of a local excess of events

In searching for new phenomena in a wide range of possible signal hypotheses (e.g. a narrow resonance of unknown mass over a broad range background), a special care must be exercised in evaluating the true significance of observing a local excess of events. In the past, this fact was given substantial scrutiny by statisticians (e.g. [764, 765]) and physicists (e.g., [766–770]) alike. The purpose of this Appendix is to quantify a possible scope of this effect on an example of a search for the Standard Model Higgs boson in the $H \to ZZ^{(*)} \to 4\mu$ decay channel. As the case study, we chose a counting experiment approach widely used in this volume.

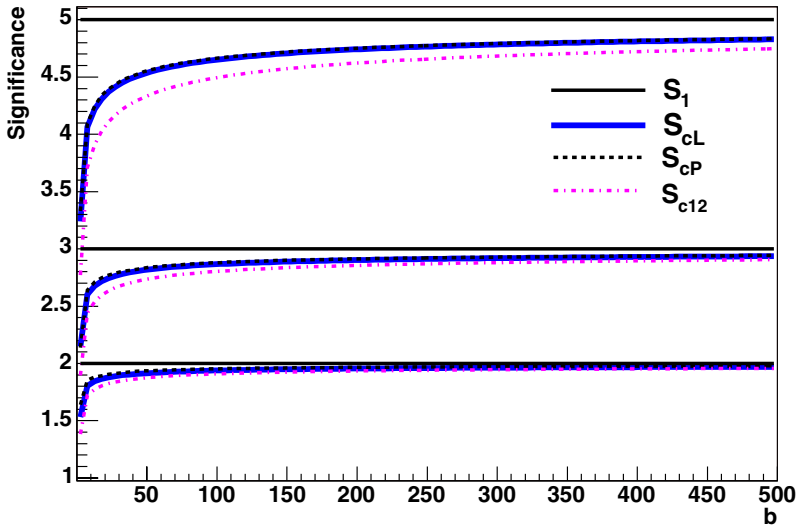

Figure A.2. Comparison of the various significance estimators as a function of the number of background events, b. The number of signal events was taken as $s = S_{c1}\sqrt{b}$, hence the constant black lines represent the value of S_{c1}. As can be seen, S_{cP} and S_{cL} agree perfectly, while S_{12} leads to slightly smaller values of significance. S_1 significantly overestimates the significance at small event numbers.

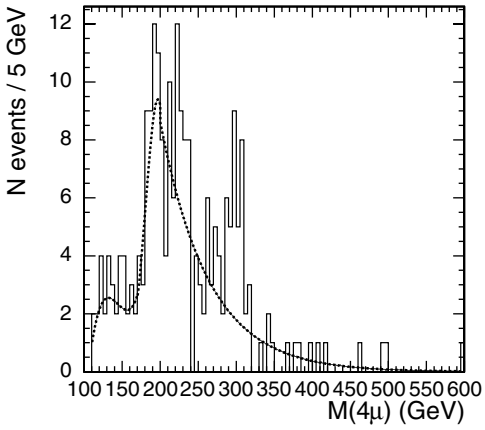

Figure A.3. The background *pdf* and an example of one pseudo-experiment with a statistical fluctuation appearing just like a signal.

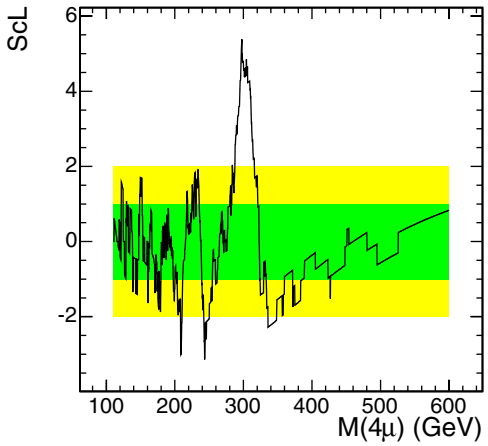

Figure A.4. Profile of the S_{cL} scan corresponding to the pseudo-experiment example shown on the left. Green (inner) and yellow (outer) bands denote $\pm 1\sigma$ and $\pm 2\sigma$ intervals. Spikes that can be seen are due to events coming in or dropping off the trial-window, a feature of low-statistics searches.

The dashed line in Fig. A.3 shows the expected 4μ invariant mass distribution for background at $\mathcal{L} = 30\,\text{fb}^{-1}$ after applying all the $m_{4\mu}$-dependent analysis cuts described in Sec. . Using this distribution, we played out $\sim 10^8$ pseudo-experiments; an example is shown in Fig. A.3. For each pseudo-experiment, we slid a *signal region window* across the spectrum looking for a local event excess over the expectation. The size of the window $\Delta m = w(m_{4\mu})$ was optimised and fixed *a priori* (about $\pm 2\sigma$) to give close to the best significance for a

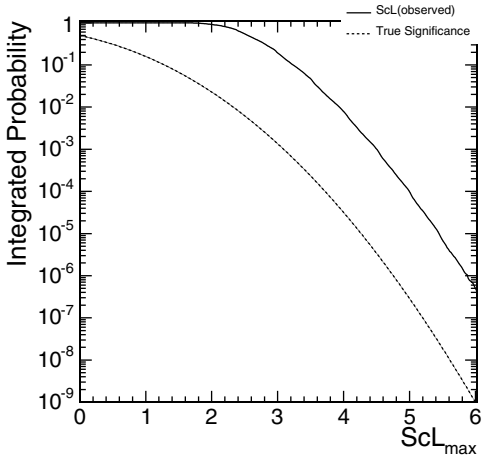

Figure A.5. S_{cL} cumulative probability density function.

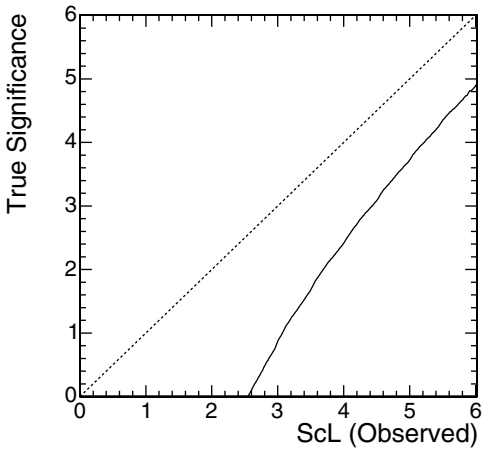

Figure A.6. Local significance "renormalisation" from an observed value to the true significance with a proper probabilistic interpretation.

resonance with a width corresponding to the experimental SM Higgs boson width $\sigma(m_{4\mu})$. The step of probing different values of $m_{4\mu}$ was "infinitesimally" small ($0.05\,\mathrm{GeV/c^2}$) in comparison to the Higgs boson width of more than $1\,\mathrm{GeV/c^2}$. The scanning was performed in *a priori* defined range of 115–600 $\mathrm{GeV/c^2}$.

We used a significance estimator $S_{cL} = \mathrm{sign}(s)\,\sqrt{2\,n_o \ln(1+s/b) - 2\,s}$, where b is the expected number of background events, n_o is the number of observed events, and the signal is defined as $s = n_o - b$. This estimator, based on the Log-Likelihood Ratio, is known to follow very closely the true Poisson significance, only slightly over-estimating it in the limit of small statistics [51]. Figure A.4 presents the results of such a scan for the pseudo-experiment shown in Fig. A.3. The maximum value of S_{cL}, S_{max}, and the corresponding mass of a "Higgs boson candidate" obtained in each pseudo-experiment were retained for further statistical studies.

After performing 10^8 pseudo-experiments, the differential probability density function for S_{max} and its corresponding cumulative probability function $P(S_{max} > S)$ (Fig. A.5) were calculated. From Fig. A.5, one can see that the frequency of observing some large values of S_{cL} (solid line) is much higher than its naive interpretation might imply (dashed line). If desired, the actual probability can be converted to the true significance. The result of such "renormalisation" is presented in Fig. A.6. One can clearly see that the required de-rating of significance is not negligible; in fact, it is larger than the effect of including all theoretical and instrumental systematic errors for this channel (see Section 3.1). More details on the various aspects of these studies can be found in [51].

There are ways of reducing the effect. A more detailed analysis of the shape of the $m_{4\mu}$ distribution will help somewhat. Using the predicted number of signal events $s = s_{theory}$ in the significance estimator to begin with and, then, for validating the statistical consistency of an excess $n_o - b$ with the expectation s_{theory} will reduce the effect further. One can also use a non-flat prior on the Higgs mass as it comes out from the precision electroweak measurements. Whether one will be able to bring the effect to a negligible level by using all these additional constraints on the signal hypotheses is yet to be seen. The purpose of this Appendix is not to give the final quantitative answer, but rather to assert that these studies must become an integral part of all future search analyses when multiple signal hypotheses are tried.

Appendix B. Systematic Errors

B.1. Theoretical uncertainties

The simulation of events at the LHC is complex and can be conventionally divided into different parts which either involve the description of the interesting physics process or the description of the initial scattering conditions and the physics environment.

The simulation of the hardest part of the physics process is done via matrix element (ME) calculations at a certain order in the coupling constants and continues with the parton showering (PS) of the resulting partons until a cut-off scale, over which the perturbative evolution stops and the fragmentation of the final partons takes on. This cut-off is often referred to as factorisation scale, because it is the scale at which the two processes (showering and fragmentation) are supposed to factorise.

The interesting event is accompanied by the so-called underlying event (UE), term which identifies all the remnant activity from the same proton-proton (p–p) interaction and whose definition often includes ISR as well, and the pile-up, composed by other minimum bias (MB) p–p interactions in the same bunch crossing (up to 25 at high luminosity at the LHC). Moreover, since the initial state is not defined in p–p collisions, a proper description of the proton parton density functions (PDFs) should be included in the calculations.

Each of these effects needs to be modelled to the best of our knowledge, and the associated uncertainties need to be determined and propagated to the physics measurements. Moreover, many of the sources are correlated: for instance, fragmentation and showering are obviously dependent on each other, and in turn they assume a certain description of the underlying event. The task of assessing systematics due to theory and modelling can therefore be a difficult one and can sometime contain a certain degree of arbitrariness.

In what follows we propose some guidelines for the estimation of errors coming from the above, trying to divide the systematics sources into wider categories as much uncorrelated as possible: QCD radiation, fragmentation description, PDFs, UE and MB.

In attributing systematic errors we believe that one should use motivated recipes, avoiding unrealistic scenarios which will lead to unnecessarily conservative errors or, much worse, totally arbitrary assumptions.

B.1.1. Hard process description and parametric uncertainties

The description of the hard process should be done with Monte Carlo tools which are best suited to the specific analysis. For instance, when precise description of hard gluon emission becomes an issue, then next-to-leading order (NLO) generator tools like MC@NLO [771], or higher leading order (LO) α_s generators like COMPHEP [43], MADGRAPH [81], ALPGEN [161], and SHERPA [194] should be considered. This is in general true for both the signal and the background description.

When adopting a ME tool, one should always keep in mind that its output is often (if not always) supposed to be interfaced to PS Monte Carlo such as HERWIG [196], PYTHIA [24] or ISAJET [672], that treat the soft radiation and the subsequent transition of the partons into observable hadrons. One of the most difficult problems is to eliminate double counting where jets can arise from both higher order ME calculations and from hard emission during the shower evolution. Much theoretical progress has been made recently in this field [772–775]. For what concerns the ME/PS matched description of multi-jet final states, a rich spectrum of processes is currently available in ALPGEN. However, adopting general purpose generators like PYTHIA can still be the best option for topologies that are better described in the Leading

Logarithm Approximation (LLA), for instance in the case of two leading jets and much softer secondary jets. The two different descriptions should be regarded as complementary.

In general, a sensible choice for the selection of the best generation tools can be driven by the HEPCODE data base [776]. However, comparison between different generators is recommended whenever applicable.

Each analysis needs then to make sure that other important effects (e.g. spin correlations in the final state, NLO ME corrections to top decays) are included in the generation mechanism. For example, TopReX [44], as long with some of the Monte Carlo generators already introduced in this section, provides a correct treatment of top quark spin correlations in the final state. Neglecting some of these effects corresponds to introducing an error in the analysis that cannot be considered as coming from a theoretical uncertainty.

For both signal and backgrounds, missing higher orders are a delicate source of uncertainty. Formally, the associated error cannot be evaluated unless the higher order calculation is available. This is often not possible, unless extrapolating by using comparisons with analytical calculations of total or differential cross-sections at the next order, if available. One should keep in mind that simple K-factors are not always enough and that the inclusion of higher orders typically also involves distortions in differential distributions.

Moreover, one should not forget that any Standard Model calculation is performed in certain schemes and that the input parameters are subject to their experimental uncertainties; if the error on most of those and the choice of the renormalisation scheme are expected to give negligible effects in comparison with other uncertainties, this might not be so for the choice of the hard process scale, which we will discuss in the next section, and some of the input parameters.

Among the input parameters, by far the one known with less accuracy will be the top mass. The current uncertainty of about 2% [777] enters in the LO calculations for processes which involve top or Higgs production. For instance, the total $t\bar{t}$ cross-section is known to have a corresponding 10% uncertainty due to this [45]. As far as Higgs production (in association or not with tops) is concerned, gluon–gluon fusion proceeds via a top loop and therefore the total cross-section can have a strong dependence on the top mass when $m_H \approx 2m_t$. Analyses which include Higgs bosons or top are encouraged to estimate the dependence of the significant observables on the top mass itself. Effects of m_t variation on acceptances of these analyses should instead be negligible.

B.1.2. Hard process scale

The hard process under study drives the definition of the Q^2 scale, which directly enters in the parametrisation of PDFs and α_s, hence in the expression of the cross sections.

The dependence of the observables on the choice for the Q^2 hard process scale is unphysical and should be regarded as one important contribution to the total uncertainty in the theoretical predictions. The sensitivity of the predicted observables to such choice is expected to decrease with the increasing order in which the calculation is performed, and can be tested by changing the hard process scale parameters in the generation (where applicable) using a set of sound values according to the characteristics of the hard process.

A sensible choice for the hard process scale in $2 \to 1$ processes is often $\hat{s}$, which is the default in general purpose generators like PYTHIA. Alternative choices to quote theoretical uncertainties can be $0.25\hat{s}$ and $4.0\hat{s}$. In PYTHIA this can be obtained acting on PARP(34).

For $2 \to n$ processes, many reasonable alternatives for the Q^2 scale definition exist. The PYTHIA default (MSTP(32) = 8), corresponds to the average squared transverse mass of the outgoing objects. It is possible to test the sensitivity on the Q^2 scale switching to different options, for example trying $Q^2 = \hat{s}$ (MSTP(32) = 4 in PYTHIA).

B.1.3. PDF description

The parton distribution functions of interacting particles describe the probability density for partons undergoing hard scattering at the hard process scale Q^2 and taking a certain fraction x of the total particle momentum. Since the Q^2 evolution can be calculated perturbatively in the framework of QCD, PDFs measurements can be cross checked using heterogeneous DIS, Drell–Yan and jet data, and achieve predictivity for points where no direct measurements are available yet, for example in a large region of the (x,Q^2) space for p–p interactions at the LHC energy.

Various approaches are currently available to quote the PDFs of the proton, which propose different solutions for what concerns the functional form, the theoretical scheme, the order of the QCD global analysis (including possible QED corrections), and the samples of data retained in the fits: CTEQ [778], MRST [779], Botje [780], Alekhin [781], etc. The CTEQ and MRST PDFs, including Tevatron jet data in the fits, seem to be well suited for use in Monte Carlo simulations for the LHC.

The best way to evaluate theoretical uncertainties due to a certain proton PDFs is to vary the errors on the parameters of the PDF fit itself. With the Les Houches accord [95] PDF (LHAPDF) errors should be easily propagated via re-weighting to the final observables. However, errors are available only for NLO PDF, whereas in most of the cases only LO tools are available for the process calculation. Correctly performing evaluation of theoretical uncertainties in these cases requires some care. The proposed solution is to adopt CTEQxL (LO) for the reference predictions using CTEQxM (NLO) only to determine the errors.

For analyses which are known to be particularly sensitive to PDFs, like cross-section measurements, it would be also desirable to compare two different sets of PDFs (typically CTEQ vs MRST) taking then the maximum variation as an extra error. This is important since, even considering the error boundaries, different set of PDFs may not overlap in some region of the phase space.

The LHAGLUE interface [95] included from the most recent LHAPDF versions simplifies the use of the Les Houches accord PDF in PYTHIA by the switches MSTP(52) = 2, MSTP(51) = LHAPDF$_{id}$.

B.1.4. QCD radiation: the parton shower Monte Carlo

The showering algorithm is basically a numeric Markov-like implementation of the QCD dynamic in the LLA. After the generation of a given configuration at partonic level, the initial state radiation (ISR) and the final state radiation (FSR) are produced following unitary evolutions with probabilities defined by the showering algorithm.

The probability for a parton to radiate, generating a $1\rightarrow 2$ branching, are given by the Altarelli–Parisi equations [782], however various implementations of the showering algorithm exist in parton shower Monte Carlo, which mostly differ for the definition of the Q^2 evolution variable (virtuality scale) in the $1\rightarrow 2$ radiation branching and for the possible prescriptions limiting the phase space accessible to the radiation: PYTHIA, HERWIG, ARIADNE [783], ISAJET etc.

The virtuality scales for both ISR and FSR need to be matched to the hard process scale, the latter setting an upper limit on the former ones; such limit has to be considered in a flexible way, given the level of arbitrariness in the scale definitions. While this matching is somewhat guaranteed if one adopts the same simulation tool for both hard scattering and parton shower, a careful cross check is recommended in all other cases. In general, a critical judgement taking into account the hard process type is needed. Allowing a virtuality scale higher than the hard

process scale may give rise to double counting. This is the case of gg→gg processes with additional hard gluons added in the showering. However other processes are safer from this point of view, for instance the case of the $q\bar{q} \rightarrow Z$ process at LO.

Quantum interference effects in hadronic collisions have been observed by CDF [784] and DØ [785] studying the kinematical correlations between the third jet (regarded as the result of a soft branching in the LLA) and the second one. The implementation of the so called colour coherence in PS Monte Carlo is made in the limit of large number of colours and for soft and collinear emissions, restricting the phase space available to the radiation depending on the developed colour configuration. Different implementations of the colour coherence are available in HERWIG and PYTHIA, while ISAJET doesn't take into account such effects.

The theoretical uncertainty associated to the parton showering descriptions, includes what is normally referred to as ISR or FSR and their interference. In order to achieve practical examples for the recommended parton shower settings, we will consider PYTHIA as the default tool for showering from now on.

Turning OFF ISR and FSR (MSTP(61) = 0, MSTP(71) = 0 respectively) or even the interference part (MSTP(62) = 0, MSTP(67) = 0) is certainly a too crude approach and, to a large extent, a totally arbitrary procedure to assess a systematic error. We believe it is much more realistic to vary, according to sound boundaries, the switches regulating the amount and the strength of the radiation of the showering. These can correspond to Λ_{QCD} and the maximum virtuality scales up to which ISR stops and from which FSR starts. It would be important to switch the parameters consistently going from low to high values in both ISR and FSR.

Notice that the radiation parameters were typically fitted at LEP1 together with the fragmentation parameters, benefiting from a much simplified scenario where no ambiguity on the maximum virtuality scale applies, the only relevant energy scale of the problem being $\hat{s} = s$. One has to take into account that while for instance FSR accompanying heavy boson decays at the LHC can be directly related to the LEP experience, FSR in processes like $gg \rightarrow b\bar{b}$ entails additional uncertainties arising from the maximum allowed virtuality scale and ISR/FSR interference. On top of that, additional complications arise from the fact that ISR at hadron machines contributes to the description of the underlying event. Matching two different tunings of the same parameter (in particular PARP(67)) can be very subtle at the LHC.

These are the suggested settings in PYTHIA, which have been cross-checked with the ones adopted by the CDF experiment and also follow the prescription by the main author:

- Λ_{QCD}: PARP(61), PARP(72), PARJ(81) from 0.15 to 0.35 GeV consistently, symmetric with respect to 0.25. Notice that these settings have been optimised for the CTEQ6L PDFs. In general different ranges apply when changing PDFs. In order to give the user full control on these parameters the option MSTP(3) = 1 has to be set, otherwise Λ_{QCD} is assumed to be derived from the PDFs parametrisation.
- Q^2_{max}: PARP(67) from 0.25 to 4 and PARP(71) from 1 to 16 going from low to high emission in a correlated way. In doing so one should also make sure that the tuning of the underlying event is not changing at the same time. Possible re-tuning of the underlying event in different radiation scenarios may be needed, in particular for what concerns PARP(82).

B.1.5. Fragmentation

Perturbative QCD cannot provide the full description of the transition from primary quarks to observable hadrons, but only the part which involves large momentum transfer. The formation of final hadrons involves a range of interactions which goes above the Fermi scale and where

the strong coupling constant α_s increases above unity, making it necessary to describe this part in a non-perturbative way, normally referred to as fragmentation or hadronisation.

The non-perturbative description of fragmentation is realised via models, which need to be tuned to experimental data. The data correspond, typically, to event shapes and multiplicities at leptonic machines or to the inclusive jet shapes at hadronic machines. A comprehensive overview of the models can be found in [786].

Fragmentation is said to depend only on the factorisation scale if jet universality is assumed, i.e. assuming that jets fragment in the same way at hadron and lepton machines. Jet universality will be ultimately verified at the LHC; one should clarify whether instrumental effects and the LHC environment will have an impact on the final observables. For instance, the much larger fraction of gluon jets or the different description of the underlying event can change the values of the parameters that regulate the fragmentation. Moreover, for events with high multiplicity of jets it will also be crucial to properly describe fragmentation in conditions where large jet overlapping is to be expected and where inclusive tunings might not be ideal.

The consequence of jet universality is that, once the PS cut-off scale is fixed, the fragmentation description for light quarks should be universal, and the LEP/SLD tunings (or the Tevatron ones) could be used as they are for the LHC.

It is important to underline that the description of the non-perturbative part of the radiation also depends on the way the perturbative one is described. This means that one should not use a tuning of fragmentation done with LO(+LL) tools (typically PYTHIA at LEP) attached to perturbative calculation which are done at higher (or different) order.

B.1.5.1. Light quarks fragmentation. In the absence of LHC data, the best choice is therefore to use a model tuned to the LEP and SLD data [787–789]. It is important to choose the tuning in a consistent way from the same experiment, given that a combined LEP/SLD tuning has never been attempted. As a possibility, suggested by the major success in describing the data and by its extensive use in the experimental collaborations, is the use of PYTHIA, which uses the string (or Lund) fragmentation model [790]. The parameters that we consider more relevant in PYTHIA for the description of fragmentation are the following, where the central value is taken by the fit performed by the OPAL Collaboration, as an example:

PARJ(81) = 0.250
PARJ(82) = 1.90
PARJ(41) = 0.11
PARJ(42) = 0.52
PARJ(21) = 0.40

where PARJ(81) (Λ_{QCD}) and PARJ(82) (Q^2_{min}) refer to the radiation part. To properly evaluate a systematic error due to pure fragmentation one should vary only PARJ(42) and PARJ(21) by their respective errors (0.04 and 0.03 for OPAL). The variation should account for the proper parameter correlation if the effect is critical for the analysis. PARJ(41) is totally correlated to PARJ(42).

Alternatively, or additionally, it would also be important to compare PYTHIA with HERWIG with consistent tunings from LEP [787–789]; in doing so it is important to factorise the UE description (see next section) that can induce important differences in the results.

B.1.5.2. Heavy quarks fragmentation. The description of the heavy quarks fragmentation is important for top physics and for those processes with large b production in the final states. Exclusive channels are particularly influenced by the description of the fragmentation of the b quark.

The description of the fragmentation of the heavy quarks has been tuned to Z data at LEP and SLD[778, 791–793] (via a measurement of x_B and x_D) and $b\bar{b}$ data at the Tevatron, using different fragmentation functions like Lund, Bowler [794], Peterson [795], Kartvelishvili [796].

In the spirit of fragmentation universality the LEP/SLD tunings can be adopted for the LHC, but with much care. Significant differences among the fitted values in different experiment can point out that the factorisation scale used for the PS is not the same everywhere. One should make sure that the scale used is set consistently with the chosen fragmentation function parameters. This can be done by using the tuning from only one experiment, making sure to also use the main switches of the parton showering, (PARJ(81) and PARJ(82) in PYTHIA).

The fragmentation function that best describes heavy flavour data at LEP is Bowler. With the same OPAL tuning reported above the best fit of the Bowler parameters, a and $bm_\perp^2$, to data gives:

$bm_\perp^2 = 65^{+17}_{-14}$
$a = 15.0 \pm 2.3.$

The Bowler model would extend the string model to heavy flavours, describing the corrections in terms of the charm and bottom masses. Unfortunately, no tuning exists in the literature which is capable to describe at the same time light and heavy quark fragmentation, i.e. adopting universal parameters $a = \text{PARJ}(41)$ and $b = \text{PARJ}(42)$ for both light and heavy quarks.

Alternatively, the widely used Peterson function can be used, and its parameters are directly switchable in PYTHIA for just b and c fragmentation:

$\text{PARJ}(54) = -0.031 \pm 0.011$
$\text{PARJ}(55) = -0.0041 \pm 0.0004$

where the two parameters correspond, respectively, to ε_c and ε_b fitted in the OPAL tuning. The systematic can then be evaluated by varying the errors on the fitted parameters or by comparing with a different fragmentation function like Kartvelishvili, or Lund.

An important feature of the b fragmentation that should be considered by those analyses in the top sector sensitive to the details of the fragmentation, is the way the b fragments in top decays. At the LHC the b from a t is hadronising with a beam remnant, introducing potentially worrying differences with respect to the fragmentation at LEP. The main effects are presented in [797] and are known as *cluster collapse*, happening when a very low mass strings quark-remnant directly produces hadrons without fragmenting, hence enhancing the original flavour content, and *beam drag*, which is an angular distortion of hadron distribution toward the end of the string in the remnant. If, under reasonable assumptions on the transverse momentum in top events at the LHC, one can exclude to a large extent the importance of the first effect, beam drag could potentially introduce B meson production asymmetries, even though estimations are keeping the effect at the level of 1% at the LHC [797].

B.1.6. Minimum bias and underlying event

Multiple parton interaction models, extending the QCD perturbative picture to the soft regime, turn out to be particularly adequate to describe the physics of minimum bias and underlying event. Examples of these models are implemented in the general purpose simulation programs PYTHIA, HERWIG/JIMMY [193] and SHERPA. Other successful descriptions of underlying event and minimum bias at hadron colliders are achieved by alternative approaches like PHOJET [798], which rely on both perturbative QCD and Double Pomeron Models (DPM).

Huge progress in the phenomenological study of the underlying event in jet events have been achieved by the CDF experiment at Tevatron [799], using the multiplicity and transverse momentum spectra of charged tracks in different regions in the azimuth-pseudorapidity space defined with respect to the direction of the leading jet. Regions that receive contributions only by the underlying event have been identified. The average charged multiplicity per unit of pseudorapidity in these regions turns out to be significantly higher with respect to the one measured in minimum bias events. This effect, referred to as "pedestal effect", is well reproduced only by varying impact parameters models with correlated parton-parton interactions (MSTP(82) $>$ 1 in PYTHIA). Simpler models are definitely ruled out.

The main problem of extrapolating the predictions of the multiple interactions models to the LHC is that some of the parameters are explicitly energy dependent, in particular the colour screening p_T cut-off (PARP(82) at the tuning energy PARP(89) in PYTHIA). The CDF tuning, often referred to as Tune-A, is not concentrating on this particular aspect. Other works [197, 800] have put more emphasis on this issue. However, one of their results is that currently only PYTHIA can be tuned to provide at the same time description of CDF and lower energy minimum bias data from UA5. One of these tunings can be summarised as follows:

- PARP(82) = 2.9
- PARP(83) = 0.5
- PAPR(84) = 0.4
- PARP(85) = 0.33
- PARP(86) = 0.66
- PARP(89) = 14000
- PARP(90) = 0.16
- PARP(91) = 1.0
- MSTP(81) = 1
- MSTP(82) = 4.

Sensible estimation of theoretical uncertainties arising from underlying event and minimum bias modelling can be performed assigning $\pm 3\sigma$ variations to the colour screening p_T cut-off parameter tuned on minimum bias CDF and UA5 data and extrapolated to the LHC energy [800], i.e. varying PARP(82) in the range [2.4–3.4], while keeping the other parameters listed above to their tuned values.

As a new tool for the description of UE and MB we would like to mention PYTHIA 6.3 [801], that allows for new interesting features, including the new p_T-ordered initial- and final-state showers and a new very sophisticated multiple interactions model that achieves description of colliding partons in the proton in terms of correlated multi-parton distribution functions of flavours, colours and longitudinal momenta. However, as stressed by the PYTHIA authors, the new model (PYEVNW) is still not so well explored. Therefore the old model (PYEVNT) is retained as the default choice, with full backward compatibility. Moreover, in the use of PYTHIA 6.3, one should be careful when switching to the new p_T-ordered showers and multiple interaction models, as their parameters are not tuned yet, in particular for what concerns the energy dependence, necessary to get meaningful extrapolations at the LHC energy.

B.1.7. Pile-up and LHC cross sections

The design parameters of the LHC at both low and high luminosity are such that, on top of possible signal events, additional minimum bias interactions are produced in the same beam crossing, the so-called pile-up effect.

Pile-up is a purely statistical effect. The number of minimum bias interactions generated in a single beam crossing is a Poissonian distribution that depends on the instantaneous luminosity, which varies of about a factor 2 during a LHC fill. Although luminosity variation is not arising from theoretical uncertainties, it is recommended to cross check the stability of the results against variation of the nominal luminosity.

An issue which can affect the pile-up is the definition of the minimum bias itself. The latter, indeed, may or may not include the diffractive and elastic contributions, with figures for the total cross section which can vary from 100 mb to 50 mb respectively. If the PYTHIA generator is adopted, these two different options correspond to MSEL 2 and MSEL 1, however, in order to get full control on the different contributions to the cross sections, one can use MSEL 2, setting MSTP(31) = 0, and providing explicit input through SIGT(0, 0, J), where the meaning of the index J is described below:

$J = 0$ Total cross section (reference value = 101.3 mb)
$J = 1$ Elastic cross section (reference value = 22.2 mb)
$J = 2$ Single diffractive cross section XB (reference value = 7.2 mb)
$J = 3$ Single diffractive cross section AX (reference value = 7.2 mb)
$J = 4$ Double diffractive cross section (reference value = 9.5 mb)
$J = 5$ Inelastic, non-diffractive cross section (reference value = 55.2 mb).

Where J = 0 has to correspond to the sum of the contributions for J = 1, . . . , 5. With respect to alternative cross section predictions [802], PYTHIA reference values for diffractive cross sections might be slightly shifted on the high side. A possible sound alternative could be to reduce the diffractive cross sections of around 30%, keeping constant the total cross section.

In order to assess the sensitivity of one analysis to the diffractive variations in the pile-up, at least the two options MSEL 1 and MSEL 2 should be tried. Diffractive contribution will in general result in few additional soft charged particles spiralling in the high magnetic fields of the LHC experiments. This effect is most likely to be relevant in the tracker detectors, where multiple hits in the same layer can be generated by the same track.

B.1.8. Decays

In contrast to the simple decay models available in the common PS Monte Carlo, alternative hadron decay models exist, for example EVTGEN [803], which have huge collections of exclusive hadron decays up to branching ratios as low as 10^{-4}.

EVTGEN follows the spin density matrix formalism and has an easily tuneable and upgradeable hadron decay data base which currently constitutes the largest and most refined collection of hadron decay models.

Comparison between the simple default decay models implemented in PS Monte Carlo and those available in EVTGEN should be recommended at least for analyses dealing with B hadrons or relying on b-tagging. However, since switching to a new hadron decay model could have a deep spin-offs on the exclusive description of the final states (multiplicity of kaons, pions, photons and muons, multiplicity of tracks reconstructed in secondary vertices) it might be worth to study also effects on trigger performances.

The LHC version of EVTGEN was initially provided by the LHCb experiment and is currently maintained by LCG Generator [804]. It comprises an interface to PYTHIA simulation that solves the technical problems of switching between the two different scenarios (i.e. hadron decays performed by PYTHIA, hadron decays performed by EVTGEN).

B.1.9. LHAPDF and PDF uncertainties

The detailed investigations of processes at LHC required a well understanding of the systematic theoretical uncertainties [201]. One of the important source of such errors is the parton distribution functions (PDFs).

The Les Houches Accord Parton Density Functions (LHAPDF) package [95] is designed to work with the different PDF sets[53]. In this approach a "fit" to the data is no longer described by a single PDF, but by a PDF set consisting of many individual PDF members. Indeed, PDFs are specified in a parameterised form at a fixed energy scale Q_0, such as

$$f(x, Q_0) = a_0 x^{a_1}(1-x)^{a_2}(1 + a_3 x^{a_4} \ldots). \tag{B.1}$$

The PDFs at all higher Q are determined by NLO perturbative QCD evolution equations. The total number of PDF parameters (d) could be large (for example, for CTEQ parametrisation one has $d = 20$ [12]). Fitting procedure is used for evaluation an effective χ^2 function, which can be used to extract the "best fit" (the global minimum of χ^2) and also to explore the neighbourhood of the global minimum in order to quantify the uncertainties. As a result one has the "best-fit" PDF and $2d$ subsets of PDF [12, 95]:

$$f_0(x, Q), \;\; f_i^{\pm}(x, Q) = f\left(x, Q; \{a_i^{\pm}\}\right), \;\; i = 1, \ldots, d. \tag{B.2}$$

B.1.9.1. Master equations for calculating uncertainties. Let $X(\{a\})$ be any variable that depends on the PDFs. It can be a physical quantity such as the W production cross section, or a differential distribution.

Let $X_0 = X(\{a_0\})$ be the estimate for X calculated with the best-fit PDF and $X_i^{\pm}$ be the observable X calculated with i-th subset $f_i^{\pm}(x, Q)$.

Following to CTEQ6 collaboration one can estimate the variation of X by using a master formula [12]:

$$\Delta X = \sqrt{\sum_{i=1}^{d} \left(X_i^+ - X_i^-\right)^2}. \tag{B.3}$$

However, very often many X_i^+ and X_i^- have different magnitudes and even signs! This failure of the master formula is a result of the simple observation that the PDF set that minimises the uncertainty in a given observable X is not necessarily the same as the one that minimises the fit to the global data set.

The better estimator for the uncertainty of a generic observable X was proposed in [805]. It is defined as the maximum positive and negative errors on an observable X by

$$\begin{aligned} \Delta X_+ &= \sqrt{\textstyle\sum_{i=1}^{d} \left(\max[(X_i^+ - X_0),\ (X_i^- - X_0)\,,\ 0]\right)^2}, \\ \Delta X_- &= \sqrt{\textstyle\sum_{i=1}^{d} \left(\max[(X_0 - X_i^+),\ (X_0 - X_i^-),\ 0]\right)^2}. \end{aligned} \tag{B.4}$$

In Eqs. (B.4) one sums the maximum deviations on the observable in each of the parameter directions, and hence retain both maximal sensitivity to the parameters that vary most and estimate the range of allowed values of the cross section. Note, that the errors in Table C.2 were evaluated with this Eq. (B.4).

[53] Note, at CMS it was recommended to use the CTEQ 5L set for PTDR simulation. Since there is only *one* CTEQ 5L PDF set (without corresponding subsets), it was recommended to use CTEQ 6M for evaluation of uncertainties due to PDFs for PTDR estimates and only in a special case can one use another sets (e.g. MRST).

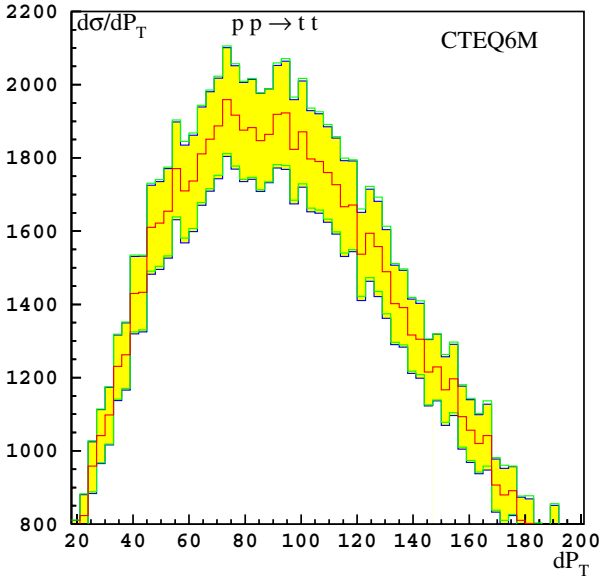

Figure B.1. $d\sigma/dP_{\mathrm{T}}$ distribution for $t\bar{t}$-pair production at LHC. The central histogram corresponds to the 'best-fit' of CTEQ6M PDF, while the shaded area represents the deviation due to PDF uncertainties.

Eq. (B.4 could also be used for calculations of differential distribution. Fig. B.1 presents the differential distribution $d\sigma/dP_{\mathrm{T}}$ for $t\bar{t}$-pair production at LHC.

B.1.9.2. How to calculate $X(\{a_i\})$. The most simple and straightforward method is to simulate a sample with the "best-fit" PDFs and then to repeat a such simulation $2d$ times with different $2d$ PDF subsets. As a results one gets $(1+2d)$ samples of *unweighted* events with *different* kinematics for each samples. Then use these samples to calculate $(1+2d)$ values for observable:

$$X_0 = \sum_{\text{events}} X_n(\{a_0\})), \quad X_i^{\pm} = \sum_{\text{events}} X_n(\{a_i^{\pm}\}), \quad i = 1, \ldots, d. \tag{B.5}$$

In practice, such method requires a large CPU-time and can be recommended only to be used for very few special cases, when a high accuracy is required.

In the second approach (*"re-weighting" method*) one needs to simulate only **one** sample with the 'best-fit' PDF. In doing so the additional weights, corresponding to all other PDF subsets are evaluated. This weight is the ratio of the parton luminosity [PDF($\{a_i\}$) – the product of PDFs] evaluated with PDF subset to the parton luminosity, calculated with the 'best-fit' PDF. As a result, for any n-event one has $2d$ additional weights:

$$w_{(0)} = 1(\text{best fit PDF}), \quad w_{(i)}^{\pm} = \frac{\text{PDF}(\{a_i^{\pm}\})_n}{\text{PDF}(\{a_0\})_n}; \quad w_{(i)}^{\pm} = \mathcal{O}(1). \tag{B.6}$$

The corresponding $(1+2d)$ values for observable X are evaluated as follows:

$$X_0 = \sum_{\text{events}} X_n(\{a_0\})), \quad X_i^{\pm} = \sum_{\text{events}} w_{(i)}^{\pm}\, X_n(\{a_0\}). \tag{B.7}$$

Contrary to the first method (see (B.5)) these $(1+2d)$ samples have the events with *different* weights, but with *identical* kinematics for each samples. Note, that all additional samples have

different "total number of events":

$$N_0 = \sum_{\text{events}} w_{(0)}(=1),\ N_i^{\pm} = \sum_{\text{events}} w_{(i)}^{\pm} \neq N_0,\ \text{and}\ N_i^{\pm} = \mathcal{O}(N_0). \tag{B.8}$$

Starting from CMKIN_6_0_0 version it is possible for each event the evaluation of the additional weights, corresponding to different PDF subsets (i.e. $w_{(i)}^{\pm}$, see (B.6)). This option is available for CMKIN run with PYTHIA-like generators (PYTHIA, MADGRAPH, COMPHEP, ALPGEN, TOPREX, STAGEN, etc) and HERWIG. This information is written in `/mc_param/` user block after all variables filled by CMKIN and a user (by using of `kis_xxx` routines).

B.2. Experimental uncertainties

The systematic uncertainties associated with the detector measurements contributing to an analysis are mostly covered in the corresponding chapters of Volume 1 of this Report [7] and are summarised here.

B.2.1. Luminosity uncertainty

As discussed in Chapter 8 of [7], the design goal for the precision of the luminosity measurement at CMS is 5%, which is assumed to be achieved after 1 fb^{-1} of data has been collected. For integrated luminosities of less than 1 fb^{-1}, it is assumed that the precision is limited to 10%. For studies based on 30 fb^{-1} or more in this Report, it is assumed that further improvement on the uncertainty can be achieved and a 3% uncertainty is assumed, via e.g. W, Z based luminosity measurements.

B.2.2. Track and vertex reconstruction uncertainties

The uncertainty in the silicon track reconstruction efficiency is taken to be 1% for all tracks. The primary vertex precision along the z coordinate is expected to be about 10 μm once 1 fb^{-1} has been collected. The transverse vertex precision is expected to be about 1 μm.

The effects of uncertainties on the alignment of silicon sensors on track and vertex reconstruction are studied using a dedicated software tool (Section 6.6.4 of [7]) that is able to displace tracker elements according to two scenarios: a "First Data Taking Scenario" with placement uncertainties as expected at LHC start-up from measurements using the laser alignment system for the strip tracker and from in-situ track-based alignment of the pixel detector, and a "Long Term Scenario" appropriate after the first few fb^{-1} have been collected and a complete track-based alignment has been carried out for all tracker elements.

The effect of the magnetic field uncertainty in the central region of CMS is expected to contribute a momentum scale uncertainty of 0.0003 GeV/c to $1/p_{\text{T}}$. When combined with the aggregate effect from alignment uncertainties, the overall momentum scale uncertainty is 0.0005 GeV/c at start-up.

B.2.3. Muon reconstruction uncertainties

As with the silicon tracker studies, a dedicated software tool has been developed (Section 3.2.2 of [7]) to study the effects of muon detector placement uncertainties on muon reconstruction. Two scenarios, a "First Data Taking Scenario" with placement uncertainties as expected at LHC start-up and a "Long Term Scenario" appropriate after the first few fb^{-1}, are available and used in analyses sensitive to the alignment precision of the muon detectors. The latter

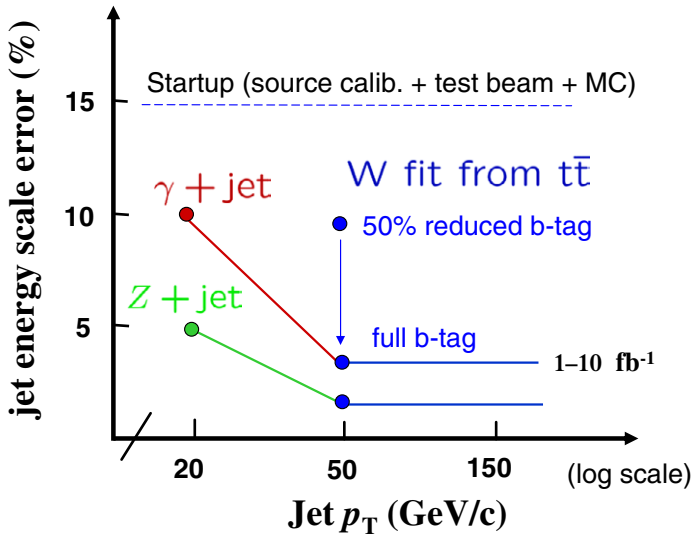

Figure B.2. Jet energy scale uncertainty is applied as a rescaling of the four-momentum of the reconstructed jet $p^{\mu,jet}_{scaled\pm} = (1 \pm \alpha) \cdot p^{\mu,jet}_{meas}$ where α is the percentage uncertainty plotted above.

scenario describes a detector alignment precision of 200 μm in the plane transverse to the beam axis using the laser alignment system and track-based alignment strategies.

The effect of magnetic field uncertainties on the muon momentum will be dominated by the uncertainty in the central region and its impact on the momentum scale determined by fits to the silicon tracker hits for muon momenta well below the TeV/c scale.

B.2.4. Electromagnetic calibration and energy scale uncertainties

The precision to which the ECAL crystals can be intercalibrated from a variety of techniques is discussed in Section 4.4 of [7], and ranges from 0.4–2.0% using about 5 fb^{-1} of *in situ* single isolated electron data. A software tool is used to apply calibration constants to the accuracy expected to be obtained with either 1 fb^{-1} or 10 fb^{-1} of integrated luminosity. The absolute energy scale can be determined using the Z mass constraint in Z $\rightarrow$ ee decays, and is expected to be measured to a precision of about 0.05%.

B.2.5. Jet and missing transverse energy uncertainties

The estimated systematic uncertainty on the jet energy scale is shown in Fig. B.2. At startup the accuracy of the jet energy scale relies on the understanding of single-particle test beam calibration and the level of agreement achieved in the data-to-Monte Carlo simulation comparisons of the detector response. The response of an individual tile or crystals is known to limited accuracy from source calibration in the HCAL and test stand measurements for crystals in the ECAL. Hence, given the limitations of the precalibration of the calorimeters, an overall uncertainty of 15% is expected for the "day-one" absolute energy scale. This applies equally for jet response and the energy scale uncertainty of the missing transverse energy.

In the first 1–10 fb^{-1} of data, the γ+ jet calibration [283] and the hadronic W boson mass calibration in top quark pair production events [287] are currently the best estimates for the accuracy on the absolute jet energy scale. The hadronic W jets in the selected

sample have a mean p_{T} that is approximately 50 GeV/c. A lowering of the jet selection threshold increases the effects of the offset correction from pile-up. The systematic on offset corrections and backgrounds puts the absolute jet energy scale at 3%. The jet reconstruction efficiencies are flat above 50 GeV/c, but drop in the low p_{T} region. The current estimate of the high p_{T} jet energy scale based on the hadronic W calibration is 3%. The calorimeter response curves that are required to extrapolate to high p_{T} are not expected to significantly increase the energy scale uncertainty beyond the 3% from the W calibration. In the low p_{T} region excluded from the hadronic W analysis, the absolute jet energy scale will be set by the γ+jet calibration which will extend down to 20 GeV. Below 20 GeV, only the single-particle calibration methods apply and these will have an accuracy of 10%. The recommended treatment for the jet energy systematic in this report is to apply an uncertainty according to this functional form:

$$\sigma_E^{jet}/E = \begin{cases} 10\% & p_{\mathrm{T}} < 20\,\mathrm{GeV/c} \\ 10\% - 7\% * (p_{\mathrm{T}} - 20\,\mathrm{GeV/c})/(30\,\mathrm{GeV/c}) & 20\,\mathrm{GeV/c} < p_{\mathrm{T}} < 50\,\mathrm{GeV/c} \\ 3\% & p_{\mathrm{T}} > 50\,\mathrm{GeV/c} \end{cases}.$$

It is expected that the Z+jet sample and further analysis of the hadronic W systematics will reduce the overall jet energy scale uncertainty, but these analyses remain under active study.

The low p_{T} region is particularly important for the missing transverse energy (MET) response. As the MET will have significant contributions from low p_{T} jets and unclustered energy, it is expected that the low p_{T} component of the MET will not be understood to better than 10% following the first 1–10 fb^{-1} of data. The recommended treatment of the MET energy scale uncertainty has two approaches (one simple and one more detailed). For a MET which is known to be dominated by low p_{T} jets and unclustered energy, an uncertainty of 10% should be applied to the components of the MET uncorrelated to the jet energy scale uncertainty of the jets. This is the simple approach and gives a conservative error on the MET. For events with reconstructed high p_{T} jets, the contributions to the MET uncertainty are correlated to the jet energy scale uncertainty of the high p_{T} jets. The recommended treatment of the MET uncertainty is to apply separate uncertainties on the low p_{T} and high p_{T} components of the MET. The MET is reconstructed as described in [147] and [148]. This gives a type-1 correction of the following form:

$$E^{\mathrm{miss}}_{\mathrm{Tx(y)}} = -\left[E^{\mathrm{raw}}_{\mathrm{Tx(y)}} + \sum_{\mathrm{jets}} \left(p^{\mathrm{corr.\ jet}}_{\mathrm{Tx(y)}} - p^{\mathrm{raw\ jet}}_{\mathrm{Tx(y)}}\right)\right]$$

where $E^{\mathrm{raw}}_{\mathrm{Tx(y)}}$ is the sum over the raw calorimeter tower energies and the jet sum in the equation is over jets with a reconstructed p_{T} above a given jet $p_{\mathrm{T}}^{\mathrm{cut}}$ selection cut, typically 20–25 GeV/c. The jet p_{T} is used in these formula to account for the angular separation of the towers included in the jet sum, contributing to the jet mass. Rewriting the above equation in this form

$$E^{\mathrm{miss}}_{\mathrm{Tx(y)}} = -\left[\left(E^{\mathrm{raw}}_{\mathrm{Tx(y)}} - \sum_{\mathrm{jets}} p^{\mathrm{raw\ jet}}_{\mathrm{Tx(y)}}\right)_{\mathrm{low}\ p_{\mathrm{T}}} + \left(\sum_{\mathrm{jet}} p^{\mathrm{corr.\ jet}}_{\mathrm{Tx(y)}}\right)_{\mathrm{high}\ p_{\mathrm{T}}}\right]$$

shows explicitly the low p_{T} (in the first set of brackets) and the high p_{T} components (second set of brackets) of the MET. The proposed systematics treatment is to vary the components of the low p_{T} MET by 10% scale uncertainty uncorrelated with the high p_{T} component and to vary the high p_{T} component according the jet energy scale uncertainty for the measured jets.

If a subset of the high p_T jets are identified as electromagnetic objects, isolated electrons or photons, then these EM-jets should be given EM-scale energy corrections which are closer to unity than hadronic jet corrections. The energy scale uncertainty on an EM-object will also be much lower than the jet energy scale systematic. Therefore, if the EM-objects are not removed from the jet list, the quoted energy scale uncertainty will be conservative relative to the lower errors associated with separate treatment of identified EM-objects.

In addition to the jet energy scale uncertainty, there are uncertainties on the jet resolution. At startup the jet resolution is estimated to be accurate to 20% of the quoted resolution based on the test-beam data and simulation studies. The dijet balancing resolution will be determined from data and will further constrain this uncertainty. It is expected that the systematics on the third jet veto and other selection criteria will limit the uncertainty on the jet resolution to 10% in the 1–10 fb^{-1} dataset. The recommended treatment for this systematic is to add an additional smearing to the jet energy which broadens the overall jet resolution by 10%. This can be done by throwing a Gaussian random number and adding an energy term which is 46% of the jet resolution. Therefore, the jet-by-jet event-by-event smearing should be done as follows:

$$E'^{\mathrm{jet}}_{\mathrm{T}} = E^{\mathrm{jet}}_{\mathrm{T}} + \mathrm{Gaus}[0,\ 0.46 * \sigma(E_{\mathrm{T}}, \eta)] \tag{B.9}$$

where $\sigma(E_{\mathrm{T}}, \eta)$ is the reference jet resolution which for the central barrel is given by (using Monte Carlo simulation derived jet calibrations where $E^{\mathrm{MC}}_{\mathrm{T}}$ is equal to $E^{\mathrm{rec}}_{\mathrm{T}}$ on average)

$$\sigma(E^{\mathrm{jet}}_{\mathrm{T}}, |\eta| < 1.4) = (5.8\,\mathrm{GeV}) \oplus \left(1.25 * \sqrt{E^{\mathrm{jet}}_{\mathrm{T}}}\right) \oplus 0.033 * E^{\mathrm{jet}}_{\mathrm{T}} \tag{B.10}$$

(terms added in quadrature) and $\mathrm{Gaus}[0, 0.46 * \sigma(E_{\mathrm{T}}, \eta)]$ is a randomly thrown sampling of a normal distribution per jet with a mean of zero and a width of 46% of the jet resolution and therefore $E'^{\mathrm{jet}}_{\mathrm{T}}$ is the smeared jet energy to be used in the estimation of the jet resolution systematic uncertainty of the measurement. The 46% is chosen so that when added in quadrature to the nominal resolution gives an overall widening of the energy resolution of 10%. The resolutions of the endcap and forward jet regions are found in [165, Table 5]. These are

$$\sigma(E^{\mathrm{jet}}_{\mathrm{T}}, 1.4 < |\eta| < 3.0) = (4.8\mathrm{GeV}) \oplus \left(0.89 * \sqrt{E^{\mathrm{jet}}_{\mathrm{T}}}\right) \oplus 0.043 * E^{\mathrm{jet}}_{\mathrm{T}}$$

$$\sigma(E^{\mathrm{jet}}_{\mathrm{T}}, 3.0 < |\eta| < 5.0) = (3.8\mathrm{GeV}) \oplus 0.085 * E^{\mathrm{jet}}_{\mathrm{T}}$$

where for these jet resolution fits the stochastic term in the forward region is small compared to the noise and constant terms (hence the missing $\sqrt{E^{\mathrm{jet}}_{\mathrm{T}}}$ term for $3.0 < |\eta| < 5.0$). The shift in the +10% direction can be symmetrised to account for the −10% shift. Otherwise, the difference between the reconstructed and generated jet energies must be reduced by 10% in order to estimate the −10% uncertainty from the nominal Monte Carlo jet resolution. The jet resolution uncertainty is particularly important when searching for signals that are on a rapidly falling QCD multi-jet p_T spectrum.

B.2.6. Heavy-flavour tagging uncertainties

A strategy for measuring the b-tag efficiency using an enriched sample of b-jets from $\mathrm{t\bar{t}}$ events, and its estimated precision, is described in Section 12.2.8 of [7]. The relative uncertainty on the b-efficiency measurement is expected to be about 6% (4%) in the barrel and 10% (5%) in

the endcaps for 1 fb^{-1} (10 fb^{-1}) of integrated luminosity. These uncertainties correspond to a b-tag working point efficiency of 50%.

The light-quark (and gluon) mis-tag uncertainty is expected to be larger than the b efficiency uncertainty; however, for this Report a global uncertainty of 5% is assumed for the mis-tag uncertainty. As with the efficiency determination, it is important to identify strategies to measure the mis-tagging probabilities in data as well.

Likewise, a strategy to measure the uncertainty on the efficiency for identifying τ leptons is described in Section 12.1.4 of [7], and involves comparing the ratio of $Z \to \tau\tau \to \mu +$ jet to $Z \to \mu\mu$ events. With a 30 fb^{-1} data sample, the relative uncertainty on τ-tagging is estimated to be about 4%. A measurement of the τ misidentification probability can be determined from a sample of $\gamma+$ jet events, and with a 10 fb^{-1} data sample is expected to have an uncertainty at the level of 4–10%.

Appendix C. Monte Carlo Models and Generators

C.1. Introduction

This section presents a short description of the basic event generators used in CMS during preparation of the PTDR (see CMS "Generator Tools group" for details). A comprehensive review of the present Monte Carlo models and generators is given elsewhere [806]. Note that only MC generators used in CMS are described here, and a full description of several popular packages (like ISAJET or ACERMC, see [806]) is omitted.

There are several available Monte Carlo event generators for pp, pA and AA collisions, namely HERWIG [196], HIJING [807], ISAJET [672], PYTHIA [69] and SHERPA [808]. Each of these simulates a hadronic final state corresponding to some particular model of the underlying physics. The details of the implementation of the physics are different in each of these generators, however the underlying philosophy of the generators is the same.

The cross section values and the differential distribution for almost all processes are evalueated as follows:

$$\sigma(pp \to CX) = \sum_{ij} \int f_i^p(x_1, Q^2)\, f_j^p(x_2, Q^2) \hat{\sigma}(ij \to C) \mathrm{d}x_1 \mathrm{d}x_2, \qquad \text{(C.1)}$$

where $f_i^p(x, Q^2)$ are the Parton Distribution Functions (PDF) of ith parton, that carried a fraction x of the initial proton momentum at a scale (Q^2); $\sigma(ij \to C)$ is the cross section for the hard process (i.e. describing two partons, i and j, interaction).

A general scheme of event generation assumes the evaluation of the hard process (the cross section value, the incoming and outgoing particle's momenta and colours), then evolves the event through a parton showering and hadronisation step, and the decay of the unstable particles. The event information (stored in `/HEPEVT/` common block [69]) contains the momenta of the final hadrons, leptons and photons and positions of their decay vertexes. Typically such information contains also the characteristics (momenta, colours, `KF`-codes, mother's and daughter's relations) of all intermediate partons (quarks, gluons, gauge bosons, unstable physical particles, etc) that provide a trace-back the history of particle production inside of an event. By using an acceptance-rejection methods weighted events can be returned.

Parton showering is based on the expansion around the soft and collinear evolution limits and is often ascribed to either the initial or final state. The algorithm used by HERWIG and SHERPA also include some effects due to quantum interference. The events that have more energy in the parton process have more showering, and consequently more jet activity.

The collection of quarks and gluons must then be hadronised into mesons and baryons. This is done differently in each of the event generators, but is described by a set of (fragmentation) parameters that must be adjusted to agree with experimental results. HERWIG looks for colour singlet collections of quarks and gluons with low invariant mass and groups them together; this set then turns into hadrons. PYTHIA splits gluons into quark-anti-quark pairs and turns the resulting set of colour singlet quark-anti-quark pairs into hadrons via a string model. ISAJET simply fragments each quark independently paying no attention to the colour flow.

The dominant cross-section at the LHC consists of events with no hard scattering. There is little detailed theoretical understanding of these minimum-bias events and the event generators must rely on present data. These minimum-bias events are important at LHC, particularly at design luminosity, as they overlap with interesting hard-scattering events. The generators use a different approach in this case. HERWIG uses a parametrisation of data mainly from the CERN $p\bar{p}$ Collider. PYTHIA uses a mini-jet model where the jet cross-section is used at very low

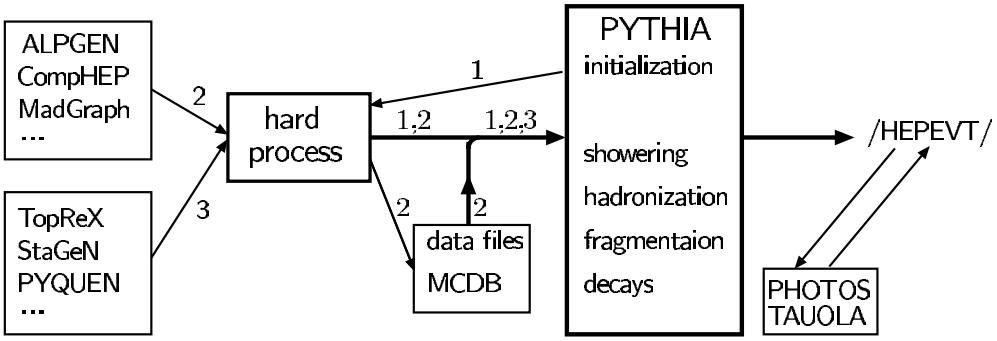

Figure C.1. Purely schematic data flow in PYTHIA and HERWIG.

transverse momenta, i.e the hard scattering process is extrapolated until it saturates the total cross-section. CMS has used the PYTHIA approach with dedicated modifications that agree with present data from Tevatron [69]. The model of the hadronic interactions implemented in the physics generator has a direct impact on physical observables such as jet multiplicity, their average transverse momentum, internal structure of the jets and their heavy flavour content. This led to the choice to use PYTHIA for most processes, allowing for a consistent set of signal and background events to be generated.

Table C.2 presents the predicted cross-section values for the basic SM processes, as used in the simulations for PTDR. The cross-section values (at leading order) were calculated by using PYTHIA 6.327 with `CTEQ5L` (default PDF for PTDR) and with `CTEQ6M` PDFs. α_s at 1st (2nd) order is used with `CTEQ5L` (`CTEQ6M`) PDFs. For `CTEQ6M` the quoted errors are related to the uncertainties due to PDFs (see Subsection B.1.9).

C.2. General scheme of generator usage in CMS

All event generators, included in CMS simulation software, can be separated into two groups.

The first group (HERWIG, HIJING, ISAJET, PYTHIA) provides the *full simulation* of events. The basic package explored in CMS is PYTHIA and only few specific processes were simulated with HERWIG or HIJING.

A purely schematic data flow in PYTHIA and HERWIG is presented in Fig. C.1.

After initialisation the package (HERWIG or PYTHIA) calls "hard process" routines (see "1" arrow lines in Fig. C.1). Then information (the momenta of initial and final partons, the colours and `KF`-codes) is passed to package for parton showering, hadronisation, fragmentation and decays of the unstable particles.

However, all these "full event simulation" generators have very limited number of the hard process matrix elements (typically for $2 \to 2$ reaction at LO). Therefore, several special generators are used for simulation of many other LO processes. In fact, such packages generate the hard processes kinematic quantities, such as masses and momenta, the spin, the colour connection, and the flavour of initial- and final-state partons. The information is stored in the "Les Houches" format [809] (`/HEPEUP/` common block) and is passed to full event simulation package like PYTHIA or HERWIG (see thick "output" line on Fig. C.1).

Three generators, namely ALPGEN [161], COMPHEP [355], and MADGRAPH [81, 493], are widely used for simulation of many processes, especially for the generation of the hard processes with multi-jet final states. For example, ALPGEN allows to generate $Q\bar{Q}$ pair

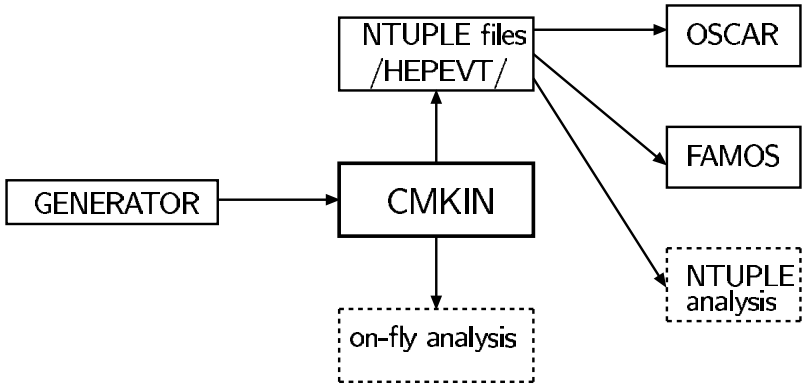

Figure C.2. Illustration of the CMKIN interface.

production with up to 6 jets. Due to the complexity of the matrix elements, describing the multi-jet processes, and a re-weighting procedure the generation of events is very CPU-time consuming. As a result, the information with kinematics is stored in the output files. (see "2" lines on Fig. C.1). Then, like in a generic PYTHIA process, such information is passed to PYTHIA (see thick "output" line on Fig. C.1).

There are several *"dedicated generators"*, TOPREX [44], STAGEN, SINGLETOP, COSMIC, SIMUB, PHASE, PYQUEN [810, 811], HYDJET [812], EDDE. These generators are used for simulation of several specific process (see below for a short description of these codes). The information with hard processes kinematic quantities is stored in `/HEPEUP/` common block [809] and is passed to the "full event simulation" package (see "3" lines on Fig. C.1).

After full simulation of event with PYTHIA or HERWIG the output information is stored in the `/HEPEVT/` common block. In addition two *special functionality* codes provide a better description of photon radiation from a charge final particles (PHOTOS [39]) and $\tau^{\pm}$-lepton decays (TAUOLA [155]). Typically, these codes read information from `/HEPEVT/` common, perform simulation and then add generated information (new particles) into the `/HEPEVT/` common block (see Fig. C.1).

C.3. CMKIN

Almost all generators available in CMS could be used with the CMKIN package. Now the CMKIN is used for OSCAR and FAMOS detector simulation input. This software package provides a common interface between physics event generators and CMS detector simulation (see Fig. C.2). It also provides an environment to make physics plots of generated events. CMKIN provides an interface to a number of physics generators like PYTHIA, ISAJET and HERWIG. It also offers the possibility to use different 'external generators' like ALPGEN [161], COMPHEP [355], MADGRAPH [81, 493] and TOPREX [44]. Cosmic muon simulation is available as well. Simple particle generation is also included, i.e. single and double particles as well as simple multi particle events. The interface is based on a common block `HEPEVT` - a HEP standard to store particle kinematics information for one event [69]. The `/HEPEVT/` common block is converted to HBOOK n-tuples. The event output format follows the `HEPEVT` standard and additional information can be included by the user in the block `/MC_PARAM/`.

There is a unified compilation script which is used as follows:

```
kine_make_ntpl.com <generator> [lhapdf]
```

where the first parameter can have one of the following values: *pythia, herwig, isajet, simple, single, double, simplemulti, cosmic, comphep, alpgen, madgraph, phase, toprex* or *stagen*. The optional second parameter *lhapdf* is given when the user wants to use LHAPDF library [95].

C.4. Full event simulation generators

C.4.1. PYTHIA

The PYTHIA package [69] is a general-purpose generator for hadronic events in pp, e^+e^- and ep colliders. It contains a subprocess library and generation machinery, initial- and final-state parton showers, underlying event, hadronisation and decays, and analysis tools. PYTHIA contains around 240 different $2 \to 2$ (and some $2 \to 1$ or $2 \to 3$) subprocesses, all at leading order. The subsequent decays of unstable resonances (W, Z, top, Higgs, SUSY, ...) brings up the partonic multiplicity, for many processes with full spin correlations in the decays. The external processes can be evolved through the showering and hadronisation (like internal ones).

The final-state shower is based on forward evolution in terms of a decreasing timelike virtuality m^2, with angular ordering imposed by veto. The framework is leading-log, but includes many NLL aspects such as energy–momentum conservation, $\alpha_s(p_\perp^2)$ and coherence. Further features include gluon polarisation effects and photon emission.

The initial-state shower is based on backward evolution, i.e. starting at the hard scattering and moving backwards in time to the shower initiators, in terms of a decreasing spacelike virtuality Q^2. Initial and final showers are matched to each other by maximum emission cones.

The composite nature of hadrons (and resolved photons) allows for several partons from each of the incoming hadrons to undergo scatterings. Such multiple parton–parton interactions are instrumental in building up the activity in the underlying event, in everything from charged multiplicity distributions and long-range correlations to minijets and jet pedestals. The interactions are described by perturbation theory, approximated by a set of more or less separate $2 \to 2$ scatterings; energy conservation and other effects introduce (anti)correlations. The scatterings are colour-connected with each other and with the beam remnants.

The Lund string model, used for hadronisation, is based on a picture with linear confinement, where (anti)quarks or other colour (anti)triplets are located at the ends of the string, and gluons are energy and momentum carrying kinks on the string. The string breaks by the production of new $q\bar{q}$ pairs, and a quark from one break can combine with an anti-quark from an adjacent one to form a colour singlet meson.

Unstable particles are allowed to decay. In cases where better decay models are available elsewhere, e.g. for $\tau^\pm$ with spin information or for B hadrons, such decays can be delegated to specialised packages.

At present the parameters from almost all PYTHIA common blocks (see BLOCK DATA PYDATA) could be set via data cards. With the CMKIN these parameters could be set in data card file with the following format (note, that only capital letters should be used):

PYTHIA	CMKIN	COMMENT
parameter		
MSEL = 6	MSEL6	$t\bar{t}$ production
one- *and* two-dimensional arrays		
CKIN(1) = 100	CKIN1 = 100	min.$\sqrt{\hat{s}}$
i.e. PMAS(6, 1) = 178	PMAS6, 1 = 178	top-quark mass

• *Common cards for* CMKIN

Below we present a list of PYTHIA parameters used for full event simulation for PTDR. Some of these parameters correspond to the old multiple interactions scenario, namely *Tune A* [813].

`MSTP(2)` = 1 : 1(first)/2(second) order running α_s
`MSTP(33)` = 0 : do not include of K-factors in hard cross sections
`MSTP(51)` = 7 : PDF set (here is CTEQ5L)
`MSTP(81)` = 1 : multiple parton interactions is switched ON
`MSTP(82)` = 4 : defines the multiple parton interactions model
`PARP(67)` = 1 : amount of initial-state radiation
`PARP(82)` = 1.9 : P_{T} cut-off for multi-parton interactions
`PARP(83)` = 0.5 : fraction of total hadronic matter in core
`PARP(84)` = 0.4 : radius of core
`PARP(85)` = 0.33 : gluon production mechanism in multiple interactions
`PARP(86)` = 0.66 : gluon prod. mechanism in multiple interactions
`PARP(88)` = 0.5
`PARP(89)` = 1000 : reference energy scale for which `PARP(82)` is set
`PARP(90)` = 0.160 : effective P_{T} cut − off = [PARP(82)/PARP(89)]**PARP(90)
`PARP(91)` = 1.0 : width of Gaussian primordial $k_{\perp}$ distribution inside hadron
`PARJ(71)` = 10 : maximum average $c\tau$ for particles allowed to decay
`MSTJ(11)` = 3 : choice of the fragmentation function
`MSTJ(22)` = 2 : allow to decay those unstable particles
`PMAS(5,1)` = 4.8 : the mass of the b-quark
`PMAS(6,1)` = 175.0 : the mass of the t-quark

C.4.2. HERWIG

HERWIG contains a wide range of Standard Model, Higgs and supersymmetric processes [196]. HERWIG uses the parton-shower approach for initial- and final-state QCD radiation, including colour coherence effects and azimuthal correlations both within and between the jets.

In the treatment of supersymmetric processes, HERWIG itself doesn't calculate the SUSY mass spectrum or decay rates, but reads in an input file containing the low-energy parameters (masses, couplings, decays, ...). This file can be written by hand or more conveniently be generated with the ISAWIG program. This program provides an interface to ISAJET (and therefore to all models in ISASUSY and ISASUGRA), to HDECAY (for NLO Higgs decays), and can also add R-parity violating decays.

Colour coherence effects of (initial and final) partons are taken into account in all hard subprocesses, including the production and decay of heavy quarks and supersymmetric particles. HERWIG uses the angular ordered parton shower algorithm which resumes both soft and collinear singularities. HERWIG includes spin correlation effects in the production and decay of top quarks, tau leptons and supersymmetric particles. For the SUSY decays, there is an option for using either the matrix elements (fast) or the full spin correlations. HERWIG uses a cluster hadronisation model based on non-perturbative gluon splitting, and a similar cluster model for soft and underlying hadronic events. This model gives a good agreement with the LEP data on event shapes, but does not fit the identified particle spectrum well.

C.4.3. ISAJET

ISAJET is a Monte Carlo program which simulates pp, $p\bar{p}$, e^+e^- interactions at high energies [672]. ISAJET is based on perturbative QCD plus phenomenological models for parton and beam jet fragmentation. At CMS ISAJET is used for calculations of SUSY parameters.

C.4.4. HIJING

Hard or semi-hard parton scatterings with transverse momentum of a few GeV/c are expected to dominate high energy heavy ion collisions. The HIJING (Heavy Ion Jet INteraction Generator) Monte Carlo model [807] was developed by M Gyulassy and X-N Wang with special emphasis on the role of minijets in pp, pA and AA reactions at collider energies.

Detailed systematic comparison of HIJING results with a very wide range of data demonstrates that a quantitative understanding of the interplay between soft string dynamics and hard QCD interaction has been achieved. In particular, HIJING reproduces many inclusive spectra two particle correlations, and can explain the observed flavour and multiplicity dependence of the average transverse momentum.

C.5. Tree level matrix element generators

C.5.1. ALPGEN

ALPGEN is designed for the generation of Standard Model processes in hadronic collisions, with emphasis on final states with large jet multiplicities [161]. It is based on the exact leading order evaluation of partonic matrix elements and t and gauge boson decays with helicity correlations. The code generates events in both a weighted and unweighted mode. Weighted generation allows for high-statistics parton-level studies. Unweighted events can be processed in an independent run through shower evolution and hadronisation programs.

The current available processes are:

- $W/Z/H\ Q\bar{Q} + N$ jets ($Q = c, b, t$) with $N \leqslant 4$
- $Q\bar{Q} + N$ jets, with $N \leqslant 6$
- $Q\bar{Q}Q'\bar{Q}' + N$ jets, with $N \leqslant 4$
- W + charm + N jets, with $N \leqslant 5$
- N jets, $W/Z + N$ jets, with $N \leqslant 6$
- $nW + mZ + lH + N$ jets, with $n + m + l + N \leqslant 8$, $N \leqslant 3$
- $N\gamma + M$ jets, with $N \geqslant 1$, $N + M \leqslant 8$ and $M \leqslant 6$
- $H + N$ jets ($N \leqslant 4$), with the Higgs produced via ggH vertex
- single top production.

C.5.2. CompHEP

CompHEP [814] is a package for evaluating Feynman diagrams, integrating over multi-particle phase space and generating events with a high level of automation. CompHEP includes the Feynman rules for SM and several versions of MSSM (SUGRA, GMSB, MSSM with R-parity violation).

CompHEP computes squared Feynman diagrams symbolically and then numerically calculates cross sections and distributions. After numerical computation one can generate the unweighted events with implemented colour flow information. The events are in the form of the Les Houches Accord event record [809] to be used in the PYTHIA program for showering and hadronisation.

CompHEP allows for the computation of scattering processes with up to 6 particles and decay processes with up to 7 particles in the final state.

C.5.3. MadGraph *and* madevent

madevent [81] is a multi-purpose, tree-level event generator which is powered by the matrix element generator MadGraph [493]. Given a user process, MadGraph automatically generates the amplitudes for all the relevant subprocesses and produces the mappings for the integration over the phase space. This process-dependent information is packaged into madevent, and a stand-alone code is produced. It allows the user to calculate cross sections and to obtain unweighted events automatically. Once the events have been generated – event information, (e.g. particle id's, momenta, spin, colour connections) is stored in the "Les Houches" format [809]. Events may be passed directly to a shower Monte Carlo program (interfaces are available for herwig and pythia).

The limitation of the code are related to the maximum number of final state QCD particles. Currently, the package is limited to ten thousand diagrams per subprocess. So, for example, $W+5$ jets is close to its practical limit. At present, only the Standard Model Feynman rules are implemented and the user has to provide his/her own rules for beyond Standard Model physics, such as MSSM.

C.5.4. TopReX

The event generator TopReX [44] provides the simulation of several important processes in pp and $p\bar{p}$ collisions, not implemented in pythia. In the matrix elements used in TopReX the decays of the final t-quarks, $W^{\pm}$, Z and charged Higgs bosons are also included. The final top quark could decay into SM channel ($t \to qW^{+}$, $q = d, s, b$), b-quark and charged Higgs ($t \to bH^{+}$) and the channels with flavour changing neutral current (FCNC): $t \to u(c)V$, $V = g, \gamma, Z$. The implemented matrix elements take into account spin polarisations of the top quark, that provides a correct description of the differential distributions and correlations of the top quarks decay products.

C.6. Supplementary packages

C.6.1. photos

photos is a universal package to simulate QED photon radiative corrections [39]. The precision of the generation may in some cases be limited, in general it is not worse than the complete double bremsstrahlung in LL approximation. The infrared limit of the distributions is also correctly reproduced. The action of the algorithm consists of generating, with internally calculated probability, bremsstrahlung photon(s), which are later added to the `/HEPEVT/` record. Kinematic configurations are appropriately modified. Energy-momentum conservation is assured. When using photos, the QED bremsstrahlung of the principal generator must be switched off. For example in case of pythia one has to use `MSTJ 41=1`.

C.6.2. tauola

tauola is a package for simulation of the $\tau^{\pm}$-lepton decays [155]. It uses the photos package to simulate radiative corrections in the decay. The tauola interface is made with the pythia generator. This interface evaluates also the position of τ-lepton decay (i.e. the information on the production vertex of the decay products of τ-lepton).

C.6.3. PYQUEN

The event generator PYQUEN (PYthia QUENched) [810, 811] provides the simulation of rescattering and energy loss of hard partons in dense QCD-matter (quark-gluon plasma) created in ultrarelativistic heavy ion collisions. The approach relies on an accumulative energy losses, when gluon radiation is associated with each scattering in expanding medium together including the interference effect by the modified radiation spectrum $dE/d\ell$ as a function of decreasing temperature T. The model is implemented as fast Monte Carlo tool, to modify standard PYTHIA jet event.

C.6.4. HYDJET

The event generator HYDJET [812] (HYDrodynamics + JETs) provides the fast simulation of heavy ion events at LHC energy including longitudinal, transverse and elliptic flow effects together with jet production and jet quenching (rescattering and energy loss of hard partons in dense QCD-matter, quark-gluon plasma). The model merges a fast generator of flow effects HYDRO [815] with PYTHIA (for jet production) and PYQUEN [810, 811] (for jet quenching) by simulating full heavy ion event as a superposition of soft, hydro-type state and hard multi-jets.

First of all, HYDJET calculates the number N^{hard} of hard nucleon-nucleon sub-collisions and number N^{part} nucleons-participants (at given impact parameter b of AA collision and minimum P_{T} of hard parton scattering) and generates the initial parton spectra by calling PYTHIA N^{hard} times (fragmentation off). After each jet parton affected by medium-induced rescattering and energy loss according with PYQUEN model. In the end of each PYTHIA sub-event adding new (in-medium emitted) gluons into PYTHIA parton list and rearrangements of partons to update string formation are performed. Then PYQUEN forms final hadrons with `PYEXEC` subroutine (fragmentation on). Finally, HYDJET calculates the multiplicity of soft, hydro-induced part of the event and add new particles in the end of the event record.

C.7. K-factors for dilepton production

Some event generators such as PYTHIA do not employ the most advanced matrix-element calculations. They must be reasonably fast since in most applications, many millions of events must be generated. Experimenters apply an *ad-hoc* correction or "kludge" called the K-factor so that the cross-section value used for, say, the production of muon pairs, is correct. This K-factor amounts to the ratio of a highly accurate cross-section calculation to a less accurate one, typically a leading-order calculation:

$$K_{\text{NLO}} = \frac{\sigma_{\text{NLO}}}{\sigma_{\text{LO}}} \qquad \text{and} \qquad K_{\text{NNLO}} = \frac{\sigma_{\text{NNLO}}}{\sigma_{\text{LO}}}.$$

Clearly the K-factor reflects the accuracy of the better theoretical calculation, and there can be significant differences between K_{NNLO} and K_{NLO}. The most significant contributions to the K-factor come from QCD radiative corrections are expected to be on the order of 10% or more. Usually one does not include electroweak radiative corrections in the K-factor.

We have examined the K-factor for the Drell–Yan production of charged lepton pairs, as well as the signal for new Z' neutral gauge bosons. The program PHOZPRMS is used to compute mass-dependent cross-sections [348], and a generalised version called WUWD is used to study Z' cross-sections [816]. We checked carefully the differential cross-section, $d\sigma/dM$ obtained from PHOZPRMS with the program RESBOS [817, 818] and found very good agreement. We use the MRST parton distribution functions [819] for these calculations. Very similar results are obtained using CTEQ6M [12].

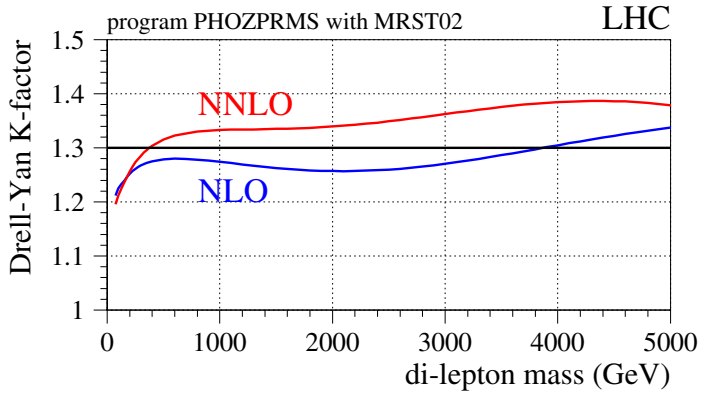

Figure C.3. K-factors as a function of mass for the LHC.

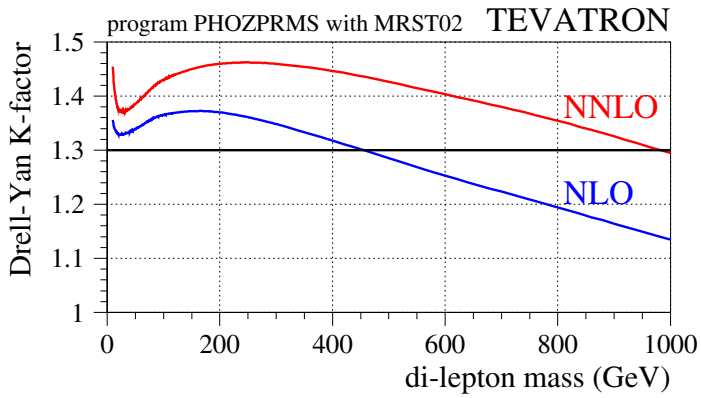

Figure C.4. K-factors as a function of mass for the Tevatron.

Usually experimenters use a constant value for the K-factor, but in fact this is not accurate. The variation of the K-factor with mass is substantial, as shown in Fig. C.3. (There is a similar, though different, variation in the K-factor for Drell–Yan production at the Tevatron – see Fig. C.4.) Notice that $K_{\mathrm{NLO}} \neq K_{\mathrm{NNLO}}$, in general, and the difference can be as large as 7%. A number of values for the K-factor are listed in Table C.1.

It is customary to take the difference $K_{\mathrm{NNLO}} - K_{\mathrm{NLO}}$ as a measure of the theoretical uncertainty due to missing higher orders. According to the results obtained with PHOZPRMS, this uncertainty is on the order of 5%. It is interesting to compare this to the uncertainty coming from the parton distribution functions (PDFs). We used the CTEQ6M set which contains "error" PDFs with which one can estimate this uncertainty [12]. The relative uncertainty of the Drell–Yan cross-section as a function of mass is shown in Fig. C.5. The positive and negative variations of the cross-section were summed separately. The error bands show the full uncertainty obtained from the twenty error-PDFs – no rescaling was done to take into account the fact that these error-PDF's correspond to 2σ variations of the PDF parameters. One sees that the PDF uncertainty varies from about 3% at low masses to 20% toward the upper reach of the LHC. Of course, these uncertainties will be reduces as data from HERA, the Tevatron and fixed-target experiments are used to improve the PDFs.

Table C.1. Values for K_{NNLO}, K_{NLO} and $K_{\mathrm{NNLO}}/K_{\mathrm{NLO}}$ as a function of mass.

mass (GeV/c^2)	K_{NNLO}	K_{NLO}	$K_{\mathrm{NNLO}}/K_{\mathrm{NLO}}$
100	1.212	1.225	0.989
200	1.256	1.252	1.003
300	1.286	1.268	1.014
400	1.303	1.275	1.022
600	1.323	1.280	1.033
800	1.330	1.278	1.040
1000	1.333	1.274	1.046
2000	1.339	1.257	1.065
3000	1.362	1.270	1.073
4000	1.385	1.304	1.061
5000	1.378	1.338	1.031

Table C.2. Leading order cross sections for some typical process at the LHC calculated by using PYTHIA 6.327 with `CTEQ5L` (default PDF for PTDR) and with `CTEQ6M` PDFs. P_0 denotes $\hat{p}_{\mathrm{T}}$-min. for the hard process.

process	cross section	comment	
$\sigma_{\mathrm{tot}}(pp \to X)$	110 ± 10 mb	different models	
$\sigma_{\mathrm{tot}}(pp \to X)$	$111.5 \pm 1.2^{+4.1}_{-2.1}$ mb	COMPETE Coll.	
process	`CTEQ5L`	`CTEQ6M`	comment
Z-boson	48.69 nb	$50.1^{+4.19\%}_{-4.76\%}$ nb	
Z + jet($g+q$)	13.94 nb	$12.73^{+3.16\%}_{-3.94\%}$ nb	$P_0 = 20$ GeV
$q\bar{q} \to Z\gamma$	44.21 pb	$46.7^{+3.93\%}_{-4.22\%}$ nb	$P_0 = 20$ GeV
$W^{\pm}$-boson	158.5 pb	$161.3^{+4.32\%}_{-4.93\%}$ nb	
$W^{\pm}$ + jet($g+q$)	41.42 nb	$37.24^{+3.34\%}_{-4.10\%}$ nb	$P_0 = 20$ GeV
$W^{\pm}\gamma$	56.21 pb	$56.42^{+4.11\%}_{-4.38\%}$ nb	$P_0 = 20$ GeV
W^+W^-	69.69 pb	$75.0^{+3.87\%}_{-4.03\%}$ pb	
$W^{\pm}Z$	26.69 pb	$28.76^{+3.93\%}_{-4.08\%}$ pb	
$q\bar{q} \to ZZ$	11.10 pb	$10.78^{+4.02\%}_{-4.21\%}$ pb	
$WQ\bar{Q}$	$m_b = 4.8$ GeV, $m_c = 1.5$ GeV, TopReX		
$W^{\pm}c\bar{c}$	1215 pb	$1086^{+4.12\%}_{-4.53\%}$ pb	$M_{c\bar{c}} \geqslant 3.0$ GeV
$W^{\pm}c\bar{c}$	33.5 pb	$31.3^{+4.00\%}_{-4.18\%}$ pb	$M_{c\bar{c}} \geqslant 50$ GeV
$W^{\pm}b\bar{b}$	328 pb	$297^{+4.04\%}_{-4.37\%}$ pb	$M_{b\bar{b}} \geqslant 9.6$ GeV
$W^{\pm}b\bar{b}$	34.0 pb	$31.3^{+4.00\%}_{-4.18\%}$ pb	$M_{b\bar{b}} \geqslant 50$ GeV
$Zb\bar{b}$, $m_b = 4.62$ GeV	789.6 ± 3.66 pb	MCFM	$M_{b\bar{b}} \geqslant 9.24$ GeV
dijet processes	819 μb	$583^{+4.78\%}_{-6.02\%}$ μb	$P_0 = 20$ GeV
γ + jet	182 nb	$135^{+4.92\%}_{-6.14\%}$ nb	$P_0 = 20$ GeV
$\gamma\gamma$	164 pb	$137^{+4.62\%}_{-5.65\%}$ pb	$P_0 = 20$ GeV
$b\bar{b}$, $m_b = 4.8$ GeV	479 μb	$187^{+9.7\%}_{-13.2\%}$ μb	
$t\bar{t}$, $m_t = 175$ GeV	488 pb	$493^{+3.24\%}_{-3.31\%}$ pb	
$t\bar{t}$, $m_t = 175$ GeV	830 ± 90 pb	NLO+NNLO	
$t\bar{t}\,b\bar{b}$	10 pb		AcerMC 1.2
inclusive Higgs	$m_H = 150$ GeV	23.8 pb	
inclusive Higgs	$m_H = 500$ GeV	3.8 pb	

The variation of the K-factors with mass comes in part because of the Z-resonance. The size of the Z-peak relative to the continuum production of lepton pairs is therefore relevant. This relative size depends on the coupling of the Z-boson to the up and down quarks in

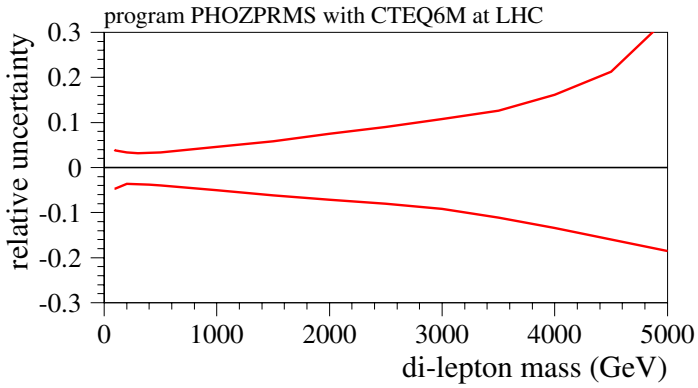

Figure C.5. Uncertainty from the parton distribution functions, evaluated using the CTEQ6M set.

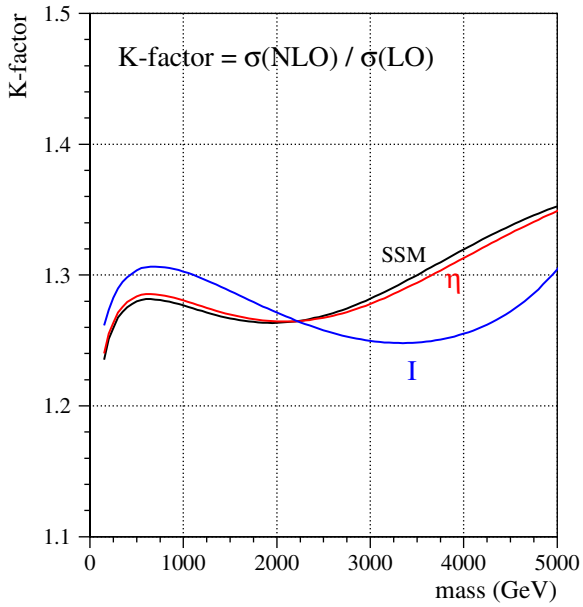

Figure C.6. K-factors as a function of mass of a new Z' resonance, for two cases: η and I (see text). The curve 'SSM' refers to a sequential Standard Model Z'.

the proton. There is practically no uncertainty on those couplings, and they are completely determined in the Standard Model. However, if a new Z' resonances is present, its couplings will not be known *a priori*. Thus it is interesting to consider to what extent the K-factor will depend on those couplings.

We have considered two examples of possible Z' resonances, and computed $K_{\rm NLO}$ as a function of the resonance mass, as shown in Fig. C.6. The first model, labelled "η," illustrates the case of a Z' which couples primarily to up-quarks, and the second one, labelled "I," couples mainly to down-quarks [816]. As is clear from the figure, the radiative corrections as a function of mass are quite different in these two extreme cases. Thus, there will be an ambiguity in the cross-section measurement of a new Z' resonance at the level of about 5% until the relative couplings of that Z' to up and down quarks can be established.

Appendix D. GARCON: Genetic Algorithm for Rectangular Cuts OptimizatioN

Typically HEP analysis has quite a few selection criteria (cuts) to optimise for example a significance of the "signal" over "background" events: transverse energy/momenta cuts, missing transverse energy, angular correlations, isolation and impact parameters, etc. In such cases simple scan over multi-dimensional cuts space (especially when done on top of a scan over theoretical predictions parameters space like for SUSY e.g.) leads to CPU time demand varying from days to many years... One of the alternative methods, which solves the issue is to employ a Genetic Algorithm (GA), see e.g. [820–822].

We wrote a code, GARCON [63], which automatically performs an optimisation and results stability verification effectively trying $\sim 10^{50}$ cut set parameters/values permutations for millions of input events in hours time. Examples of analyses are presented in this Physics TDR; see, for example, Sections 3.1, 8.4.1, 13.6, 13.7, 13.14 and recent papers [51, 317, 675, 676].

The GARCON program among many other features allows user:

- to select an optimisation function among known significance estimators, as well as to define user's own formula, which may be as simple as signal to background ratio, or a complicated one including different systematic uncertainties separately on different signal and background processes, different weights per event and so on;
- to define a precision of the optimisation;
- to restrict the optimisation using different kind of requirements, such us minimum number of signal/background events to survive after final cuts, variables/processes to be used for a particular optimisation run, number of optimisations inside one run to ensure that optimisation converges/finds not just a local maximum(s), but a global one as well (in case of a complicated phase space);
- to automatically verify results stability.

GARCON, like GA-based programs in general, exploits evolution-kind algorithms and uses evolution-like terms:

- Individual is a set of qualities, which are to be optimised in a particular environment or set of requirements. In HEP analysis case Individual is a set of lower and upper rectangular cut values for each of variables under study/optimization.
- Environment or set of requirements of evolutionary process in HEP analysis case is a Quality Function (QF) used for optimisation of individuals. The better QF value the better is an Individual. Quality Function may be as simple as $S/\sqrt{B}$, where S is a number of signal events and B is a total number of background events after cuts, or almost of any degree of complexity, including systematic uncertainties on different backgrounds, etc.
- A given number of individuals constitute a Community, which is involved in evolution process.
- Each individual involved in the evolution: breeding with possibility of mutation of new individuals, death, etc. The higher is the QF of a particular individual, the more chances this individual has to participate in breeding of new individuals and the longer it lives (participates in more breeding cycles, etc.), thus improving community as a whole.
- Breeding in HEP analysis example is a producing of a new individual with qualities (set of min/max cut values) taken in a defined way from two "parent" individuals.
- Death of an individual happens, when it passes over an age limit for it's quality: the bigger it's quality, the more it lives.

- Cataclysmic Updates may happen in evolution after a long period of stagnation in evolution, at this time the whole community gets renewed and gets another chance to evolve to even better quality level. In HEP analysis case it corresponds to a chance to find another local and ultimately a global maximum in terms of quality function. Obviously, the more complicated phase space of cut variables is used the more chances exist that there are several local maximums in quality function optimisation.
- There are some other algorithms involved into GAs. For example mutation of a new individual. In this case newly "born" individual has not just qualities of its "parents", but also some variations, which in terms of HEP analysis example helps evolution to find a global maximum, with less chances to fall into a local one. There are also random creation mechanisms serving the same purpose.

There is nothing special involved in GARCON input preparation. One would need to prepare a set of arrays for each background and a signal process of cut variable values for optimisation. Similar to what is needed to have to perform a classical eye-balling cut optimisation.

In comparison to other automatised optimisation methods GARCON output is transparent to user: it just says what rectangular cut values are optimal and recommended in an analysis. Interpretation of these cut values is absolutely the same as with eye-balling cuts when one selects a set of rectangular cut values for each variable in a "classical" way by eye.

All-in-all it is a simple yet powerful ready-to-use tool with flexible and transparent optimisation and verification parameters setup. It is publicly available along with a paper on it [63] consisting of an example case study and user's manual.

Appendix E. Online Selection

E.1. Introduction

The CMS trigger menu depends upon the luminosity delivered by the LHC and the available bandwidth between and out of the systems. The LHC luminosity is expected to start at $\mathcal{L} = 10^{32}\,\mathrm{cm}^{-2}\,\mathrm{s}^{-1}$ in 2007 and gradually rise to $\mathcal{L} = 10^{34}\,\mathrm{cm}^{-2}\,\mathrm{s}^{-1}$ by 2010. The CMS data acquisition can be operated with one to eight slices of Event Filter Farms that execute High-Level Trigger (HLT) algorithms. It is expected that we start with one slice in 2007, allowing a bandwidth of 12.5 kHz between Level-1 and HLT, and build up to the full eight slices by 2010, when the Level-1 to HLT bandwidth can be raised to 100 kHz. It is assumed that the data logging capability after the HLT selection will remain constant at a rate between 100 Hz to 150 Hz[54]. The Level-1 and HLT algorithms will be configured to operate with the lowest possible thresholds making the best use of the available bandwidth.

Here we focus solely on trigger studies for $\mathcal{L} = 2 \times 10^{33}\,\mathrm{cm}^{-2}\,\mathrm{s}^{-1}$. The scenario of operation assumes that CMS uses four DAQ slices capable of 50 kHz. While the actual choice of trigger thresholds, especially at HLT, depends strongly upon the physics of interest at the time of operation, we propose here an example set of trigger menus within the constraints of the data acquisition system. An effort has been made to optimise the Level-1 and HLT thresholds coherently, taking into account possible bandwidth limitations.

The structure of this note is as follows: first we overview the object-identification algorithms used for these studies. The emphasis is given to the changes that have been introduced since a similar study was performed in the DAQ TDR [76]. We then introduce a series of new trigger paths, aiming at increasing the event yield for various physics analyses. The central idea is to exploit various multi-object (or *cross-channel*) triggers in an attempt to improve the rejection and, at the same time, lower the kinematic thresholds of the corresponding objects. We finally present the performance of the triggers, and we calculate the overlap among them and the total HLT output rate.

E.2. Description of trigger tools

E.2.1. Level-1 reconstruction

There have been no significant changes in the Level-1 algorithms since the DAQ TDR. We have introduced an H_{T} algorithm which sums the corrected jet E_{T} of all the jets found above a programmable threshold, within $|\eta| < 5$. It does not account for E_{T} carried by muons and neutrinos.

The Level-1 strategy is the following: We have made an effort to keep the thresholds at the same levels, or even reduce them in order to be able to study cross-channel triggers (typically appearing with lower kinematic cuts). The notable exception is the tau triggers, where an increase in the HCAL noise and the usage of a new pile-up model in the simulation do affect the Level-1 τ identification tools, and therefore the related trigger rates. We have introduced additional Level-1 conditions for all HLT paths. The determination of thresholds and prescales is a compromise between the desire to distribute reasonably the available L1 bandwidth to the various triggers, and the need to optimise the L1 and HLT thresholds coherently in well-defined trigger paths.

[54] At the time of the writing of this document, several scenarios for the HLT output rate, the disk requirements for the storage manager and the associated cost are under discussion.

E.2.2. HLT reconstruction

Well defined Level-1 terms are used in order to obtain triggers whose behaviour and efficiency can be studied with real data. We have replaced some of the Level-1 conditions with respect to the DAQ TDR with new Level-1 terms when this leads to more reasonable trigger paths or triggers that are more stable and carry less of a bias. The optimisation of the thresholds for the various triggers has been a compromise between the physics needs of the CMS experiment and the total HLT rate available. This study serves only as an intermediate step in a long-term trigger study project. Further improvements in the reconstruction tools, better optimisation of the thresholds, implementation of additional triggers and a CMS-wide discussion of the allocation of the HLT bandwidth to the physics groups according to the priorities of the experiment, are foreseen.

A general and detailed description of the HLT system can be found in Ref. [76]. Here we summarise the recent modifications of the HLT tools, and the expected changes in the rates of the various triggers with respect to the earlier studies.

- **Muons:** The muon algorithm has not changed, with the exception of the drift-tube local reconstruction and segment building. Therefore, no significant changes in the rates of single- and dimuon trigger paths are expected. The option of constructing muon triggers without isolation has been added.
- **Electrons–Photons.** Here the most important change is that all saturated trigger towers at Level-1 are now considered isolated. This increases both the signal efficiency and the background. At HLT, the photon rate can be reduced by increasing the thresholds or by applying some isolation cuts. For the electrons the options include a matching with pixel lines and tracks, as well as isolation requirements in the hadron calorimeter and the tracker. A study of the algorithm optimisation can be found in Ref. [7]. An improvement of the rejection power of the electron–photon algorithms is achieved with a simultaneous decrease of the HLT thresholds. Similar enhancements are expected for cross-channel triggers where one of the objects under consideration is an electron or a photon.
- **Jets and $\boldsymbol{E_{\mathrm{T}}^{\mathrm{miss}}}$.** The main jet-finder algorithm (Iterative Cone with $R = 0.5$) has not been modified. Some optimisations of the tower thresholds have been added, and the jet corrections have been updated ("Scheme C"). Similarly, there are no major algorithm changes for $E_{\mathrm{T}}^{\mathrm{miss}}$, however it has been ensured that all triggers including a $E_{\mathrm{T}}^{\mathrm{miss}}$ object do not have any off-line corrections applied. Another improvement that has been recently introduced is the ability to construct *acoplanar* triggers by combining two jets, or a jet and a $E_{\mathrm{T}}^{\mathrm{miss}}$ object that do not lie "back-to-back" Details of the physics algorithms can be found in Refs. [165] and [148].
- ***b*-jets.** The algorithm now uses muon information for fast rejection. Further improvements have been made for faster decisions and for an increased efficiency in fully hadronic final states. The documentation for the *b*-jet HLT algorithm can be found in Ref. [290].
- **Taus:** The HLT τ algorithm has not changed. However, the increase in the Level-1 rate does propagate into the HLT. The isolation parameters for the electromagnetic calorimeter and the tracker have been tuned after recent studies performed by the Higgs group, described in Ref. [280]. The overall rate for τ-related triggers is expected to be slightly increased.

A new addition to the HLT reconstruction tools is the H_{T} algorithm. It sums the corrected jet E_{T} of all the $E_{\mathrm{T}} > 5\,\mathrm{GeV}$ jets found within $|\eta| < 5$, along with the energy of the $p_{\mathrm{T}} > 5\,\mathrm{GeV/c}$ HLT muons found in the event, and the $E_{\mathrm{T}}^{\mathrm{miss}}$ computed using the calorimeter deposits. It is meant to be driven off the corresponding L1 H_{T} term.

E.3. Triggering with forward detectors

E.3.1. Objective

We discuss[55] the feasibility of a special forward detectors trigger stream, with target output rate of $\mathcal{O}(1)$ kHz at L1 and $\mathcal{O}(1)$ Hz on the HLT, as well as the potential of the already foreseen CMS L1 trigger streams for retaining events with diffractive processes.

The proposed forward detectors trigger stream combines the information of the central CMS detector with that from detectors further downstream of the CMS IP. The forward detectors considered are the TOTEM T1 and T2 tracker telescopes as well as the TOTEM Roman Pot (RP) detectors up to 220 m downstream of CMS [823, 824]. Information from TOTEM will be available to the CMS L1 trigger. We also consider detectors at a distance of 420 m, in the cryogenic region of the LHC ring, currently being studied by the FP420 project [254].

Topologically, diffractive events are characterised by a gap in the rapidity distribution of final-state hadrons. In addition, the fractional momentum loss, ξ, of diffractively scattered protons peaks at $\xi = 0$ ("diffractive peak"). The TOTEM RP detectors will permit to measure protons in the region $0.2 > \xi > 0.02$. Detectors at a distance of 420 m from the IP would provide a coverage of $0.02 > \xi > 0.002$, complementary to that of the TOTEM detectors, but cannot be included in the Level-1 trigger without an increase in the Level-1 latency of 3.2 μs (though a special, long latency running mode might be feasible at lower luminosities).

The studies discussed in the following assume that the RP detectors are 100% efficient in detecting all particles that emerge at a distance of at least $10\,\sigma_{\text{beam}} + 0.5$ mm from the beam axis (1.3 mm at 220 m, 4 mm at 420 m). Their acceptance was calculated for the nominal LHC optics ($\beta^* = 0.55$ m), version V6.5 [825, 826], and by way of a simulation program that tracks particles through the accelerator lattice [827]. LHC bunches with 25 ns spacing were assumed.

The results presented below do not depend on the specific hardware implementation of the TOTEM T1, T2 and RP detectors; they hold for any tracker system with the T1, T2 η coverage in conjunction with RPs at 220 m from the IP.

E.3.2. Level-1 trigger rates for forward detectors trigger stream

E.3.2.1. 2-Jet conditions. A particularly interesting and challenging diffractive channel is the central exclusive production of a Higgs Boson, $pp \to pHp$, with Higgs mass close to the current exclusion limit. The dominant decay of a SM Higgs Boson of mass $\sim$120 GeV/c^2 is into two b-quarks and generates 2 jets with at most 60 GeV/c transverse momentum each. In order to retain as large a signal fraction as possible, as low an E_{T} threshold as possible of the Level-1 2-jet trigger is desirable. In practice, the threshold value cannot be chosen much lower than 40 GeV per jet. The Level-1 trigger applies cuts on the calibrated E_{T} value of the jet. Thus, a threshold of 40 GeV corresponds to 20–25 GeV in reconstructed E_{T}, i.e. to values where noise starts becoming sizable.

For luminosities of $10^{32}\,\text{cm}^{-2}\text{s}^{-1}$ and above, the Level-1 rate from standard QCD processes for events with at least 2 central jets ($|\eta| < 2.5$) with $E_{\text{T}} > 40$ GeV exceeds by far the target output rate of $\mathcal{O}(1)$ kHz. Thus additional conditions need to be employed to reduce the rate from QCD processes. The efficacy of several conditions was investigated [247, 248, 828–830]. In the following, the corresponding rate reduction factors are always quoted with respect to the rate of QCD events that contain at least 2 central jets with $E_{\text{T}} > 40$ GeV per jet.

[55] These studies were carried out in collaboration with TOTEM.

Table E.1. Reduction of the rate from standard QCD processes for events with at least 2 central Level-1 jets with $E_T > 40$ GeV, achievable with requirements on the tracks seen in the RP detectors. Additional rate reductions can be achieved with the H_T condition and with a topological condition. Each of them yields, for all luminosities listed, an additional reduction by about a factor 2.

				Reduction when requiring track in RPs at					
				220 m		420 m	220 & 420 m (asymmetric)		420 & 420 m
Luminosity [$\mathrm{cm^{-2}\,s^{-1}}$]	Pile-up events per BX	Level-1 2-jet rate [kHz] for $E_T > 40$ GeV	Total reduction needed		$\xi < 0.1$			$\xi < 0.1$	
1×10^{32}	0	2.6	2	370					
1×10^{33}	3.5	26	20	7	15	27	160	380	500
2×10^{33}	7	52	40	4	10	14	80	190	150
5×10^{33}	17.5	130	100	3	5	6	32	75	30
1×10^{34}	35	260	200	2	3	4	17	39	10

The QCD background events were generated with the Pythia Monte Carlo generator. In order to assess the effect when the signal is overlaid with pile-up, a sample of 500,000 pile-up events was generated with Pythia. This sample includes inelastic as well as elastic and single diffractive events. Pythia underestimates the number of final state protons in this sample. The correction to the Pythia leading proton spectrum described in [831] was used to obtain the results discussed in the following.

Given a Level-1 target rate for events with 2 central Level-1 jets of $\mathcal{O}(1)$ kHz, a total rate reduction between a factor 20 at $1 \times 10^{33}\,\mathrm{cm^{-2}\,s^{-1}}$ and 200 at $1 \times 10^{34}\,\mathrm{cm^{-2}\,s^{-1}}$ is necessary. Table E.1 summarises the situation for luminosities between $10^{32}\,\mathrm{cm^{-2}\,s^{-1}}$ and $10^{34}\,\mathrm{cm^{-2}\,s^{-1}}$, and for different RP detector conditions: a track at 220 m on one side of the IP (single-arm 220 m), without and with a cut on ξ; a track at 420 m on one side of the IP (single-arm 420 m); a track at 220 m and 420 m (asymmetric); a track at 420 m on both sides of the IP (double-arm 420 m). Because the detectors at 220 m and 420 m have complementary coverage in ξ, the asymmetric condition in effect selects events with two tracks of very different ξ value, in which one track is seen at 220 m on one side of the IP and a second track is seen on the other side at 420 m. If not by the L1 trigger, these asymmetric events can be selected by the HLT and are thus of highest interest. At luminosities where pile-up is present, the rate reduction achievable with the RP detector conditions decreases because of the diffractive component in the pile-up.

A collimator located in front of the LHC magnet Q5, planned to be operative at higher luminosities, will have an effect on the acceptance of the RP detectors resembling that of a ξ cut. This effect has not been taken into account in Table E.1.

Using T1 and T2 as vetoes in events with 2 central Level-1 jets was found to be effective only in the absence of pile-up [832].

In addition to the E_T values of individual Level-1 jets, the CMS Calorimeter Trigger has at its disposal the scalar sum, H_T, of the E_T values of all jets. Requiring that essentially all the E_T be concentrated in the two central Level-1 jets with highest E_T, i.e. $[E_T^1 + E_T^2]/H_T > 0.9$ (H_T condition), corresponds to imposing a rapidity gap of at least 2.5 units with respect to the beam direction. This condition reduces the rate of QCD events by approximately a factor 2, independent of the presence of pile-up and with only a small effect on the signal efficiency.

A further reduction of the QCD rate could be achieved with the help of a topological condition. The 2-jet system has to balance the total momentum component of the two protons along the beam axis. In signal events with asymmetric ξ values, the proton seen on one side

Table E.2. Estimated threshold values that result in a L1 output rate of ~ 1 kHz, for various conditions on central CMS detector quantities and on tracks seen in the RP detectors at 220 m and 420 m.

	L1 E_T or p_T threshold [GeV] at $\mathcal{O}(1)$ KHz L1 output rate for luminosity [cm^{-2} s^{-1}]			
L1 condition	1×10^{33}	2×10^{33}	5×10^{33}	1×10^{34}
1 Jet	115	135	160	190
2 Jet	90	105	130	150
1 Jet+220s	90	115	155	190
2 Jet+220s	65	90	125	150
1 Jet+220d	55	85	130	175
2 Jet+220d	30	60	100	140
1 Jet+220s(c)	70	90	150	185
2 Jet+220s(c)	60	70	115	145
1 Jet+220d(c)	30	65	110	155
2 Jet+220d(c)	20	45	85	125
1 Jet+420s	65	90	125	165
2 Jet+420s	45	70	100	130
1 Jet+420d	20	40	80	115
2 Jet+420d	< 10	30	60	90
1 μ+220s	12	16	23	> 100
1 μ + 220d	4	9	17	80
1 μ+220s(c)	–	11	22	100
1 μ+220d(c)	–	6	13	30
1 μ+420s	7	11	14	37
1 μ+420d	< 2	4	7	14

in the RP detectors at 220 m distance is the one with the larger ξ and thus has lost more of its initial momentum component along the beam axis. Hence the jets tend to be located in the same η-hemisphere as the RP detectors that detect this proton. A trigger condition requiring that $[\eta^{jet1} + \eta^{jet2}] \times \text{sign}(\eta^{220\,mRP}) > 0$ reduces the QCD background by a factor 2, independent of pile-up, and with no loss in signal efficiency.

A reduction of the QCD rate to levels compatible with a Level-1 output target rate of $\mathcal{O}(1)$ kHz by including RP detectors at a distance of 220 m from the CMS IP thus appears feasible for luminosities up to 2×10^{33} cm^{-2} s^{-1}, as long as a ξ cut can be administered in the L1 trigger.

E.3.2.2. Other conditions. The effect of combining already foreseen Level-1 trigger conditions with conditions on the RP detectors is illustrated in Table E.2 [829]. Single- and double-arm RP detector conditions are indicated with 's' and 'd' endings, respectively. Entries marked with a '(c)' indicate thresholds applicable if a cut on $\xi < 0.1$ is implemented for the RP detectors at 220 m. The jet conditions consider all Level-1 jets with $|\eta| < 5$.

A further rate reduction by approximately a factor two can be obtained at luminosities with negligible pile-up by imposing a rough large rapidity gap cut at L1. This was implemented by requiring that there be no forward jets, i.e. jets in the HF, in either hemisphere in the event.

E.3.3. Level-1 signal efficiencies

Of the Level-1 conditions discussed so far, only those based on the RP detectors have a significant impact on the signal efficiency. Of further interest is the question how many signal events are being retained by the already foreseen trigger streams, notably the muon trigger.

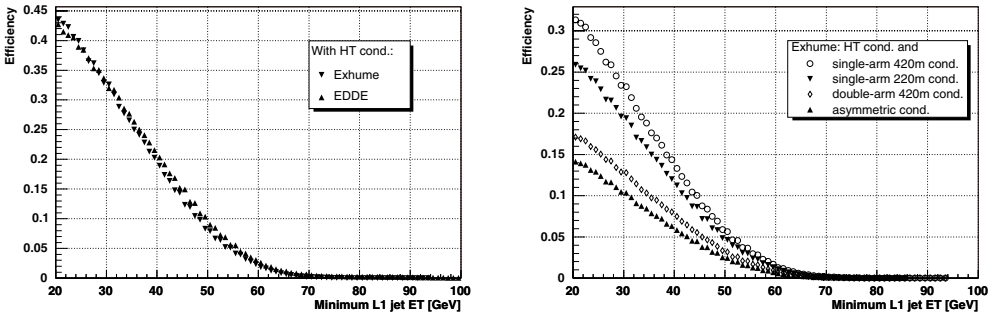

Figure E.1. L1 selection efficiency for $pp \to pHp$ and $H(120, \mathrm{GeV/c^2}) \to b\bar{b}$ as function of the E_T threshold value when at least 2 central Level-1 jets with E_T above threshold are required. All plots are for the non-pile-up case and the H_T condition has been applied. Left: Comparison between the EDDE and Exhume Monte Carlo generators, without applying any additional RP conditions. Right: Comparison of the effect of different RP conditions on the efficiency in the Exhume Monte Carlo sample.

E.3.3.1. Central exclusive Higgs production ($H(120\,\mathrm{GeV/c^2}) \to b\bar{b}$). In order to study the effect of the Level-1 trigger selection on the Higgs signal, signal samples of 100,000 events with central exclusive production of a Higgs Boson were generated with the Monte Carlo programs EDDE [261] (version 1.1) and Exhume [259] (version 1.0).

Figure E.1 shows the Level-1 selection efficiency as a function of the E_T threshold values when at least 2 central Level-1 jets with E_T above threshold are required [829]. For a threshold of 40 GeV per jet, Exhume and EDDE both yield an efficiency of about 20%. The plot on the right-hand side overlays the efficiency curves obtained with Exhume when the 2-jet condition is combines with RP detector conditions. With an E_T threshold of 40 GeV per jet, the single-arm 220 m (420 m) condition results in an efficiency of the order 12% (15%), the double-arm 420 m condition in one of 8% and the asymmetric condition in one of 6%. This also means that, even without the possibility of including the RP detectors at 420 m from the CMS IP in the Level-1 trigger, 6% of the signal events can be triggered on with the single-arm 220 m condition, but will have a track also in the 420 m detectors that can be used in the HLT.

An alternative trigger strategy is to exploit the relatively muon-rich final state from B-decays: about 20% of the events have at least a muon in the final state. Requiring at least one (two) L1 muon(s) with p_T above 14 GeV/c (3 GeV/c) yields an efficiency of 6% (2%). Demanding at least 1 muon and 1 jet, the latter with E_T >40 GeV, is a condition not yet foreseen in the CMS trigger tables. For a muon p_T threshold of 3 GeV/c, the rate at a luminosity of $10^{33}\,\mathrm{cm^{-2}}$ is slightly less than 3 kHz, and about half of the decays with muons in the final state (i.e. 9%) are retained [830].

E.3.3.2. Central exclusive Higgs production ($H(140\,\mathrm{GeV/c^2}) \to WW$). For SM Higgs Boson masses above 120 GeV/c^2, the $H \to WW$ branching ratio becomes sizable; in this case the final state contains high-p_T leptons that can be used for triggering. Efficiencies are in general high [830]. About 23% of the events have at least one muon in the final state. Approximately 70% of these (i.e. 16%) are retained by requiring at least one muon with a p_T threshold of 14 GeV/c. An extra $\approx$ 10% (i.e. 2%) would be retained by implementing the muon/jet slot discussed above with thresholds of 3 GeV/c on the muon p_T and 40 GeV on the jet E_T.

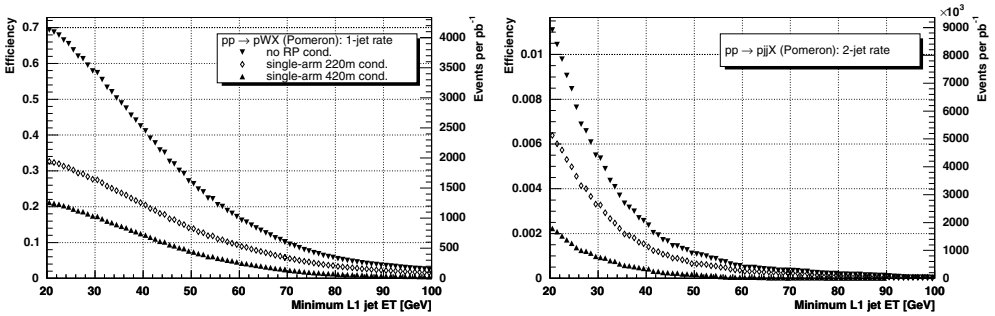

Figure E.2. L1 selection efficiency as function of the E_{T} threshold value for $pp \to pWX$ (left) and $pp \to pjjX$ (right), when at least one (left) or two (right) Level-1 jets ($|\eta| < 5$) above threshold are required. All plots are for the non-pile-up case.

E.3.3.3. Single diffractive hard processes. Double-Pomeron exchange processes constitute only a small part of the diffractive cross section. Hard single-diffraction, $pp \to pX$, where only one proton remains intact and the other is diffractively excited, have much higher cross sections than hard double-Pomeron exchange events. Efficiencies have been studied for $pp \to pX$, with X containing a W or a Z boson that decay to jets and to muons, as well as with X containing a dijet system. Samples of 100,000 signal events each were generated with the POMWIG Monte Carlo generator [833] (version 1.3).

For two example processes, Figure E.2 shows the efficiency as a function of the Level-1 threshold value, normalised to the number of events where for the diffractively scattered proton $0.001 < \xi < 0.2$ holds [829]. Three different trigger conditions are considered: trigger on central detector quantities alone (i), trigger on central detector quantities in conjunction (ii) with the single-arm 220 m condition, and (iii) with the single-arm 420 m condition. Also shown is the number of events expected to pass the L1 selection per pb^{-1} of LHC running. A significant part of events is retained when a proton is required in the 220 m RPs.

E.3.4. Effect of pile-up, beam-halo and beam-gas backgrounds

Pile-up effects are included in all rate and efficiency studies presented. In the 220 m stations, 0.055 protons/pile-up event are expected on average, in the 420 m stations, 0.012 protons/pile-up event. At a luminosity of $10^{34}\,\mathrm{cm}^{-2}\,\mathrm{s}^{-1}$, there are 35 pile-up events on average; this entails, on average, 2 extra tracks in the 220 m stations and less than one in the 420 m stations.

The effect from beam-halo and beam-gas events on the Level-1 rate is not yet included in the studies discussed here. Preliminary estimates suggest that they are chiefly a concern for any trigger condition based solely on the forward detectors. For any trigger condition that includes a requirement on central CMS detector quantities the size of their contribution is such that they do not lead to a significant increase of the Level-1 output rate.

E.3.5. HLT strategies

Jets are reconstructed at the HLT with an iterative cone ($R < 0.5$) algorithm. The Level-1 selection cuts are repeated with HLT quantities. The following conditions are imposed [829]:

(A) The event pass the single-arm 220 m Level-1 condition with $\xi < 0.1$ cut. As demonstrated in Table E.1, this condition reduces the Level-1 output rate to below $\mathcal{O}(1)$ kHz. Additional

Table E.3. Results of HLT selection.

HLT selection condition	A + B + C	A + B + D	A + B + C + E
HLT rate at $1 \times 10^{33}\,\mathrm{cm}^{-2}\,\mathrm{s}^{-1}$	15 Hz	20 Hz	< 1 Hz
line HLT rate at $2 \times 10^{33}\,\mathrm{cm}^{-2}\,\mathrm{s}^{-1}$	60 Hz	80 Hz	1 Hz
e Signal eff. $H(120)\,\mathrm{GeV/c^2} \to b\bar{b}$	11%	7%	6%

rate reduction factors of ~ 300 (~ 1000) at $1(2) \times 10^{33}$ cm $^{-2}$ s $^{-1}$ are needed to reach the HLT target output rate of $\mathcal{O}(1)$ Hz.

(B) The two jets are back-to-back in the azimuthal angle ϕ ($2.8 < \Delta\phi < 3.48$ rad), and have $(E_{\mathrm{T}}^1 - E_{\mathrm{T}}^2)/(E_{\mathrm{T}}^1 + E_{\mathrm{T}}^2) < 0.4$, and $E_{\mathrm{T}} > 40$ GeV for each jet.

(C) The proton fractional momentum loss ξ is evaluated with the help of calorimeter quantities [834–836]:

$$\xi_{+-} = (1/\sqrt{s})\,\Sigma_i E_{Ti} \exp(\mp\eta_i), \tag{E.1}$$

where the sum runs over the two jets and the $+, -$ signs denote the two hemispheres. The result is compared with the ξ value measured by the RP detectors. At present, no simulation of the RP reconstruction is available. As estimate of the ξ resolution, 15% (10%) is assumed at 220 m (420 m). Events are rejected if the difference between the two values of ξ is larger than $2\,\sigma$.

(D) At least one of the two jets is b-tagged.

(E) A proton is seen at 420 m.

The case without pile-up presents no difficulty: essentially no QCD background events survive the selection. If conditions A+B+C are applied, the signal efficiency for $pp \to pHp$ with $H(120\ \mathrm{GeV/c^2}) \to b\bar{b}$ is at 11% essentially unchanged with respect to the Level-1 selection, but the HLT output rate exceeds the target output rate, see Table E.3. If b-tagging is required but no ξ matching (conditions A +B+D), the efficiency drops to 7%, without any improvement in the rate reduction. The combination of conditions A+B+C+E finally leads to the targeted HLT output rate of $\mathcal{O}(1)$ Hz, without any loss in signal efficiency compared to L1.

E.4. High-Level Trigger paths

We are starting with the DAQ-TDR trigger table as the baseline. This includes single- and double-triggers for the basic objects (e, γ, μ, τ) along with jets and b-jets. Some cross-channel triggers are also present. We are expanding the cross-channel "menu" by introducing additional triggers. We introduce an H_{T} algorithm, which we combine with other objects. We are also adding a series of central single-jets, non-isolated muons, and a diffractive trigger discussed earlier.

E.4.1. Level-1 conditions

Table E.4 summarises the Level-1 conditions used to drive all the trigger paths. A pseudo "L1 bit number" has been assigned for easy reference in the following sections.

E.4.2. Evolution of DAQ-TDR triggers

The trigger paths that have been studied in Ref. [76] have been inherited and constitute the "bulk" of this next iteration of the CMS Trigger Menu for $\mathcal{L} = 2 \times 10^{33}\,\mathrm{cm}^{-2}\,\mathrm{s}^{-1}$.

Table E.4. Level-1 conditions used in High Level Trigger paths.

Level-1 bit #	Trigger	(GeV)	Prescale
0	Single μ	14	1
1	Double μ	3	1
2	Single isolated $e\gamma$	23	1
3	Double isolated $e\gamma$	11	1
4	Double $e\gamma$ (isolated/non-isolated)	19	1
8	Single central jet	177	1
9	Single forward jet	177	1
10	Single τ-jet	100	1
11	2 central jets	130	1
12	2 forward jets	130	1
13	2 τ-jets	66	1
14	3 central jets	86	1
15	3 forward jets	86	1
16	3 τ-jets	40	1
17	4 central jets	70	1
18	4 forward jets	70	1
19	4 τ-jets	30	1
26	(isolated) $e\gamma$ + τ	14, 52	1
31	H_{T}	300	1
32	$E_{\mathrm{T}}^{\mathrm{miss}}$	60	1
33	Single jet (central, forward or τ)	140	10
34	Single jet (central, forward or τ)	60	1 000
35	Single jet (central, forward or τ)	20	100 000
36	Single jet (central, forward or τ)	150	1
37	2 jets (central, forward or τ)	100	1
38	3 jets (central, forward or τ)	70	1
39	4 jets (central, forward or τ)	50	1

Modifications (optimisation of isolation cuts and thresholds) have been made for certain of the triggers, to reflect changes in the physics algorithms, or the improved understanding of the background from Monte Carlo (MC) simulations. The proposed Trigger Tables includes:

- **Muons.** The standard muon triggers include calorimeter-based isolation at L2, and both calorimeter and tracker isolation at L3. The p_{T} thresholds remain at 19 GeV/c for the single-muon and (7, 7) GeV/c for the dimuon trigger. A second set of relaxed single- and double-muons has been added with $p_{\mathrm{T}} > 37$ GeV and $p_{\mathrm{T}} > 10$ GeV, respectively. The main motivation here is Drell–Yan studies. In general, physics analyses that do not need a low p_{T} muon but do suffer from the isolation requirement on the muon. The reduced rejection caused by the removal of the isolation cuts is compensated by the higher-p_{T} thresholds on the muons, without affecting the event yield for the physics signal. The relaxed triggers have the advantage that the muons here are immune to radiative losses for the higher energy spectrum ($p_{\mathrm{T}} > 500$ GeV/c). Both isolated and relaxed triggers run off the corresponding non-isolated single- and double-muon bits at L1.
- **Electrons.** The p_{T} threshold remains at 26 GeV/c for the single electron trigger and has a new value of (12, 12) GeV/c for the dielectron trigger. An additional relaxed dielectron trigger appears with $p_{\mathrm{T}} > 19$ GeV/c. The single-electron and double-electron triggers run off the corresponding Level-1 bits.
- **Photons.** The new p_{T} thresholds are 80 GeV/c for the single-photon trigger and (30, 20) GeV/c for the diphoton trigger (both relaxed and non-relaxed flavours). A few prescaled

single- and double-photon triggers have also been introduced, for the purpose of studying trigger efficiencies. The photon HLT algorithms run off the corresponding Level-1 $e\gamma$ bits (single- and double-triggers).

- **Taus.** The single-τ trigger runs off the corresponding Level-1 bit. The double-τ trigger is driven by the `.OR.`-ing of the single- and double-τ trigger bits at L1. There is no explicit kinematic cut on the tau at HLT. There is, however, a match-to-track requirement in addition to the $p_{\mathrm{T}} > 100(66)\,\mathrm{GeV/c}$ L1 precondition for the inclusive (double) tau trigger. The single-τ has also a $E_{\mathrm{T}}^{\mathrm{miss}} > 65\,\mathrm{GeV}$ requirement at HLT.
- **Tau and electron.** The Level-1 condition is the corresponding τ+$e\gamma$ trigger. The p_{T} threshold remains at $16\,\mathrm{GeV/c}$ for the electron. There is no explicit p_{T} cut for the τ at HLT, but there is the match-to-track requirement for the τ candidate.
- **Jets.** The Level-1 conditions for the single-, double-, triple- and quadruple-jet triggers have been simplified considerably. Single jet triggers run off an `OR.` of a central-, forward- or tau-jet trigger at L1. Double-, triple- and quadruple-jet triggers use an `.OR.` of the all the Level-1 terms requiring the same number of jets or less. For example, the triple-jet trigger is driven by an `OR.` of the single-, double- and triple-jet Level-1 bits. In all cases, jets can be found in either the central or the forward region of the detector, and they include the τ candidates. The additional p_{T} cuts at HLT are: 400 (single), 350 (double), 195 (triple) and 80 (quadruple) GeV. The new double-jet trigger is expected to have a large overlap with the single-jet trigger path. However, it is useful for testing the additional bias introduced by the requirement for a second jet in the event. A series of prescaled triggers have also been introduced, which are discussed later (Sec. E.4.3.2).
- ***b*-jet.** This trigger is also based on the logical `.OR.` of the single-, double-, triple- and quadruple-jet Level-1 terms. At HLT, we have the additional requirement that the event is consistent with *b*-content. The E_{T} cut for the HLT jets is one of the following: 350 GeV if the event has one jet, 150 GeV if the event has three jets, or 55 GeV if the event has four jets.
- **Jet and $\boldsymbol{E}_{\mathbf{T}}^{\mathbf{miss}}$.** The E_{T} thresholds are 180 and 80 GeV, respectively. The Level-1 condition is a single $E_{\mathrm{T}}^{\mathrm{miss}}$ object above 60 GeV.

E.4.3. New triggers

E.4.3.1. Cross-channel triggers. The trigger studies presented in the DAQ TDR [76] have been the most comprehensive CMS effort to date to calculate rates for various trigger paths across many physics channels. For those studies the focus has been the optimisation of the rejection of the individual object-id algorithms (muon, electron, tau, etc.) rather than the combination of them into more powerful trigger tools. However, single (or even double) trigger objects are limited by the rate and, therefore, have their thresholds often higher than desired for many physics analyses. If the signal contains more than one trigger objects, using trigger paths combining different objects may yield a considerable gain by allowing lower trigger thresholds and higher efficiency. Cross-channel triggers can be much more stable and less prone to rate fluctuations from operating conditions. The correlations among trigger objects can help reduce difficult backgrounds and instrumental fakes. The additional advantage is that such cross-channel triggers have noticeably lower rates than the single trigger channels and therefore contribute fairly little to the overall bandwidth.

Some cross-channel triggers have already been considered and their rates estimated [76], such as τ + e and τ + $E_{\mathrm{T}}^{\mathrm{miss}}$, motivated by the Higgs searches with hadronic decays of τ and leptons, and jet + $E_{\mathrm{T}}^{\mathrm{miss}}$, important for searches of super-symmetric particles. The new addition

to the Trigger Menu, expanding the scope of Higgs searches, is a combined $\tau + \mu$ trigger with p_T thresholds at 40 and 15 GeV/c, respectively. It is driven by the single-μ Level-1 bit.

We are presenting here a few additional cross-channel triggers, along with the physics motivation.

- A new category of triggers introduced here is the acoplanar dijet and jet+E_T^{miss} for SUSY signals. The gain is the lower thresholds that become possible because of the topology constraint. Possible biases should be studied, so these triggers are meant to run in parallel with the standard jet and jet + E_T^{miss} triggers without the acoplanarity requirements. We introduce a double-jet trigger with E_T thresholds at (200, 200) GeV and $|\Delta\phi| < 2.1$, and a new jet + E_T^{miss} trigger with E_T thresholds at (100, 80) GeV and $|\Delta\phi| < 2.1$. The former is driven by an `.OR.` of the single- and double-jet requirements at Level-1 (bits 36, 37). The latter is driven by a simple $E_T^{miss} > 60$ GeV Level-1 requirement.
- "$E_T^{miss} + X$" triggers. A combination of an E_T^{miss} object with an H_T cut, one (or more) jet or lepton may be the only way to access E_T^{miss}-enhanced triggers if there are problems (*e.g.* instrumental fakes) that prevent CMS from running an inclusive E_T^{miss} trigger. At this point we have implemented:
  - Multi-jets and E_T^{miss}. These will be useful for SUSY studies, just like the series of jet triggers. However, the additional E_T^{miss} requirement allows us to lower the thresholds on the jets, and therefore increase the sensitivity of the analyses. We introduce here a dijet + E_T^{miss} trigger with $E_T^{jet} > 155$ GeV, $E_T^{miss} > 80$ GeV, a triple − jet + E_T^{miss} trigger with $E_T^{jet} > 85$ GeV, $E_T^{miss} > 80$ GeV and a quadruple − jet + E_T^{miss} trigger with $E_T^{jet} > 35$ GeV, $E_T^{miss} > 80$ GeV. These all run off the single Level-1 requirement for $E_T^{miss} > 60$ GeV.
  - H_T + E_T^{miss} and H_T + e. It is difficult to contain the rate for an inclusive H_T trigger without any additional cuts. The requirement for a E_T^{miss} cut or an additional electron in the event allows us to access events with lower E_T^{miss} or softer electrons. This can give an increased efficiency for W+jets, top physics, SUSY cascades, and other similar physics channels. Here we propose an H_T + E_T^{miss} trigger with $H_T > 350$ GeV, $E_T^{miss} > 80$ GeV and an H_T + e trigger with $H_T > 350$ GeV and $p_T > 20$GeV/c for the electron. They are both driven by the $E_T^{miss} > 60$ GeV condition at L1.

Some additional cross-channel triggers that have not been included in this Trigger Table iteration but should be considered in future trigger studies are:

- An $e + \mu$ trigger is of interest in many studies, for example:
  - $qqH, H \to \tau\tau \to 2\ell$, with an expected gain thanks to the lower lepton thresholds compared to the single-electron and single-muon trigger paths,
  - many SUSY decays including leptons in the final state,
  - top measurements in the double leptonic channel ($t\bar{t} \to b\bar{b}\ell\nu\ell\nu$), gaining sensitivity at the lower p_T spectrum, and
  - $B_s \to \ell\ell$, to allow for the lepton-number-violating channel to be studied.
- $E_T^{miss} + \ell$. The idea here is to exploit the presence of a W boson or a top decay in many channels. This could be used in many SM channels where lowering the lepton threshold extends the range of the measurement. For example:
  - top measurement in the double leptonic and semi-leptonic channels,
  - single top production, and
  - W measurements.

  Furthermore, this is a typical signature of an event containing super-symmetric particles.

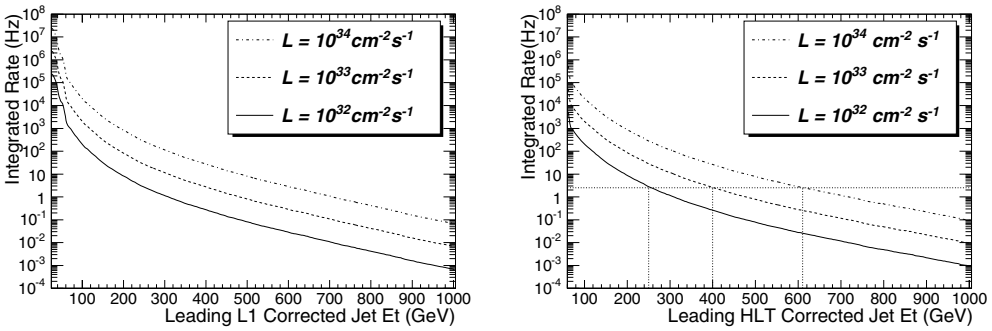

Figure E.3. The integrated trigger rates at Level-1 (left) and HLT (right) above the E_{T} thresholds for the highest E_{T} jet is plotted versus the E_{T} threshold for three luminosity scenarios: $\mathcal{L} = 10^{32}\,\mathrm{cm}^{-2}\,\mathrm{s}^{-1}$ (solid), and $\mathcal{L} = 10^{33}\,\mathrm{cm}^{-2}\,\mathrm{s}^{-1}$ (dashed), and $\mathcal{L} = 10^{34}\,\mathrm{cm}^{-2}\,\mathrm{s}^{-1}$ (dot-dashed). HLT thresholds that give 2.5 Hz are shown by vertical dotted lines.

- Triggers combining a lepton and a jet, or a lepton and a b-jet could be of interest for top measurements. The ℓ + jet signature is also very common in super-symmetric events.
- Finally, a combination of a lepton and a photon ($e+\gamma$ and $\mu+\gamma$) is ideal for Flavour Changing Neutral Current analyses, exploiting the extraordinary capabilities of CMS in detecting photons. These triggers allow to lower the thresholds on the lepton and the photon, increasing the event yield compared to the single-e, μ or γ trigger paths.

E.4.3.2. Single jet triggers. In this section we propose the single jet trigger paths. These have been driven by the needs of the inclusive jet and dijet analysis. The full study can be found in Ref. [118]. Here we summarise conclusions, along with a short description of the strategy for adjusting thresholds and prescales as the luminosity changes. This study looks at the evolution of the single-jet triggers for various luminosities. It serves as an example of how to preserve the long-term continuity of the triggers used for physics analyses. It is, therefore, interesting and instructive beyond the strict scope of the single-jet trigger suite.

To measure jet spectra down to low jet E_{T} and dijet mass requires multiple triggers, of roughly equal total rate, and with appropriately chosen E_{T} thresholds and prescales. In Fig. E.3 we show estimates of the Level-1 and HLT single jet trigger rates vs. corrected jet E_{T}. In Table E.5 we show the single jet trigger paths from Level-1 to HLT including thresholds, prescales and estimates of the rates. We find that the maximum allowed HLT rate is the constraining factor for triggering on jets. For luminosity $\mathcal{L} = 10^{32}\,\mathrm{cm}^{-2}\,\mathrm{s}^{-1}$, $\mathcal{L} = 10^{33}\,\mathrm{cm}^{-2}\,\mathrm{s}^{-1}$ and $\mathcal{L} = 10^{34}\,\mathrm{cm}^{-2}\,\mathrm{s}^{-1}$ the highest E_{T} threshold at HLT was chosen to give a rate of roughly 2.5 Hz, as illustrated in Fig. E.3, so that four triggers would saturate an allowed jet rate of roughly 10 Hz at HLT.

The highest E_{T} threshold in each scenario is not prescaled. Lower thresholds are prescaled and are chosen at roughly half the E_{T} of the next highest threshold. This allows reasonable statistics in the overlap between the two samples, necessary for measuring trigger efficiencies and producing a continuous jet spectrum. Note that the total L1 jet rate required is only around 0.3 KHz, a small fraction of the Level-1 total bandwidth. Since we are limited by HLT, not L1, for each trigger path the Level-1 thresholds are chosen low enough to have a Level-1 trigger efficiency of more than 95% at the corresponding HLT threshold in the path, as shown in Figure E.4. This strategy utilizes ten times more bandwidth at L1 than at HLT to insure that all of the resulting HLT sample has high enough trigger efficiency to be useful for analysis.

Table E.5. Single jet trigger table showing path names, trigger thresholds in corrected E_T, prescales, and estimated rates at Level-1 and HLT for four different luminosity scenarios.

	L1				HLT	
Path	E_T Cut (GeV)	Unpres. Rate (KHz)	Prescale (N)	Presc. Rate (KHz)	E_T Cut GeV)	Rate (Hz)
Single Jet Triggers in Scenario 1: $\mathcal{L} = 10^{32}$ cm^{-2} s^{-1}						
High	140	0.044	1	0.044	250	2.8
Med	60	3.9	40	0.097	120	2.4
Low	25	2.9×10^2	2,000	0.146	60	2.8
Single Jet Triggers in Scenario 2: $\mathcal{L} = 10^{33}$ cm^{-2} s^{-1}						
Ultra	270	0.019	1	0.019	400	2.6
High	140	0.44	10	0.044	250	2.8
Med	60	39	400	0.097	120	2.4
Low	25	2.9×10^3	20,000	0.146	60	2.8
Single Jet Triggers in Scenario 3: $\mathcal{L} = 2 \times 10^{33}$ cm^{-2} s^{-1}						
Ultra	270	0.038	1	0.038	400	5.2
High	140	0.88	20	0.044	250	2.8
Med	60	78	800	0.097	120	2.4
Low	25	5.8×10^3	40,000	0.146	60	2.8
Single Jet Triggers in Scenario 4: $\mathcal{L} = 10^{34}$ cm^{-2} s^{-1}						
Super	450	0.014	1	0.014	600	2.8
Ultra	270	0.19	10	0.019	400	2.6
High	140	4.4	100	0.044	250	2.8
Med	60	3.9×10^2	4,000	0.097	120	2.4
Low	25	2.9×10^4	200,000	0.146	60	2.8

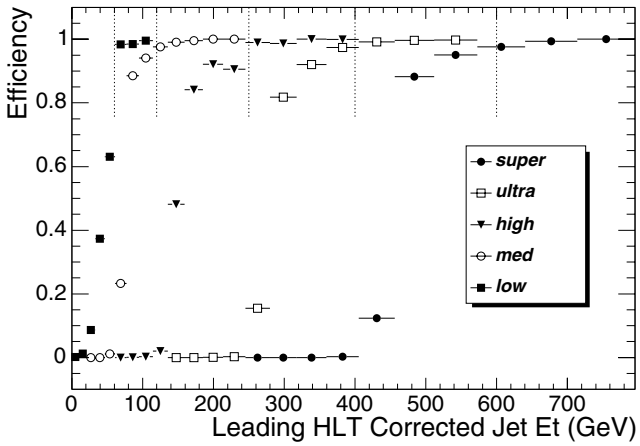

Figure E.4. The efficiency for passing the Level-1 jet trigger is shown as a function of HLT corrected jet E_T for each of the trigger paths shown in table E.5. The Level-1 thresholds were chosen to give an efficiency of greater than 95% at the corresponding HLT threshold.

Table E.5 illustrates a trigger strategy to maintain the continuity of jet analysis as the luminosity increases over a time span of years. The most important feature is that each luminosity scenario maintains the thresholds introduced in the previous scenario, allowing

combination of trigger samples over time. For the prescaled thresholds, we may increase the prescales, either in discrete steps or dynamically, to maintain the allowed HLT rate with increasing luminosity. However, to maintain maximum sensitivity to new physics, the highest E_T threshold must never be prescaled. For example, in table E.5 when the luminosity increases by only a factor of 2 from $\mathcal{L} = 10^{33}\,\mathrm{cm}^{-2}\,\mathrm{s}^{-1}$ to $\mathcal{L} = 2 \times 10^{33}\,\mathrm{cm}^{-2}\,\mathrm{s}^{-1}$, we double the prescales on the prescaled triggers but don't change either the threshold or the prescale of the highest E_T trigger labelled Ultra. This allows us to maintain stability of the single jet trigger thresholds, and analyses that depend on them, with only modest increases in the total rate for single jets. When the HLT rate in the unprescaled trigger becomes intolerably high, a higher E_T threshold unprescaled trigger is introduced, and the old unprescaled trigger can then be prescaled as necessary.

For the particular case of single-jet triggers: To commission the calorimeters, or perform a one-time jet study, it may be desirable to have more jets. If we want to write more than roughly 10 Hz of single jets at HLT, we can still use the same suite of single-jets, but lower the prescales to obtain more jets at low E_T. This is preferable to moving the threshold for the unprescaled trigger, or any of the triggers, and ending up with a special trigger that is only applicable for a given running period and difficult to combine with other samples.

For $\mathcal{L} = 2 \times 10^{33}\,\mathrm{cm}^{-2}\,\mathrm{s}^{-1}$, the suggested jet thresholds have been studied again in the scope of the global High-Level trigger analysis (Sec. E.5) and new Level-1 prescales and rates have been determined. For the trigger table proposed in this study, we have chosen four triggers, with E_T thresholds of 400, 250, 120 and 60 GeV, amd prescales of 1, 10, 1000 and 100 000, respectively.

E.4.3.3. Other triggers. The remaining triggers that have been introduced since the DAQ TDR are:

- Inclusive E_T^{miss} trigger. As discussed earlier, this is a difficult trigger that is subject to the good understanding and control of the detector noise. We suggest here a single E_T^{miss} trigger with $E_T > 91\,\mathrm{GeV}$, driven by the $E_T^{miss} > 60\,\mathrm{GeV}$ L1 condition. This is just an indicative value, rather on the low side, as E_T^{miss} rates appear lower compared to Ref. [76]. It is foreseen that additional E_T^{miss} triggers with different thresholds and prescales will be introduced in the future.
- Diffractive trigger. This trigger is different than all others described earlier in that it uses the TOTEM detector [823, 824]. At Level-1 we ask for two central jets with $E_T > 40\,\mathrm{GeV}$, along with a proton tagged with the 220 m Roman Pot. At HLT, a similar dijet cut and a "back-to-back" azimuthal condition are applied. We also require that we have a consistent measurement of the proton energy loss ξ in the two hemispheres (within $2\,\sigma$, measured at the Roman Pots). A final condition for a tagged proton seen by the 420 m Roman Pot brings the HLT rate down to $\mathcal{O}(1)$ Hz. This trigger is discussed in detail in Sec. E.3.

E.5. Performance

The performance of the trigger system is studied by using simulated data that has been digitised with appropriate pileup[56], taking into account both the inelastic (55.2 mb) and the diffractive (24.1 mb) cross sections. To reduce the amount of simulation time, about 50 million

[56] We have estimated the average number of in-time interactions per bunch crossing to be 5 for $\mathcal{L} = 2 \times 10^{33}\,\mathrm{cm}^{-2}\,\mathrm{s}^{-1}$. Additional, out-of-time interactions have been ignored.

Table E.6. Description and sizes of MC Samples used for the trigger studies. The contribution to the HLT rate does not include pre-scaled triggers.

Sample description	Cuts (Momenta in GeV/c)	Cross section (mb)	# of events	HLT rate (Hz)
Minimum bias with in-time pile-up; $\langle$ # of interactions $\rangle = 5$	—	79.3	50 000 000	—
QCD	$\hat{p_T} \in [15, 20]$	1.46×10^{0}	49 491	
QCD	$\hat{p_T} \in [20, 30]$	6.32×10^{-1}	49 244	
QCD	$\hat{p_T} \in [30, 50]$	1.63×10^{-1}	49 742	
QCD	$\hat{p_T} \in [50, 80]$	2.16×10^{-2}	99 486	
QCD	$\hat{p_T} \in [80, 120]$	3.08×10^{-3}	96 238	
QCD	$\hat{p_T} \in [120, 170]$	4.94×10^{-4}	99 736	
QCD	$\hat{p_T} \in [170, 230]$	1.01×10^{-4}	99 226	
QCD	$\hat{p_T} \in [230, 300]$	2.45×10^{-5}	99 481	
QCD	$\hat{p_T} \in [300, 380]$	6.24×10^{-6}	98 739	
QCD	$\hat{p_T} \in [380, 470]$	1.78×10^{-6}	46 491	
QCD	$\hat{p_T} \in [470, 600]$	6.83×10^{-7}	47 496	
QCD	$\hat{p_T} \in [600, 800]$	2.04×10^{-7}	48 986	
QCD	$\hat{p_T} \in [800, 1000]$	3.51×10^{-8}	45 741	
	Partial total		930 099	55.3 ± 6.9
$W \to e\nu$	1 electron with$\lvert\eta\rvert < 2.7$, $p_T > 25$	7.9×10^{-6}	3 944	9.7 ± 0.2
$Z \to ee$	2 electrons with $\lvert\eta\rvert < 2.7$, $p_T > 5$	8.2×10^{-7}	4 000	1.4 ± 0.0
$pp \to$ jet(s) $+ \gamma$, $\hat{p_T} > 30$ GeV/c	jet: $p_T > 20$,γ: $p_T > 30$	2.5×10^{-6}	4 000	1.0 ± 0.0
$W \to \mu\nu$	1 muon with $\lvert\eta\rvert < 2.5$, $p_T > 14$	9.8×10^{-6}	4 000	14.0 ± 0.3
$Z \to \mu\mu$	2 muons with $\lvert\eta\rvert < 2.5$, $p_T > 20$, 10	7.9×10^{-7}	2 941	1.5 ± 0.0
$pp \to \mu + X$	1 muon with $p_T > 3$	2.4×10^{-2}	839 999	25.5 ± 1.2

minimum bias events were simulated and reused in random combinations. It was ensured that these events do not cause triggers by themselves to avoid over estimating the rates due to this reuse of events.

In the following sections we list trigger rates along with their statistical uncertainties. These take into account the luminosity-dependent weight of the events from the different samples, the corresponding cross sections and the $\hat{p_T}$ of the main interaction and the pile-up contribution. They do *not* take into account the uncertainties of these individual factors, i.e. no systematic effects are studied here.

The Level-1 calorimeter trigger object rate studies are performed using QCD data that has been generated in several bins of $\hat{p_T}$. A special event-weighting procedure has been applied to properly take into account the cross sections of the sub-samples. The Level-1 muon and E_T^{miss} rate studies are performed using a purely minimum bias sample.

The HLT rates are estimated using specially enriched samples. For the triggers invoking muons, electrons and photons we have used a minimum bias sample enriched in muons, as well as $W \to e/\mu\nu$, $Z \to ee/\mu\mu$ and jet(s) + γ MC datasets. For the triggers including jets we have used QCD samples. These samples also contribute to the electron and photon triggers. Events triggered exclusively with muons have been excluded from the QCD samples, to avoid double-counting with the muon-enriched sample. Table E.6 summarises the MC samples used for the trigger studies, and their corresponding contribution to the HLT rate. A more detailed breakdown of the contributions to the electron, photon and muon trigger rates from

Table E.7. Trigger table showing Level-1 rates for DAQ TDR chosen thresholds for $\mathcal{L} = 2 \times 10^{33}\,\mathrm{cm}^{-2}\,\mathrm{s}^{-1}$. Whenever the "95% efficiency point" is reported in DAQ TDR, we also give the actual kinematic threshold that has been applied.

Trigger	95% Eff. point	Threshold (GeV)	Rate (kHz)	Cumulative Rate (kHz)
Single $e\gamma$	29	23.4	3.38 ± 0.23	3.4 ± 0.2
Double $e\gamma$	17	11.5	0.85 ± 0.12	4.0 ± 0.3
Single μ	—	14	2.53 ± 0.20	6.5 ± 0.3
Double μ	—	3	4.05 ± 0.26	10.3 ± 0.4
Single τ	86	93	3.56 ± 0.24	9.7 ± 0.4
Double τ	59	66	1.97 ± 0.18	10.6 ± 0.4
1-, 3-, 4-jets	177, 86, 70	135, 58, 45	2.43 ± 0.20	11.9 ± 0.4
Jet + $E_{\mathrm{T}}^{\mathrm{miss}}$	—	88, 46	1.07 ± 0.13	12.2 ± 0.4
$e\gamma$ + τ	—	21, 45	3.64 ± 0.24	12.9 ± 0.5
	Level-1 Trigger Total			12.9 ± 0.5

the different samples is discussed later (Sec. E.5.3-rates). For our calculations, we have used the standard HLT physics algorithms (`ORCA/_8/_13/_3` [10]) for the implementation of all trigger paths. At the time of this writing, this includes the latest algorithms and jet calibrations. For the global evaluation of the trigger rates we have used the "HLT steering code"

E.5.1. Level-1 rates

The background at Level-1 is entirely dominated by strong interactions. The muon rates at Level-1 are dominated by low p_{T} muons which are reconstructed as high p_{T} muons due to limited resolution at the trigger level. For the electron/photon trigger the rate is dominated by jets that fragment to high E_{T} π^0 s. The jet rates are dominated by true jets in the QCD events. The $E_{\mathrm{T}}^{\mathrm{miss}}$ background is due to the limited energy resolution, and pile-up of minimum bias interactions.

We first produce a trigger table with Level-1 rates for DAQ TDR chosen thresholds for comparison. For the calculations we use a sample of 2 million minimum bias crossings with an average of 5 events per crossing, constructed from the minbias events, without reuse of events. The out-of-time pile-up is neglected. Even though there are small differences for the individual triggers, the integral rate is consistent with the rates reported in Ref. [76]. This comparison serves as a cross-check and is a necessary intermediate step before the introduction of new trigger terms. Table E.7 summarises the Level-1 rate calculations for the DAQ TDR triggers with the new MC samples. Besides the "95% efficiency points" (used throughout the DAQ TDR), the applied L1 thresholds are also given.

For the new trigger table: We select several thresholds for each trigger object type and quote corresponding rates and prescales for $\mathcal{L} = 2 \times 10^{33}\,\mathrm{cm}^{-2}\,\mathrm{s}^{-1}$. For the single objects we have added a series of prescaled triggers to determine the efficiency turn-on. For the multi-object triggers we have picked the lowest common threshold that is allowed for the allocated bandwidth. For the cross-channel triggers we have attempted to keep the lepton thresholds as low as possible, within the allocated bandwidth based on the physics needs of the experiment. The prescales are chosen such that the simulated rate at all times falls below the DAQ bandwidth taking into account a safety factor of 3. The total Level-1 rate for all triggers (including prescaled ones) is 22.6 ± 0.3 kHz.

Table E.8. Comparison of HLT bandwidth given to various trigger paths calculated in this study with the DAQ TDR. See text for details on different kinematic cuts and changes in the HLT algorithms.

Trigger	DAQ TDR Rate (Hz)	New Rate (Hz)
Inclusive e	33.0	23.5 ± 6.7
e-e	1.0	1.0 ± 0.1
Relaxed e-e	1.0	1.3 ± 0.1
Inclusive γ	4.0	3.1 ± 0.2
γ-γ	5.0	1.6 ± 0.7
Relaxed γ-γ	5.0	1.2 ± 0.6
Inclusive μ	25.0	25.8 ± 0.8
μ-μ	4.0	4.8 ± 0.4
τ + $E_{\mathrm{T}}^{\mathrm{miss}}$	1.0	0.5 ± 0.1
τ + e	2.0	< 1.0
Double Pixel τ	1.0	4.1 ± 1.1
Double Tracker τ	1.0	6.0 ± 1.1
Single jet	1.0	4.8 ± 0.0
Triple jet	1.0	1.1 ± 0.0
Quadruple jet	7.0	8.9 ± 0.2
jet + $E_{\mathrm{T}}^{\mathrm{miss}}$	5.0	3.2 ± 0.1
b-jet (leading jet)	5.0	10.3 ± 0.3
b-jet (2^{nd} leading jet)	5.0	8.7 ± 0.3

E.5.2. Level-1 trigger object corrections

The trigger decisions are based on E_{T} of the objects reconstructed by various algorithms. Unfortunately, the energy deposition in the calorimeter and the size of the trigger towers, are not entirely uniform. We have used fits to the reconstructed-to-generated E_{T} ratios to correct for non-uniformity of the response for jets and electron/photon candidates found at all levels of trigger [830]. This correction procedure adjusts the mean response to the generated level.

The energy response of the calorimeters and the limited number of bits used in trigger calculations result in a finite resolution for the reconstructed trigger objects. Similarly, misalignments of the tracking systems and the limited number of patterns in the muon trigger look-up-tables also result in a finite resolution. To avoid systematic problems in understanding the trigger efficiency turn-on with the E_{T} of the trigger objects, it is envisioned that only data where high trigger efficiency is assured is used for analysis.

E.5.3. HLT rates

A rough comparison of the HLT bandwidth given to various triggers, calculated with the latest algorithms and the ones reported in Ref. [76] is shown in Table E.8. It must be noted that not only thresholds but also other cuts are different in the two trigger studies. Furthermore, additional changes in the HLT algorithms (summarised in Sec. E.2.2) must be taken into account. This comparison serves only as a consistency check. It reaffirms that despite the evolution of the CMS reconstruction algorithms over the years, trigger rates remain under control and that no major bandwidth changes are expected.

Table E.10 shows in a similar way the contributions to the single and double standard and relaxed muon rates from the various MC samples.

The contributions to the single and double electron and photon trigger rates at HLT from the various MC samples is given at Table E.9-egamma. The main contributions to the single

Table E.9. Contributions to the HLT rates for the electron and photon triggers from the various MC datasets.

Trigger	Threshold (GeV)	Rates (Hz)			
		QCD	$W \to e\nu$	$Z \to ee$	jet(s) + γ
Inclusive e	26	12.6 ± 6.7	9.7 ± 0.2	1.2 ± 0.0	—
e-e	12, 12	0.1 ± 0.1	—	1.0 ± 0.0	—
Relaxed e-e	19, 19	0.3 ± 0.1	—	1.0 ± 0.0	—
Inclusive γ	80	1.1 ± 0.2	—	—	2.0 ± 0.1
γ-γ	30, 20	1.3 ± 0.8	—	—	0.3 ± 0.0
Relaxed γ-γ	30, 20	0.9 ± 0.6	—	—	0.3 ± 0.0

Table E.10. Contributions to the HLT rates for the muon triggers from the various MC datasets.

Trigger	Threshold	Rates (Hz)		
	(GeV)	Enriched-μ sample	$W \to \mu\nu$	$Z \to \mu\mu$
Inclusive μ	19	10.9 ± 0.8	13.4 ± 0.3	1.5 ± 0.0
Relaxed μ	37	5.1 ± 0.5	5.7 ± 0.1	1.1 ± 0.0
μ-μ	7, 7	3.4 ± 0.4	—	1.3 ± 0.0
Relaxed μ-μ	10, 10	7.1 ± 0.5	—	1.4 ± 0.0

Table E.11. The Level-1 Trigger Menu at $\mathcal{L} = 2 \times 10^{33}\,\mathrm{cm}^{-2}\,\mathrm{s}^{-1}$. Individual and cumulative rates are given for the different trigger paths and selected kinematic thresholds.

Trigger	Level-1 Threshold (GeV)	Level-1 Rate (kHz)	Cumulative Level-1 Rate (kHz)
Inclusive $e\gamma$	22	4.2 ± 0.1	4.2 ± 0.1
Double $e\gamma$	11	1.1 ± 0.1	5.1 ± 0.1
Inclusive μ	14	2.7 ± 0.1	7.8 ± 0.2
Double μ	3	3.8 ± 0.1	11.4 ± 0.2
Inclusive τ	100	1.9 ± 0.1	13.0 ± 0.2
Double τ	66	1.8 ± 0.1	14.1 ± 0.2
1-,2-,3-,4-jets	150, 100, 70, 50	1.8 ± 0.1	14.8 ± 0.3
H_{T}	300	1.2 ± 0.1	15.0 ± 0.3
$E_{\mathrm{T}}^{\mathrm{miss}}$	60	0.3 ± 0.1	15.1 ± 0.3
H_{T} + $E_{\mathrm{T}}^{\mathrm{miss}}$	200, 40	0.7 ± 0.1	15.3 ± 0.3
jet + $E_{\mathrm{T}}^{\mathrm{miss}}$	100, 40	0.8 ± 0.1	15.4 ± 0.3
τ + $E_{\mathrm{T}}^{\mathrm{miss}}$	60, 40	2.7 ± 0.1	17.4 ± 0.3
μ + $E_{\mathrm{T}}^{\mathrm{miss}}$	5, 30	0.3 ± 0.1	17.6 ± 0.3
$e\gamma$ + $E_{\mathrm{T}}^{\mathrm{miss}}$	15, 30	0.7 ± 0.1	17.7 ± 0.3
μ + jet	7, 100	0.1 ± 0.1	17.8 ± 0.3
$e\gamma$ + jet	15, 100	0.6 ± 0.1	17.8 ± 0.3
μ + τ	7, 40	1.2 ± 0.1	18.4 ± 0.3
$e\gamma$ + τ	14, 52	5.4 ± 0.2	20.7 ± 0.3
$e\gamma$ + μ	15, 7	0.2 ± 0.1	20.7 ± 0.3
Prescaled			22.6 ± 0.3
	Total Level-1 Rate		22.6 ± 0.3

Table E.12. The High-Level Trigger Menu at $\mathcal{L} = 2 \times 10^{33}\,\mathrm{cm}^{-2}\,\mathrm{s}^{-1}$ for an output of approximately 120 Hz. The E_T values are the kinematic thresholds for the different trigger paths.

Trigger	Level-1 bits used	Level-1 Prescale	HLT Threshold (GeV)	HLT Rate (Hz)
Inclusive e	2	1	26	23.5 ± 6.7
e-e	3	1	12, 12	1.0 ± 0.1
Relaxed e-e	4	1	19, 19	1.3 ± 0.1
Inclusive γ	2	1	80	3.1 ± 0.2
γ-γ	3	1	30, 20	1.6 ± 0.7
Relaxed γ-γ	4	1	30, 20	1.2 ± 0.6
Inclusive μ	0	1	19	25.8 ± 0.8
Relaxed μ	0	1	37	11.9 ± 0.5
μ-μ	1	1	7, 7	4.8 ± 0.4
Relaxed μ-μ	1	1	10, 10	8.6 ± 0.6
$\tau + E_\mathrm{T}^\mathrm{miss}$	10	1	65 ($E_\mathrm{T}^\mathrm{miss}$)	0.5 ± 0.1
Pixel τ-τ	10, 13	1	—	4.1 ± 1.1
Tracker τ-τ	10, 13	1	—	6.0 ± 1.1
$\tau + e$	26	1	52, 16	< 1.0
$\tau + \mu$	0	1	40, 15	< 1.0
b-jet (leading jet)	36, 37, 38, 39	1	350, 150, 55 (see text)	10.3 ± 0.3
b-jet (2 $^{\mathrm{nd}}$ leading jet)	36, 37, 38, 39	1	350, 150, 55 (see text)	8.7 ± 0.3
Single-jet	36	1	400	4.8 ± 0.0
Double-jet	36, 37	1	350	3.9 ± 0.0
Triple-jet	36, 37, 38	1	195	1.1 ± 0.0
Quadruple-jet	36, 37, 38, 39	1	80	8.9 ± 0.2
$E_\mathrm{T}^\mathrm{miss}$	32	1	91	2.5 ± 0.2
jet + $E_\mathrm{T}^\mathrm{miss}$	32	1	180, 80	3.2 ± 0.1
acoplanar 2 jets	36, 37	1	200, 200	0.2 ± 0.0
acoplanar jet + $E_\mathrm{T}^\mathrm{miss}$	32	1	100, 80	0.1 ± 0.0
2 jets + $E_\mathrm{T}^\mathrm{miss}$	32	1	155, 80	1.6 ± 0.0
3 jets + $E_\mathrm{T}^\mathrm{miss}$	32	1	85, 80	0.9 ± 0.1
4 jets + $E_\mathrm{T}^\mathrm{miss}$	32	1	35, 80	1.7 ± 0.2
Diffractive	Sec. E.3	1	40, 40	< 1.0
$H_\mathrm{T} + E_\mathrm{T}^\mathrm{miss}$	31	1	350, 80	5.6 ± 0.2
$H_\mathrm{T} + e$	31	1	350, 20	0.4 ± 0.1
Inclusive γ	2	400	23	0.3 ± 0.0
γ-γ	3	20	12, 12	2.5 ± 1.4
Relaxed γ-γ	4	20	19, 19	0.1 ± 0.0
Single-jet	33	10	250	5.2 ± 0.0
Single-jet	34	1 000	120	1.6 ± 0.0
Single-jet	35	100 000	60	0.4 ± 0.0
	Total HLT rate			119.3 ± 7.2

electron trigger come from the QCD and $W \to e\nu$ samples, whereas for the single photon trigger the primary source is the jet(s) + γ events.

E.5.4. Trigger tables

Table E.11 summarises the Level-1 triggers used in this study, their kinematic thresholds, the individual and cumulative rates. We have assumed a DAQ capability of 50 kHz, taking into account a safety factor of 3.

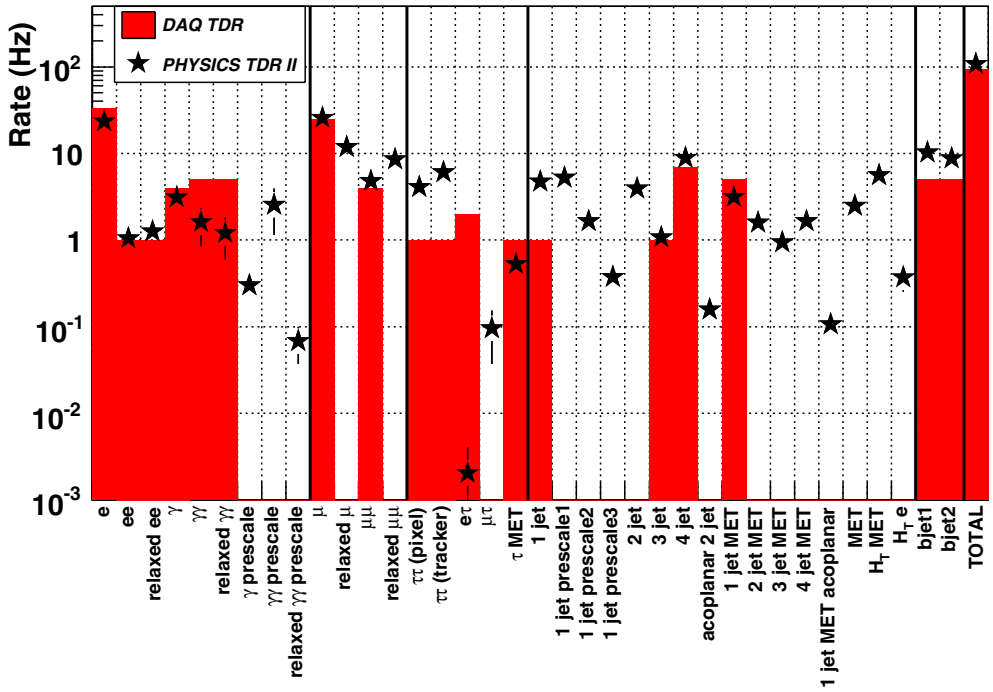

Figure E.5. Heuristic comparison of HLT bandwidth assigned to various trigger paths calculated in this study with the DAQ TDR. For the triggers introduced in this study the DAQ TDR entries appear empty. See text for details on different kinematic cuts and changes in the HLT algorithms.

Table E.12 gives the full list of trigger paths proposed for $\mathcal{L} = 2 \times 10^{33}\,\mathrm{cm}^{-2}\,\mathrm{s}^{-1}$ that have been described earlier for an HLT output rate of approximately 120 Hz.

Fig. E.5 shows a graphic representation of the HLT bandwidth assigned to all trigger paths presented in this study. For the triggers that appeared in the DAQ TDR, the corresponding rates are overlaid, in a heuristic comparison.

Glossary

ADC	Analog to Digital Converter
AdS	Anti de Sitter space
ALEPH	An experiment at LEP
ALICE	A Large Ion Collider Experiment at the LHC
ALPGEN	Monte Carlo event generator for multi-parton processes in hadronic collisions
ATLAS	A Toroidal LHC ApparatuS experiment
BMU	Barrel Muon system
BR	Branching Ratio
BX	Bunch Crossing
BXN	Bunch Crossing Number
CASTOR	Calorimeter in the forward region of CMS
CDF	Collider Detector Facility experiment at the FNAL Tevatron
CL	Confidence Level
CLHEP	Class Library for HEP
CMKIN	CMS Kinematics Package (legacy Fortran)
CMS	Compact Muon Solenoid experiment
CMSIM	CMS Simulation Package (legacy Fortran)
CMSSW	CMS Software framework
CPT	Computing, Physics, TriDAS and software projects of CMS
CPU	Central Processing Unit
CompHEP	Monte Carlo event generator for high-energy physics collisions
CSC	Cathode Strip Chamber muon system
CVS	Concurrent Versions System
DØ	Experiment at the FNAL Tevatron
DAQ	Data Acquisition
DELPHI	An experiment at LEP
DESY	Deutsches Elektronen SYnchrotron laboratory, Hamburg
DST	Data Summary Tape – a compact event format
DT	Drift Tube muon system
DY	Drell–Yan
EB	Electromagnetic Calorimeter (Barrel)
ECAL	Electromagnetic Calorimeter
ED	Extra Dimensions
EE	Electromagnetic Calorimeter (Endcap)
EM	Electromagnetic
EMU	Endcap Muon system
ES	Endcap preShower detector
EW	ElectroWeak
FAMOS	CMS Fast Simulation
FLUKA	Computer program for hadron shower calculations
FNAL	Fermi National Accelerator Laboratory, USA
FSR	Final State Radiation

Gb	Gigabit (10^9 bits)
GB	Gigabyte (10^9 bytes)
GCALOR	Computer program for hadron shower calculations
GEANT	Detector simulation framework and toolkit
GMSB	Gauge Mediated Symmetry Breaking
GUT	Grand Unified Theory
H1	An experiment at the DESY HERA collider
HAD	Hadronic
HCAL	Hadron Calorimeter
HB	Hadron Calorimeter (Barrel)
HE	Hadron Calorimeter (Endcap)
HEP	High Energy Physics
HEPEVT	HEP Event (generated event format)
HERA	Electron-proton collider at DESY
HERWIG	Hadron Emission Reactions With Interfering Gluons, a Monte Carlo event generator for high-energy physics collisions
HF	Hadron Calorimeter (Forward)
HI	Heavy Ion(s)
HIJING	Heavy Ion Jet INteraction Generator, Monte Carlo event generator for heavy-ion collisions
HLT	High-Level Trigger
HO	Hadron Calorimeter (Outer Barrel)
IGUANA	Interactive Graphics for User ANAlysis – used for the CMS Event Display Package
I/O	Input/Output
IP	Impact Parameter, also Impact Point or Internet Protocol
ISR	Initial State Radiation, also Intersecting Storage Ring collider at CERN
JES	Jet Energy Scale
Kalman Filter	Computational method for fitting tracks
kb	kilobit (10^3 bits)
kB	kilobytes (10^3 bytes)
L1	Level-1 hardware-based trigger
L3	An experiment at LEP
LCG	LHC Computing Grid (a common computing project)
LED	Large Extra Dimenstions, also Light Emitting Diode
LEP	Large Electron Positron collider at CERN
LHC	Large Hadron Collider
LHCb	Large Hadron Collider Beauty experiment
LHCC	LHC (review) Committee
LHEP	Physics model of GEANT4
LL	Leading Logarithm, also Log Likelihood
LO	Leading Order calculation
LOI	Letter Of Intent
LPC	LHC Physics Center, Fermilab
LS	Like-Sign
LSP	Lightest Supersymmetric Particle

Mb	Megabit (10^6 bits)
MB	Muon system (Barrel), also Mother Board or Megabyte (10^6 bytes)
MC	Monte Carlo simulation program/technique, also Mini-Crate of DT system
ME	Muon system (Endcap), also Matrix Element or Monitoring Element
MET	Missing Transverse Energy
metadata	Data describing characteristics of other data
MIP	Minimum Ionizing Particle
MSUGRA	Minimal SUper GRAvity model of supersymmetry
MSSM	Minimal SuperSymmetric Model
MTCC	Magnet Test Cosmic Challenge
ndf	number of degrees of freedom
NLO	Next-to-Leading Order calculation
NN	Neural Network
NNLO	Next-to-Next-to-Leading Order calculation
NS	Numbering Scheme
OO	Object Oriented
OPAL	An experiment at LEP
ORCA	Object-oriented Reconstruction for CMS Analysis
OS	Opposite-Sign, also Operating System
OSCAR	Object-oriented Simulation for CMS Analysis and Reconstruction
P5	Point 5 collision area of LHC
PAW	Physics Analysis Workstation (legacy interactive analysis application)
PB	Petabyte (10^5 bytes)
PC	Personal Computer
PD	Pixel Detector
PDF	Parton Density Function, also Probability Distribution Function (p.d.f.)
PRS	Physics Reconstruction and Selection groups
PS	Proton Synchrotron, also Parton Showers
PV	Primary Vertex
PYTHIA	Monte Carlo event generator for high-energy physics collisions
QCD	Quantum Chromodynamics
QED	Quantum Electrodynamics
QGSP	Physics model of GEANT4
RecHit	Reconstructed hit in a detector element
RHIC	Relativistic Heavy Ion Collider (at Brookhaven, USA)
RMS	Root Mean Square
ROOT	An object-oriented data analysis framework
RPC	Resistive Plate Chamber muon system

SLT	Soft Lepton Tag
SM	Standard Model, also SuperModule (ECAL) or Storage Manager (DAQ)
S/N	Signal to Noise ratio
SPS	Super Proton Synchrotron collider at CERN
SS	Same-Sign
SST	Silicon Strip Tracker
SUSY	SUperSYmmetry
SV	Secondary Vertex
T1, T2	Tracking telescopes of TOTEM
TAG	Event index information such as run/event number, trigger bits, etc.
Tb	Terabit (10^{12} bits)
TB	Terabyte (10^{12} bytes)
TDR	Technical Design Report
TEC	Tracker EndCap
TIB	Tracker Inner Barrel
TID	Tracker Inner Disks
TOB	Tracker Outer Barrel
TOTEM	Separate experiment at P5 for forward physics
TPD	Tracker Pixel Detector
TriDAS	Trigger and Data Acquisition project
UA1	An experiment at the CERN SPS collider
UA2	An experiment at the CERN SPS collider
UE	Underlying Event
UED	Universal Extra Dimensions
VBF	Vector Boson Fusion
VPT	Vacuum PhotoTriode
WWW	World Wide Web
ZDC	Zero Degree Calorimeter
ZEUS	An experiment at the DESY HERA collider

References

Blue font in the online PDF indicates links to full-text articles.

DOI numbers are given for some published articles, for which the full text may be accessed by prefixing the number with http://dx.doi.org/

CMS Notes are available at http://cms.cern.ch/iCMS/ unless otherwise noted.

[1] TLS Group 1995 The Large Hadron Collider Conceptual Design *CERN-AC-95-05 Preprint* hep-ph/0601012

[2] CMS Collaboration 1992 The Compact Muon Solenoid Letter of Intent *CERN/LHCC* 1992-3, LHCC/I 1

[3] CMS Collaboration 1994 The Compact Muon Solenoid Technical Proposal *CERN/LHCC* 94-38, LHCC/P1

[4] ATLAS and CMS Collaboration, Branson J G *et al* 2002 High transverse momentum physics at the Large Hadron Collider: The ATLAS and CMS Collaborations *Eur. Phys. J. direct* C **4** N1 (*Preprint* hep-ph/0110021)

[5] LHC/LC Study Group Collaboration, Weiglein G *et al* 2004 Physics interplay of the LHC and the ILC *Preprint* hep-ph/0410364

[6] Krasnikov N and Matveev V 2004 Search for new physics at LHC *Phys. Usp.* **47** 643 (*Preprint* hep-ph/0309200)

[7] CMS Collaboration 2006 The CMS Physics Technical Design Report, Volume 1 *CERN/LHCC* 2006-001, CMS TDR 8.1

[8] OSCAR: CMS Simulation Package Home Page http://cmsdoc.cern.ch/oscar

[9] GEANT4 Collaboration, Agostinelli S *et al* 2003 GEANT4: A simulation toolkit *Nucl. Instrum. Methods* A **506** 250–303

[10] ORCA: CMS reconstruction Package Site located at http://cmsdoc.cern.ch/orca

[11] CMS Collaboration, Acosta D *et al* 2006 CMS Physics Technical Design Report, Volume 1, Section 2.6: Fast simulation p 55 *CERN/LHCC* 2006-001

[12] Pumplin J *et al* 2002 New generation of parton distributions with uncertainties from global QCD analysis *J. High. Energy Phys.* JHEP07(2002)012 (*Preprint* hep-ph/0201195)

[13] Martin A D, Roberts R G, Stirling W J and Thorne R S 2002 MRST2001: Partons and alpha(s) from precise deep inelastic scattering and Tevatron jet data *Eur. Phys. J.* C **23** 73 (*Preprint* hep-ph/0110215)

[14] Alekhin S *et al* 2005 HERA and the LHC - A workshop on the implications of HERA for LHC physics: Proceedings Part A

[15] Seez C *et al* 1990 Photon decay modes of the intermediate mass Higgs *Proceedings of the Large Hadron Collider Workshop* (*Aachen, 4–9 October, 1990), CERN 90-10* volume II ed G Jarlskog and D Rein

[16] CMS Collaboration 1997 The Electromagnetic Calorimeter Technical Design Report *CERN/LHCC*, 97-033 CMS TDR 4, Addendum *CERN/LHCC* 2002-027

[17] Favara A and Pieri M 1997 Confidence Level Estimation and Analysis Optimization *Preprint* DFF 278/4/1997

[18] L3 Collaboration, Acciarri M *et al* 1997 Search for the Standard Model Higgs Boson in e^+e^- Interactions at 161 GeV $< \sqrt{s} <$ 172 GeV *Phys. Lett.* B **411** 373

[19] CMS Collaboration, Pieri M *et al* 2006 Inclusive search for the Higgs boson in the $H \to \gamma\gamma$ channel *CMS Note* AN 2006/112

[20] Spira M 1998 QCD effects in Higgs physics *Fortsch. Phys.* **46** 203–284 (*Preprint* hep-ph/9705337)

[21] Djouadi A, Kalinowski J and Spira M 1998 HDECAY: a program for Higgs boson decays in the Standard Model and its supersymmetric extension *Comput. Phys. Commun.* **108** 56–74 (doi:10.1016/S0010-4655(97)00123-9)

[22] CMS Collaboration, Dubinin M *et al* 2006 The vector boson fusion production with $H \to \gamma\gamma$ *CMS Note* 2006/097

[23] CMS Collaboration, Lethuillier M 2006 Search for SM Higgs boson with W/Z+H, H$\to 2\gamma$ channel *CMS Note* 2006/110

[24] Sjostrand T, Lonnblad L and Mrenna S 2001 PYTHIA 6.2: Physics and manual *Preprint* hep-ph/0108264

[25] CMSIM home page http://cmsdoc.cern.ch/cmsim/cmsim.html

[26] Giele W *et al* 2002 The QCD/SM working group: Summary report *Preprint* hep-ph/0204316

[27] Dobbs M *et al* 2004 The QCD/SM working group: Summary report *Preprint* hep-ph/0403100

[28] Binoth T 2000 Two photon background for Higgs boson searches at the LHC *Preprint* hep-ph/0005194

[29] Bern Z, Dixon L J and Schmidt C 2002 Isolating a light Higgs boson from the di-photon background at the LHC *Phys. Rev.* D **66** 074018 (*Preprint* hep-ph/0206194)

[30] Binoth T, Guillet J P, Pilon E and Werlen M 2002 A next-to-leading order study of photon pion and pion pair hadro-production in the light of the Higgs boson search at the LHC *Eur. Phys. J. Direct* C **4** (doi:10.1007/s1010502c0007)
[31] CMS Collaboration, Agostino L *et al* 2006 HLT Selection of Electrons and Photons *CMS Note* 2006/078
[32] CMS Collaboration, Meschi E *et al* 2001 Electron Reconstruction in the CMS Electromagnetic Calorimeter *CMS Note* 2001/034
[33] CMS Collaboration, Marinelli N 2006 Track Finding and Identification of Converted Photons *CMS Note* 2006/005
[34] CMS Collaboration, Litvin V *et al* 2002 The Rejection of Background to the HGG Process Using Isolation Criteria Based on Information from the Calorimeter and Tracker *CMS Note* 2002-030
[35] CMS Collaboration, Pieri M *et al* 2006 Distinguishing Isolated Photos from Jets *CMS Note* 2006/007
[36] The LEP Collaborations: ALEPH, DELPHI, L3 and OPAL1998 Lower Bound for the Standard Model Higgs Boson Mass from Combining the Results of the Four LEP Experiments *CERN EP* 98-046
[37] CMS Collaboration, Baffioni S *et al* 2006 Discovery potential for the SM Higgs boson in the $H \to ZZ^{(*)} \to e^+e^-e^+e^-$ decay channel *CMS Note* 2006/115
[38] Barberio E, van Eijk B and Was Z 1991 PHOTOS: A Universal Monte Carlo for QED radiative corrections in decays *Comput. Phys. Commun.* **66** 115–128
[39] Barberio E and Was Z 1994 PHOTOS: A Universal Monte Carlo for QED radiative corrections. Version 2.0 *Comput. Phys. Commun.* **79** 291–308 (doi:10.1016/0010-4655(94)90074-4)
[40] Spira M 1995 HIGLU: A Program for the Calculation of the Total Higgs Production Cross Section at Hadron Colliders via Gluon Fusion including QCD Corrections *Preprint* hep-ph/9510347
[41] Djouadi A, Kalinowski J and Spira M 1998 HDECAY: A Program for Higgs Boson Decays in the Standard Model and its Supersymmetric Extension *Comput. Phys. Commun.* **108** 56–74 (*Preprint* hep-ph/9704448)
[42] Zecher C *et al* 1994 Leptonic Signals from off-shell Z Boson Pairs at Hadron Colliders *Preprint* hep-ph/9404295
[43] CompHEP Collaboration, Boos E *et al* 2004 CompHEP 4.4: Automatic computations from Lagrangians to events *Nucl. Instrum. Meth.* A **534** 250–259 (*Preprint* hep-ph/0403113)
[44] Slabospitsky S R and Sonnenschein L 2002 TopReX generator (version 3.25): Short manual *Comput. Phys. Commun.* **148** 87–102 (doi:10.1016/S0010-4655(02)00471-X)
[45] Beneke M *et al* 2000 Top quark physics *Preprint* hep-ph/0003033
[46] CMS Collaboration, Baffioni S, Charlot C, Ferri F, Futyan D, Meridiani P, Puljak I, Rovelli C, Salerno R and Sirois Y 2006 Electron Reconstruction in CMS *CMS Note* 2006/040
[47] Abdullin S *et al* 2006 Study of PDF and QCD scale uncertainties in $H \to ZZ^{(*)} \to 4\mu$ events at the LHC *CMS Note* 2006/068 See also hep-ph/0604120, Les Houches Physics at TeV Colliders 2005, Standard Model and Higgs working group: Summary report. April 2006
[48] Meridiani P and Paramatti R 2006 Use of $Z \to e^+e^-$ events for ECAL calibration *CMS Note* 2006/039
[49] Bartsch V and Quast G 2006 Expected signal observability at future experiments *CMS Note* 2005-004
[50] Bityukov S and Krasnikov N 1998 New physics discovery potential in future experiments *Mod. Phys. Lett.* A **13** 3235–3249
[51] Abdullin S *et al* 2006 Search Strategy for the Standard Model Higgs Boson in the $H \to ZZ^{(*)} \to 4\mu$ Decay Channel using $M(4\mu)$-Dependent Cuts *CMS Note* 2006/122
[52] Karimaki V *et al* 2004 CMKIN v3 User's Guide *CMS IN* 2004-016
[53] Spira M 2005 'SM Higgs boson production cross sections at NLO' and 'SM Higgs boson BRs'Available at http://cmsdoc.cern.ch/∼anikiten/cms-higgs/
[54] Particle Data Group, Eidelman S *et al* 2004 Review of Particle Physics *Phys. Lett.* B **592** 1 (doi:10.1016/j.physletb.2004.06.001)
Particle Data Group, Yao W-M *et al* 2006 Review of Particle Physics *J. Phys. G: Nucl. Part. Phys.* **33** 1 (doi:10.1088/0954-3899/33/1/001)
[55] Maltoni F 2005 Theoretical Issues and Aims at the Tevatron and LHC *Proceedings of the 1st Hadron Collider Physics Symposium (HCP 2005) (Les Diablerets, Switzerland 2005 July)* Available at http://hcp-2005.web.cern.ch/HCP-2005
[56] Campbell J M 2001 W/Z + B anti-B/jets at NLO using the Monte Carlo MCFM Talk given at 36th Rencontres de Moriond on QCD and Hadronic Interactions (*Les Arcs, France, 17–24 March 2001*) *Preprint* hep-ph/0105226
[57] Abdullin S *et al* 2006 Relative Contributions of t- and s-Channels to the $ZZ \to 4\mu$ Process *CMS Note* 2006/057, See also hep-ph/0604120, Les Houches Physics at TeV Colliders 2005, Standard Model and Higgs working group: Summary report. April 2006

[58] Bartalini P *et al* 2006 NLO vs. LO: kinematical differences for signal and background in the H $\rightarrow$ ZZ* $\rightarrow 4\mu$ analysis *CMS Note* 2006/130

[59] Acosta D *et al* 2006 Measuring Muon Reconstruction Efficiency from Data *CMS Note* 2006/060

[60] Aldaya M, Arce P, Caballero J, de la Cruz B, Garcia-Abia P, Hernandez J M, Josa M and Ruiz E 2006 Discovery potential and search strategy for the Standard Model Higgs boson in the $H \rightarrow ZZ^\star \rightarrow 4\mu$ decay channel using a mass-independent analysis *CMS Note* 2006/106

[61] Read A 2000 Modified Frequentist Analysis of Search Results (The CLs Method) *1st Workshop on Confidence Limits, CERN, Geneva CERN-EP* /2000-005

[62] LEP Working Group for Higgs boson searches Collaboration, Barate R *et al* 2003 Search for the standard model Higgs boson at LEP *Phys. Lett.* B **565** 61–75 (*Preprint* hep-ex/0306033)

[63] Abdullin S and Drozdetskiy A *et al* 2006 GARCON: Genetic Algorithm for Rectangular Cuts Optimization. User's manual for version 2.0 *Preprint* hep-ph/0605143 See also http://drozdets.home.cern.ch/drozdets/home/genetic/

[64] Abdullin S *et al* 2006 Sensitivity of the Muon Isolation Cut Efficiency to the Underlying Event Uncertainties *CMS Note* 2006/033, See also hep-ph/0604120, Les Houches Physics at TeV Colliders 2005, Standard Model and Higgs working group: Summary report. April 2006

[65] Aldaya M *et al* 2006 A method for determining the mass, cross-section and width of the Standard Model Higgs boson using the H $\rightarrow$ ZZ* $\rightarrow 4\mu$ decay channel *CMS Note* 2006/107

[66] Bartsch V Simulation of Silicon Sensors and Study of the Higgs Decay

[67] Dittmar M and Dreiner H 1997 How to find a Higgs boson with a mass between 155GeV to to 180GeV at the CERN LHC *Phys. Rev.* D **55** 167–172 (*Preprint* hep-ph/9608317) (doi:10.1103/PhysRevD.55.167)

[68] Dittmar M and Dreiner H 1997 LHC Higgs Search with $l^+\nu l^-\overline{\nu}$ final states *CMS Note* 1997/083

[69] Sjostrand T *et al* 2001 High-energy-physics event generation with PYTHIA 6.1 *Comput. Phys. Commun.* **135** 238–259 (doi:10.1016/S0010-4655(00)00236-8)

[70] Binoth T, Ciccolini M, Kauer N and Kramer M 2005 Gluon-induced W W background to Higgs boson searches at the LHC *J. High. Energy Phys.* JHEP03(2005)065 (*Preprint* hep-ph/0503094)

[71] Davatz G *et al* 2004 Effective k-factors for $H \rightarrow WW^{(*)} \rightarrow 2\mu 2\nu$ at the LHC *J. High. Energy Phys.* JHEP0405(2004)009 (*Preprint* hep-ph/0402218) (doi:10.1088/1126-6708/2004/05/009)

[72] Frixione S and Webber B R 2002 Matching NLO QCD computations and parton shower simulations *J. High. Energy Phys.* JHEP0206(2002)029 (*Preprint* hep-ph/0204244)

[73] Davatz G, Dittmar M and Giolo-Nicollerat A S 2006 Standard Model Higgs Discovery Potential of CMS in the $H \rightarrow WW^{(*)} \rightarrow l\nu l\nu$ Channel *CMS Note* 2006/047

[74] Campbell J M and Ellis R K 1999 An update on vector boson pair production at hadron colliders *Phys. Rev.* D **60** 113006 (doi:10.1103/PhysRevD.60.113006)

[75] Campbell J and Tramontano F 2005 Next-to-leading order corrections to Wt production and decay *Nucl. Phys.* B **726** 109–130 (doi:10.1016/j.nuclphysb.2005.08.015)

[76] CMS Collaboration 2002 The TriDAS Project Technical Design Report, Volume 2: Data Acquisition and High-Level Trigger *CERN/LHCC* 2002-26, CMS TDR 6.2

[77] Drollinger V, Gasparini U, Torassa E and Zanetti M 2006 Physics study of the Higgs decay chanel $H \rightarrow WW^{(*)} \rightarrow 2\mu 2\nu$ *CMS Note* 2006/055

[78] Chekanov S V 2002 Jet algorithms: a mini review *Proceedings of the 14th Topical Conference on Hadron Collider Physics (HCP 2002)* September-October (Karlsruhe, Germany)

[79] Bityukov S I and Krasnikov N V 2002 Uncertainties and discovery potential in planned experiments *CMS CR* 2002/05

[80] Davatz G, Giolo-Nicollerat A and Zanetti M 2006 Systematics uncertainties of the top background in the $H \rightarrow WW$ channel *CMS Note* 2006/048

[81] Maltoni F and Stelzer T 2003 MadEvent: Automatic event generation with MadGraph *J. High. Energy Phys.* JHEP02(2003)027 (doi:10.1088/1126-6708/2003/02/027)

[82] Kauer N 2004 Top background extrapolation for $H \rightarrow WW$ searches at the LHC *Preprint* hep-ph/0404045

[83] Lowette S, D'Hondt J, Heyninck J and Vanlaer P 2006 Offline Calibration of b-Jet Identification Efficiencies *CMS Note* 2006/013

[84] Drollinger V *et al* 2005 Modeling the production of W pairs at the LHC *CMS Note* 2005/024

[85] Anastasiou C *et al* 2004 High precision QCD at hadron colliders: Electroweak gauge boson rapidity distribution at NNLO *Phys. Rev.* D **69**

[86] Belotelov I *et al* 2006 Simulation of misalignment scenarios for CMS tracking devices *CMS Note* 2006-008

[87] Cvetic M and Langacker P 1996 Implications of abelian extended gauge structures from string models *Phys. Rev.* D **54** 3570–3579 (*Preprint* hep-ph/9511378)

[88] Cvetic M and Langacker P 1996 New gauge bosons from string models *Mod. Phys. Lett.* A **11** 1247–1262 (*Preprint* hep-ph/9602424)
[89] Leike A 1999 The phenomenology of extra neutral gauge bosons *Phys. Rept.* **317** 143–250 (*Preprint* hep-ph/9805494)
[90] Hill C T and Simmons E H 2003 Strong dynamics and electroweak symmetry breaking *Phys. Rept.* **381** 235–402 (*Preprint* hep-ph/0203079)
[91] Han T, Logan H, McElrath B and Wang L-T 2003 Phenomenology of the little Higgs model *Phys. Rev.* D **67** 095004 (doi:10.1103/PhysRevD.67.095004)
[92] Cvetic M and Godfrey S 1996 Discovery and identification of extra gauge bosons *Electroweak symmetry breaking and new physics at the TeV scale* ed T L Barlow and S Dawson (World Scientific) 383–415 *Preprint* hep-ph/9504216
[93] Godfrey S 2001 Update of discovery limits for extra neutral gauge bosons at hadron colliders *Proceedings of Snowmass 2001* (Snowmass, Colorado: June–July) p P344 *Preprint* hep-ph/0201093
[94] Randall L and Sundrum R 1999 A large mass hierarchy from a small extra dimension *Phys. Rev. Lett.* **83** 3370–3373 (doi:10.1103/PhysRevLett.83.3370)
[95] Whalley M R, Bourilkov D and Group R C 2005 The Les Houches accord PDFs (LHAPDF) and LHAGLUE *Preprint* hep-ph/0508110
[96] Rosner J L 1987 Off peak lepton asymmetries from new Zs *Phys. Rev.* D **35** 2244
[97] Rosner J L 1996 Forward-Backward asymmetries in hadronically produced lepton pairs *Phys. Rev.* D **54** 1078–1082 (*Preprint* hep-ph/9512299)
[98] Mohapatra R N, Goldstein S A and Money D (eds) 2002 *Unification and supersymmetry: The Frontiers of quark - lepton physics* 3rd ed. (Springer-Verlag)
[99] Belotelov I *et al* 2006 Influence of misalignment scenarios on muon reconstruction *CMS Note* 2006-017
[100] Cousins R, Mumford J and Valuev S 2005 Detection of Z' gauge bosons in the dimuon decay mode in CMS *CMS Note* 2005-002
[101] Cousins R, Mumford J and Valuev V 2006 Detection of Z′ gauge bosons in the dimuon decay mode in CMS *CMS CR* 2004/050
[102] Bartsch V and Quast G 2005 Expected signal observability at future experiments *CMS Note* 2005-004
[103] Wilks S S 1938 The large-sample distribution of the likelihood ratio for testing composite hypotheses *Annals of Math. Stat.* **9** 60
[104] Baur U, Brein O, Hollik W, Schappacher C and Wackeroth D 2002 Electroweak radiative corrections to neutral-current Drell–Yan processes at hadron colliders *Phys. Rev.* D **65** 033007 (*Preprint* hep-ph/0108274)
[105] Zykunov V 2005 Weak radiative corrections to Drell–Yan process for large invariant mass of di-lepton pair *Preprint* hep-ph/0509315
[106] De Roeck A and Slabospitsky S Evaluation of the PDF Uncertainties (in CMS) available at http://cmsdoc.cern.ch/cms/PRS/gentools/www/pdfuncert/uncert.html
[107] Cerminara G private communication
[108] Langacker P, Robinett R W and Rosner J L 1984 New heavy gauge bosons in pp and $p\bar{p}$ collisions *Phys. Rev.* D **30** 1470
[109] Rosner J L 1989 Observability of charge asymmetries for lepton pairs produced in present collider experiments *Phys. Lett.* B **221** 85
[110] Cheng T P and Li L F 1988 *Gauge theory of elementary particle physics* (Oxford University Press)
[111] Cousins R, Mumford J and Valuev V 2005 Measurement of Forward-Backward Asymmetry of Simulated and Reconstructed $Z' \to \mu^+\mu^-$ Events in CMS *CMS Note* 2005-022
[112] Dittmar M 1997 Neutral current interference in the TeV region: The experimental sensitivity at the LHC *Phys. Rev.* D **55** 161–166 (*Preprint* hep-ex/9606002)
[113] Wulz C-E 1996 Z' at LHC *Proceedings of the 1996 DPF/DPB Summer Study on New Directions in High-Energy Physics* available at http://www.slac.stanford.edu/pubs/snowmass96
[114] Collins J C and Soper D E 1977 Angular distribution of dileptons in high-energy hadron collisions *Phys. Rev.* D **16** 2219
[115] Allanach B C, Odagiri K, Parker M A and Webber B R 2000 Searching for narrow graviton resonances with the ATLAS detector at the Large Hadron Collider *J. High. Energy Phys.* JHEP09(2000)019 (*Preprint* hep-ph/0006114)
[116] Cousins R, Mumford J, Tucker J and Valuev V 2005 Spin discrimination of new heavy resonances at the LHC *J. High. Energy Phys.* JHEP11(2005)046 (doi:10.1088/1126-6708/2005/11/046)
[117] Belotelov I *et al* 2006 Search for Randall-Sandrum Graviton Decay into Muon Pairs *CMS Note* 2006/104
[118] Esen S and Harris R M 2006 Jet Triggers and Dijet Mass *CMS Note* 2006/069

[119] CMS Collaboration, Acosta D *et al* 2006 CMS Physics Technical Design Report, Volume 1, Section 11.3: Monte Carlo Corrections *CERN/LHCC*, 2006-001 p 409

[120] CDF Collaboration, Abe F *et al* 1997 Search for new particles decaying to dijets at CDF *Phys. Rev.* D **55** 5263–5268 (doi:10.1103/PhysRevD.55.R5263)

[121] DØ Collaboration, Abazov V M *et al* 2004 search for new particles in the two-jet decay channel with the DØdetector *Phys. Rev.* D **69** 111101 (*Preprint* hep-ex/0308033)

[122] DØ Collaboration, Abbott B *et al* 1999 The dijet mass spectrum and a search for quark compositeness in $\bar{p}p$ collisions at $\sqrt{s} = 1.8$-TeV *Phys. Rev. Lett.* **82** 2457–2462 (doi:10.1103/PhysRevLett.82.2457)

[123] Eichten E, Lane K D and Peskin M E 1983 New tests for quark and lepton substructure *Phys. Rev. Lett.* **50** 811–814 (doi:10.1103/PhysRevLett.50.811)

[124] Lane K D 1996 Electroweak and flavor dynamics at hadron colliders *Preprint* hep-ph/9605257

[125] CDF Collaboration, Abe F *et al* 1996 Measurement of dijet angular distributions at CDF *Phys. Rev. Lett.* **77** 5336–5341 (doi:10.1103/PhysRevLett.77.5336)

[126] CMS Collaboration, Acosta D *et al* 2006 CMS Physics Technical Design Report, Volume 1, Section 11.6.1: Data-driven calibration strategy *CERN/LHCC*, 2006-001 p 421

[127] CMS Collaboration, Acosta D *et al* 2006 CMS Physics Technical Design Report, Volume 1, Section 11.6.2: Dijet Balancing *CERN/LHCC*, 2006-001 p 422

[128] CDF Collaboration, Acosta D *et al* 2005 Measurement of the lifetime difference between B_s mass eigenstates *Phys. Rev. Lett.* **94** 101803 (*Preprint* hep-ex/0412057) (doi:10.1103/PhysRevLett.94.101803)

[129] DØ Collaboration 2006 Measurement of the lifetime difference in the B_s system *DØ Conference note 5052*

[130] Belkov A and Shulga S 2004 Studies of angular correlations in the decays $B_s^0 \to J/\psi\phi$ by using the SIMUB generator *Comput. Phys. Commun.* **156** 221–240 (*Preprint* hep-ph/0310096) (doi:10.1016/S0010-4655(03)00465-X)

[131] Dighe A S, Dunietz I and Fleischer R 1999 Extracting CKM phases and $B_s - \bar{B}_s$ mixing parameters from angular distributions of non-leptonic B decays *Eur. Phys. J.* C **6** 647–662 (doi:10.1007/s100529800954)

[132] Dighe A S, Dunietz I, Lipkin H J and Rosner J L 1996 Angular distributions and lifetime differences in $B_s \to J/\psi\phi$ decays *Phys. Lett.* B **369** 144–150 (doi:10.1016/0370-2693(95)01523-X)

[133] CDF Collaboration, Abe F *et al* 1997 Production of J/ψ mesons from χ_c meson decays in $p\bar{p}$ collisions at $\sqrt{s} = 1.8$ TeV *Phys. Rev. Lett.* **79** 578–583 (doi:10.1103/PhysRevLett.79.578)

[134] Cano-Coloma B and Sanchis-Lozano M A 1997 Charmonia production in hadron colliders and the extraction of colour-octet matrix elements *Nucl. Phys.* B **508** 753–767 (*Preprint* hep-ph/9706270) (doi:10.1016/S0550-3213(97)00660-3)

[135] Cucciarelli S, Konecki M, Kotlinski D and Todorov T 2006 Track reconstruction, primary vertex finding and seed generation with the Pixel Detector *CMS Note* 2006/026

[136] Prokofiev K and Speer T 2005 A kinematic fit and a decay chain reconstruction library *CERN Yellow Report* http://doc.cern.ch/yellowrep/2005/2005-002/p411.pdf, 2005-002 Proc. of the 2004 Conference for Computing in High-Energy and Nuclear Physics (CHEP 04) (Interlaken, Switzerland, 2004) available at http://indico.cern.ch

[137] Dunietz I, Fleischer R and Nierste U 2001 In pursuit of new physics with B_s decays *Phys. Rev.* D **63** 114015 (doi:10.1103/PhysRevD.63.114015)

[138] BABAR Collaboration, Aubert B *et al* 2005 Ambiguity-free measurement of $\cos(2\beta)$: Time-integrated and time-dependent angular analyses of $B \to J/\psi K\pi$ *Phys. Rev.* D **71** 032005 (doi:10.1103/PhysRevD.71.032005)

[139] Dunietz I, Quinn H, Snyder A, Toki W and Lipkin H J 1991 How to extract CP-violating asymmetries from angular correlations *Phys. Rev.* D **43** 2193–2208 (doi:10.1103/PhysRevD.43.2193)

[140] Vanlaer P *et al* 2006 Impact of CMS Silicon Tracker Misalignment on Track and Vertex Reconstruction *CMS Note* 2006/029

[141] Speer T *et al* 2006 Vertex Fitting in the CMS Tracker *CMS Note* 2006/032

[142] Heinemeyer S, Hollik W and Weiglein G 2000 FeynHiggs: A program for the calculation of the masses of the neutral CP-even Higgs bosons in the MSSM *Comput. Phys. Commun.* **124** 76–89 (*Preprint* hep-ph/9812320)

[143] Heinemeyer S, Hollik W and Weiglein G 1999 The masses of the neutral CP-even Higgs bosons in the MSSM: accurate analysis at the two-loop level *Eur. Phys. J.* C **9** 343–366 (*Preprint* hep-ph/9812472)

[144] Degrassi G, Heinemeyer S, Hollik W, Slavich P and Weiglein G 2003 Towards high-precision predictions for the MSSM Higgs sector *Eur. Phys. J.* C **28** 133–143 (*Preprint* hep-ph/0212020)

[145] Lehti S 2006 Study of bbZ as a benchmark for MSSM bbH *CMS Note* 2006/099

[146] Bagliesi G, Dutta S, Gennai S, Kalinowski A, Konecki M, Kotlinski D, Moortgat F, Nikitenko A, Wendland L and Wakefield S 2006 Tau jet reconstruction and tagging at high level trigger and off-line *CMS Note* 2006/028
[147] Kunori S, Kinnunen R and Nikitenko A 2001 Missing transverse energy measurement with jet energy correctioins *CMS Note* 2001/040
[148] Pi H *et al* 2006 Measurement of missing transverse energy with the CMS detector at the LHC *CMS Note* 2006/035
[149] Kalinowski A and Nikitenko A 2006 Measurement of the τ-tagging efficiency using the Z$\rightarrow \tau\tau \rightarrow \mu$ + hadrons + X events *CMS Note* 2006/074
[150] Gennai S, Nikitenko A and Wendland L 2006 Search for MSSM Heavy Neutral Higgs Boson in $\tau\tau \rightarrow$ two Jet Decay Mode *CMS Note* 2006/126
[151] Rizzi A, Palla F and Segneri G 2006 Track impact parameter based b-tagging with CMS *CMS Note* 2006/019
[152] Kalinowski A, Konecki M and Kotlinski D 2006 Search for MSSM Heavy Neutral Higgs Boson in $\tau\tau \rightarrow \mu$ + jet Decay Mode *CMS Note* 2006/105
[153] Kalinowski A, Konecki M and Kotliński D 2006 Search for MSSM heavy neutral Higgs boson in $\tau + \tau \rightarrow \mu +$ jet decay mode *CMS Note* 2006/105
[154] Kinnunen R and Lehti S 2006 Search for the Heavy Neutral MSSM Higgs Bosons with the H/A$\rightarrow \tau\tau \rightarrow$ Electron plus Jet Decay Mode *CMS Note* 2006/075
[155] Jadach S, Was Z, Decker R and Kuhn J H 1993 The tau decay library TAUOLA: Version 2.4 *Comput. Phys. Commun.* **76** 361–380 (doi:10.1016/0010-4655(93)90061-G)
[156] Giolo-Nicollerat A-S 2006 *CMS Note*
[157] Weiser C 2006 A Combined Secondary Vertex Based B-Tagging Algorithm in CMS *CMS Note* 2006/014
[158] Haywood S *et al* 1999 Electroweak physics *Preprint* hep-ph/0003275 In 'Standard Model Physics (and more) at the LHC', Geneva, 1999
[159] Chakraborty D, Konigsberg J and Rainwater D L 2003 Review of top quark physics *Ann. Rev. Nucl. Part. Sci.* **53** 301–351 (*Preprint* hep-ph/0303092)
[160] Benedetti D, Cucciarelli S, Hill C, Incandela J, Koay S, Riccardi C, Santocchia A, Schmidt A, Torre P and Weiser C 2006 Search for $H \rightarrow bb$ in association with a tt pair at CMS *CMS Note* 2006/119
[161] Mangano M L, Moretti M, Piccinini F, Pittau R and Polosa A D 2003 ALPGEN, a generator for hard multiparton processes in hadronic collisions *J. High. Energy Phys.* JHEP07(2003)001 (*Preprint* hep-ph/0206293) (doi:10.1088/1126-6708/2003/07/001)
[162] Beenakker W, Dittmaier S, Kraemer M, Pluemper B, Spira M and Zerwas P 2003 NLO QCD corrections to $t\bar{t}H$ production in hadron collisions *Nucl. Phys.* B **653** 151–203 (*Preprint* hep-ph/0211352)
[163] Roberfroid V *et al* 2006 Validation and status of the HLT Steering Code and default menu *CMS IN* 2006/001
[164] James E, Maravin Y, Mulders M and Neumeister N 2006 Muon Identification in CMS *CMS Note* 2006/010
[165] Heister A, Kodolova O, Konoplianikov V, Petrushanko S, Rohlf J, Tully C and Ulyanov A 2006 Measurement of Jets with the CMS Detector at the LHC *CMS Note* 2006/036
[166] Santocchia A 2006 Optimization of Jet Reconstruction Settings and Parton-Level Correction for the ttH Channel *CMS Note* 2006/059
[167] D'Hondt J, Lowette S, Buchmuller O, Cucciarelli S, Schilling F P, Spiropulu M, Mehdiabadi S, Benedetti D and Pape L 2006 Fitting of Event Topologies with External Kinematic Constraints in CMS *CMS Note* 2006/023
[168] Mangano M private communication
[169] Wang X-N and Gyulassy M 1991 HIJING: A Monte Carlo model for multiple jet production in p p, p A and A A collisions *Phys. Rev.* D **44** 3501–3516
[170] Bedjidian M *et al* 2004 Hard probes in heavy ion collisions at the LHC: heavy flavour physics *Preprint* hep-ph/0311048
[171] Eskola K J, Kolhinen V J and Salgado C A 1999 The scale dependent nuclear effects in parton distributions for practical applications *Eur. Phys. J.* C **9** 61–68 (*Preprint* hep-ph/9807297)
[172] Kodolova O, Bedjidian M and Petrouchanko S 1999 Dimuon reconstruction in heavy ion collisions using a detailed description of CMS geometry *CMS Note* 1999-004
[173] Bedjidian M and Kodolova O 2006 Quarkonia measurements in heavy-ion collisions in CMS *CMS Note* 2006/089
[174] Sterman G and Weinberg S 1977 Jets from Quantum Chromodynamics *Phys. Rev. Lett.* **39** 1436
[175] JADE Collaboration, Bartel W *et al* 1986 Experimental studies on multi-jet production in e^+e^+ annihilation at petra energies *Z. Phys.* C **33** 23
[176] JADE Bethke S *et al* 1988 Experimental investigation of the energy dependence of the strong coupling strength *Phys. Lett.* B **213** 235

[177] Catani S, Dokshitzer Y L, Olsson M, Turnock G and Webber B R 1991 New clustering algorithm for multi-jet cross-sections in e^+e^+ annihilation *Phys. Lett.* B **269** 432–438

[178] CDF Run II Collaboration, Abulencia A *et al* 2005 Measurement of the inclusive jet cross section in $p\bar{p}$ interactions at $\sqrt{s} = 1.96$ TeV using a cone-based jet algorithm *Preprint* hep-ex/0512020

[179] DØ, Collaboration, Strohmer R 2006 Inclusive jet cross-sections and dijet azimuthal decorrelations with DØ*PoS* HEP **2005** 051 (*Preprint* hep-ex/0601016)

[180] Butterworth J, Couchman J, Cox B and Waugh B 2003 KtJet: A C^{++} implementation of the K(T) clustering algorithm *Comput. Phys. Commun.* **153** 85–96 (*Preprint* hep-ph/0210022)

[181] ed U Baur, R K Ellis and D Zeppenfeld 2000 *QCD and Weak Boson Physics in Run II* (Batavia, IL, USA: FERMILAB) Prepared for Physics at Run II: QCD and Weak Boson Physics Workshop: Final General Meeting, Batavia, Illinois, 4–6 November, 1999

[182] Ellis S D, Huston J and Tonnesmann M 2001 On building better cone jet algorithms *eConf* C 010630 P513 (*Preprint* hep-ph/0111434)

[183] Wobisch M private communication

[184] Sjostrand T 1994 High-energy physics event generation with PYTHIA 5.7 and JETSET 7.4 *Comput. Phys. Commun.* **82** 74–90

[185] Nagy Z 2002 Three-jet cross sections in hadron hadron collisions at next-to-leading order *Phys. Rev. Lett.* **88** 122003 (*Preprint* hep-ph/0110315)

[186] Kluge T, Rabbertz K and Wobisch M fast NLO—fast pQCD calculations for hadron-induced processes To be published, available at http://hepforge.cedar.ac.uk/fastnlo

[187] Moretti S, Nolten M R and Ross D A 2005 Weak corrections and high E(T) jets at Tevatron *Preprint* hep-ph/0503152

[188] DØ Collaboration, Abazov V M *et al* 2002 The inclusive jet cross-section in p anti-p collisions at s**(1/2)=1.8-TeV using the k(T) algorithm *Phys. Lett.* B **525** 211–218 (*Preprint* hep-ex/0109041)

[189] DØ Collaboration, Abbott B *et al* 2001 High-p_T jets in $\bar{p}p$ collisions at $\sqrt{s} = 630$ GeV and 1800 GeV *Phys. Rev.* D **64** 032003 (doi:10.1103/PhysRevD.64.032003)

[190] CDF Collaboration, Affolder A A *et al* 2002 Charged jet evolution and the underlying event in proton anti-proton collisions at 1.8-TeV *Phys. Rev.* D **65** 092002

[191] CDF Collaboration, Acosta D *et al* 2004 The underlying event in hard interactions at the Tevatron anti-p p collider *Phys. Rev.* D **70** 072002 (*Preprint* hep-ex/0404004)

[192] Sjostrand T and van Zijl M 1987 A multiple interaction model for the event structure in hadron collisions *Phys. Rev.* D **36** 2019

[193] Butterworth J, Forshaw J R and Seymour M 1996 Multiparton interactions in photoproduction at HERA *Z. Phys.* C **72** 637–646 (*Preprint* hep-ph/9601371)

[194] Gleisberg T *et al* 2004 SHERPA 1.alpha, a proof-of-concept version *J. High. Energy Phys.* JHEP02(2004)056 (*Preprint* hep-ph/0311263)

[195] Bopp F W, Engel R and Ranft J 1998 Rapidity gaps and the PHOJET Monte Carlo *Preprint* hep-ph/9803437

[196] Corcella G *et al* 2001 HERWIG 6: An event generator for hadron emission reactions with interfering gluons (including supersymmetric processes) *J. High. Energy Phys.* JHEP01(2001)010 (*Preprint* hep-ph/0011363) (doi:10.1088/1126-6708/2001/01/010)

[197] Buttar C M, Clements D, Dawson I and Moraes A 2004 Simulations of minimum bias events and the underlying event, MC tuning and predictions for the LHC *Acta Phys. Polon.* B **35** 433–441

[198] CDF Collaboration, Field R 2005 Min-bias and the underlying event in Run 2 at CDF *Acta Phys. Polon.* B **36** 167–178

[199] Acosta D *et al* 2006 The underlying event at the LHC *CMS Note* 2006/067

[200] CDF Collaboration, Abe F *et al* 1991 Measurement of the Z-boson p_T distribution in $\bar{p}p$ collisions at $\sqrt{s} = 1.8$ TeV *Phys. Rev. Lett.* **67** 2937–2941 (doi:10.1103/PhysRevLett.67.2937)

[201] Bartalini P, Chierici R and De Roeck A 2005 Guidelines for the estimation of theoretical uncertainties at the LHC *CMS Note* 2005/013

[202] Adam W, Mangano B, Speer T and Todorov T 2006 Track reconstruction in the CMS tracker *CMS Note* 2006/041

[203] Andreev V P, Cline D.B and Otwinowski S 2006 Inclusive b quark production *CMS Note* 2006/120

[204] CDF Collaboration, Abe F *et al* 1993 Measurement of the bottom quark production cross section using semileptonic decay electrons in $p\bar{p}$ collisions at $\sqrt{s} = 1.8$ TeV *Phys. Rev. Lett.* **71** 500 (doi:10.1103/PhysRevLett.71.500)

[205] CDF Collaboration, Abe F *et al* 1994 Measurement of the B meson and b quark cross sections at $\sqrt{s} = 1.8$ TeV using the exclusive decay $B^0 \to J/\psi K^*(892)^0$ *Phys. Rev.* D **50** 4252 (doi:10.1103/PhysRevD.50.4252)

[206] CDF Collaboration, Abe F *et al* 1995 Measurement of the B Meson Differential Cross Section $d\sigma/dp_{\mathrm{T}}$ in $p\bar{p}$ Collisions at $\sqrt{s} = 1.8$ TeV *Phys. Rev. Lett.* **75** 1451 (doi:10.1103/PhysRevLett.75.1451)
[207] CDF Collaboration Abe F *et al* 2002 Measurement of the B^+ total cross section and B^+ differential cross section $d\sigma/dp_{\mathrm{T}}$ in $p\bar{p}$ collisions at $\sqrt{s} = 1.8$ TeV *Phys. Rev.* D **65** 052005 (doi:10.1103/PhysRevD.65.052005)
[208] CDF Collaboration, Abe F *et al* 2002 Measurement of the ratio of b quark production cross sections in $\bar{p}p$ collisions at $\sqrt{s} = 630$ GeV and $\sqrt{s} = 1800$ GeV *Phys. Rev.* D **66** 032002 (doi:10.1103/PhysRevD.66.032002)
[209] DØ Collaboration, Abachi S *et al* 1995 Inclusive μ and b-quark production cross-sections in $p\bar{p}$ collisions at $\sqrt{s} = 1.8$ TeV *Phys. Rev. Lett.* **74** 3548 (doi:10.1103/PhysRevLett.74.3548)
[210] DØ Collaboration, Abbott B *et al* 2000 The $b\bar{b}$ production cross section and angular correlations in $p\bar{p}$ collisions at $\sqrt{s} = 1.8$ TeV *Phys. Lett.* B **487** 264 (doi:10.1016/S0370-2693(00)00844-3)
[211] DØ Collaboration, Abbott B *et al* 2000 Cross section for b-Jet production in $\bar{p}p$ collisions at $\sqrt{s} = 1.8$ TeV *Phys. Rev. Lett.* **85** 5068 (doi:10.1103/PhysRevLett.85.5068)
[212] H1 Collaboration, Adloff C *et al* 1999 Measurement of open beauty production at HERA *Phys. Lett.* B **467** 156 (doi:10.1016/S0370-2693(99)01099-0)
[213] H1 Collaboration, Adloff C *et al* 2001 Erratum *Phys. Lett.* B **518** 331
[214] ZEUS Collaboration, Breitweg J *et al* 2001 Measurement of open beauty production in photoproduction at HERA *Eur. Phys. J.* C **18** 625–637 (doi:10.1007/s100520100571)
[215] H1 Collaboration, Aktas A *et al* 2005 Measurement of F2(c anti-c) and F2(b anti-b) at high Q**2 using the H1 vertex detector at HERA *Eur. Phys. J.* C **40** 349–359 (*Preprint* hep-ex/0411046)
[216] ZEUS Collaboration, Chekanov S *et al* 2004 Bottom photoproduction measured using decays into muons in dijet events in e p collisions at s**(1/2)=318 GeV *Phys. Rev.* D **70** 012008
[217] ZEUS Collaboration, Chekanov S *et al* 2004 Measurement of beauty production in deep inelastic scattering at HERA *Phys. Lett.* B **599** 173–189 (*Preprint* hep-ex/0405069)
[218] H1 Collaboration, Aktas A *et al* 2005 Measurement of beauty production at HERA using events with muons and jets *Eur. Phys. J.* C **41** 453–467 (*Preprint* hep-ex/0502010)
[219] L3 Collaboration, Acciarri M *et al* 2001 Measurements of the cross sections for open charm and beauty production in $\gamma\gamma$ collisions at $\sqrt{s} = 189$ GeV–202 GeV *Phys. Lett.* B **503** 10 (doi:10.1016/S0370-2693(01)00134-4)
[220] L3 Collaboration, Achard P *et al* 2005 Measurement of the cross section for open-beauty production in photon photon collisions at LEP *Phys. Lett.* B **619** 71
[221] Nason P, Dawson S and Ellis R K 1988 The total cross-section for the production of heavy quarks in hadronic collisions *Nucl. Phys.* B **303** 607
[222] Nason P, Dawson S and Ellis R K 1989 The one particle inclusive differential cross-section for heavy quark production in hadronic collisions *Nucl. Phys.* B **327** 49–92
[223] Beenakker W, Van Neerven W L, Meng R, Schuler G A and Smith J 1991 QCD corrections to heavy quark production in hadron-hadron collisions *Nucl. Phys.* B **351** 507–560 (doi:10.1016/S0550-3213(05)80032-X)
[224] Cacciari M, Frixione S, Mangano M L, Nason P and Ridolfi G 2004 QCD analysis of first b cross section data at 1.96-TeV *J. High. Energy Phys.* JHEP07(2004)033 (doi:10.1088/1126-6708/2004/07/033)
[225] Mangano M L 2005 The saga of bottom production in proton antiproton collisions *AIP Conf. Proc.* **753** 247–260 (*Preprint* hep-ph/0411020)
[226] Frixione S 2004 Bottom production *Preprint* hep-ph/0408317
[227] Weinberg S 1990 Unitarity vonstraints on CP nonconservation in Higgs exchange *Phys. Rev.* D **42** 860–866
[228] Lavoura L 1993 Maximal CP violation via Higgs boson exchange *Int. J. Mod. Phys.* A **8** 375–390
[229] Jenkins E, Luke M E, Manohar A V and Savage M J 1993 Semileptonic B_c decay and heavy quark spin symmetry *Nucl. Phys.* B **390** 463–473 (*Preprint* hep-ph/9204238)
[230] Kiselev V V, Kovalsky A E and Likhoded A K 2000 B_c decays and lifetime in QCD sum rules *Nucl. Phys.* B **585** 353–382 (doi:10.1016/S0550-3213(00)00386-2)
[231] Wu X-G, Chang C-H, Chen Y-Q and Fang Z-Y 2003 The meson B_c annihilation to leptons and inclusive light hadrons *Phys. Rev.* D **67** 094001 (doi:10.1103/PhysRevD.67.094001)
[232] Chang C-H and Chen Y-Q 1992 The Production of B_c or $\bar{B}_c$ meson associated with two heavy quark jets in Z^0 boson decay *Phys. Rev.* D **46** 3845–3855 (doi:10.1103/PhysRevD.46.3845)
[233] Chang C-H and Chen Y-Q 1993 Hadronic production of the B_c meson at TeV energies *Phys. Rev.* D **48** 4086 (doi:10.1103/PhysRevD.48.4086)
[234] Chang C-H, Chen Y-Q, Han G-P and Jiang H-T 1995 On hadronic production of the B_c meson *Phys. Lett.* B **364** 78 (doi:10.1016/0370-2693(95)01235-4)

[235] Chang C-H, Chen Y-Q and Oakes R J 1996 Comparative study of the hadronic production of B_c mesons *Phys. Rev.* D **54** 4344 (doi:10.1103/PhysRevD.54.4344)
[236] Chang C-H and Wu X-G 2004 Uncertainties in estimating hadronic production of the meson B/c and comparisons between TEVATRON and LHC *Eur. Phys. J.* C **38** 267–276 (doi:10.1140/epjc/s2004-02015-0)
[237] CDF Collaboration, Abe F *et al* 1998 Observation of the B_c meson in $p\bar{p}$ collisions at $\sqrt{s} = 1.8$ TeV *Phys. Rev. Lett.* **81** 2432–2437 (doi:10.1103/PhysRevLett.81.2432)
[238] CDF Collaboration, Acosta D *et al* 2006 Evidence for the exclusive decay $B_c^{\pm} \to J/\psi\pi^{\pm}$ and measurement of the mass of the B_c meson *Phys. Rev. Lett.* **96** 082002 (doi:10.1103/PhysRevLett.96.082002)
[239] Berezhnoi A V, Kiselev V V, Likhoded A K and Onishchenko A I 1997 B_c meson at LHC *Phys. Atom. Nucl.* **60** 1729–1740 (*Preprint* hep-ph/9703341)
[240] Gouz I P, Kiselev V V, Likhoded A K, Romanovsky V I and Yushchenko O P 2004 Prospects for the B_c studies at LHCb *Phys. Atom. Nucl.* **67** 1559–1570 (doi:10.1134/1.1788046)
[241] Chang C-H and Chen Y-Q 1994 Decays of the B_c meson *Phys. Rev.* D **49** 3399–3411 (doi:10.1103/PhysRevD.49.3399)
[242] Kwong W-K and Rosner J L 1991 Masses of new particles containing b quarks *Phys. Rev.* D **44** 212–219 (doi:10.1103/PhysRevD.44.212)
[243] Eichten E J and Quigg C 1994 Mesons with beauty and charm: Spectroscopy *Phys. Rev.* D **49** 5845–5856 (*Preprint* hep-ph/9402210)
[244] Chen Y-Q and Kuang Y-P 1992 Improved QCD motivated heavy quark potentials with explicit $\Lambda_{\overline{MS}}$ dependence *Phys. Rev.* D **46** 1165–1171 (doi:10.1103/PhysRevD.46.1165)
[245] Chen G, Meng X and Tao J 2006 Feasibility to study the B_c meson at CMS *CMS Note* 2006/118
[246] Sjostrand T, Lonnblad L, Mrenna S and Skands P 2003 PYTHIA 6.3: Physics and manual *Preprint* hep-ph/0308153
[247] Grothe M *et al* 2006 Triggering on Forward Physics *CMS Note* 2006/054. Also available as TOTEM NOTE 2006-01
[248] CMS/TOTEM Collaboration, CMS/TOTEM document on diffractive and forward physics, in preparation 2006
[249] UA8 Collaboration, Bonino R *et al* 1988 Evidence for transverse jets in high mass diffraction *Phys. Lett.* B **211** 239
[250] Arneodo M and Diehl M 2005 Diffraction for non-believers *Preprint* hep-ph/0511047
[251] UA8 Collaboration, Brandt A *et al* 1998 Measurements of single diffraction at $\sqrt{s} = 630$ GeV: Evidence for a non-linear $\alpha(t)$ of the pomeron *Nucl. Phys.* B **514** 3–44 (doi:10.1016/S0550-3213(97)00813-4)
[252] Erhan S and Schlein P E 2000 Inelastic diffraction data and the Pomeron trajectory *Phys. Lett.* B **481** 177–186 (doi:10.1016/S0370-2693(00)00467-6)
[253] Goulianos K 2005 Twenty years of diffraction at the TevatronPresented at 11th international conference on elastic and diffractive scattering: towards high energy frontiers: the 20th anniversary of the blois workshops *Preprint* hep-ph/0510035
[254] FP420 Collaboration, Albrow M G *et al* 2005 FP420: A proposal to investigate the feasibility of installing proton tagging detectors in the 420 m region of the LHC *CERN/LHCC*, 2005-025
[255] CDF Collaboration, Affolder A A *et al* 2000 Diffractive dijets with a leading antiproton in anti-p p collisions at $\sqrt{s}$ = 1800 GeV *Phys. Rev. Lett.* **84** 5043–5048
[256] De Roeck A, Khoze V A, Martin A D, Orava R and Ryskin M G 2002 Ways to detect a light Higgs boson at the LHC *Eur. Phys. J.* C **25** 391–403 (*Preprint* hep-ph/0207042)
[257] Khoze V, Martin A and Ryskin M 2002 Prospects for new physics observations in diffractive processes at the LHC and Tevatron *Eur. Phys. J.* C **23** 311–327 (*Preprint* hep-ph/0111078)
[258] Kisselev A, Petrov V and Ryutin R 2005 5-dimensional quantum gravity effects in exclusive double diffractive events *Phys. Lett.* B **630** 100–107 (doi:10.1016/j.physletb.2005.09.059)
[259] Monk J and Pilkington A 2005 ExHuME: a Monte Carlo event generator for exclusive diffraction *Preprint* hep-ph/0502077
[260] Boonekamp M *et al* 2005 Monte-Carlo generators for central exclusive diffraction *Proceedings of the HERA-LHC Workshop (CERN/DESY, January, 2005)* available at http://www.desy.de/ heralhc/proceedings/wg4montecarlo.pdf
[261] Ryutin R 2004 EDDE Monte Carlo event generator *Preprint* hep-ph/0409180
[262] Kaidalov A, Khoze V A, Martin A D and Ryskin M G 2003 Central exclusive diffractive production as a spin parity analyser: From hadrons to Higgs *Eur. Phys. J.* C **31** 387–396 (*Preprint* hep-ph/0307064)
[263] Carena M, Heinemeyer S, Wagner C E M and Weiglein G 2006 MSSM Higgs boson searches at the Tevatron and the LHC: Impact of different benchmark scenarios *Eur. Phys. J.* C **45** 797–814 (*Preprint* hep-ph/0511023)

[264] Ellis J R, Lee J S and Pilaftsis A 2005 Diffraction as a CP and lineshape analyzer for MSSM Higgs bosons at the LHC *Phys. Rev.* D **71** 075007 (*Preprint* hep-ph/0502251)
[265] Petrov A, Ryutin R, Sobol A and Guillaud J-P 2005 Azimuthal angular distributions in EDDE as spin-parity analyser and glueball filter for LHC *J. High. Energy Phys.* JHEP06(2005)007 (*Preprint* hep-ph/0409118)
[266] Piotrzkowski K 2001 Tagging two-photon production at the LHC *Phys. Rev.* D **63** 071502 (*Preprint* hep-ex/0009065)
[267] Budnev V, Ginzburg I, Meledin G and Serbo V 1974 The Two photon particle production mechanism. physical problems. applications. equivalent photon approximation *Phys. Rept.* **15** 181–281 (doi:10.1016/0370-1573(75)90009-5)
[268] Khoze V, Martin A and Ryskin M 2002 Photon-exchange processes at hadron colliders as a probe of the dynamics of diffraction *Eur. Phys. J.* C **24** 459–468 (*Preprint* hep-ph/0201301) (doi:10.1007/s10052-002-0964-4)
[269] White A R 2005 The physics of a sextet quark sector *Phys. Rev.* D **72** 036007 (*Preprint* hep-ph/0412062)
[270] Piotrzkowski K 2002 High energy two-photon interactions at the LHC *Preprint* hep-ex/0201027
[271] Kalmykov N N, Ostapchenko S S and Pavlov A I 1997 Quark-gluon string model and EAS simulation problems at ultra-high energies *Nucl. Phys. Proc. Suppl.* B **52** 17–28
[272] Engel R, Gaisser T K, Stanev T and Lipari P 1999 Air shower calculations with the new version of SIBYLL *Prepared for 26th International Cosmic Ray Conference* (ICRC 99) (Salt Lake City, Utah, 17–25 August 1999)
[273] Roesler S, Engel R and Ranft J The Event generator DPMJET-III at cosmic ray energies Prepared for 27th International Cosmic Ray Conference (ICRC 2001) (Hamburg, Germany, 7-15 Aug 2001)
[274] Karsch Frithjof 2002 Lattice QCD at high temperature and density *Lect. Notes Phys.* **583** 209–249 (*Preprint* hep-lat/0106019)
[275] Iancu Edmond and Venugopalan Raju 2003 The color glass condensate and high energy scattering in QCD *Preprint* hep-ph/0303204
[276] Schwarz Dominik J 2003 The first second of the universe *Annalen Phys.* **12** 220–270 (*Preprint* astro-ph/0303574)
[277] Starinets Andrei O 2005 Transport coefficients of strongly coupled gauge theories: Insights from string theory *Preprint* nucl-th/0511073
[278] Bonciani Roberto, Catani Stefano, Mangano Michelangelo L and Nason Paolo 1998 NLL resummation of the heavy-quark hadroproduction cross-section *Nucl. Phys.* B **529** 424–450 (*Preprint* hep-ph/9801375)
[279] Davids M *et al* 2006 Measurement of top-pair cross section and top-quark mass in the di-lepton and full-hadronic channels with CMS *CMS Note* http://cms.cern.ch/iCMS/jsp/openfile.jsp?tp=draft&files=2907_ttbar.pdf2006/077
[280] Gennai S *et al* 2006 Tau jet reconstruction and tagging at High Level Trigger and off-line *CMS Note* http://cms.cern.ch/iCMS/jsp/openfile.jsp?type=NOTE&year=2006&files=NOTE2006_028.pdf2006/028
[281] D'Hondt J, Heyninck J and Lowette S 2006 Measurement of the cross section of single leptonic $t\bar{t}$ events *CMS Note* http://cms.cern.ch/iCMS/jsp/openfile.jsp?type=NOTE&year=2006&files=NOTE2006_064.pdf2006/064
[282] Buttar C *et al* 2006 Les Houches Physics at TeV Colliders 2005, Standard Model and Higgs working group: Summary report *Preprint* hep-ph/0604120
[283] Konoplianikov V, Kodolova O and Ulyanov A 2006 Jet calibration using γ+jet events in the CMS Detector *CMS Note* http://cms.cern.ch/iCMS/jsp/openfile.jsp?type=NOTE&year=2006&files=NOTE2006_042.pdf2006/042
[284] D'Hondt J *et al* 2006 Electron and muon reconstruction in single leptonic $t\bar{t}$ events *CMS Note* http://cms.cern.ch/iCMS/jsp/openfile.jsp?type=NOTE&year=2006&files=NOTE2006_024.pdf2006/024
[285] CMS Collaboration, Acosta D *et al* 2006 CMS Coll. Physics TDR Vol. I, Section 12.2.8 *CERN/LHCC* 2006-001
[286] Lowette S, D'Hondt J, Heyninck J and Vanlaer P 2006 Offline calibration of b-jet identification efficiency, *CERN-CMS-NOTE* -2006-013
[287] D'Hondt J, Lowette S, Heyninck J and Kasselmann S 2006 Light quark jet energy scale calibration using the W mass constraint in single-leptonic $t\bar{t}$ events *CERN-CMS-NOTE* -2006-025
[288] The CDF Collaboration, Acosta D *et al* 2005 Measurement of the $t\bar{t}$ cross section in $p\bar{p}$ collisions at $\sqrt{s}$=1.96 TeV using kinematic characteristics of lepton plus jets events *Phys. Rev.* D **71** 072005 (doi:10.1103/PhysRevD.71.072005)
[289] DØ Collaboration, Abazov V M *et al* 2005 Measurement of the $t\bar{t}$ cross section in $p\bar{p}$ collisions at $\sqrt{s}$=1.96 TeV using kinematic characteristics of lepton plus jets events *Phys. Lett.* B **626** 55 (doi:10.1016/j.physletb.2005.08.105)

[290] Vos M and Palla F 2006 B-tagging in the High Level Trigger *CMS Note* http://cmsdoc.cern.ch/documents/06/note06_030.pdf2006-030
[291] CDF and DØ, Wicke D 2005 Top pair production cross-section measurement in the all-hadronic channel at CDF and DØCollaboration *Int. J. Mod. Phys. A* **20** 3183–3186 (*Preprint* hep-ex/0411009) (doi:10.1142/S0217751X05026091)
[292] D'Hondt J, Heyninck J and Lowette S 2006 Top Quark mass measurement in single-leptonic $t\bar{t}$ events *CMS Note* http://cms.cern.ch/iCMS/jsp/openfile.jsp?type=NOTE&year=2006&files=NOTE2006_066.pdf2006/066
[293] CDF Collaboration, Abe F *et al* 1997 First Observation of the All-Hadronic Decay of $t\bar{t}$ pairs *Phys. Rev. Lett.* **79** 1992–1997 (doi:10.1103/PhysRevLett.79.1992)
[294] Tevatron Electroweak Working Group Collaboration 2006 Combination of CDF and DØresults on the mass of the top quark *Preprint* hep-ex/0603039
[295] Kharchilava Avto 2000 Top mass determination in leptonic final states with J/psi *Phys. Lett.* **B476** 73–78 (*Preprint* hep-ph/9912320)
[296] Grenier P 2001 *ATLAS Physics Note* 2001-023
[297] Chierici R and Dierlamm A 2006 Determination of the top mass in exclusive JPsi decays *CMS Note* http://cmsdoc.cern.ch/documents/06/note06_058.pdf2006-058
[298] Tevatron Electroweak Working Group Collaboration 2006 Combination of CDF and DØ results on the mass of the top quark *Preprint* hep-ex/0603039
[299] Hill C S, Incandela J R and Lamb J M 2005 A method for measurement of the top quark mass using the mean decay length of *b* hadrons in *t* anti-*t* events *Phys. Rev.* D **71** 054029 (*Preprint* hep-ex/0501043)
[300] Borjanovic I *et al* 2005 Investigation of top mass measurements with the ATLAS detector at LHC *Eur. Phys. J.* **C39S2** 63–90 (*Preprint* hep-ex/0403021)
[301] Lyons Louis, Gibaut Duncan and Clifford Peter 1988 How to combine correlated estimates of a single physical quantity *Nucl. Instrum. Methods* A **270** 110
[302] Valassi A 2003 Combining correlated measurements of several different physical quantities *Nucl. Instrum. Methods* A **500** 391–405
[303] Mahlon G and Parke S 1996 Angular correlation in top quark pair production and decay at hadron collider *Phys. Rev.* D **53** 4886–4896 (*Preprint* hep-ph/9512264)
[304] Stelzer T and Willenbrock S 1996 Spin correlation in top-quark production at hadron collider *Phys. Lett.* B **374** 169–172 (*Preprint* hep-ph/9512292)
[305] Brandenburg A 1996 Spin-spin correlations of top quark pairs at Hadron colliders *Phys. Lett.* B **387** 626–632 (*Preprint* hep-ph/9606379)
[306] Baarmand M, Mermerkaya H and Vodopiyanov I 2006 Measurement of spin correlation in top quark pair production in semi-leptonic final state *CMS Note* 2006/111
[307] Tait T 2000 The tW^- mode of single top production *Phys. Rev.* D **61** 034001 (*Preprint* hep-ph/9909352) (doi:10.1103/PhysRevD.61.034001)
[308] Belyaev A and Boos E 2001 Single top quark t W + X production at the LHC: A closer look *Phys. Rev.* D **63** 034012 (*Preprint* hep-ph/0003260)
[309] Zhu S 2002 Next-to-leading order QCD corrections to b g $\rightarrow$ t W- at the CERN Large Hadron Collider *Phys. Lett.* B **524** 283–288
[310] Boos E, Bunichev V, Dudko L, Savrin V and Sherstnev A 2005 A simulation method of the electroweak top quark production events in the NLO approximation: a Monte-Carlo generator 'singletop'abstract available at http://www.npi.msu.su/eng/science.php3?sec=preprint&ref_pp=1262
[311] CMS Collaboration, Acosta D *et al* 2006 CMS Physics Technical Design Report, Volume 1, Section 9.1.2: Global muon reconstruction *CERN/LHCC*, 2006-001 p 333
[312] CMS Collaboration, Acosta D *et al* 2006 CMS Physics Technical Design Report, Volume 1, Section 9.3: Muon identification *CERN/LHCC*, 2006-001 p 351
[313] CMS Collaboration, Acosta D *et al* 2006 CMS Physics Technical Design Report, Volume 1, Section 10.4: Electron reconstruction and selection *CERN/LHCC*, 2006-001 p 390
[314] CMS Collaboration, Acosta D *et al* 2006 CMS Physics Technical Design Report, Volume 1, Section 11.2.1: Iterative cone *CERN/LHCC*, 2006-001 p 408
[315] CMS Collaboration, Acosta D *et al* 2006 CMS Physics Technical Design Report, Volume 1, Section 11.6.3: γ+jet events *CERN/LHCC*, 2006-001 423
[316] CMS Collaboration, Acosta D *et al* 2006 CMS Physics Technical Design Report, Volume 1, Section 12.2: b-tagging tools *CERN/LHCC*, 2006-001 p 461
[317] Abramov V *et al* 2006 Selection of single top events with the CMS detector at LHC *CMS Note* 2006/084
[318] Yeh P *et al* 2006 Search for W-associated Production of Single Top Quarks in CMS *CMS Note* 2006/086

[319] Campbell J, Ellis R K and Rainwater D L 2003 Next-to-leading order QCD predictions for W + 2jet and Z + 2jet production at the CERN LHC *Phys. Rev.* D **68** 094021 (doi:10.1103/PhysRevD.68.094021)
[320] CMS Collaboration, Acosta D *et al* 2006 CMS Coll. Physics Technical Design Physics, Volume I, Section 11.6.5 *CERN/LHCC*, 2006-001
[321] CMS Collaboration, Acosta D *et al* 2006 CMS Physics Technical Design Physics, Volume I, Section 8.5: Sources of systematic effects *CERN/LHCC*, 2006-001 p 229
[322] Fisher R A 1936 The use of multiple measurements in taxonomic problems *Annuals of Eugenics* **7** 179–188
[323] Mele B, Petrarca S and Soddu A 1998 A new evaluation of the $t \to cH$ decay width in the standard model *Phys. Lett.* B **435** 401–406 (*Preprint* hep-ph/9805498)
[324] Huang C-S, Wu X-H and Zhu S-H 1999 Top-charm associated production at high energy $e^+ e^-$ colliders in standard model *Phys. Lett.* B **452** 143–149 (*Preprint* hep-ph/9901369)
[325] de Divitiis G M, Petronzio R and Silvestrini L 1997 Flavour changing top decays in supersymmetric extensions of the standard model *Nucl. Phys.* B **504** 45–60 (*Preprint* hep-ph/9704244)
[326] Guasch J and Sola J 1999 FCNC top quark decays: A door to SUSY physics in high luminosity colliders? *Nucl. Phys.* B **562** 3–28 (*Preprint* hep-ph/9906268)
[327] Eilam G, Gemintern A, Han T, Yang J M and Zhang X 2001 Top quark rare decay $t \to ch$ in R-parity-violating SUSY *Phys. Lett.* B **510** 227–235 (*Preprint* hep-ph/0102037) (doi:10.1016/S0370-2693(01)00598-6)
[328] Li C S, Zhang X-M and Zhu S H 1999 SUSY-QCD effect on top charm associated production at linear collider *Phys. Rev.* D **60** 077702 (*Preprint* hep-ph/9904273)
[329] Bejar S, Guasch J and Sola J 2001 FCNC top quark decays beyond the standard model *Preprint* hep-ph/0101294
[330] Diaz R A, Martinez R and Alexis Rodriguez J 2001 The rare decay $t \to c\gamma$ in the general 2HDM type III *Preprint* hep-ph/0103307
[331] Han T and Hewett J L 1999 Top charm associated production in high energy $e^+ e^-$ collisions *Phys. Rev.* D **60** 074015 (*Preprint* hep-ph/9811237)
[332] del Aguila F, Aguilar-Saavedra J A and Miquel R 1999 Constraints on top couplings in models with exotic quarks *Phys. Rev. Lett.* **82** 1628–1631 (*Preprint* hep-ph/9808400)
[333] Aguilar-Saavedra J A and Nobre B M 2003 Rare top decays $t \to c\gamma$, $t \to cg$ and CKM unitarity *Phys. Lett.* B **553** 251–260 (*Preprint* hep-ph/0210360)
[334] CDF and DØ Collaboration, Paulini M 1996 Heavy flavor physics from top to bottom *Preprint* hep-ex/9701019
[335] CDF Collaboration, Abe F *et al* 1998 Search for flavor-changing neutral current decays of the top quark in $p\bar{p}$ collisions at $\sqrt{s} = 1.8$ TeV *Phys. Rev. Lett.* **80** 2525–2530 (doi:10.1103/PhysRevLett.80.2525)
[336] Heinson A 1996 Future top physics at the Tevatron and LHC *Preprint* hep-ex/9605010
[337] Aguilar-Saavedra J A and Branco G C 2000 Probing top flavour-changing neutral scalar couplings at the CERN LHC *Phys. Lett.* B **495** 347–356 (*Preprint* hep-ph/0004190)
[338] Aguilar-Saavedra J A 2001 Top flavour-changing neutral coupling signals at a linear collider *Phys. Lett.* B **502** 115–124 (*Preprint* hep-ph/0012305)
[339] Aguilar-Saavedra J A and Riemann T 2001 Probing top flavor-changing neutral couplings at TESLA *Preprint* hep-ph/0102197
[340] Karafasoulis K *et al* 2006 Study of flavour changing neutral currents in top quark decays with the CMS detector *CMS Note* 2006/093
[341] Dissertori G *et al* 2006 How accurately can we count the number of $pp \to ZX$ and $pp \to WX$ events using decays to electrons *CMS Note* 2006/124
[342] Alcaraz J 2006 Measurement of Z $\to \mu^+\mu^-$ and W $\to \mu\nu$ rates in CMS *CMS Note* 2006/082
[343] Frixione S and Webber B R 2006 The MC@NLO 3.2 event generator *Preprint* hep-ph/0601192
[344] For further details see Proceedings of the 2004/2005 HERA-LHC workshop
[345] Dittmar M, Pauss F and Zurcher D 1997 Towards a precise parton luminosity determination at the CERN LHC *Phys. Rev.* D **56** 7284–7290 (*Preprint* hep-ex/9705004)
[346] Drell S D and Yan T-M 1970 Massive lepton pair production in hadron-hadron collisions at high-energies *Phys. Rev. Lett.* **25** 316–320 (doi:10.1103/PhysRevLett.25.316)
[347] Belotelov I *et al* 2006 Study of Drell–Yan di-muon production with the CMS detector *CMS Note* 2006/123
[348] Hamberg R, van Neerven W L and Matsuura T 1991 A Complete calculation of the order α_s^2 correction to the Drell–Yan K-factor *Nucl. Phys.* B **359** 343–405 (doi:10.1016/0550-3213(91)90064-5)
[349] Bourilkov D 2006 Compositeness search with di-muons in CMS *CMS Note* 2006/085
[350] Baur U and Wackeroth D 2003 Electroweak radiative corrections to weak boson production at hadron colliders *Nucl. Phys. Proc. Suppl.* **116** 159–163 (*Preprint* hep-ph/0211089)

[351] Bourilkov D 2003 Study of parton density function uncertainties with LHAPDF and PYTHIA at LHC*Prepared for the LHC/LC Study Group Meeting (Geneva, Switzerland, 9 May 2003) Preprint* hep-ph/0305126
[352] Buege V *et al* 2006 Prospects for the precision measurement of the W mass with the CMS detector *CMS Note* 2006-061
[353] Giele W T and Keller S 1998 Determination of W boson properties at hadron colliders *Phys. Rev.* D **57** 4433–4440 (*Preprint* hep-ph/9704419)
[354] Brigljević V *et al* 2006 Study of di-boson production with the CMS detector at the LHC *CMS Note* 2006/108
[355] Pukhov A *et al* 1999 CompHEP: A package for evaluation of Feynman diagrams and integration over multi-particle phase space. User's manual for version 33 *Preprint* hep-ph/9908288
[356] Higgs P W 1964 Broken symmetries, massless particles and gauge fields *Phys. Lett.* **12** 132–133
[357] Higgs P W 1966 Spontaneous symmetry breakdown without massless bosons *Phys. Rev.* **145** 1156–1163
[358] Englert F and Brout R 1964 Broken symmetry and the mass of gauge vector mesons *Phys. Rev. Lett.* **13** 321–322
[359] Guralnik G S, Hagen C R and Kibble T W B 1964 Global conservation laws and massless particles *Phys. Rev. Lett.* **13** 585–587
[360] Cornwall J M, Levin D N and Tiktopoulos G 1973 Uniqueness of spontaneously broken gauge theories *Phys. Rev. Lett.* **30** 1268–1270 (doi:10.1103/PhysRevLett.30.1268)
[361] Cornwall J M, Levin D N and Tiktopoulos G 1974 Derivation of gauge invariance from high-energy unitarity bounds on the S-Matrix *Phys. Rev.* D **10** 1145
[362] Llewellyn Smith C H 1973 High-energy behavior and gauge symmetry *Phys. Lett.* B **46** 233–236
[363] Joglekar S D 1974 S-matrix derivation of the Weinberg model *Ann. Phys.* **83** 427
[364] Veltman M 1968 Perturbation theory of massive Yang-Mills fields *Nucl. Phys.* B **7** 637–650
[365] 't Hooft G 1971 Renormalization of massless Yang-Mills fields *Nucl. Phys.* B **33** 173–199
[366] 't Hooft G 1971 Renormalizable lagrangians for massive Yang-Mills fields *Nucl. Phys.* B **35** 167–188
[367] 't Hooft G and Veltman M J G 1972 Regularization and renormalization of gauge fields *Nucl. Phys.* B **44** 189–213
[368] 't Hooft G and Veltman M J G 1972 Combinatorics of gauge fields *Nucl. Phys.* B **50** 318–353
[369] Djouadi A 2005 The anatomy of electro-weak symmetry breaking I: The Higgs boson in the standard model *Preprint* hep-ph/0503172
[370] Djouadi A 2005 The anatomy of electro-weak symmetry breaking II: The Higgs bosons in the minimal supersymmetric model *Preprint* hep-ph/0503173
[371] Cabibbo N, Maiani L, Parisi G and Petronzio R 1979 Bounds on the fermions and higgs boson masses in grand unified theories *Nucl. Phys.* B **158** 295
[372] Chanowitz M S, Furman M A and Hinchliffe I 1978 Weak interactions of ultraheavy fermions *Phys. Lett.* B **78** 285
[373] Flores R A and Sher M 1983 Upper limits to fermion masses in the Glashow-Weinberg-Salam model *Phys. Rev.* D **27** 1679
[374] Lindner M 1986 Implications of triviality for the standard model *Zeit. Phys.* C **31** 295
[375] Sher M 1989 Electroweak Higgs potentials and vacuum stability *Phys. Rept.* **179** 273–418
[376] Sher M 1993 Precise vacuum stability bound in the standard model *Phys. Lett.* B **317** 159–163 (*Preprint* hep-ph/9307342)
[377] Altarelli G and Isidori G 1994 Lower limit on the Higgs mass in the standard model: an update *Phys. Lett.* B **337** 141–144
[378] Espinosa J and Quiros M 1995 Improved metastability bounds on the standard model Higgs mass *Phys. Lett.* B **353** 257–266 (*Preprint* hep-ph/9504241)
[379] Hasenfratz A, Jansen K, Lang C B, Neuhaus T and Yoneyama H 1987 The triviality bound of the four component phi**4 model *Phys. Lett.* B **199** 531
[380] Kuti J, Lin L and Shen Y 1988 Upper bound on the Higgs mass in the standard model *Phys. Rev. Lett.* **61** 678
[381] Luscher M and Weisz P 1989 Scaling laws and triviality bounds in the lattice φ^4 theory (III) n-component model *Nucl. Phys.* B **318** 705 (doi:10.1016/0550-3213(89)90637-8)
[382] Higgs Working Group Collaboration, Carena M *et al* 2000 Report of the Tevatron Higgs working group *Preprint* hep-ph/0010338
[383] ATLAS Collaboration, 1994 Technical Design Report *CERN/LHCC*, 94-14, ATLAS TDR 14
[384] Abdullin S *et al* 2005 Summary of the CMS potential for the Higgs boson discovery *Eur. Phys. J.* C **39S2** 41–61 (doi:10.1140/epjcd/s2004-02-003-9)
[385] Braaten E and Leveille J P 1980 Higgs boson decay and the running mass *Phys. Rev.* D **22** 715

[386] Sakai N 1980 Perturbative QCD Corrections to the hadronic decay width of the Higgs boson *Phys. Rev.* D **22** 2220
[387] Inami T and Kubota T 1981 Renormalization group estimate of the Hadronic decay width of the Higgs boson *Nucl. Phys.* B **179** 171
[388] Gorishnii S G, Kataev A L and Larin S A 1984 The width of Higgs Boson decay into Hadrons: three loop corrections of strong interactions *Sov. J. Nucl. Phys.* **40** 329–334
[389] Drees M and Hikasa K-i 1990 Heavy quark thresholds in Higgs physics *Phys. Rev.* D **41** 1547
[390] Drees M and Hikasa K 1990 Note on QCD corrections to Hadronic Higgs decay *Phys. Lett.* B **240** 455
[391] Chetyrkin K G 1997 Correlator of the quark scalar currents and Gamma(tot)(H → hadrons) at O(alpha(s)**3) in pQCD *Phys. Lett.* B **390** 309–317 (*Preprint* hep-ph/9608318)
[392] Fleischer J and Jegerlehner F 1981 Radiative Corrections to Higgs Decays in the Extended Weinberg-Salam Model *Phys. Rev.* D **23** 2001–2026
[393] Bardin D Y, Vilensky B M and Khristova P K 1991 Calculation of the Higgs boson decay width into fermion pairs *Sov. J. Nucl. Phys.* **53** 152–158
[394] Dabelstein A and Hollik W 1992 Electroweak corrections to the fermionic decay width of the standard Higgs boson *Z. Phys.* C **53** 507–516
[395] Kniehl B A 1992 Radiative corrections for $H \to f\bar{f}(\gamma)$ in the standard model *Nucl. Phys.* B **376** 3–28 (doi:10.1016/0550-3213(92)90065)-J
[396] Zheng H-Q and Wu D-D 1990 First order QCD corrections to the decay of the Higgs boson into two photons *Phys. Rev.* D **42** 3760–3763
[397] Djouadi A, Spira M, van der Bij J and Zerwas P 1991 QCD corrections to gamma gamma decays of Higgs particles in the intermediate mass range *Phys. Lett.* B **257** 187–190
[398] Dawson S and Kauffman R P 1993 QCD corrections to H → gamma gamma *Phys. Rev.* D **47** 1264–1267
[399] Djouadi A, Spira M and Zerwas P 1993 Two photon decay widths of Higgs particles *Phys. Lett.* B **311** 255–260 (*Preprint* hep-ph/9305335)
[400] Melnikov K and Yakovlev O I 1993 Higgs → two photon decay: QCD radiative correction *Phys. Lett.* B **312** 179–183 (*Preprint* hep-ph/9302281)
[401] Inoue M, Najima R, Oka T and Saito J 1994 QCD corrections to two photon decay of the Higgs boson and its reverse process *Mod. Phys. Lett.* A **9** 1189–1194
[402] Steinhauser M 1996 Corrections of O(alpha(s)**2) to the decay of an intermediate-mass Higgs boson into two photons *Preprint* hep-ph/9612395
[403] Djouadi A, Gambino P and Kniehl B A 1998 Two-loop electroweak heavy-fermion corrections to Higgs-boson production and decay *Nucl. Phys.* B **523** 17–39 (*Preprint* hep-ph/9712330)
[404] Aglietti U, Bonciani R, Degrassi G and Vicini A 2004 Two-loop light fermion contribution to Higgs production and decays *Phys. Lett.* B **595** 432–441 (*Preprint* hep-ph/0404071)
[405] Degrassi G and Maltoni F 2005 Two-loop electroweak corrections to the Higgs-boson decay H→ gamma gamma *Preprint* hep-ph/0504137
[406] Kniehl B A 1991 Radiative corrections for $H \to ZZ$ in the standard model *Nucl. Phys.* B **352** 1–26 (doi:10.1016/0550-3213(91)90126-I)
[407] Kniehl B A 1991 Radiative corrections for $H \to W^+W^-(\gamma)$ in the standard model *Nucl. Phys.* B **357** 439–466 (doi:10.1016/0550-3213(91)90476-E)
[408] Georgi H, Glashow S, Machacek M and Nanopoulos D 1978 Higgs bosons from two gluon annihilation in proton proton collisions *Phys. Rev. Lett.* **40** 692 (doi:10.1103/PhysRevLett.40.692)
[409] Graudenz D, Spira M and Zerwas P M 1993 QCD corrections to Higgs boson production at proton proton colliders *Phys. Rev. Lett.* **70** 1372–1375 (doi:10.1103/PhysRevLett.70.1372)
[410] Spira M, Djouadi A, Graudenz D and Zerwas P 1993 SUSY Higgs production at proton colliders *Phys. Lett.* B **318** 347–353 (doi:10.1016/0370-2693(93)90138-8)
[411] Spira M, Djouadi A, Graudenz D and Zerwas P 1995 Higgs boson production at the LHC *Nucl. Phys.* B **453** 17–82 (*Preprint* hep-ph/9504378) (doi:10.1016/0550-3213(95)00379-7)
[412] Kramer M, Laenen E and Spira M 1998 Soft gluon radiation in Higgs boson production at the LHC *Nucl. Phys.* B **511** 523–549 (*Preprint* hep-ph/9611272) (doi:10.1016/S0550-3213(97)00679-2)
[413] Djouadi A, Spira M and Zerwas P 1991 Production of Higgs bosons in proton colliders: QCD corrections *Phys. Lett.* B **264** 440–446
[414] Dawson S 1991 Radiative corrections to Higgs boson production *Nucl. Phys.* B **359** 283–300
[415] Kauffman R P and Schaffer W 1994 QCD corrections to production of Higgs pseudoscalars *Phys. Rev.* D **49** 551–554 (*Preprint* hep-ph/9305279)
[416] Dawson S and Kauffman R 1994 QCD corrections to Higgs boson production: nonleading terms in the heavy quark limit *Phys. Rev.* D **49** 2298–2309 (*Preprint* hep-ph/9310281)

[417] Harlander R V and Kilgore W B 2002 Next-to-next-to-leading order Higgs production at hadron colliders *Phys. Rev. Lett.* **88** 201801 (*Preprint* hep-ph/0201206)
[418] Harlander R V and Kilgore W B 2002 Production of a pseudo-scalar Higgs boson at hadron colliders at next-to-next-to leading order *J. High. Energy Phys.* JHEP10(2002)017 (*Preprint* hep-ph/0208096)
[419] Anastasiou C and Melnikov K 2002 Higgs boson production at hadron colliders in NNLO QCD *Nucl. Phys.* B **646** 220–256 (*Preprint* hep-ph/0207004)
[420] Ravindran V, Smith J and van Neerven W L 2003 NNLO corrections to the total cross section for Higgs boson production in hadron hadron collisions *Nucl. Phys.* B **665** 325–366 (*Preprint* hep-ph/0302135)
[421] Catani S, de Florian D, Grazzini M and Nason P 2003 Soft-gluon resummation for Higgs boson production at hadron colliders *J. High. Energy Phys.* JHEP07(2003)028 (*Preprint* hep-ph/0306211)
[422] Djouadi A and Gambino P 1994 Leading electroweak correction to Higgs boson production at proton colliders *Phys. Rev. Lett.* **73** 2528–2531 (*Preprint* hep-ph/9406432)
[423] Chetyrkin K G, Kniehl B A and Steinhauser M 1997 Virtual top-quark effects on the H → b anti-b decay at next-to-leading order in QCD *Phys. Rev. Lett.* **78** 594–597 (*Preprint* hep-ph/9610456)
[424] Chetyrkin K G, Kniehl B A and Steinhauser M 1997 Three-loop O(alpha(s)**2 G(F) M(t)**2) corrections to hadronic Higgs decays *Nucl. Phys.* B **490** 19–39 (*Preprint* hep-ph/9701277)
[425] Ghinculov A and van der Bij J J 1996 The Higgs resonance shape in gluon fusion: Heavy Higgs effects *Nucl. Phys.* B **482** 59–72 (*Preprint* hep-ph/9511414)
[426] Ellis R K, Hinchliffe I, Soldate M and van der Bij J J 1988 Higgs Decay to tau + tau-: A Possible Signature of Intermediate Mass Higgs Bosons at the SSC *Nucl. Phys.* B **297** 221
[427] Baur U and Glover E W N 1990 Higgs Boson Production at Large Transverse Momentum in Hadronic Collisions *Nucl. Phys.* B **339** 38–66
[428] Schmidt C R 1997 $H \to ggg(gq\bar{q})$ at two loops in the large-M_t limit *Phys. Lett.* B **413** 391–395 (doi:10.1016/S0370-2693(97)01102-7)
[429] de Florian D, Grazzini M and Kunszt Z 1999 Higgs production with large transverse momentum in hadronic collisions at next-to-leading order *Phys. Rev. Lett.* **82** 5209–5212 (*Preprint* hep-ph/9902483)
[430] Ravindran V, Smith J and Van Neerven W L 2002 Next-to-leading order QCD corrections to differential distributions of Higgs boson production in hadron hadron collisions *Nucl. Phys.* B **634** 247–290 (*Preprint* hep-ph/0201114)
[431] Glosser C J and Schmidt C R 2002 Next-to-leading corrections to the Higgs boson transverse momentum spectrum in gluon fusion *J. High. Energy Phys.* JHEP12(2002)016 (*Preprint* hep-ph/0209248)
[432] Anastasiou C, Melnikov K and Petriello F 2005 Fully differential Higgs boson production and the di-photon signal through next-to-next-to-leading order *Nucl. Phys.* B **724** 197–246 (*Preprint* hep-ph/0501130)
[433] Catani S, D'Emilio E and Trentadue L 1988 The Gluon Form-Factor to Higher Orders: Gluon Gluon Annihilation at Small Q-Transverse *Phys. Lett.* B **211** 335–342
[434] Hinchliffe I and Novaes S F 1988 On the Mean Transverse Momentum of Higgs Bosons at the SSC *Phys. Rev.* D **38** 3475–3480
[435] Kauffman R P 1991 Higgs boson p(T) in gluon fusion *Phys. Rev.* D **44** 1415–1425
[436] Kauffman R 1992 Higher order corrections to Higgs boson p(T) *Phys. Rev.* D **45** 1512–1517
[437] Balazs C and Yuan C P 2000 Higgs boson production at the LHC with soft gluon effects *Phys. Lett.* B **478** 192–198 (*Preprint* hep-ph/0001103)
[438] Berger E L and Qiu J-w 2003 Differential cross section for Higgs boson production including all-orders soft gluon resummation *Phys. Rev.* D **67** 034026 (*Preprint* hep-ph/0210135)
[439] Kulesza A and Stirling W J 2003 Non-perturbative effects and the resummed Higgs transverse momentum distribution at the LHC *J. High. Energy Phys.* JHEP12(2003)056 (*Preprint* hep-ph/0307208)
[440] Kulesza A, Sterman G and Vogelsang W 2004 Joint resummation for Higgs production *Phys. Rev.* D **69** 014012 (*Preprint* hep-ph/0309264)
[441] Gawron A and Kwiecinski J 2004 Resummation effects in Higgs boson transverse momentum distribution within the framework of unintegrated parton distributions *Phys. Rev.* D **70** 014003 (*Preprint* hep-ph/0309303)
[442] Watt G, Martin A and Ryskin M 2004 Unintegrated parton distributions and electroweak boson production at hadron colliders *Phys. Rev.* D **70** 014012 (*Preprint* hep-ph/0309096)
[443] Lipatov A and Zotov N 2005 Higgs boson production at hadron colliders in the k(T)-factorization approach *Eur. Phys. J.* C **44** 559–566 (*Preprint* hep-ph/0501172)
[444] de Florian D and Grazzini M 2000 Next-to-next-to-leading logarithmic corrections at small transverse momentum in hadronic collisions *Phys. Rev. Lett.* **85** 4678–4681 (*Preprint* hep-ph/0008152)

[445] Catani S, De Florian D and Grazzini M 2001 Higgs production at hadron colliders in (almost) NNLO QCD *Bologna 2001, Deep Inelastic Scattering (Bologna, Italy, April, 2001)* pp 518–521 *Preprint* hep-ph/0106049
[446] Catani S, de Florian D and Grazzini M 2001 Universality of non-leading logarithmic contributions in transverse momentum distributions *Nucl. Phys.* B **596** 299–312 (*Preprint* hep-ph/0008184)
[447] Bozzi G, Catani S, de Florian D and Grazzini M 2003 The q(T) spectrum of the Higgs boson at the LHC in QCD perturbation theory *Phys. Lett.* B **564** 65–72 (*Preprint* hep-ph/0302104)
[448] Bozzi G, Catani S, de Florian D and Grazzini M 2006 Transverse-momentum resummation and the spectrum of the Higgs boson at the LHC *Nucl. Phys.* B **737** 73–120 (*Preprint* hep-ph/0508068)
[449] Cahn R N and Dawson S 1984 Production of Very Massive Higgs Bosons *Phys. Lett.* B **136** 196
[450] Hikasa K-i 1985 Heavy Higgs Production in e+ e- and e- e- Collisions *Phys. Lett.* B **164** 385
[451] Altarelli G, Mele B and Pitolli F 1987 Heavy Higgs production at future colliders *Nucl. Phys.* B **287** 205–224
[452] Han T, Valencia G and Willenbrock S 1992 Structure function approach to vector boson scattering in p p collisions *Phys. Rev. Lett.* **69** 3274–3277 (*Preprint* hep-ph/9206246)
[453] Figy T, Oleari C and Zeppenfeld D 2003 Next-to-leading order jet distributions for Higgs boson production via weak-boson fusion *Phys. Rev.* D **68** 073005 (*Preprint* hep-ph/0306109)
[454] Glashow S, Nanopoulos D and Yildiz A 1978 Associated production of Higgs bosons and Z particles *Phys. Rev.* D **18** 1724–1727
[455] Kunszt Z, Trocsanyi Z and Stirling W J 1991 Clear signal of intermediate mass Higgs boson production at LHC and SSC *Phys. Lett.* B **271** 247–255
[456] Han T and Willenbrock S 1991 QCD correction to the p p → W H and Z H total cross- sections *Phys. Lett.* B **273** 167–172
[457] Brein O, Djouadi A and Harlander R 2004 NNLO QCD corrections to the Higgs-strahlung processes at hadron colliders *Phys. Lett.* B **579** 149–156 (*Preprint* hep-ph/0307206)
[458] Ciccolini M L, Dittmaier S and Kramer M 2003 Electroweak radiative corrections to associated W H and Z H production at hadron colliders *Phys. Rev.* D **68** 073003 (*Preprint* hep-ph/0306234)
[459] Raitio R and Wada W W 1979 Higgs Boson production at large transverse momentum in QCD *Phys. Rev.* D **19** 941
[460] Ng J N and Zakarauskas P 1984 A QCD Parton calculation of conjoined production of Higgs Bosons and heavy flavors in p anti-p collision *Phys. Rev.* D **29** 876
[461] Kunszt Z 1984 Associated production of heavy Higgs boson with top quarks *Nucl. Phys.* B **247** 339
[462] Gunion J F 1991 Associated top anti-top Higgs production as a large source of W H events: Implications for Higgs detection in the lepton neutrino gamma gamma final state *Phys. Lett.* B **261** 510–517
[463] Marciano W J and Paige F E 1991 Associated production of Higgs bosons with t anti-t pairs *Phys. Rev. Lett.* **66** 2433–2435
[464] Beenakker W, Dittmaier S, Kraemer M, Pluemper B, Spira M and Zerwas P 2001 Higgs radiation off top quarks at the Tevatron and the LHC *Phys. Rev. Lett.* **87** 201805 (*Preprint* hep-ph/0107081)
[465] Dawson S, Orr L H, Reina L and Wackeroth D 2003 Associated top quark Higgs boson production at the LHC *Phys. Rev.* D **67** 071503 (*Preprint* hep-ph/0211438)
[466] Dawson S and Reina L 1998 QCD corrections to associated Higgs boson production *Phys. Rev.* D **57** 5851–5859 (*Preprint* hep-ph/9712400)
[467] Futyan D, Fortin D and Giordano D 2006 Search for the Standard Model Higgs Boson in the Two-Electron and Two-Muon Final State with CMS *CMS Note* 2006/136
[468] Bartalini P *et al* 2006 NLO vs. LO: kinematical differences for signal and background in the $H \to ZZ^{(*)} \to 4\mu$ analysis *CMS Note* 2006/130
[469] Baffioni S *et al* 2006 Discovery potential for the SM Higgs boson in the $H \to ZZ^{(*)} \to e^+e^-e^+e^-$ decay channel *CMS Note* 2006/115
[470] Dittmar M and Dreiner H K 1997 How to find a Higgs boson with a mass between 155-GeV to 180-GeV at the LHC *Phys. Rev.* D **55** 167–172 (*Preprint* hep-ph/9608317)
[471] Davatz G, Dittmar M and Giolo-Nicollerat A-S 2006 Standard Model Higgs Discovery Potential of CMS in H→WW→ $\ell\nu\ell\nu$ Channel *CMS Note* 2006/047
[472] Davatz G, Dissertori G, Dittmar M, Grazzini M and Pauss F 2004 Effective K-factors for $gg \to H \to WW \to \ell\nu\ell\nu$ at the LHC *J. High. Energy Phys.* JHEP05(2004)009 (*Preprint* hep-ph/0402218)
[473] Campbell J and Tramontano F 2005 Next-to-leading order corrections to W t production and decay *Nucl. Phys.* B **726** 109–130 (*Preprint* hep-ph/0506289)
[474] CMS Collaboration, Beaudette F *et al* 2006 Search for a Light Standard Model Higgs Boson in the $H \to WW^{(*)} \to e^+\nu e^-\bar{\nu}$ Channel *CMS Note* 2006/114

[475] Plehn T, Rainwater D L and Zeppenfeld D 2000 A method for identifying $H \to \tau\tau \to e^{\pm}\mu^{\mp}_{P_T}$ at the CERN LHC *Phys. Rev.* D **61** 093005 (doi:10.1103/PhysRevD.61.093005)

[476] Rainwater D L, Zeppenfeld D and Hagiwara K 1999 Searching for $H \to \tau\tau$ in weak boson fusion at the LHC *Phys. Rev.* D **59** 014037 (doi:10.1103/PhysRevD.59.014037)

[477] Cavalli D *et al* 2002 The Higgs working group: Summary report *Preprint* hep-ph/0203056

[478] Zeppenfeld D, Kinnunen R, Nikitenko A and Richter-Was E 2000 Measuring Higgs boson couplings at the LHC *Phys. Rev.* D **62** 013009 (*Preprint* hep-ph/0002036)

[479] Duhrssen M *et al* 2004 Extracting Higgs boson couplings from LHC data *Phys. Rev.* D **70** 113009 (*Preprint* hep-ph/0406323)

[480] Plehn T, Rainwater D L and Zeppenfeld D 1999 Probing the MSSM Higgs sector via weak boson fusion at the LHC *Phys. Lett.* B **454** 297–303 (*Preprint* hep-ph/9902434)

[481] Foudas C, Nikitenko A and Takahashi M 2006 Observation of the Standard Model Higgs boson via H$\to \tau\tau \to$ lepton+jet Channel *CMS Note* 2006/088

[482] Pi H, Avery P, Rohlf J, Tully C and Kunori S 2006 Search for Standard Model Higgs Boson via Vector Boson Fusion in the H$\to$W$^+$W$^-$ to $\ell^{\pm}\nu$jj with $120 < m_H < 250$ GeV/c^2 *CMS Note* 2006/092

[483] Dubinin M, Litvin V, Ma Y, Newman H and Pieri M 2006 Vector Boson Fusion Production with H$\to \gamma\gamma$ *CMS Note* 2006/097

[484] Delaere C 2006 Study of associated WH production with H$\to$WW* in the 3 leptons final state *CMS Note* 2006/053

[485] CDF Collaboration, Acosta D *et al* 2005 Measurement of the ttbar Production Cross Section in ppbar Collisions at sqrt(s) = 1.96 TeV using Lepton + Jets Events with Secondary Vertex b-tagging *Phys. Rev.* D **71** 052003

[486] Djouadi A and Ferrag S 2003 PDF Uncertainties In Higgs Production At Hadron Colliders *Preprint* hep-ph/0310209

[487] Higgs Working Group Collaboration, Assamagan K *et al* 2004 The Higgs working group: Summary report 2003 *Preprint* hep-ph/0406152

[488] Belanger G, Boudjema F and Sridhar K 2000 SUSY Higgs at the LHC: Large stop mixing effects and associated production *Nucl. Phys.* B **568** 3–39 (*Preprint* hep-ph/9904348)

[489] Dubinin M, Ilyin V and Savrin V 1997 Light Higgs Boson Signal at LHC in the reaction pp $\to \gamma\gamma$+jet and pp $\to \gamma\gamma$+lepton *CMS Note* 1997/101

[490] Kinnunen R and Denegri D 1997 Expected SM/SUSY Higgs Observability in CMS *CMS Note* 1997/057

[491] ATLAS Collaboration, 1999 ATLAS Detector and Physics Performance. Technical Design Report. Vol. 2 *CERN/LHCC, CERN-LHCC* -99-15

[492] Beauchemin P, Azuelos G and Burgess C 2004 Dimensionless coupling of bulk scalars at the LHC *J. Phys.* **G30** N17 (doi:10.1088/0954-3899/30/10/N01)

[493] Stelzer T and Long W F 1994 Automatic generation of tree level helicity amplitudes *Comput. Phys. Commun.* **81** 357–371 (doi:10.1016/0010-4655(94)90084-1)

[494] Murayama H, Watanabe I and Hagiwara K HELAS: HELicity amplitude subroutines for Feynman diagram evaluations KEK-91-11

[495] Mangano M, Moretti M and Pittau R 2002 Multijet matrix elements and shower evolution in hadronic collisions: $Wb\bar{b}+n$-jets as a case study *Nucl. Phys.* B **632** 343–362 (*Preprint* hep-ph/0108069) (doi:10.1016/S0550-3213(02)00249-3)

[496] Caravaglios F, Mangano M, Moretti M and Pittau R 1999 A new approach to multi-jet calculations in hadron collisions *Nucl. Phys.* B **539** 215–232 (*Preprint* hep-ph/9807570)

[497] Buttar C *et al* Les Houches physics at TeV colliders 2005, standard model, QCD, EW, and Higgs working group: Summary report 2006 *Preprint* hep-ph/0604120

[498] Bityukov S, Erofeeva S, Krasnikov N and Nikitenko A 2005 Program for evaluation of significance, confidence intervals and limits by direct calculation of probabilities *Proceedings of PhyStat 2005*

[499] Lethuillier M *et al* 2006 Search for a neutral Higgs boson with WH / ZH, H$\to \gamma\gamma$ channel *CMS Note* 2006/110

[500] Ravat O 2004 Etude du Calorimètre électromagnétique de l'expérience CMS et recherche de bosons de Higgs neutres dans le canal de production associée PhD Thesis, IPN, Lyon, 2004. LYCEN-T2004-29

[501] Graham D J 1995 An algorithm using tracks to locate the two photon vertex at high luminosity *CMS TN* 1995/115

[502] Djouadi A 1998 Squark effects on Higgs boson production and decay at the LHC *Phys. Lett.* B **435** 101–108 (*Preprint* hep-ph/9806315)

[503] Eynard G 1998 Study of associated Higgs boson production HW, Ht$\bar{t}$, HZ $\to \gamma\gamma + e^{\pm}/\mu^{\pm} +$ X with the ATLAS detector at LHC. (In French) PhD Thesis, Annecy, *CERN-THESIS* -2000-036

[504] Beauchemin P-H and Azuelos G 2004 Search for the Standard Model Higgs Boson in the $\gamma\gamma + E_{\mathrm{T}}^{miss}$ channel *ATL-PHYS-2004-028*
[505] Lethuillier M, Agram J-L, Baty C, Gascon-Shotkin S, Perries S and Ravat O 2006 Search for a Neutral Higgs Boson with WH/ZH, H$\rightarrow \gamma\gamma$ Channel *CMS Note* 2006/110
[506] CMS Collaboration 2000 The TriDAS Project Technical Design Report, Volume 1: The Trigger Systems *CERN/LHCC*, 2000-38, CMS TDR 6.1
[507] CMS Collaboration, Acosta D *et al* 2006 CMS Physics Technical Design Report, Volume 1, Section 10.3.2: Photon isolation *CERN/LHCC*, 2006-001 p 376
[508] Read A L 2002 Presentation of search results: The CL(s) technique *J. Phys.* G **28** 2693–2704
[509] Junk T 1999 Confidence level computation for combining searches with small statistics *Nucl. Instrum. Meth.* A **434** 435–443 (*Preprint* hep-ex/9902006)
[510] Djouadi A and Ferrag S 2004 PDF uncertainties in Higgs production at hadron colliders *Phys. Lett.* B **586** 345–352 (*Preprint* hep-ph/0310209)
[511] Dell'Aquila J R and Nelson C A 1986 Simple tests for CP or P violation by sequential decays: V_1V_2 modes with decays into $\bar{\ell}_A\ell_B$ and/or $\bar{q}_Aq_B$ *Phys. Rev.* D **33** 101 (doi:10.1103/PhysRevD.33.101)
[512] Skjold A and Osland P 1994 Signals of CP violation in Higgs decay *Phys. Lett.* B **329** 305–311 (*Preprint* hep-ph/9402358)
[513] Choi S Y, Miller D J, Muhlleitner M M and Zerwas P M 2003 Identifying the Higgs spin and parity in decays to Z pairs *Phys. Lett.* B **553** 61–71 (*Preprint* hep-ph/0210077)
[514] Buszello C P, Fleck I, Marquard P and van der Bij J J 2004 Prospective analysis of spin- and CP-sensitive variables in H $\rightarrow$ ZZ $\rightarrow$ l(1)+ l(1)- l(2)+ l(2)- at the LHC *Eur. Phys. J.* C **32** 209–219 (*Preprint* hep-ph/0212396)
[515] Bluj M 2006 A Study of Angular Correlations in H$\rightarrow$ZZ$\rightarrow$2e2μ *CMS Note* 2006/094
[516] Wess J and Zumino B 1974 Supergauge transformations in four-dimensions *Nucl. Phys.* B **70** 39–50
[517] Fayet P and Ferrara S 1977 Supersymmetry *Phys. Rept.* **32** 249–334
[518] Nilles H P 1984 Supersymmetry, supergravity and particle physics *Phys. Rept.* **110** 1
[519] Barbieri R 1988 Looking beyond the standard model: the supersymmetric option *Riv. Nuovo Cim.* **11N4** 1–45
[520] Haber H E and Kane G L 1985 The search for supersymmetry: probing physics beyond the standard model *Phys. Rept.* **117** 75
[521] Witten E 1981 Mass hierarchies in supersymmetric theories *Phys. Lett.* B **105** 267
[522] Dimopoulos S, Raby S and Wilczek F 1981 Supersymmetry and the scale of unification *Phys. Rev.* D **24** 1681–1683
[523] Ibanez L E and Ross G G 1981 Low-energy predictions in supersymmetric grand unified theories *Phys. Lett.* B **105** 439
[524] Ibanez L E and Ross G G 1982 $SU(2)_L \times U(1)$ Symmetry breaking as a radiative effect of supersymmetry breaking in GUTs *Phys. Lett.* B **110** 215–220 (doi:10.1016/0370-2693(82)91239-4)
[525] Inoue K, Kakuto A, Komatsu H and Takeshita S 1982 Aspects of grand unified models with softly broken supersymmetry *Prog. Theor. Phys.* **68** 927
[526] Alvarez-Gaume L, Claudson M and Wise M B 1982 Low-energy supersymmetry *Nucl. Phys.* B **207** 96
[527] Ellis J R, Nanopoulos D V and Tamvakis K 1983 Grand unification in simple supergravity *Phys. Lett.* B **121** 123
[528] Dimopoulos S and Georgi H 1981 Softly broken supersymmetry and SU(5) *Nucl. Phys.* B **193** 150
[529] Sakai N 1981 Naturalness in supersymmetric 'GUTS' *Zeit. Phys.* C **11** 153
[530] Okada Y, Yamaguchi M and Yanagida T 1991 Upper bound of the lightest Higgs boson mass in the minimal supersymmetric standard model *Prog. Theor. Phys.* **85** 1–6
[531] Haber H E and Hempfling R 1991 Can the mass of the lightest Higgs boson of the minimal supersymmetric model be larger than m(Z)? *Phys. Rev. Lett.* **66** 1815–1818
[532] Ellis J R, Ridolfi G and Zwirner F 1991 Radiative corrections to the masses of supersymmetric Higgs bosons *Phys. Lett.* B **257** 83–91
[533] Barbieri R, Frigeni M and Caravaglios F 1991 The supersymmetric Higgs for heavy superpartners *Phys. Lett.* B **258** 167–170
[534] Yamada A 1991 Radiative corrections to the Higgs masses in the minimal supersymmetric standard model *Phys. Lett.* B **263** 233–238
[535] Brignole A, Ellis J R, Ridolfi G and Zwirner F 1991 The supersymmetric charged Higgs boson mass and LEP phenomenology *Phys. Lett.* B **271** 123–132
[536] Chankowski P H, Pokorski S and Rosiek J 1992 Charged and neutral supersymmetric Higgs boson masses: Complete one loop analysis *Phys. Lett.* B **274** 191–198

[537] Espinosa J R and Quiros M 1991 Two loop radiative corrections to the mass of the lightest Higgs boson in supersymmetric standard models *Phys. Lett.* B **266** 389–396
[538] Hempfling R and Hoang A H 1994 Two loop radiative corrections to the upper limit of the lightest Higgs boson mass in the minimal supersymmetric model *Phys. Lett.* B **331** 99–106 (*Preprint* hep-ph/9401219)
[539] Casas J A, Espinosa J R, Quiros M and Riotto A 1995 The lightest Higgs boson mass in the minimal supersymmetric standard model *Nucl. Phys.* B **436** 3–29 (*Preprint* hep-ph/9407389)
[540] Carena M, Espinosa J R, Quiros M and Wagner C 1995 Analytical expressions for radiatively corrected Higgs masses and couplings in the MSSM *Phys. Lett.* B **355** 209–221 (*Preprint* hep-ph/9504316)
[541] Carena M, Quiros M and Wagner C E M 1996 Effective potential methods and the Higgs mass spectrum in the MSSM *Nucl. Phys.* B **461** 407–36 (*Preprint* hep-ph/9508343)
[542] Heinemeyer S, Hollik W and Weiglein G 1998 QCD corrections to the masses of the neutral CP-even Higgs bosons in the MSSM *Phys. Rev.* D **58** 091701 (*Preprint* hep-ph/9803277)
[543] Heinemeyer S, Hollik W and Weiglein G 1998 Precise prediction for the mass of the lightest Higgs boson in the MSSM *Phys. Lett.* B **440** 296–304 (*Preprint* hep-ph/9807423)
[544] Heinemeyer S, Hollik W and Weiglein G 2000 Constraints on tan(beta) in the MSSM from the upper bound on the mass of the lightest Higgs boson *J. High. Energy Phys.* JHEP06(2000)009 (*Preprint* hep-ph/9909540)
[545] Espinosa J R and Zhang R-J 2000 Complete two-loop dominant corrections to the mass of the lightest CP-even Higgs boson in the minimal supersymmetric standard model *Nucl. Phys.* B **586** 3–38 (*Preprint* hep-ph/0003246)
[546] Brignole A, Degrassi G, Slavich P and Zwirner F 2002 On the $\mathcal{O}(\alpha_t^2)$ two-loop corrections to the neutral Higgs boson masses in the MSSM *Nucl. Phys.* B **631** 195–218 (doi:10.1016/S0550-3213(02)00184-0)
[547] Brignole A, Degrassi G, Slavich P and Zwirner F 2002 On the two-loop sbottom corrections to the neutral Higgs boson masses in the MSSM *Nucl. Phys.* B **643** 79–92 (*Preprint* hep-ph/0206101)
[548] Heinemeyer S, Hollik W, Rzehak H and Weiglein G 2005 High-precision predictions for the MSSM Higgs sector at $\mathcal{O}(\alpha_b\alpha_s)$ *Eur. Phys. J.* C **39** 465–481 (doi:10.1140/epjc/s2005-02112-6)
[549] Coarasa J A, Jimenez R A and Sola J 1996 Strong effects on the hadronic widths of the neutral Higgs Bosons in the MSSM *Phys. Lett.* B **389** 312–320 (*Preprint* hep-ph/9511402)
[550] Chankowski P H, Pokorski S and Rosiek J 1994 Complete on-shell renormalization scheme for the minimal supersymmetric Higgs sector *Nucl. Phys.* B **423** 437–496 (*Preprint* hep-ph/9303309)
[551] Dabelstein A 1995 The One loop renormalization of the MSSM Higgs sector and its application to the neutral scalar Higgs masses *Z. Phys.* C **67** 495–512 (*Preprint* hep-ph/9409375)
[552] Brignole A 1992 Radiative corrections to the supersymmetric neutral Higgs boson masses *Phys. Lett.* B **281** 284–294
[553] Haber H E, Hempfling R and Hoang A H 1997 Approximating the radiatively corrected Higgs mass in the minimal supersymmetric model *Z. Phys.* C **75** 539–554 (*Preprint* hep-ph/9609331)
[554] Zhang R-J 1999 Two-loop effective potential calculation of the lightest CP-even Higgs-boson mass in the MSSM *Phys. Lett.* B **447** 89–97 (*Preprint* hep-ph/9808299)
[555] Espinosa J R and Zhang R-J 2000 MSSM lightest CP-even Higgs boson mass to O(alpha(s) alpha(t)): The effective potential approach *J. High. Energy Phys.* JHEP03(2000)026 (*Preprint* hep-ph/9912236)
[556] Degrassi G, Slavich P and Zwirner F 2001 On the neutral Higgs boson masses in the MSSM for arbitrary stop mixing *Nucl. Phys.* B **611** 403–422 (*Preprint* hep-ph/0105096)
[557] Hempfling R 1994 Yukawa coupling unification with supersymmetric threshold corrections *Phys. Rev.* D **49** 6168–6172
[558] Hall L J, Rattazzi R and Sarid U 1994 The Top quark mass in supersymmetric SO(10) unification *Phys. Rev.* D **50** 7048–7065 (*Preprint* hep-ph/9306309)
[559] Carena M, Olechowski M, Pokorski S and Wagner C 1994 Electroweak symmetry breaking and bottom-top Yukawa unification *Nucl. Phys.* B **426** 269–300 (*Preprint* hep-ph/9402253)
[560] Guasch J, Hafliger P and Spira M 2003 MSSM Higgs decays to bottom quark pairs revisited *Phys. Rev.* D **68** 115001 (*Preprint* hep-ph/0305101)
[561] Dedes A, Degrassi G and Slavich P 2003 On the two-loop Yukawa corrections to the MSSM Higgs boson masses at large tan(beta) *Nucl. Phys.* B **672** 144–162 (*Preprint* hep-ph/0305127)
[562] Eberl H, Hidaka K, Kraml S, Majerotto W and Yamada Y 2000 Improved SUSY QCD corrections to Higgs boson decays into quarks and squarks *Phys. Rev.* D **62** 055006 (*Preprint* hep-ph/9912463)
[563] Carena M, Garcia D, Nierste U and Wagner C 2000 Effective Lagrangian for the $\bar{t}bH^+$ interaction in the MSSM and charged Higgs phenomenology *Nucl. Phys.* B **577** 88–120 (doi:0.1016/S0550-3213(00)00146-2)

[564] Heinemeyer S, Hollik W and Weiglein G 2006 Electroweak precision observables in the minimal supersymmetric standard model *Phys. Rept.* **425** 265–368 (*Preprint* hep-ph/0412214)
[565] Carena M and Haber H E 2003 Higgs boson theory and phenomenology. ((V)) *Prog. Part. Nucl. Phys.* **50** 63–152 (*Preprint* hep-ph/0208209)
[566] ALEPH, DELPHI, L3, OPAL Collaboration 2006 LEP Working Group for Higgs Boson Searches, Search for neutral MSSM Higgs bosons at LEP *Preprint* hep-ex/0602042
[567] LEP Higgs Working Group for Higgs boson searches Collaboration 2001 Search for charged Higgs bosons: Preliminary combined results using LEP data collected at energies up to 209 GeV *Preprint* hep-ex/0107031
[568] Dabelstein A 1995 Fermionic decays of neutral MSSM Higgs bosons at the one loop level *Nucl. Phys.* B **456** 25–56 (*Preprint* hep-ph/9503443)
[569] Heinemeyer S, Hollik W and Weiglein G 2000 Decay widths of the neutral CP-even MSSM Higgs bosons in the Feynman-diagrammatic approach *Eur. Phys. J.* C **16** 139–153 (*Preprint* hep-ph/0003022)
[570] Djouadi A, Janot P, Kalinowski J and Zerwas P M 1996 SUSY Decays of Higgs Particles *Phys. Lett.* B **376** 220–226 (*Preprint* hep-ph/9603368)
[571] Djouadi A, Kalinowski J, Ohmann P and Zerwas P M 1997 Heavy SUSY Higgs bosons at e+ e- linear colliders *Z. Phys.* C **74** 93–111 (*Preprint* hep-ph/9605339)
[572] Dawson S, Djouadi A and Spira M 1996 QCD Corrections to SUSY Higgs Production: The Role of Squark Loops *Phys. Rev. Lett.* **77** 16–19 (*Preprint* hep-ph/9603423)
[573] Harlander R V and Steinhauser M 2003 Hadronic Higgs production and decay in supersymmetry at next-to-leading order *Phys. Lett.* B **574** 258–268 (*Preprint* hep-ph/0307346)
[574] Harlander R and Steinhauser M 2003 Effects of SUSY-QCD in hadronic Higgs production at next-to-next-to-leading order *Phys. Rev.* D **68** 111701 (*Preprint* hep-ph/0308210)
[575] Harlander R V and Steinhauser M 2004 Supersymmetric Higgs production in gluon fusion at next-to-leading order *J. High. Energy Phys.* JHEP09(2004)066 (*Preprint* hep-ph/0409010)
[576] Harlander R V and Hofmann F 2005 Pseudo-scalar Higgs production at next-to-leading order SUSY-QCD *Preprint* hep-ph/0507041
[577] Langenegger U, Spira M, Starodumov A and Trueb P 2006 SM and MSSM Higgs boson production: spectra at large transverse momentum *Preprint* hep-ph/0604156
[578] Djouadi A and Spira M 2000 SUSY-QCD corrections to Higgs boson production at hadron colliders *Phys. Rev.* D **62** 014004 (*Preprint* hep-ph/9912476)
[579] Wu P *et al* 2005 NLO supersymmetric QCD corrections to t anti-t h0 associated production at hadron colliders *Preprint* hep-ph/0505086
[580] Dittmaier S, Kramer M and Spira M 2004 Higgs radiation off bottom quarks at the Tevatron and the LHC *Phys. Rev.* D **70** 074010 (*Preprint* hep-ph/0309204)
[581] Dawson S, Jackson C B, Reina L and Wackeroth D 2004 Exclusive Higgs boson production with bottom quarks at hadron colliders *Phys. Rev.* D **69** 074027 (*Preprint* hep-ph/0311067)
[582] Dicus D A and Willenbrock S 1989 Higgs boson production from heavy quark fusion *Phys. Rev.* D **39** 751
[583] Dicus D, Stelzer T, Sullivan Z and Willenbrock S 1999 Higgs boson production in association with bottom quarks at next-to-leading order *Phys. Rev.* D **59** 094016 (*Preprint* hep-ph/9811492)
[584] Balazs C, He H-J and Yuan C P 1999 QCD corrections to scalar production via heavy quark fusion at hadron colliders *Phys. Rev.* D **60** 114001 (*Preprint* hep-ph/9812263)
[585] Harlander R V and Kilgore W B 2003 Higgs boson production in bottom quark fusion at next-to-next-to-leading order *Phys. Rev.* D **68** 013001 (*Preprint* hep-ph/0304035)
[586] Aivazis M A G, Olness F I and Tung W-K 1994 Leptoproduction of heavy quarks. 1. General formalism and kinematics of charged current and neutral current production processes *Phys. Rev.* D **50** 3085–3101 (*Preprint* hep-ph/9312318)
[587] Aivazis M A G, Collins J C, Olness F I and Tung W-K 1994 Leptoproduction of heavy quarks. 2. A unified QCD formulation of charged and neutral current processes from fixed target to collider energies *Phys. Rev.* D **50** 3102–3118 (*Preprint* hep-ph/9312319)
[588] Campbell J *et al* 2004 Higgs boson production in association with bottom quarks *Preprint* hep-ph/0405302 Contributed to 3rd Les Houches Workshop: Physics at TeV Colliders, Les Houches, France, 26 May–6 June 2003
[589] Campbell J, Ellis R K, Maltoni F and Willenbrock S 2003 Higgs boson production in association with a single bottom quark *Phys. Rev.* D **67** 095002 (*Preprint* hep-ph/0204093)
[590] Dawson S, Jackson C B, Reina L and Wackeroth D 2005 Higgs boson production with one bottom quark jet at hadron colliders *Phys. Rev. Lett.* **94** 031802 (doi:10.1103/PhysRevLett.94.031802)
[591] Bawa A C, Kim C S and Martin A D 1990 Charged Higgs production at hadron colliders *Z. Phys.* C **47** 75–82

[592] Borzumati F, Kneur J-L and Polonsky N 1999 Higgs-strahlung and R-parity violating slepton-strahlung at hadron colliders *Phys. Rev.* D **60** 115011 (*Preprint* hep-ph/9905443)

[593] Belyaev A, Garcia D, Guasch J and Sola J 2002 Prospects for heavy supersymmetric charged Higgs boson searches at hadron colliders *J. High. Energy Phys.* JHEP06(2002)059 (*Preprint* hep-ph/0203031)

[594] Wu P *et al* 2006 NLO supersymmetric QCD corrections to the t anti-b H-associated production at hadron colliders *Phys. Rev.* D **73** 015012 (*Preprint* hep-ph/0601069) (doi:10.1103/PhysRevD.73.015012)

[595] Zhu S-H 2003 Complete next-to-leading order QCD corrections to charged Higgs boson associated production with top quark at the CERN large hadron collider *Phys. Rev.* D **67** 075006 (doi:10.1103/PhysRevD.67.075006)

[596] Plehn T Charged Higgs boson production in bottom-gluon fusion Prepared for 10th International Conference on Supersymmetry and Unification of Fundamental Interactions (SUSY02), Hamburg, Germany, 17–23 June 2002

[597] Berger E L, Han T, Jiang J and Plehn T 2005 Associated production of a top quark and a charged Higgs boson *Phys. Rev.* D **71** 115012 (*Preprint* hep-ph/0312286)

[598] Gao G, Lu G, Xiong Z and Yang J M 2002 Loop effects and non-decoupling property of SUSY QCD in $gb \to tH^-$ *Phys. Rev.* D **66** 015007 (doi:10.1103/PhysRevD.66.015007)

[599] Willenbrock S S D 1987 Pair production of supersymmetric charged Higgs bosons *Phys. Rev.* D **35** 173

[600] Krause A, Plehn T, Spira M and Zerwas P M 1998 Production of charged Higgs boson pairs in gluon–gluon collisions *Nucl. Phys.* B **519** 85–100 (*Preprint* hep-ph/9707430)

[601] Jiang Y, Han L, Ma W-G, Yu Z-H and Han M 1997 Pair production of charged Higgs bosons in gluon–gluon collisions *J. Phys.* **G23** 385–400 (*Preprint* hep-ph/9703275)

[602] Brein O and Hollik W 2000 Pair production of charged MSSM Higgs bosons by gluon fusion *Eur. Phys. J.* C **13** 175–184 (*Preprint* hep-ph/9908529)

[603] Barrientos Bendezu A A and Kniehl B A 2000 H^+H^- pair production at the large hadron collider *Nucl. Phys.* B **568** 305–318 (doi:10.1016/S0550-3213(99)00732-4)

[604] Hou H-S *et al* 2005 Pair production of charged Higgs bosons from bottom-quark fusion *Phys. Rev.* D **71** 075014 (doi:10.1103/PhysRevD.71.075014)

[605] Barrientos Bendezu A A and Kniehl B A 1999 $W^\pm H^\mp$ associated production at the large hadron collider *Phys. Rev.* D **59** 015009 (*Preprint* hep-ph/9807480) (doi:10.1103/PhysRevD.59.015009)

[606] Brein O, Hollik W and Kanemura S 2001 The MSSM prediction for $W^\pm H^\mp$ production by gluon fusion *Phys. Rev.* D **63** 095001 (*Preprint* hep-ph/0008308)

[607] Barrientos Bendezu A A and Kniehl B A 2001 Squark loop correction to $W^\pm H^\mp$ associated hadroproduction *Phys. Rev.* D **63** 015009 (*Preprint* hep-ph/0007336)

[608] Dicus D, Hewett J, Kao C and Rizzo T G 1989 $W^\pm H^\mp$ production at hadron colliders *Phys. Rev.* D **40** 787

[609] Hollik W and Zhu S-h 2002 $\mathcal{O}(\alpha_s)$ corrections to $b\bar{b} \to W^\pm H^\mp$ at the CERN large hadron collider *Phys. Rev.* D **65** 075015 (*Preprint* hep-ph/0109103) (doi:10.1103/PhysRevD.65.075015)

[610] Zhao J, Li C S and Li Q 2005 SUSY-QCD corrections to $W^\pm H^\mp$ associated production at the CERN large hadron collider *Phys. Rev.* D **72** 114008 (*Preprint* hep-ph/0509369)

[611] Lehti S 2006 Study of H/A$\to \tau\tau \to$ eμ+X in CMS *CMS Note* 2006/101

[612] Lehti S 2002 Study of $gg \to b\bar{b}H_{SUSY}$, $H_{SUSY} \to \tau\tau \to \ell\ell + X$ *CMS Note* 2002/035

[613] Bloch D private communication

[614] Boos E, Djouadi A, Muhlleitner M and Vologdin A 2002 The MSSM Higgs bosons in the intense-coupling regime *Phys. Rev.* D **66** 055004 (*Preprint* hep-ph/0205160)

[615] Boos E, Djouadi A and Nikitenko A 2004 Detection of the neutral MSSM Higgs bosons in the intense-coupling regime at the LHC *Phys. Lett.* B **578** 384–393 (*Preprint* hep-ph/0307079)

[616] CMS Collaboration, Acosta D *et al* 2006 CMS Physics Technical Design Report, Volume 1, Section 12.2.3: Combined secondary vertex tag *CERN/LHCC*, 2006-001 p 466

[617] Fernandez J 2006 Search for MSSM heavy neutral Higgs bosons in the four-b final state *CMS Note* 2006/080

[618] CMS Collaboration, Acosta D *et al* 2006 CMS Physics Technical Design Report, Volume 1, Section 12.2.6: HLT b tag *CERN/LHCC*, 2006-001 p 474

[619] CMS Collaboration, Acosta D *et al* 2006 CMS Physics Technical Design Report, Volume 1, Section 11.6.4: Parton-level corrections *CERN/LHCC*, 2006-001 p 428

[620] DØ Collaboration, Abazov V M *et al* 2005 Search for neutral supersymmetric Higgs bosons in multijet events at $\sqrt{s}$ =1.96 TeV *Phys. Rev. Lett.* **95** 151801 (doi:10.1103/PhysRevLett.95.151801)

[621] Baarmand M, Hashemi M and Nikitenko A 2006 Light Charged Higgs Discovery Potential of CMS in the $H^+ \to \tau\nu$ with single lepton trigger *CMS Note* 2006/056

[622] Roy D 1999 The hadronic tau decay signature of a heavy charged Higgs boson at LHC *Phys. Lett.* B **459** 607–614 (*Preprint* hep-ph/9905542)

[623] Kinnunen R 2004 Study of $A/H \to \tau\tau$ and $H^{\pm} \to \tau\nu$ in CMS *Czech. J. Phys.* **54** A93–A101
[624] Assamagan K A and Coadou Y 2002 The hadronic tau decay of a heavy $H^{\pm}$ in ATLAS *Acta Phys. Polon.* B **33** 707–720
[625] Baarmand M, Hashemi M and Nikitenko A 2006 Search for the heavy charged MSSM Higgs bosons with the $H^{+} \to \tau\nu$ decay mode in fully hadronic final state *CMS Note* 2006/100
[626] Roy D P 2004 Looking for the charged Higgs boson *Mod. Phys. Lett.* A **19** 1813–1828 (*Preprint* hep-ph/0406102)
[627] Alwall J and Rathsman J 2004 Improved description of charged Higgs boson production at hadron colliders *J. High Energy Phys.* JHEP12(2004)050 (*Preprint* hep-ph/0409094)
[628] Plehn T 2003 Charged Higgs boson production in bottom gluon fusion *Phys. Rev.* D **67** 014018 (*Preprint* hep-ph/0206121)
[629] Lowette S, D'Hondt J and Vanlaer P 2006 Charged MSSM Higgs boson observability in the $H^{\pm} \to tb$ Decay *CMS Note* 2006/109
[630] CMS Collaboration, Anagnostou G and Daskalakis G 2006 Search for the MSSM A → Zh decay with Z → $\ell^{+}\ell^{-}$, h → bb *CMS Note* 2006/063
[631] CMS Collaboration, Charlot C, Salerno R and Sirois Y 2006 Observability of the heavy neutral SUSY Higgs Bosons decaying into neutralinos *CMS Note* 2006/125
[632] Allanach B C *et al* 2002 The snowmass points and slopes: benchmarks for SUSY searches *Eur. Phys. J.* C **25** 113–123 (*Preprint* hep-ph/0202233)
[633] Battaglia M *et al* 2004 Updated post-WMAP benchmarks for supersymmetry *Eur. Phys. J.* C **33** 273–296 (*Preprint* hep-ph/0306219)
[634] Carena M, Heinemeyer S, Wagner C and Weiglein G 1999 Suggestions for improved benchmark scenarios for Higgs-boson searches at LEP2 *Preprint* hep-ph/9912223
[635] Carena M, Heinemeyer S, Wagner C and Weiglein G 2003 Suggestions for benchmark scenarios for MSSM Higgs boson searches at hadron colliders *Eur. Phys. J.* C **26** 601–607 (*Preprint* hep-ph/0202167)
[636] ECFA/DESY LC Physics Working Group Collaboration, Aguilar-Saavedra J A *et al* 2001 TESLA Technical Design Report Part III: Physics at an e+e- Linear Collider *Preprint* hep-ph/0106315
[637] Bennett C L *et al* 2003 First year Wilkinson Microwave Anisotropy Probe (WMAP) observations: preliminary maps and basic results *Astrophys. J. Suppl.* **148** 1 (*Preprint* astro-ph/0302207)
[638] WMAP Collaboration, Spergel D N *et al* 2003 First year Wilkinson Microwave Anisotropy Probe (WMAP) observations: determination of cosmological parameters *Astrophys. J. Suppl.* **148** 175 (*Preprint* astro-ph/0302209)
[639] Goldberg H 1983 Constraint on the photino mass from cosmology *Phys. Rev. Lett.* **50** 1419
[640] Ellis J R, Hagelin J, Nanopoulos D, Olive K A and Srednicki M 1984 Supersymmetric relics from the big bang *Nucl. Phys.* B **238** 453–476
[641] Heavy Flavor Averaging Group Collaboration, Barberio E *et al* 2006 Averages of b-hadron properties at the end of 2005 *Preprint* hep-ex/0603003
[642] Asatrian H M, Hovhannisyan A, Poghosyan V, Greub C and Hurth T 2005 Towards the NNLL precision in anti-B→X/s gamma *Preprint* hep-ph/0512097
[643] Muon Collaboration, Bennett G W 2006 Final report of the muon E821 anomalous magnetic moment measurement at BNL *Preprint* hep-ex/0602035
[644] Czarnecki A and Marciano W J 2001 The muon anomalous magnetic moment: A harbinger for 'new physics' *Phys. Rev.* D **64** 013014 (*Preprint* hep-ph/0102122)
[645] Carena M *et al* 2000 Reconciling the two-loop diagrammatic and effective field theory computations of the mass of the lightest CP-even Higgs boson in the MSSM *Nucl. Phys.* B **580** 29–57 (*Preprint* hep-ph/0001002)
[646] Randall L and Sundrum R 1999 An alternative to compactification *Phys. Rev. Lett.* **83** 4690–4693 (doi:10.1103/PhysRevLett.83.4690)
[647] Giudice G F, Rattazzi R and Wells J D 2001 Graviscalars from higher-dimensional metrics and curvature- Higgs mixing *Nucl. Phys.* B **595** 250–276 (*Preprint* hep-ph/0002178)
[648] Chaichian M, Datta A, Huitu K and Yu Z-h 2002 Radion and Higgs mixing at the LHC *Phys. Lett.* B **524** 161–169 (*Preprint* hep-ph/0110035)
[649] Hewett J L and Rizzo T G 2003 Shifts in the properties of the Higgs boson from radion mixing *J. High. Energy Phys.* JHEP08(2003)028 (*Preprint* hep-ph/0202155)
[650] Dominici D, Grzadkowski B, Gunion J F and Toharia M 2003 The scalar sector of the Randall-Sundrum model *Nucl. Phys.* B **671** 243–292 (*Preprint* hep-ph/0206192)
[651] Battaglia M, De Curtis S, De Roeck A, Dominici D and Gunion J F 2003 On the complementarity of Higgs and radion searches at LHC *Phys. Lett.* B **568** 92–102 (*Preprint* hep-ph/0304245)

[652] Azuelos G, Cavalli D, Przysiezniak H and Vacavant L 2002 Search for the radion using the ATLAS detector *Eur. Phys. J. direct* C **4** 16
[653] Dominici D, Dewhirst G, Nikitenko A, Gennai S and Fanò L 2005 Search for radion decays into Higgs boson pairs in the $\gamma\gamma b\bar{b}$, $\tau\tau b\bar{b}$ and $b\bar{b}b\bar{b}$ final states *CMS Note* 2005/007
[654] Arkani-Hamed N, Cohen A G and Georgi H 2001 (De)constructing dimensions *Phys. Rev. Lett.* **86** 4757–4761 (*Preprint* hep-th/0104005)
[655] Cheng H-C, Hill C T, Pokorski S and Wang J 2001 The standard model in the latticized bulk *Phys. Rev.* D **64** 065007 (*Preprint* hep-th/0104179)
[656] Arkani-Hamed N, Cohen A G and Georgi H 2001 Electroweak symmetry breaking from dimensional deconstruction *Phys. Lett.* B **513** 232–240 (*Preprint* hep-ph/0105239)
[657] Arkani-Hamed N, Cohen A G, Katz E and Nelson A E 2002 The littlest Higgs *J. High Energy Phys.* JHEP07(2002)034 (*Preprint* hep-ph/0206021)
[658] Schechter J and Valle J 1980 Neutrino masses in $SU(2) \times U(1)$ Theories *Phys. Rev.* D **22** 2227 (doi:10.1103/PhysRevD.22.2227)
[659] Ma E and Sarkar U 1998 Neutrino masses and leptogenesis with heavy Higgs triplets *Phys. Rev. Lett.* **80** 5716–5719 (*Preprint* hep-ph/9802445)
[660] Ma E, Raidal M and Sarkar U 2000 Verifiable model of neutrino masses from large extra dimensions *Phys. Rev. Lett.* **85** 3769–3772 (*Preprint* hep-ph/0006046)
[661] Ma E, Raidal M and Sarkar U 2001 Phenomenology of the neutrino-mass-giving Higgs triplet and the low-energy seesaw violation of lepton number *Nucl. Phys.* B **615** 313–330 (*Preprint* hep-ph/0012101)
[662] Ma E and Sarkar U 2006 Connecting dark energy to neutrinos with an observable Higgs triplet *Preprint* hep-ph/0602116
[663] Marandella G, Schappacher C and Strumia A 2005 Little-Higgs corrections to precision data after LEP2 *Phys. Rev.* D **72** 035014 (*Preprint* hep-ph/0502096)
[664] Huitu K, Maalampi J, Pietila A and Raidal M 1997 Doubly charged Higgs at LHC *Nucl. Phys.* B **487** 27–42 (*Preprint* hep-ph/9606311)
[665] Han T, Logan H E and Wang L-T 2005 Smoking-gun signatures of little Higgs models *Preprint* hep-ph/0506313
[666] Azuelos G *et al* 2005 Exploring little Higgs models with ATLAS at the LHC *Eur. Phys. J.* C **39S2** 13–24 (*Preprint* hep-ph/0402037)
[667] Gunion J F, Grifols J, Mendez A, Kayser B and Olness F I 1989 Higgs bosons in left-right symmetric models *Phys. Rev.* D **40** 1546 (doi:10.1103/PhysRevD.40.1546)
[668] Muhlleitner M and Spira M 2003 A note on doubly-charged Higgs pair production at hadron colliders *Phys. Rev.* D **68** 117701 (*Preprint* hep-ph/0305288)
[669] Bityukov S, Krasnikov N and Taperechkina V 2001 Confidence intervals for Poisson distribution parameter *Preprint* hep-ex/0108020
[670] Martin S P 1997 A supersymmetry primer *Perspectives in Supersymmetry* ed G. Kane (World Scientific) *Preprint* hep-ph/9709356
[671] CMS Collaboration Abdullin S *et al* 2002 Discovery potential for supersymmetry in CMS *J. Phys.* G **28** 469 (doi:10.1088/0954-3899/28/3/401)
[672] Paige F E, Protopopescu S D, Baer H and Tata X 2003 ISAJET 7.69: A Monte Carlo Event Generator for pp, $\bar{p}p$, and e^+e^- Reactions (*Preprint* hep-ph/0312045)
[673] De Roeck A *et al* 2005 Supersymmetric benchmarks with non-universal scalar masses or gravitino dark matter *Preprint* hep-ph/0508198
[674] de Boer W *et al* 2004 Excess of EGRET galactic gamma ray data interpreted as dark matter annihilation *Preprint* astro-ph/0408272
[675] Acosta D *et al* 2006 Potential to Discover SUSY in Events with Muons Jets and Large Missing Transverse Energy in pp Collisions at $\sqrt{s} = 14$ TeV *CMS Note* 2006/134
[676] Acosta D *et al* 2006 CMS Discovery Potential for mSUGRA in Same Sign Di-muon Events with Jets and Large Missing Transverse Energy in pp collisions at $\sqrt{s} = 14$ TeV*CMS Note*
[677] Chiorboli M, Galanti M and Tricomi A 2006 Leptons + Jets + Missing Energy analysis at LM1 *CMS Note* 2006/133
[678] Mangeol D and Goerlach U 2006 Search for $\tilde{\tau}$ production in di-tau final states and measurements of SUSY masses in mSUGRA cascade decays *CMS Note* 2006/096
[679] Bityukov S I 2005 Uncertainty, Systematics, Limits Available at http://cmsdoc.cern.ch/bityukov
[680] Kyriazopoulou S and Markou C 2006 Search for SUSY in Final States with Z Bosons *CMS Note* 2006/116
[681] Nikitenko A, Quast G and Ciulli V Minimal requirements for significance estimates of the physics resultInfo located at http://cmsdoc.cern.ch/ anikiten/cms-higgs/stat.txt

[682] Beenakker W, Hopker R and Spira M 1996 PROSPINO: A program for the PROduction of Supersymmetric Particles In Next-to-leading Order QCD *Preprint* hep-ph/9611232
[683] Allanach B C, Lester C G, Parker M A and Webber B R 2000 Measuring sparticle masses in non-universal string inspired models at the LHC *J. High. Energy Phys.* JHEP09(2000)004 (*Preprint* hep-ph/0007009)
[684] Beenakker W *et al* 1999 The production of charginos/neutralinos and sleptons at hadron colliders *Phys. Rev. Lett.* **83** 3780–3783 (doi:10.1103/PhysRevLett.83.3780)
[685] del Aguila F and Ametller L 1991 On the detectability of sleptons at large hadron colliders *Phys. Lett.* B **261** 326–333 (doi:10.1016/0370-2693(91)90336-O)
[686] Baer H, Chen C-h, Paige F and Tata X 1994 Detecting sleptons at hadron colliders and supercolliders *Phys. Rev.* D **49** 3283–3290 (*Preprint* hep-ph/9311248)
[687] Denegri D, Rurua L and Stepanov N 1996 Detection of Sleptons in CMS, Mass Reach *CMS TN* 96-059
[688] Andreev Y M, Bityukov S I and Krasnikov N V 2005 Sleptons at post-WMAP benchmark points at LHC(CMS) *Phys. Atom. Nucl.* **68** 340–347 (*Preprint* hep-ph/0402229)
[689] Bityukov S I and Krasnikov N V 1999 The search for sleptons and lepton-flavor-number violation at LHC (CMS) *Phys. Atom. Nucl.* **62** 1213–1225 (*Preprint* hep-ph/9712358)
[690] Krasnikov N 1994 Flavor lepton number violation at LEP-2 *Mod. Phys. Lett.* A **9** 791–794
[691] Arkani-Hamed N, Cheng H-C, Feng J L and Hall L J 1996 Probing lepton flavor violation at future colliders *Phys. Rev. Lett.* **77** 1937–1940 (*Preprint* hep-ph/9603431) (doi:10.1103/PhysRevLett.77.1937)
[692] Krasnikov N V 1997 Search for flavor lepton number violation in slepton decays at LHC *JETP Lett.* **65** 148 (doi:10.1134/1.567315)
[693] Agashe K and Graesser M 2000 Signals of supersymmetric lepton flavor violation at the LHC *Phys. Rev.* D **61** 075008 (*Preprint* hep-ph/9904422)
[694] Hisano J, Kitano R and Nojiri M M 2002 Flavor mixing in slepton production at the large hadron collider *Phys. Rev.* D **65** 116002
[695] Baer H, Chen C-h, Paige F and Tata X 1994 Trileptons from chargino - neutralino production at the CERN Large Hadron Collider *Phys. Rev.* D **50** 4508–4516 (*Preprint* hep-ph/9404212) (doi:10.1103/PhysRevD.50.4508)
[696] Ellis J R, Olive K A and Santoso Y 2002 The MSSM parameter space with non-universal Higgs masses *Phys. Lett.* B **539** 107–118 (*Preprint* hep-ph/0204192)
[697] Altarelli G, Mele B and Ruiz-Altaba M 1989 Searching for new heavy vector bosons in $p\bar{p}$ colliders *Z. Phys.* C **45** 109 (doi:10.1007/BF01556677)
[698] Arkani-Hamed N, Dimopoulos S and Dvali G R 1998 The hierarchy problem and new dimensions at a millimeter *Phys. Lett.* B **429** 263–272 (*Preprint* hep-ph/9803315)
[699] Lykken J D, Poppitz E and Trivedi S P 1999 Branes with GUTs and supersymmetry breaking *Nucl. Phys.* B **543** 105–121 (*Preprint* hep-th/9806080)
[700] Antoniadis I 1990 A possible new dimension at a few TeV *Phys. Lett.* B **246** 377–384 (doi:10.1016/0370-2693(90)90617-F)
[701] Lykken J D 1996 Weak scale superstrings *Phys. Rev.* D **54** 3693–3697 (*Preprint* hep-th/9603133) (doi:10.1103/PhysRevD.54.R3693)
[702] Giudice G F, Rattazzi R and Wells J D 1999 Quantum gravity and extra dimensions at high-energy colliders *Nucl. Phys.* B **544** 3–38 (*Preprint* hep-ph/9811291)
[703] Han T, Lykken J D and Zhang R-J 1999 On Kaluza-Klein states from large extra dimensions *Phys. Rev.* D **59** 105006 (*Preprint* hep-ph/9811350) (doi:10.1103/PhysRevD.59.105006)
[704] Cullen S, Perelstein M and Peskin M E 2000 TeV strings and collider probes of large extra dimensions *Phys. Rev.* D **62** 055012 (*Preprint* hep-ph/0001166)
[705] Lykken J D and Randall L 2000 The shape of gravity *J. High. Energy Phys.* JHEP06(2000)014 (*Preprint* hep-th/9908076)
[706] Vacavant L and Hinchliffe I 2001 Signals of models with large extra dimensions in ATLAS *J. Phys.* G **27** 1839–1850
[707] Ruppert J, Rahmede C and Bleicher M 2005 Determination of the fundamental scale of gravity and the number of space-time dimensions from high energetic particle interactions *Phys. Lett.* B **608** 240–243 (*Preprint* hep-ph/0501028)
[708] Dudas E and Mourad J 2000 String theory predictions for future accelerators *Nucl. Phys.* B **575** 3–34 (doi:10.1016/S0550-3213(00)00082-1)
[709] Chialva D, Iengo R and Russo J G 2005 Cross sections for production of closed superstrings at high energy colliders in brane world models *Phys. Rev.* D **71** 106009 (*Preprint* hep-ph/0503125)
[710] Bando M, Kugo T, Noguchi T and Yoshioka K 1999 Brane fluctuation and suppression of Kaluza-Klein mode couplings *Phys. Rev. Lett.* **83** 3601–3604 (doi:10.1103/PhysRevLett.83.3601)

[711] Hewett J L 1999 Indirect collider signals for extra dimensions *Phys. Rev. Lett.* **82** 4765–4768 (doi:10.1103/PhysRevLett.82.4765)
[712] Davoudiasl H, Hewett J L and Rizzo T G 2000 Phenomenology of the Randall-Sundrum gauge hierarchy model *Phys. Rev. Lett.* **84** 2080 (doi:10.1103/PhysRevLett.84.2080)
[713] Hewett J and Spiropulu M 2002 Particle physics probes of extra spacetime dimensions *Ann. Rev. Nucl. Part. Sci.* **52** 397–424 (doi:10.1146/annurev.nucl.52.050102.090706)
[714] Clerbaux B, Mahmoud T, Collard C and Miné P 2006 Search with the CMS detector for heavy resonances decaying into an electron pair *CMS Note* 2006/083
[715] Collard C and Lemaire M-C 2004 Search with the CMS Detector for Randall-Sundrum Excitations of Gravitons Decaying Into Electron Pairs *CMS Note* 2004/024
[716] CMS Collaboration, Acosta D *et al* 2006 CMS Physics Technical Design Report Volume 1, Section 10 *CERN/LHCC*, 2006-001
[717] Clerbaux B, Mahmoud T, Collard C, Lemaire M-C and Litvin V 2006 TeV electron and photon saturation studies *CMS Note* 2006/004
[718] CDF Collaboration, Affolder T *et al* 2001 Measurement of ds/dM and Forward-Backward charge asymmetry for high-mass Drell–Yan e $^{+}$e $^{-}$ pairs from collisions at $\sqrt{s} = 1.8$ TeV *Phys. Rev. Lett.* **87** 131802
[719] CTEQ Collaboration, Lai H L *et al* 2000 Global QCD analysis of parton structure of the nucleon: CTEQ5 parton distributions *Eur. Phys. J.* C **12** 375–392 (doi:10.1007/s100529900196)
[720] CTEQ Collaboration, Stump D *et al* 2003 Inclusive jet production, parton distributions, and the search for new physics *J. High. Energy Phys.* JHEP0310(2003)046 (*Preprint* hep-ph/0303013)
[721] Davoudiasl H, Hewett J L and Rizzo T G 2001 Experimental probes of localized gravity: on and off the wall *Phys. Rev.* D **63** 075004 (*Preprint* hep-ph/0006041)
[722] Cheung K-m and Landsberg G 2000 Drell–Yan and diphoton production at hadron colliders and low scale gravity model *Phys. Rev.* D **62** 076003 (*Preprint* hep-ph/9909218)
[723] Belotelov I, Golutvin I, Bourilkov D, Lanyov A, Rogalev E, Savina M and Shmatov S 2006 Search for ADD extra dimensional gravity in di-muon channel with the CMS Detector *CMS Note* 2006/076
[724] Mohapatra R and Pati J 1975 Left-right gauge symmetry and an 'isoconjugate' model of CP violation *Phys. Rev.* D **11** 566–571 (doi:10.1103/PhysRevD.11.566)
[725] Senjanovic G and Mohapatra R 1975 Exact left-right symmetry and spontaneous violation of parity *Phys. Rev.* D **12** 1502 (doi:10.1103/PhysRevD.12.1502)
[726] Mohapatra R and Senjanovic G 1980 Neutrino mass and spontaneous parity nonconservation *Phys. Rev. Lett.* **44** 912 (doi:10.1103/PhysRevLett.44.912)
[727] Pati J and Salam A 1974 Lepton number as the fourth color *Phys. Rev.* D **10** 275–289
[728] CDF Collaboration, Affolder T *et al* 2001 Search for quark lepton compositeness and a heavy W' boson using the e nu channel in p anti-p collisions at s $^{**}(1/2) = 1.8$-TeV *Phys. Rev. Lett.* **87** 231803 (*Preprint* hep-ex/0107008)
[729] Hof C, Hebbeker T and Hoepfner K 2006 Detection of New Heavy Charged Gauge Bosons in the Muon Plus Neutrino Channel *CMS Note* 2006/117
[730] Gumus K, Akchurin N, Esen S and Harris R M 2006 CMS sensitivity to dijet resonances *CMS Note* 2006/070
[731] Baur U, Hinchliffe I and Zeppenfeld D 1987 Excited quark production at Hadron colliders *Int. J. Mod. Phys.* A **2** 1285
[732] Bagger J, Schmidt C and King S 1988 Axigluon production in hadronic collisions *Phys. Rev.* D **37** 1188
[733] Chivukula R S, Cohen A G and Simmons E H 1996 New strong interactions at the Tevatron? *Phys. Lett.* B **380** 92–98 (*Preprint* hep-ph/9603311)
[734] Hewett J L and Rizzo T G 1989 Low-energy phenomenology of superstring inspired E(6) models *Phys. Rept.* **183** 193
[735] Lane K and Mrenna S 2003 The collider phenomenology of technihadrons in the technicolor Straw man model *Phys. Rev.* D **67** 115011 (doi:10.1103/PhysRevD.67.115011)
[736] Eichten E, Hinchliffe I, Lane K D and Quigg C 1984 Super collider physics *Rev. Mod. Phys.* **56** 579–707
[737] CMS Collaboration, Lemaire M-C, Newman H and Litvin V 2006 Search for Randall-Sundrum excitations of gravitons decaying into two photons for CMS at LHC *CMS Note* 2006/051
[738] CMS Collaboration, Clerbaux B, Mahmoud T, Collard C, Lemaire M-C and Litvin V 2006 TeV electron and photon saturation studies *CMS Note* 2006/004
[739] Acosta D *et al* 2005 Measurement of the Cross Section for Prompt Diphoton Production in $p\bar{p}$ Collisions at $\sqrt{s} = 1.96$ TeV *Phys. Rev. Lett.* **95** 022003 (doi:10.1103/PhysRevLett.95.022003)
[740] Weng J *et al* 2006 Search for ADD Direct Graviton Emission in Photon plus Missing Transverse Energy Final States at CMS *CMS Note* 2006/129
[741] Myers R C and Perry M J 1986 Black holes in higher dimensional space-times *Ann. Phys.* **172** 304

[742] Hawking S W 1975 Particle creation by black holes *Commun. Math. Phys.* **43** 199–220
[743] Argyres P C, Dimopoulos S and March-Russell J 1998 Black holes and sub-millimeter dimensions *Phys. Lett.* B **441** 96–104 (*Preprint* hep-th/9808138)
[744] Harris C M, Richardson P and Webber B R 2003 CHARYBDIS: A black hole event generator *J. High. Energy Phys.* JHEP08(2003)033 (*Preprint* hep-ph/0307305)
[745] Mathews P, Ravindran V and Sridhar K 2005 NLO-QCD corrections to dilepton production in the Randall-Sundrum model *J. High. Energy Phys.* JHEP10(2005)031 (*Preprint* hep-ph/0506158)
[746] Lane K D 2000 Technicolor 2000 *Preprint* hep-ph/0007304
[747] Kreuzer P 2006 Search for Technicolour at CMS in the $\rho_{TC} \to WZ$ channel *CMS Note* 2006/135
[748] Betev B, Bourilkov D and Mavrodiev S. Shch Structure functions of pion and nucleon determined from high mass muon pair production JINR-E2-85-312
[749] Super-Kamiokande Collaboration, Fukuda Y *et al* 1998 Evidence for oscillation of atmospheric neutrinos *Phys. Rev. Lett.* **81** 1562–1567 (*Preprint* hep-ex/9807003)
[750] Esen S and Harris R 2006 CMS sensitivity to quark contact interactions using dijets *CMS Note* 2006/071
[751] Pati J C and Salam A 1975 Anomalous lepton-hadron interactions and gauge models *Phys. Rev.* D **11** 1137–1154 (doi:10.1103/PhysRevD.11.1137)
[752] CMS Collaboration, Gninenko N, Kirsanov M, Krasnikov N and Matveev N 2006 Detection of Heavy Majorana Neutrinos and Right-Handed Bosons *CMS Note* 2006/098
[753] Particle Data Group, Hagiwara K *et al* 2002 Review of Particle Physics *Phys. Rev.* D **66** 010001
[754] Barenboim G, Bernabeu J, Prades J and Raidal M 1997 Constraints on the W(R) mass and CP-violation in left-right models *Phys. Rev.* D **55** 4213–4221 (*Preprint* hep-ph/9611347)
[755] DØ Collaboration, Abachi S *et al* 1996 Search for right-handed W bosons and heavy W' in $p\bar{p}$ collisions at $\sqrt{s}$ =1.8 TeV *Phys. Rev. Lett.* **76** 3271–3276 (*Preprint* hep-ex/9512007)
[756] Datta A, Guchait M and Roy D P 1993 Prospect of heavy right-handed neutrino search at SSC/LHC energies *Phys. Rev.* D **47** 961–966 (*Preprint* hep-ph/9208228)
[757] CMS Collaboration, Karafasoulis K, Kyriakis A, Petrakou H and Mazumdar K 2006 Little Higgs model and top-like heavy quark at CMS *CMS Note* 2006/079
[758] D'Hondt J, Lowette S, Hammad G, Heyninck J and Van Mulders P 2006 Observability of same-charge lepton topology in di-leptonic ttbar events *CMS Note* 2006/065
[759] Larios F and Penunuri F 2004 FCNC production of same sign top quark pairs at the LHC *J. Phys.* G **30** 895–904 (*Preprint* hep-ph/0311056)
[760] Gouz Y P and Slabospitsky S R 1999 Double top production at hadronic colliders *Phys. Lett.* B **457** 177–185 (doi:10.1016/S0370-2693(99)00516-X)
[761] Yue C-X, Zong Z-J, Xu L-L and Chen J-X 2006 Associated production of the top-pions and single top at hadron colliders *Phys. Rev.* D **73** 015006 (*Preprint* hep-ph/0601058)
[762] Kraml S and Raklev A R 2006 Same-sign top quarks as signature of light stops at the LHC *Phys. Rev.* D **73** 075002 (*Preprint* hep-ph/0512284)
[763] Bityukov S I and Krasnikov N V 2000 On the observability of a signal above background *Nucl. Instrum. and Methods* A **452** 518–524 (doi:10.1016/S0168-9002(00)00454-X)
[764] Lehmann E L 1957 A theory of some multiple decision problems *The Annals of Mathematical Statistics* **28 1**
[765] O'Neill R and Wetherill G B 1971 The present state of multiple comparison methods *Journal of the Royal Statistical Society, Series B (Methodological)* **33 2**
[766] Hauser J 2006 Search for new physics in tails of distributionsPrivate communications, paper in preparation
[767] DØ Collaboration, Abazov V M *et al* 2005 Measurement of the $t\bar{t}$ production cross section in $p\bar{p}$ collisions at $\sqrt{s} = 1.96$ TeV using kinematic characteristics of lepton + jets events *Phys. Lett.* B **626** 45–54 (*Preprint* hep-ex/0504043) (doi:10.1016/j.physletb.2005.08.104)
[768] Abbott B *et al* 2000 Search for New physics in $e\mu X$ data at DØ Using Sleuth: a quasi-model-independent search strategy for new physics *Phys. Rev.* D **62** (doi:10.1103/PhysRevD.62.092004)
[769] Abbott B *et al* 2001 A Quasi-Model-Independent search for new physics at large transverse momentum *Phys. Rev.* D **64** (*Preprint* hep-ex/0011067)
[770] Finley C *et al* 2004 On the evidence for clustering in the arrival directions of AGASA's ultrahigh energy cosmic rays *Astroparticle Physics* **21**
[771] Frixione S, Nason P and Webber B R 2003 Matching NLO QCD and parton showers in heavy flavour production *J. High. Energy Phys.* JHEP08(2003)007 (*Preprint* hep-ph/0305252)
[772] Lonnblad L 2002 Correcting the colour-dipole cascade model with fixed order matrix elements *J. High. Energy Phys.* JHEP05(2002)046 (*Preprint* hep-ph/0112284)
[773] Frixione S and Webber B R 2002 Matching NLO QCD computations and parton shower simulations *J. High. Energy Phys.* JHEP06(2002)029 (*Preprint* hep-ph/0204244)

[774] Krauss F 2002 Matrix elements and parton showers in hadronic interactions *J. High. Energy Phys.* JHEP08(2002)015 (*Preprint* hep-ph/0205283)

[775] Mrenna S and Richardson P 2004 Matching matrix elements and parton showers with HERWIG and PYTHIA *J. High. Energy Phys.* JHEP05(2004)040 (*Preprint* hep-ph/0312274)

[776] Butterworth J, Butterworth S, Waugh B, Stirling W and Whalley M 2004 The CEDAR project *Preprint* hep-ph/0412139

[777] LEP Collaboration, 2004 A combination of preliminary electroweak measurements and constraints on the standard model *Preprint* hep-ex/0412015

[778] Stump D R 2002 A new generation of CTEQ parton distribution functions with uncertainty analysis Prepared for 31st International Conference on High Energy Physics (ICHEP 2002), (*Amsterdam, The Netherlands, 24–31 July 2002*)

[779] Stirling W J, Martin A D, Roberts R G and Thorne R S 2005 MRST parton distributions *AIP Conf. Proc.* **747** 16–21

[780] Botje M 2000 A QCD analysis of HERA and fixed target structure function data *Eur. Phys. J.* C **14** 285–297 (*Preprint* hep-ph/9912439)

[781] Alekhin S I 2001 Global fit to the charged leptons DIS data: alpha(s), parton distributions, and high twists *Phys. Rev.* D **63** 094022 (*Preprint* hep-ph/0011002)

[782] Altarelli G and Parisi G 1977 Asymptotic freedom in parton language *Nucl. Phys.* B **126** 298

[783] Lonnblad L 1992 ARIADNE version 4: A program for simulation of QCD cascades implementing the color dipole model *Comput. Phys. Commun.* **71** 15–31

[784] CDF Collaboration, Abe F *et al* 1994 Evidence for color coherence in $p\bar{p}$ collisions at $\sqrt{s} = 1.8$ TeV *Phys. Rev.* D **50** 5562–5579 (doi:10.1103/PhysRevD.50.5562)

[785] DØ Collaboration, Abbott B *et al* 1997 Color coherent radiation in multijet events from $p\bar{p}$ collisions at $\sqrt{s} = 1.8$ TeV *Phys. Lett.* B **414** 419–427 (doi:10.1016/S0370-2693(97)01190-8)

[786] Knowles I G *et al* 1995 QCD event generators *Preprint* hep-ph/9601212

[787] ALEPH Collaboration, Buskulic D *et al* 1992 Properties of hadronic Z decays and test of QCD generators *Z. Phys.* C **55** 209–234

[788] DELPHI Collaboration, Abreu P *et al* 1996 Tuning and test of fragmentation models based on identified particles and precision event shape data *Z. Phys.* C **73** 11–60 (doi:10.1007/s002880050295)

[789] OPAL Collaboration, Alexander G *et al* 1996 A Comparison of b and (u d s) quark jets to gluon jets *Z. Phys.* C **69** 543–560

[790] Andersson B, Gustafson G and Soderberg B 1983 A general model for jet fragmentation *Z. Phys.* C **20** 317

[791] ALEPH Collaboration, Heister A *et al* 2001 Study of the fragmentation of b quarks into B mesons at the Z peak *Phys. Lett.* B **512** 30–48 (*Preprint* hep-ex/0106051)

[792] OPAL Collaboration, Abbiendi G *et al* 2003 Inclusive analysis of the b quark fragmentation function in Z decays at LEP ((B)) *Eur. Phys. J.* C **29** 463–478 (*Preprint* hep-ex/0210031)

[793] SLD Collaboration, Abe K *et al* 2002 Measurement of the b-quark fragmentation function in Z^0 decays *Phys. Rev.* D **65** 092006 (doi:10.1103/PhysRevD.65.092006)

[794] Bowler M G 1981 e+ e- Production of heavy quarks in the String Model *Zeit. Phys.* C **11** 169

[795] Peterson C, Schlatter D, Schmitt I and Zerwas P M 1983 Scaling violations in inclusive e^+e^- annihilation spectra *Phys. Rev.* D **27** 105

[796] Kartvelishvili V, Likhoded A and Petrov V 1978 On the fragmentation functions of heavy quarks into hadrons *Phys. Lett.* B **78** 615

[797] Norrbin E and Sjostrand T 2000 Production and hadronization of heavy quarks *Eur. Phys. J.* C **17** 137–161 (*Preprint* hep-ph/0005110)

[798] Engel R and Ranft J 1999 Color singlet exchange between jets and the PHOJET Monte Carlo *Nucl. Phys. Proc. Suppl.* A **75** 272–274 (doi:10.1016/S0920-5632(99)00263-7)

[799] CDF Collaboration, Affolder T *et al* 2002 Charged jet evolution and the underlying event in proton anti-proton collisions at 1.8 TeV *Phys. Rev.* D **65** 092009 (doi:10.1103/PhysRevD.65.092009)

[800] Nason P *et al* 1999 Bottom production *Preprint* hep-ph/0003142

[801] Sjostrand T and Skands P Z 2005 Transverse-momentum-ordered showers and interleaved multiple interactions *Eur. Phys. J.* C **39** 129–154 (*Preprint* hep-ph/0408302) (doi:10.1140/epjc/s2004-02084-y)

[802] Sapeta S and Golec-Biernat K 2005 Total, elastic and diffractive cross sections at LHC in the Miettinen-Pumplin model *Phys. Lett.* B **613** 154–161 (*Preprint* hep-ph/0502229)

[803] Lange D J 2001 The EvtGen particle decay simulation package *Nucl. Instrum. Methods* A **462** 152–155

[804] Bartalini P 2005 Supporting Monte Carlo Generators at the LHC *Proceedings of the 10th International Conference on B-Physics at Hadron Machines* (Assisi Perugia, Italy June, 2005) ed M Biasini and S Erhan volume 156, *Published in Nucl. Phys B - Proceedings Supplements 1* (doi:10.1016/j.nuclphysbps.2006.02.123)
[805] Sullivan Z 2002 Fully differential W production and decay at next-to- leading order in QCD *Phys. Rev.* D **66** 075011 (*Preprint* hep-ph/0207290)
[806] Dobbs M A *et al* 2004 Les Houches guidebook to Monte Carlo generators for hadron collider physics *Preprint* hep-ph/0403045
[807] HIJING Web Site Located at http://www-nsdth.lbl.gov/ xnwang/hijing/index.html
[808] Gleisberg T *et al* 2005 Event generator for the LHC *Preprint* hep-ph/0508315
[809] Boos E *et al* 2001 Generic user process interface for event generators *Preprint* hep-ph/0109068
[810] Lokhtin I P and Snigirev A M 2000 Nuclear geometry of jet quenching *Eur. Phys. J.* C **16** 527–536 (*Preprint* hep-ph/0004176) (doi:10.1007/s100520000437)
[811] Lokhtin I P and Snigirev A M 2004 Fast simulation of jet quenching in ultrarelativistic heavy ion collisions SINP MSU-13/752 *Preprint* hep-ph/0406038
[812] Lokhtin I P and Snigirev A M 2003 Fast simulation of flow effects in central and semi-central heavy ion collisions at LHC *Preprint* hep-ph/0312204
[813] CDF Collaboration, Field R D 2001 The underlying event in hard scattering processes *eConf* C **010630** P501 (*Preprint* hep-ph/0201192)
[814] CompHEP Collaboration, Boos E, Bunichev V, Dubinin M, Dudko L, Edneral V, Ilyin V, Kryukov A, Savrin V, Semenov A and Sherstnev A 2004 Web site at http://theory.sinp.msu.ru/comphep. See also [355]
[815] Lokhtin I P, Sarycheva L I and Snigirev A M 2002 The method for analysing jet azimuthal anisotropy in ultrarelativistic heavy ion collisions *Phys. Lett.* B **537** 261–267 (*Preprint* hep-ph/0203144) (doi:10.1016/S0370-2693(02)01913-5)
[816] Carena M, Daleo A, Dobrescu B A and Tait T M P 2004 Z' gauge bosons at the Tevatron *Phys. Rev.* D **70** 093009 (doi:10.1103/PhysRevD.70.093009)
[817] Balazs C, Qiu J-w and Yuan C P 1995 Effects of QCD resummation on distributions of leptons from the decay of electroweak vector bosons *Phys. Lett.* B **355** 548–554 (doi:10.1016/0370-2693(95)00726-2)
[818] Balazs C and Yuan C P 1997 Soft gluon effects on lepton pairs at hadron colliders *Phys. Rev.* D **56** 5558–5583 (doi:10.1103/PhysRevD.56.5558)
[819] Martin A D, Roberts R G, Stirling W J and Thorne R S 2003 Uncertainties of predictions from parton distributions I: Experimental errors *Eur. Phys. J.* C **28** 455–473 (*Preprint* hep-ph/0211080)
[820] Holland J H 1975 Adaptation in natural and artificial systems (The University of Michigan Press, Ann Arbor)
[821] Goldberg D E 1989 Genetic algorithms in search, optimization and machine learning (Addison: Wesley)
[822] Abdullin S 2003 Genetic algorithm for SUSY trigger optimization in CMS detector at LHC *NIM A* **502** 693–695 (doi:10.1016/S0168-9002(03)00546-1)
[823] TOTEM Collaboration, 2004 TOTEM Technical Design Report *CERN/LHCC*, 2004-002
[824] TOTEM Collaboration, 2004 Addendum to the TOTEM-TDR *CERN/LHCC*, 2004-020
[825] Avati V and Österberg K 2005 TOTEM forward measurements: leading proton acceptance *Proceedings of the HERA-LHC Workshop* (CERN/DESY: January, 2005) Available at http://www.desy.de/ heralhc/proceedings/wg4avati.pdf
[826] Kalliopuska J *et al* 2005 TOTEM forward measurements: exclusive central diffraction *Proceedings of the HERA-LHC Workshop* (CERN/DESY: January, 2005) Available at http://www.desy.de/ heralhc/proceedings/wg4pXp_heralhc.pdf
[827] The MAD-X Program, Methodical Accelerator Design Information available at http://www.cern.ch/mad
[828] Arneodo M *et al* 2005 Diffractive Higgs: CMS/TOTEM Level-1 Trigger Studies *Proceedings of the HERA-LHC Workshop* (CERN/DESY: January, 2005) Available at http://www.desy.de/ heralhc/proceedings/wg4arneodo.pdf
[829] Croft R 2006 (In preparation) PhD Thesis, University of Bristol
[830] Oljemark F 2006 First level triggering of diffractively produced low-mass Higgs at The Large Hadron Collider, University of Helsinki
[831] Bruni G *et al* 2005 Leading proton production in ep and pp, experiments: how well do high-energy physics Monte Carlos reproduce the data? *Proceedings of the HERA-LHC Workshop* (CERN/DESY: January, 2005) Available at http://www.desy.de/ heralhc/proceedings/wg5lps.pdf
[832] Ferro F 2005 Diffractive Higgs in CMS/TOTEM: study of L1 trigger conditions from T1 and T2 *TOTEM Note* **04-2005**
[833] Cox B and Forshaw J 2002 Herwig for diffractive interactions *Comput. Phys. Commun.* **144** 104–110 (doi:10.1016/S0010-4655(01)00467-2)

[834] Collins J C 1997 Light-cone variables, rapidity and all that *Preprint* hep-ph/9705393
[835] Albrow M G and Rostovtsev A 2000 Searching for the Higgs at hadron colliders using the missing mass method *Preprint* hep-ph/0009336
[836] Albrow M G 2005 Double pomeron physics at the LHC *AIP Conf. Proc.* **792** 509–514 (*Preprint* hep-ex/0507095)

Colour plates CP1–CP9

Various figures are in colour throughout the online edition but only plates CP1–CP9 are in colour in both the print and online editions.

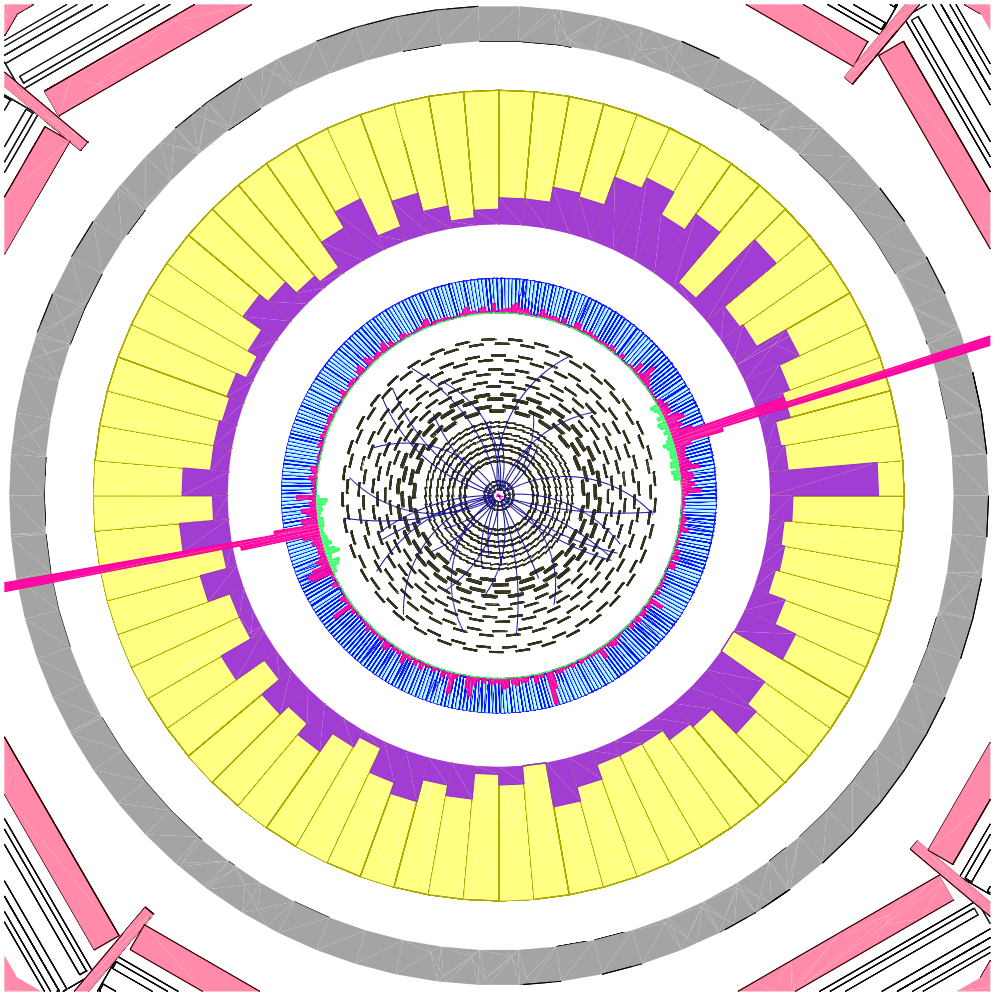

Figure CP1. Example of a $pp \to H + X$ event with Higgs particle decay $H \to \gamma\gamma$. (See section 2.1.)

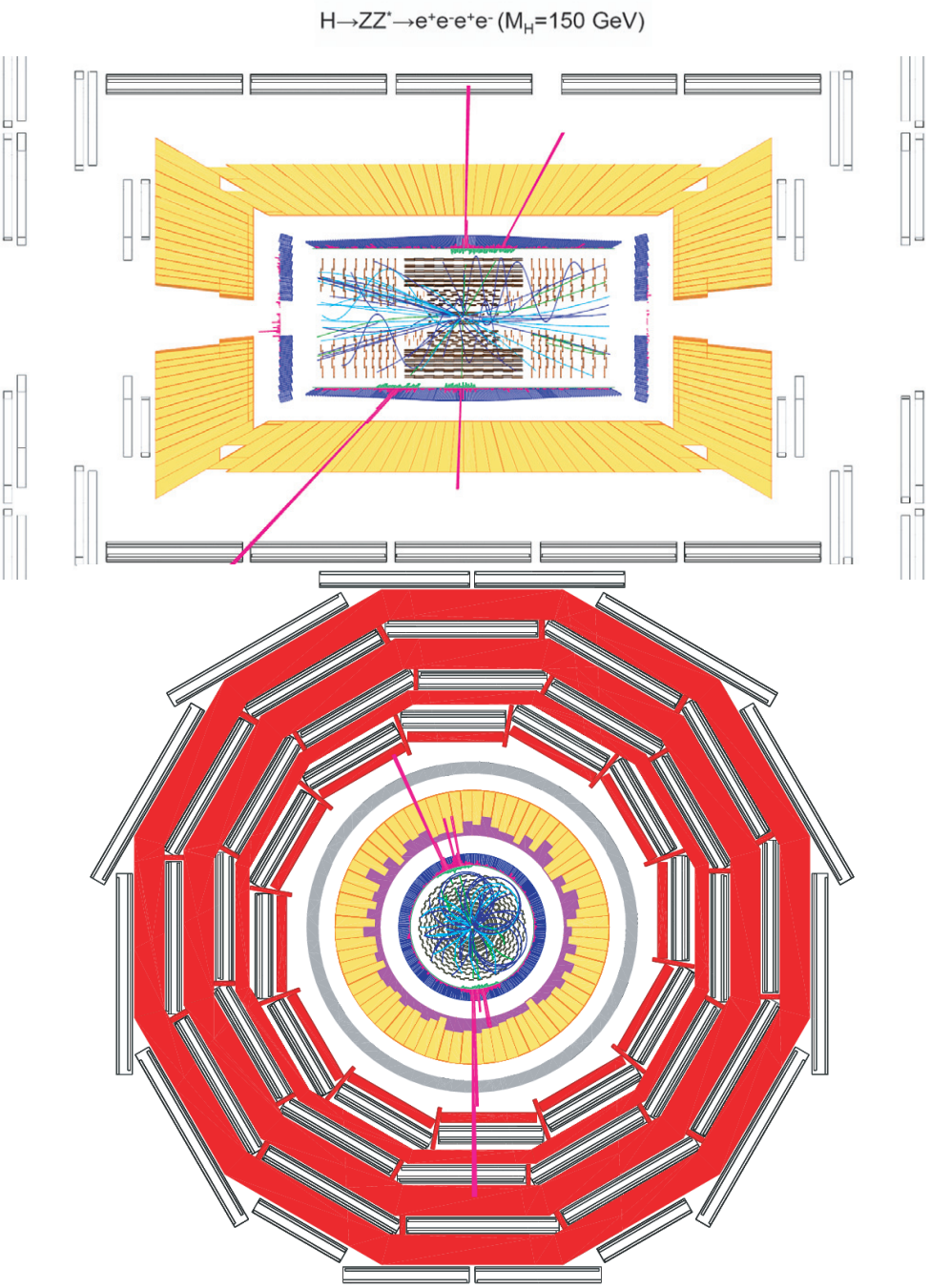

Figure CP2. Display of an event candidate in the CMS detector at the LHC for the Standard Model Higgs boson decay channel $H \rightarrow ZZ^* \rightarrow 4e$. The event is shown in a longitudinal (top) and transversal (bottom) projection of the detector. A mass of $150\,GeV/c^2$ is measured from the reconstructed electrons. (See section 2.2.)

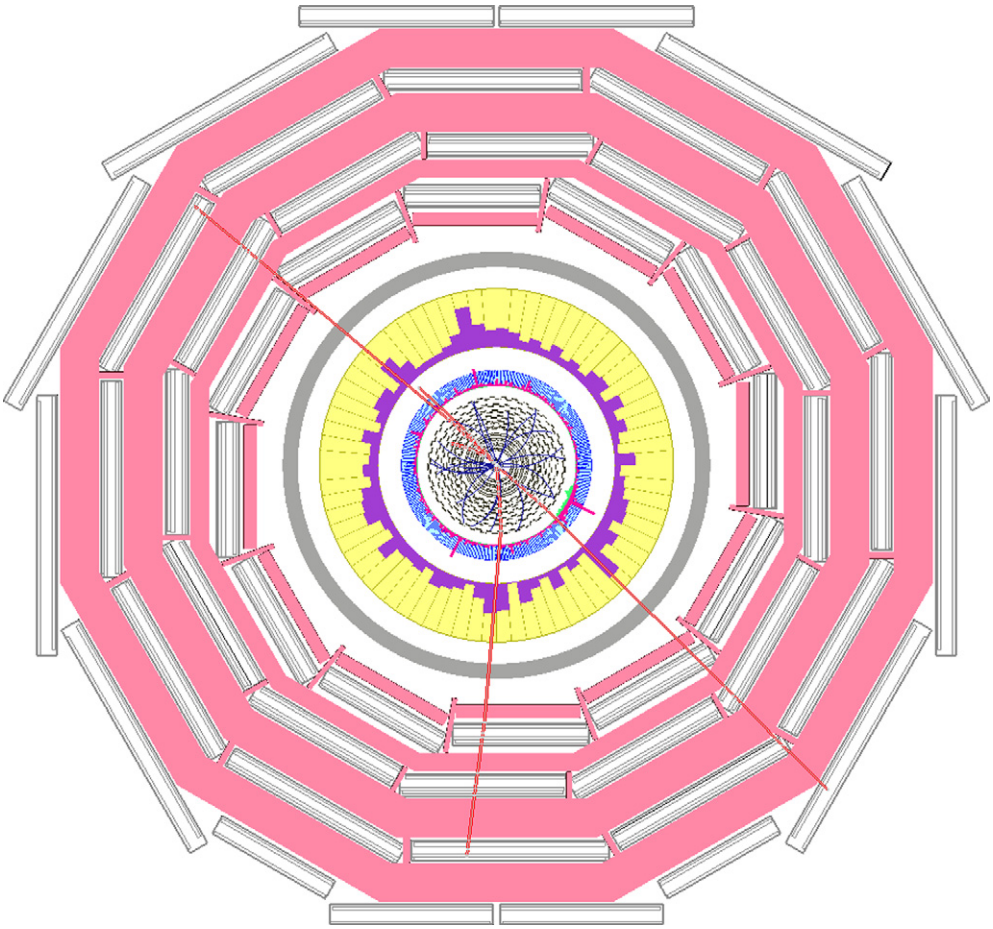

Figure CP3. Example of a $H \rightarrow ZZ \rightarrow 4\mu$ event showing only the reconstructed tracks. One muon goes in the endcap detectors. (See section 3.1.1.)

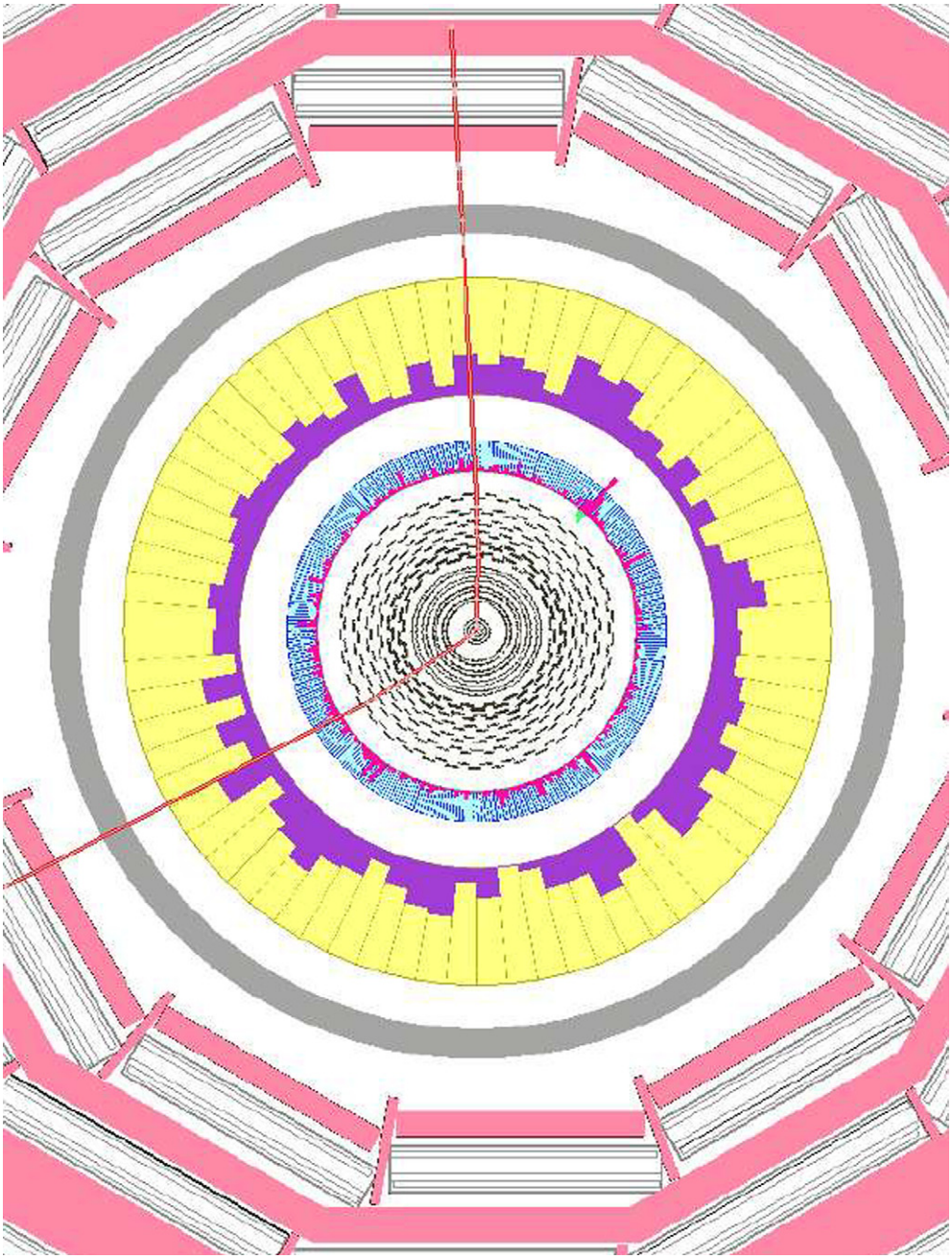

Figure CP4. Example of a pp $\rightarrow$ H + X event with H $\rightarrow$ WW $\rightarrow \mu\nu\mu\nu$. (See section 3.2.2.1.)

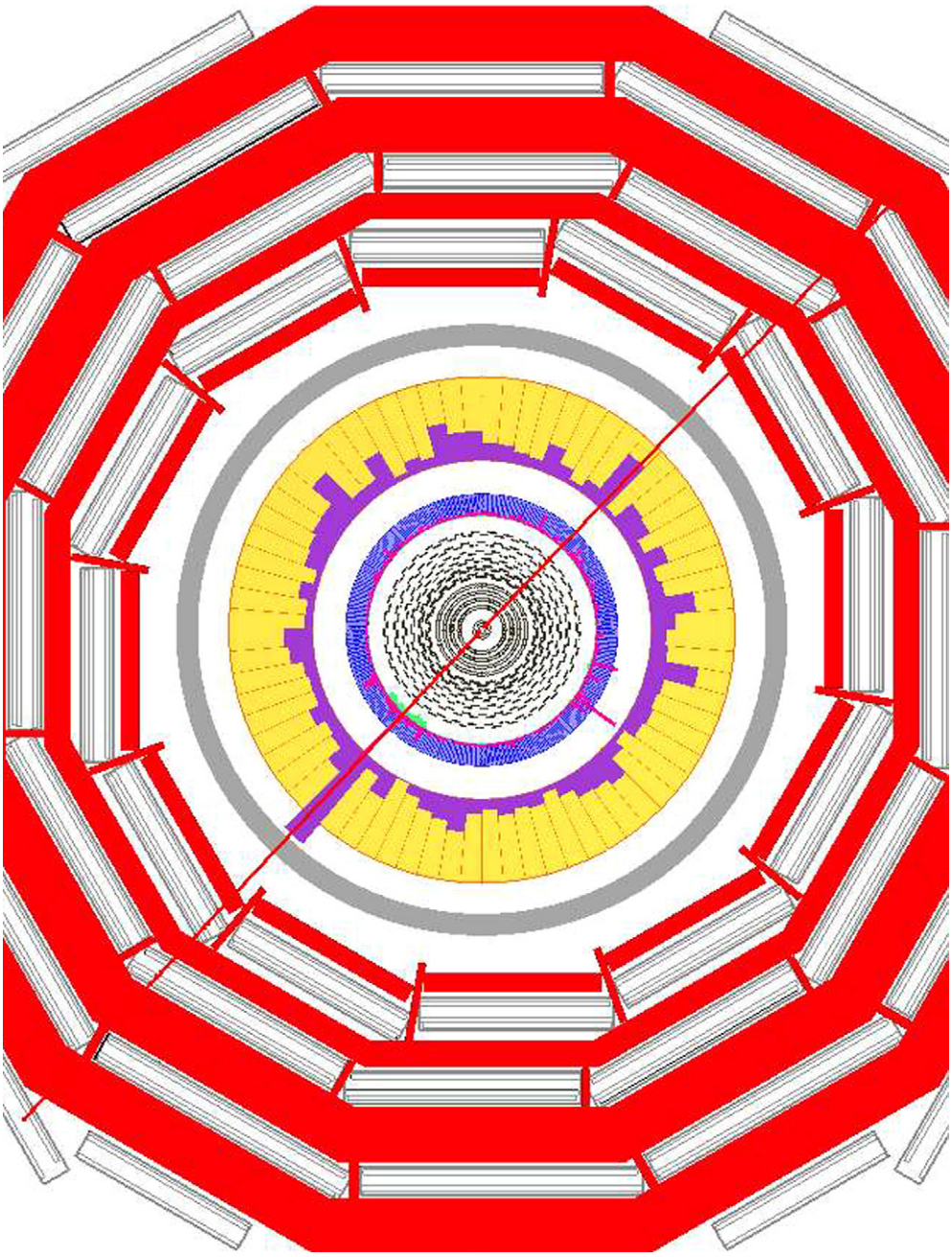

Figure CP5. Typical simulated event of a dimuon decay of $3\,\mathrm{TeV}/c^2$ Z' produced at $\mathcal{L} = 2 \times 10^{33}\,\mathrm{cm}^{-2}\,\mathrm{s}^{-1}$, showing the muon tracks only. (See section 3.3.1.)

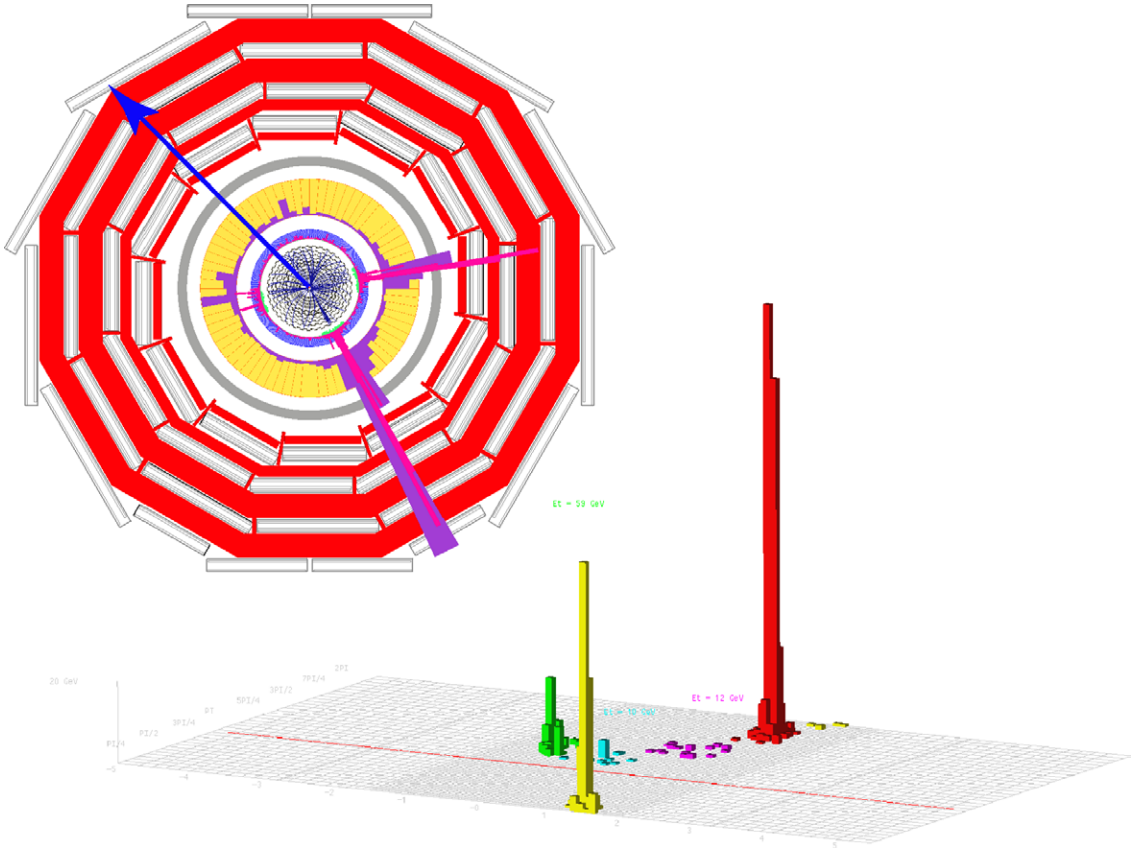

Figure CP6. Event display of SUSY candidate event that survives the requirements of the multijet + missing energy analysis of section 13.5. The three highest E_{T} jets are 330, 140 and 60 GeV while the missing transverse energy is 360 GeV. The Lego $\eta - \phi$ calorimeter display shows the three leading jets, colour coded red-yellow-green, while the missing energy ϕ is indicated with the red line. The transverse $x - y$ view shows relative depositions of the jets in the calorimeter systems as well as the reconstructed tracks and the missing energy vector direction (in blue).

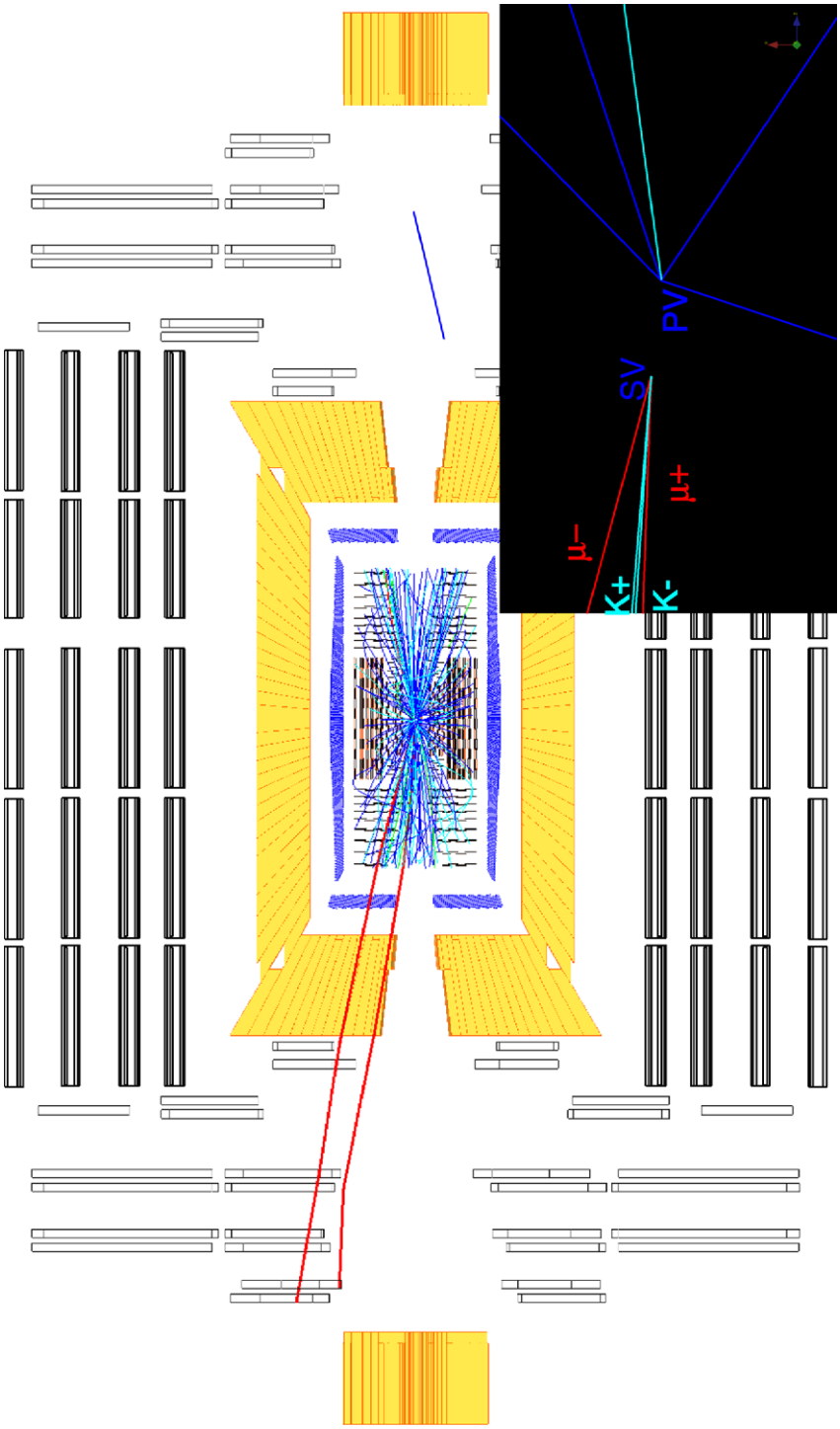

Figure CP7. Example of a pp $\rightarrow B_s + X$ event with $B_s \rightarrow J/\psi\phi$. (See section 5.1.1.)

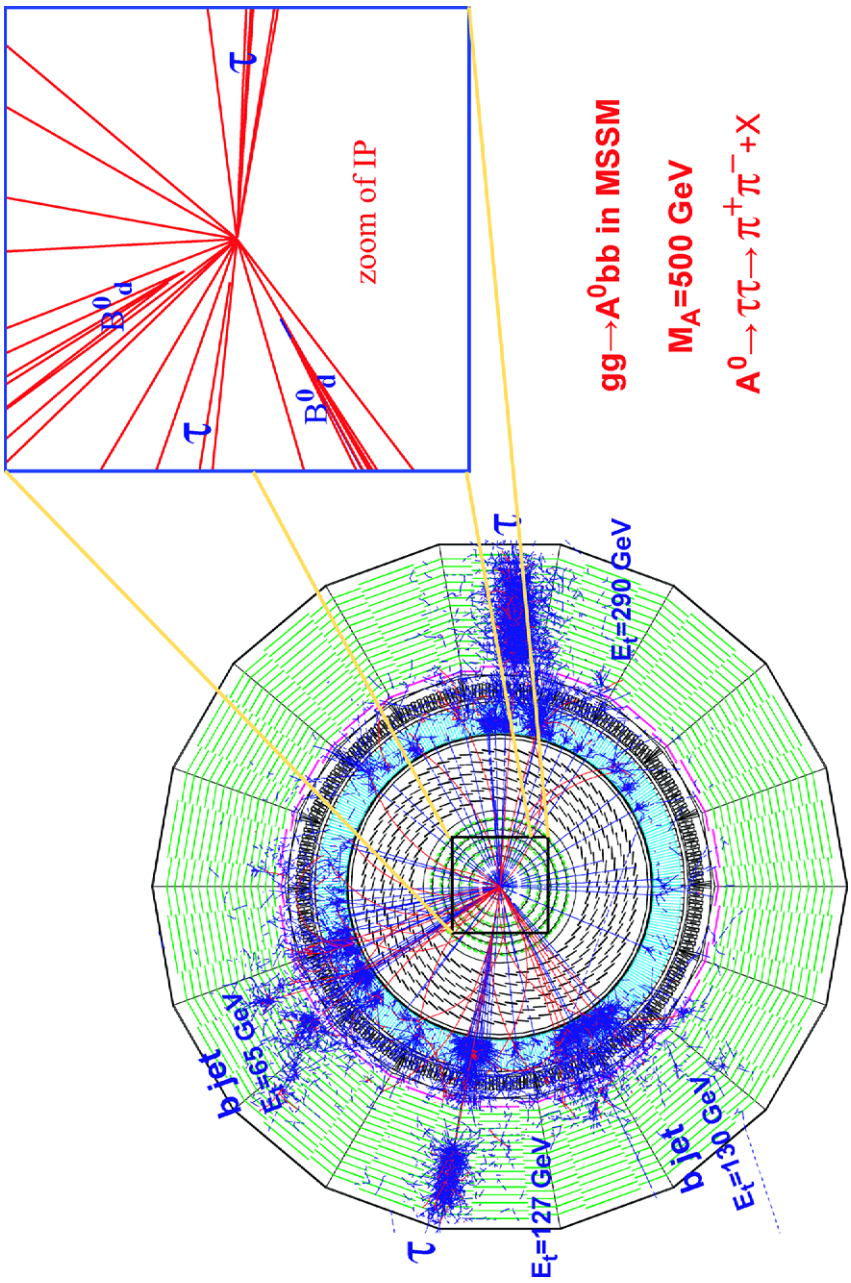

Figure CP8. Example of a pp → H + X event with H → $\tau\nu\tau\nu$. (See section 5.2.1.)

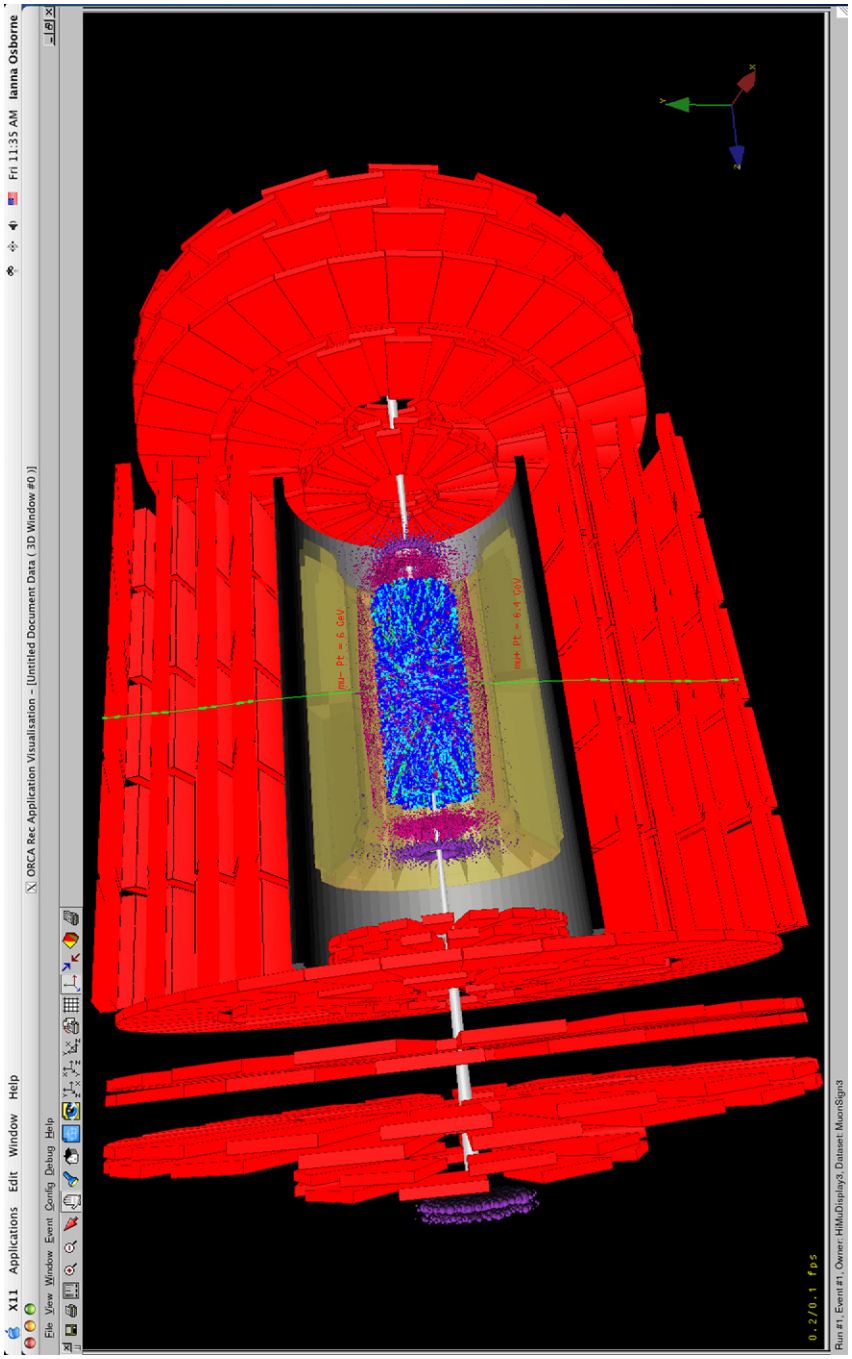

Figure CP9. $\Upsilon \to \mu^+\mu^-$ event embedded in a PbPb collision at $\sqrt{s_{NN}} = 5.5$ TeV with charged multiplicities at mid-rapidity $dN_{ch}/d\eta|_{\eta=0} = 3500$. (See section 6.1.)